Identification of parkin interactions: implications for Parkinson's disease

William Lloyd Haylett

Dissertation presented for the degree Doctor of Philosophy in Medical Sciences in the Faculty of Medicine and Health Sciences at Stellenbosch University

Supervisor: Prof. Soraya Bardien

Co-supervisors: Dr. Craig Kinnear and Prof. Jonathan Carr

December 2015

DECLARATION

By submitting this thesis electronically, I declare that the entirety of the work contained therein is my own, original work, that I am the sole author thereof (save to the extent explicitly otherwise stated), that reproduction and publication thereof by Stellenbosch University will not infringe any third party rights and that I have not previously in its entirety or in part submitted it for obtaining any qualification.

Signature: …….. Date: ……

ABSTRACT

Parkinson's disease (PD) is a progressive and debilitating neurodegenerative disorder, characterized by a distinct motor phenotype and the selective loss of dopaminergic neurons in the substantia nigra. While the etiology of PD is not fully understood, it is thought to involve a combination of different genetic, cellular and environmental factors that independently or concurrently contribute to neurodegeneration. To date, several PD-causing genes have been identified, and investigations of their function have provided novel insights into the pathobiology of disease. Particularly interesting among the known PD genes is *parkin*, mutations in which are the most common genetic cause of early onset PD. Parkin is an E3 ligase that ubiquitinates protein substrates and targets such substrates for degradation via the ubiquitin proteasome system (UPS). Therefore, the loss of parkin may result in the deleterious accumulation or dysregulation of parkin substrates and neurotoxicity. Parkin's enzymatic activity has also been implicated in the maintenance of mitochondrial health, and mitochondrial dysfunction is commonly reported in cellular and animal models of parkin deficiency.

This study aimed to investigate parkin and its role in PD on various levels. Initially, genetic screening approaches were used to assess the contribution of *parkin* mutations to PD in a group of 229 South African patients. It was concluded that *parkin* mutations are rare in the South African PD population, being present in only seven (3.1%) patients in the study group. Interestingly, this study identified two of only three Black African PD patients with mutations in a known PD-causing gene to date. The low frequency of known PD genes raises the interesting possibility that the unique South African ethnic groups may harbor mutations in novel PD-causing genes.

Although many parkin-interacting proteins have been identified in the literature, it is anticipated that novel, pathologically-relevant parkin substrates remain to be discovered. Hence, this study used a yeast two-hybrid (Y2H) approach to identify novel parkin interactions. This yielded 29 putative parkin interactors, of which four, namely ATPAF1, SEPT9, actin and 14-3-3η, were prioritized for verification by co-localization and co-immunoprecipitation experiments. Interestingly, two of the parkin interactors (ATPAF1 and SEPT9) were found to accumulate in the absence of parkin, supporting their role as authentic parkin substrates. The identification of these two intriguing proteins implicates parkin in the regulation of mitochondrial ATP synthase assembly and septin filament dynamics, which may be of significant relevance to our understanding of processes underlying neurodegeneration.

Moreover, it was aimed to assess various markers of mitochondrial function in a parkin-deficient cellular model, as previous studies had reported conflicting results regarding mitochondrial impairments in patient-derived cells with *parkin* mutations. Hence, dermal fibroblasts were obtained

from PD patients with homozygous *parkin* mutations, after which cell growth and viability, mitochondrial membrane potential, respiratory rates and the integrity of the mitochondrial network were assessed. Surprisingly, it was found that cell growth was significantly higher in the *parkin*-mutant fibroblasts compared to wild-type controls fibroblasts under basal conditions (p=0.0001), while exhibiting a greater inhibition of cell growth in the presence of the mitochondrial toxin CCCP (p=0.0013). Furthermore, whereas the mitochondrial networks of patient-derived fibroblasts were more fragmented than controls (p=0.0306), it was found that mitochondrial respiratory rates were paradoxically higher in the patients (p=0.0355). These unanticipated findings are suggestive of a compensatory response to the absence of parkin.

The parkin-deficient cellular model was also used in a pilot study of the functional effects of vitamin K_2 treatment, which has recently been identified as a promising PD therapeutic modality. It was found that treatment with vitamin K_2 resulted in more interconnected mitochondrial networks (p=0.0001) and enhanced respiratory rates (p=0.0459) in both *parkin*-mutant and wild-type control cells. While these results need to be studied further, it suggests that vitamin K_2 supplementation may be of use as a general promoter of mitochondrial integrity and function.

In conclusion, this dissertation highlights some novel interactions of the parkin protein and some interesting phenotypes of parkin deficiency. It is hoped that further investigation of parkin and its role in PD will, ultimately, aid in the development of therapeutic strategies to treat this debilitating and poorly-understood disorder.

OPSOMMING

Parkinson se siekte (PS) is 'n progressiewe en aftakelende neurodegeneratiewe kondisie, wat gekarakteriseer word deur 'n kenmerkende bewegingsfenotipe en die selektiewe afsterwing van dopaminergiese neurone in die substantia nigra. Terwyl die etiologie van PS nie ten volle verstaan is nie, behels dit waarskynlik 'n kombinasie van verskillende genetiese, sellulêre en omgewings-faktore wat onafhanklik of gelyktydig lei tot senuwee-afsterwing. Tot op hede is daar al verskeie PS-veroorsakende gene geïdentifiseer, en die bestudering van hul funksie het nuwe insigte in die patobiologie van hierdie siekte verskaf. Onder meer hierdie PS gene is *parkin* van besondere belang, aangesien mutasies in *parkin* die mees algemene genetiese oorsaak van vroeë-aanvang PS is. Parkin is 'n E3 ligase-ensiem wat proteïen substrate ubiquitineer en teiken vir degradasie via die ubiquitien proteasoomstelsel (UPS). Dus kan die verlies van parkin lei tot die beskadigende opeenhoping of wanregulasie van parkin substrate en senuwee-afsterwing. Parkin se ensiematiese aktiwiteit is ook betrokke by die instandhouding van mitokondriale gesondheid, en mitokondriale afwykings word dikwels gerapporteer in sellulêre en diermodelle van parkin tekort.

Hierdie studie het gepoog om parkin en sy rol in PS op verskillende vlakke te ondersoek. Aanvanklik is genetiese siftingsbenaderinge gebruik om die bydrae van *parkin* mutasies tot PS in 'n groep van 229 Suid-Afrikaanse pasiënte te evalueer. Die gevolgtrekking is bereik dat *parkin* mutasies skaars is in die Suid-Afrikaanse PS bevolking, aangesien dit teenwoordig is in net sewe (3.1%) pasiënte in die studie groep. Interessant genoeg, hierdie studie het twee van slegs drie gevalle van Swart Afrika-pasiënte met mutasies in 'n bekende PS geen to op datum geïdentifiseer. Die lae frekwensie van bekende PS gene versterk die stimulerende moontlikheid dat die unieke Suid-Afrikaanse sub-populasies dalk mutasies in nuwe PS-veroorsakende gene mag koester.

Alhoewel baie parkin proteïen-interaksies reeds in die literatuur geïdentifiseer is, word daar verwag dat nuwe, patologies-relevante parkin substrate nog wag om ontdek te word. Dus het hierdie studie 'n gis twee-hibried (G2H) benadering gebruik om nuwe parkin interaksies te identifiseer. Hierdie het 29 vermeende parkin interaktors opgelewer, waarvan vier, naamlik ATPAF1, SEPT9, aktien en 14-3-3η, geprioritiseer is vir verifikasie deur mede-lokalisering en mede-immunopresipitasie eksperimente. Interessant genoeg, daar is gevind dat twee van die parkin interaktors (ATPAF1 en SEPT9) ophoop in die afwesigheid van parkin, wat hul rol as werklike parkin substrate ondersteun. Die identifisering van hierdie twee interessante proteïene impliseer parkin in die regulering van mitokondriale ATP sintase vervaardiging en septienfilament dinamika, wat moontlik van beduidende belang is vir ons begrip van die onderliggende prosesse wat senuwee-afsterwing veroorsaak.

Verder is daar daarop gemik om verskeie aanwysigings van mitokondriale funksie in 'n parkin-gebrekkige sellulêre model te evalueer, aangesien vorige studies teenstrydige resultate rapporteer rakende mitokondriale afwykings in pasiënt-selle met *parkin* mutasies. Dus is daar dermale fibroblaste verkry van PS pasiënte met homosigotiese *parkin* mutasies, waarna sel-groei en lewensvatbaarheid, mitokondriale membraanpotensiaal, respiratoriese tempo en die integriteit van die mitokondriale netwerk geëvalueer is. Daar is verbasend gevind dat sel-groei aansienlik hoër is die *parkin*-mutante fibroblaste in vergelyking met wilde-tipe kontrole fibroblaste onder basale kondisies (p=0.0001), terwyl hulle 'n groter inhibisie van sel-groei in die teenwoordigheid van die mitokondriale toksien CCCP ondergaan (p=0.0013). Verder, terwyl die mitokondriale netwerke van pasiënt fibroblaste meer gefragmenteer is as die van kontroles (p=0.0306), is daar gevind dat mitokondriale respiratoriese tempo's, paradoksaal-gewys, hoër is in die pasiënte (p=0.0355). Hierdie onverwagte bevindinge is suggestief van die aanskakeling van 'n vergoedende respons-proses in die afwesigheid van parkin.

Die parkin-gebrekkige sellulêre model is ook gebruik in 'n voorlopige studie van die funksionele effekte van vitamiene K_2 behandeling, wat onlangs geïdentifiseer is as 'n belowende terapeutiese moontlikheid vir PS. Daar is gevind dat sel-behandeling met vitamiene K_2 lei tot meer geïnterkonnekteerde mitokondriale netwerke (p=0.0001) en verbeterde respiratoriese fuksie (p=0.0459) in beide *parkin*-mutante en wilde-tipe kontrole selle. Terwyl hierdie resultate verder bestudeer sal moet word, dui dit daarop dat vitamiene K_2-aanvulling moontlik gebruik kan word as 'n algehele promotor van mitochondriale integriteit en funksie.

Ten slotte, hierdie verhandeling beklemtoon 'n paar nuwe interaksies van die parkin proteïen en 'n paar interessante fenotipes van parkin tekort. Daar word gehoop dat verdere ondersoek van parkin en parkin se rol in PS sal, uiteindelik, steun in die ontwikkeling van terapeutiese strategieë om hierdie aftakelende en swak-verstaande wanorde beter te behandel.

ACKNOWLEDGEMENTS

I would like to express my sincerest gratitude to the following people and institutions that have assisted me during the course of this degree:

Prof. Soraya Bardien, my supervisor and mentor, for all her positivity, encouragement, patience and hard work. Your expert guidance and insightful suggestions have been most appreciated. Thank you for setting a wonderful example of scientific excellence.

Dr. Craig Kinnear, for his invaluable input, advice and technical assistance. Your passionate and hands-on approach to science has been a revelation.

Prof. Jonathan Carr, for helpful clinical input and sound advice.

Prof. Lize van der Merwe, for performing the statistical analyses.

Sr. Debbie Joubert for assistance with clinical information, Mrs. Ina le Roux for DNA extractions, the late Dr. Rowena Keyser for carrying out the MLPA experiments, Dr. Chrisna Swart for performing the Seahorse Analyzer assays, Dr. Ben Loos and Mrs. Lize Engelbrecht for assistance with fluorescence microscopy and Ms. Andrea Gutschmidt for assistance with flow cytometry.

My colleagues in the MAGIC lab, for creating an amiable and fun working environment. A special thank you to Drs. Sihaam Boolay and Chrisna Swart, for your advice, support and encouragement.

The National Research Foundation (NRF), Stellenbosch University and Prof. Paul van Helden for providing financial support.

My friends, particularly my friends in the sciences, who have since left the lab: Carol, Martmari, Carin, Elsje-Marie, Janine, Ilze, Ania, Carmen and Melissa. Thank you for understanding the demands of a PhD better than most, and for always being available when I needed to blow off some steam.

My parents, Travis and Suzanne, for teaching me the profound value of perseverance, diligence, inquisitiveness and imagination. I could not have finished this dissertation without your unwavering support and words of encouragement in difficult times.

Francois, for your unfailing love and endless patience.

TABLE OF CONTENTS

LIST OF ABBREVIATIONS

3'	Three-prime
3D	Three-dimensional
5'	Five-prime
A	Adenine
Å	Ångström
aa	Amino acid
AAO	Age at onset
ACTB	β-Actin gene
ACTG1	γ-Actin gene
AD	Autosomal dominant
AIMP2	Aminoacyl-tRNA synthase complex-interacting multifunctional protein-2
ALP	Autophagy-lysosomal pathway
ALS	Amyotrophic lateral sclerosis
AP-MS	Affinity purification-mass spectrometry
AR	Autosomal recessive
ARTS	Apoptosis-related protein in the TGF-β signaling pathway
ATP	Adenosine triphosphate
ATP13A2	ATPase type 13A2
ATPAF1	ATP synthase mitochondrial F1 complex assembly factor 1
ATPase	ATP hydrolyzing enzyme
BLAST	Basic local alignment search tool
BLASTn	Basic Local Alignment Search Tool nucleotide
BLASTP	Basic Local Alignment Search Tool protein
bp	Basepair
BSA	Bovine serum albumin
C	Cytosine
CAF	Central analytical facility
CCCP	Carbonyl cyanide 3-chlorophenylhydrazone
cDNA	Complementary DNA
CDS	Coding sequence
CIP	Calf intestinal alkaline phosphatase
CISD1	CDGSH iron-sulfur domain-containing protein 1

CNS	Central nervous system
co-IP	Co-immunoprecipitation
CRISPR	Clustered regularly interspaced short palindromic repeats
C-terminal	Carboxyl-terminal
DBS	Deep brain stimulation
ddH_2O	Distilled deionized water
DJ-1	Daisuke-junko-1
DMSO	Dimethyl sulfoxide
DNAJC6	Neuronally-expressed auxilin
DOPA	3,4-dihydroxy phenylalanine
Drp1	Dynamin-related protein 1
dsDNA	Double-stranded DNA
EDTA	Ethylene diamine tetra-acetic acid
EGFR	Epidermal growth factor receptor
EIF4G1	Eukaryotic translation initiation factor 4 gamma 1
EOPD	Early-onset Parkinson's disease
ER	Endoplasmic reticulum
ERK	Extracellular signal-related kinase
ESCRT	Endosomal sorting complex required for transport
ETC	Electron transport chain
ExoI	Exonuclease I
F-actin	Actin filaments
FAF1	Fas-associated factor 1
FBXO7	F-box only protein 7
FCCP	Carbonyl cyanide p-trifluoromethoxyphenyl hydrazone
FSC/SSC	Forward scatter/side scatter
FTDP-17	Frontotemporal dementia with parkinsonism linked to chromosome 17
g	Gram
G	Guanine
GAL4	Galactose transcription factor 4
GAL4-AD	GAL4 activation domain
GAL4-DNA-BD	GAL4 DNA binding domain
GAPDH	Glyceraldehyde-3-phosphate dehydrogenase
GBA	Glucoserebrosidase
gDNA	Genomic DNA
GSTO1	Glutathione S-transferase omega 1

GTPase	Guanine triphosphate hydrolyzing enzyme
GWAS	Genome-wide association studies
h	Hour
HA	Hemagglutinin
HECT	Homologous to E6 C-terminus
HIF-1α	Hypoxia-inducible factor 1α
HK1	Hexokinase 1
HK2	Hexokinase 2
HRM	High-resolution melt
HRP	Horseradish peroxidase
IBR	In-between RING domain
ID	Identifier
Indel	Insertion/deletion
IP	Immunoprecipitation
IPDGC	International Parkinson's Disease Genomics Consortium
iPSC	Induced pluripotent stem cells
JC-1	Tetraethyl benzimidazolyl carbocyanine iodide
JNK	C-Jun N-terminal kinase
kb	Kilobase
kDa	Kilodalon
L	Liter
LB	Lewy body
LB	Luria-Bertani
LiAc	Lithium acetate
log	Logarithm
LRRK2	Leucine-rich repeat kinase 2
M	Molar
MAO-B	Mitogen-activated protein kinase
MAPT	Microtubule-associated protein tau
Mcl-1	Myeloid cell leukemia-1
MCS	Multiple cloning site
MDV	Mitochondria-derived vesicle
Mfn1	Mitofusin 1
Mfn2	Mitofusin 2
mg	Milligram
min	Minute
MK-4	Menaquinone-4

ml	Milliliter
MLPA	Multiplex ligation-dependent probe amplification
mM	Millimolar
mm	Millimeter
MPTP	1-Methyl-4-phenyl-1,2,3,6-tetrahydropyridine
MRI	Magnetic resonance imaging
mRNA	Messenger RNA
mtDNA	Mitochondrial DNA
MTT	Thiazolyl blue tetrazolium bromide
ng	Nanogram
NGS	Next-generation sequencing
nM	Nanomolar
nm	Nanometer
NMDA	N-methyl-D-aspartate
NSC	Non-silencing control
N-terminal	Amino-terminal
OCR	Oxygen consumption rate
OD	Optical density
OGFOD1	2-Oxoglutarate and Fe^{2+}-dependent oxygenase domain containing protein 1
OMIM	Online Mendelian Inheritance in Man
OMM	Outer mitochondrial membrane
OPA1	Optic atrophy protein 1
OR	Odds ratio
ORF	Open reading frame
P	Patient
PACRG	Parkin co-regulated gene
PARIS	Parkin interacting substrate
PARP1	Poly(ADP-ribose)-polymerase-1
PBS	Phosphate-buffered saline
PCI	Phenol chloroform isoamyl alcohol
PCR	Polymerase chain reaction
PD	Parkinson's disease
PDmutDB	Parkinson's disease mutation database
PEG	Polyethylene glycol
PET	Positron emission tomography
PGC-1α	Peroxisome proliferator-activated receptor γ coactivator 1α

PI(3)K	Phosphoinositide 3-kinase
PINK1	Phosphatase and tensin homolog (PTEN)-induced kinase 1
PKA	Protein kinase A
pK_a	Acid dissociation constant
PLA2G6	Phospholipase A2, group VI
pmol	Picomol
PSP	Progressive supranuclear palsy
PVDF	Polyvinylidene difluoride
QDO	Quadruple dropout
q-PCR	Quantitative PCR
q-RT-PCR	Quantitative reverse-transcrition PCR
RBR	RING between RING
RE	Restriction enzyme
REP	Repressor element
RING	Really interesting new gene domain
RNAi	RNA interference
ROS	Reactive oxygen species
RPL13A	Ribosomal protein l13a
rpm	Revolutions per minute
RQI	RNA quality indicator
RR	Relative risk
RT-PCR	Reverse-transcription PCR
SAP	Shrimp alkaline phosphatase
SB	Sodium tetraborate
SCA2	Spinocerebellar ataxia type 2
SCA3	Spinocerebellar ataxia type 3
SCF	Skp1, cullin-1, Roc1 and F-box protein
SD	Synthetic defined
SD^{-Ade}	SD media lacking adenine
SD^{-His}	SD media lacking histidine
SD^{-Leu}	SD media lacking leucine
$SD^{-Leu-Trp}$	SD media lacking leucine and tryptophan
SDS	Sodium dodecyl sulfate
SDS-PAGE	SDS-polyacrylamide gel electrophoresis
SD^{-Trp}	SD media lacking tryptophan
SD^{-Ura}	SD media lacking uracil
sec	Second

SEPT4	Septin 4
SEPT4_v1	Septin 4 isoform 1
SEPT4_v2	Septin 4 isoform 2 (ARTS)
SEPT5	Septin 5
SEPT9	Septin 9
SEPT9_v1	Septin 9 isoform 1
shRNA	Small hairpin RNA
siRNA	Small interfering RNA
SNCA	α-Synuclein gene
SNpc	Substantia nigra pars compacta
SXR	Steroid and xenobiotic nuclear receptor
SYNJ1	Synaptojanin 1
T	Thymine
T_a	Annealing temperature
TBST	Tris-buffered saline with Tween-20
TDO	Triple dropout
TFAM	Mitochondrial transcription factor A
TOM	Translocase of outer membrane
TOMM7	Translocase of outer membrane member 7
U	Unit
UBIAD1	UbiA prenyltransferase domain containing 1
UBL	Ubiquitin-like domain
UCP	Uncoupling protein
UP	Unique parkin domain
UPS	Ubiquitin proteasome system
UV	Ultraviolet
V	Volt
v	Volume
VDAC1	Voltage-dependent anion-selective channel protein 1
VPS35	Vacuolar protein sorting 35
WT	Wild-type
WTCCC2	Wellcome Trust Case Control Consortium 2
X-α-gal	5-Bromo-4-chloro-3-indolyl α-D-galactopyranoside
Y2H	Yeast two-hybrid
YPDA	Yeast peptone dextrose adenine
YWHAH	Tyrosine 3-monooxygenase/tryptophan 5-monooxygenase activation protein, η polypeptide

β2M	β-2 microglobulin
$\Delta\psi_m$	Mitochondrial membrane potential
μg	Microgram
μl	Microliter
μM	Micromolar
μm	Micrometer
°C	Degrees Celsius

LIST OF FIGURES

LIST OF TABLES

OUTLINE OF THE DISSERTATION

This dissertation involves a genetic and functional investigation of parkin and its role in Parkinson's disease (PD). As such, it examines the contribution of *parkin* mutations to PD in South African patients, highlights novel parkin-interacting proteins and evaluates cellular function in a parkin-deficient cell model. Furthermore, it explores the therapeutic compound vitamin K_2 as a possible PD treatment modality.

This dissertation is divided into four chapters:

Chapter one provides an overview of what is currently known about PD, with a particular emphasis on the genetics and pathobiology of this disease. As this dissertation will be specifically focusing on the role of parkin in PD, a review of the literature on parkin is provided. Previous studies on the therapeutic potential of vitamin K_2 for PD will also be highlighted. Lastly, the overall aims and objectives of this study will be outlined.

Chapter two details the methodological approaches used in this dissertation, and is organized into three parts. The first part describes a molecular genetic screen of *parkin* for pathogenic mutations, the second part entails experimental procedures used to identify and characterize parkin-interacting proteins, and the third part provides methods employed in the functional evaluation of cellular health in a model of parkin deficiency.

Chapter three relays the results obtained from the present study. It includes the findings on the frequency of *parkin* mutations South African PD patients, the identification and verification of four parkin interactors, interesting cellular phenotypes observed in a parkin-deficient cell model and describes the effect of treatment with vitamin K_2 on several parameters of cellular health.

Chapter four provides a discussion of the important findings of this dissertation, and highlights the possible relevance of these findings to PD research. It furthermore advises on proposed future work that may expand our current understanding of parkin and its role in PD.

CHAPTER ONE: INTRODUCTION

TABLE OF CONTENTS **PAGE**

CHAPTER ONE: INTRODUCTION

PART ONE: PARKINSON'S DISEASE (PD)

1.1 PD – HISTORICAL CONTEXT

Almost two centuries ago, the English apothecary James Parkinson provided the first clear medical description of the disorder which now bears his name, in "An Essay on the Shaking Palsy" (Parkinson 1817). In this landmark publication, Parkinson described six patients with "involuntary tremulous motion, with lessened muscular power, in parts not in action and even when supported; with a propensity to bend the trunk forwards, and to pass from a walking to a running pace: the senses and the intellects being uninjured". The French neurologist Jean-Martin Charcot later expanded on the formal clinical description of this disorder and named it Parkinson's disease (PD), in recognition of the work of James Parkinson (Charcot 1880). However, Parkinson himself acknowledged that parkinsonism-like symptoms were noticed by several earlier authors, including Galen, Sylvius de la Boë, Boissier de Sauvages and Juncker (Parkinson 1817). For example, Galen described a condition involving tremors that occurred only at rest, postural instability and paralysis, whereas Sauvages described festination, a term for the gait abnormalities characteristic of PD (Raudino 2012). Ayurvedic Indian texts dating from the tenth century BC and ancient Chinese sources included descriptions highly reminiscent of PD, suggesting that this disorder was known to several ancient civilizations (Manyam 1990; Zhang et al. 2006). Nonetheless, the great merit of Parkinson's essay was its focused and careful description of PD's cardinal symptoms, accurate account of the course of the malady as well as in distinguishing PD from similar disorders. The contribution of Parkinson's work is increasingly recognized and his birthday, 11 April, is celebrated as World PD Day.

Parkinson's expressed hope that his monograph would spur pathologists to find the anatomical substrate of PD had to wait 80 years. After Paul Blocq and Georges Marinesco published their case report of a tuberculomatous lesion in the midbrain which resulted in parkinsonism (Blocq and Marinesco 1894), Edouard Brissaud speculated that an ischemic lesion of the substantia nigra might be principally responsible for PD (Brissaud 1895). Brissaud's hypothesis was later confirmed by Konstantin Tretiakoff, who consistently observed substantia nigral degeneration in autopsied PD patients and also found associated "senile lesions" in the affected areas (Tretiakoff 1919). Furthermore, a majority of the PD brains also had "corps de Lewy", neuronal inclusions described seven years earlier by Frederic Lewy (Lewy 1912). Despite Tretiakoff's study, severe damage to the substantia nigra was not generally accepted as the critical pathological hallmark of PD until later confirmatory work of Rolf Hassler (1938) and then John Greenfield and Frances Bosanquet (1953)

was published. Further noteworthy historical advances include elucidation of the biochemical basis of PD, centered on the newly discovered role of the neurotransmitter dopamine in PD (Carlsson et al. 1958), the introduction of dopamine replacement via levodopa therapy for the management of motor symptoms, and the discovery of genetic factors that contribute to PD (Polymeropoulos et al. 1997).

After two centuries since the publication of Parkinson's seminal monograph, and great leaps and bounds in our understanding of the anatomical and molecular pathology of this disorder, many key questions concerning PD pathogenesis remain unanswered, and PD remains without a cure. It is hoped that a wider and deeper understanding of the genes, proteins and pathways involved in PD will aid in the development of neuroprotective or therapeutic interventions that may prevent or treat the underlying pathology of this debilitating disorder.

1.2 EPIDEMIOLOGY OF PD

Published estimates of the prevalence and incidence of PD vary greatly according to the applied methodology, which complicates cross-study comparisons. Epidemiological studies are particularly sensitive to differences in diagnostic criteria and case-finding strategies; record-based studies and studies performed in clinical settings do not include patients who failed to seek medical attention and therefore generally underestimate the prevalence or incidence in the general population. Nonetheless, the quantity of publications on PD epidemiology, over 80 prevalence and 25 incidence studies, allow for confident estimations of PD prevalence and incidence (at least for developed nations) (Wirdefeldt et al. 2011).

1.2.1 Prevalence

The reported prevalence of PD ranges from 100 to 5703 per 100 000, with studies on the elderly population (typically over the age of 60) reporting the highest figures (Kuopio et al. 1999; de Rijk et al. 2000; Barbosa et al. 2006; Peters et al. 2006; Racette et al. 2009). A meta-analysis of twelve high-quality North American and European studies estimated the prevalence of PD in the population over the age of 65 at 950 per 100 000 (Hirtz et al. 2007). A further study that reviewed data from six European prevalence studies and country-specific population structure data estimated the worldwide total number of PD patients over the age of 50 at between 4.1 and 4.6 million in 2005; this number was projected to double to between 8.7 and 9.3 million by the year 2030 (Dorsey et al. 2007).

Age is a significant risk factor for PD: it is very rare before the age of 40 and the prevalence increases steeply after the age of 60, with up to and above 4000 per 100 000 reported in the highest age groups (de Rijk et al. 1995; Clavería et al. 2002; Benito-León et al. 2003). Most cases of PD manifest around

the age of 60 years (Jankovic 2008). Some studies report a decline in prevalence rates in the age group above 80 years (Wang et al. 1991; Benito-León et al. 2003), but this is probably an artefact resulting from PD misdiagnosis due to disease comorbidity, patient loss to follow-up or smaller patient sample sizes (de Rijk et al. 2000).

Geographic and ethnic variation in PD prevalence is interesting from an etiological point of view, as such variation might result from differences in environmental exposures or distribution of susceptibility alleles (de Lau and Breteler 2006). Several studies have reported lower prevalence figures in Africa (Schoenberg et al. 1988), Asia (Wang et al. 1991), and South America (Melcon et al. 1997) than Europe. This is supported by calculations of age-standardized prevalence proportions which found a 13-fold difference in age-standardized prevalence across populations; the study found the lowest prevalence in China, Japan and Africa (Zhang and Román 1993). However, more recent studies report PD prevalence in China (Zhang et al. 2005) and South America (Barbosa et al. 2006) as being similar to European populations. The previously reported differences may result from methodological and case-ascertainment concerns, rather than true ethnic differences (Alves et al. 2008). The low PD prevalence in Africa may be due to a shorter life expectancy in comparison to the developed world (McInerney-Leo et al. 2004). Indeed, PD prevalence estimates in Africa are lowest in countries of Eastern and Western Africa, where life expectancy is lowest, while Northern African countries have reported prevalences comparable to developed countries (Okubadejo et al. 2006). Another plausible reason for low prevalence in Africa is the relative underdiagnosis of PD in Africa due to socioeconomic and cultural factors (McInerney-Leo et al. 2004).

1.2.2 Incidence

Comparatively fewer PD incidence than prevalence studies have been published. Overall, these studies report annual incidence estimates for all age groups ranging from 2 to 22 per 100 000 (Mayeux et al. 1995; Bower et al. 1999; de Lau et al. 2004), with studies restricted to the elderly (over the age of 65) reporting estimates of 410 to 529 per 100 000 (Benito-León et al. 2004; Driver et al. 2009). A meta-analysis of eight high-quality incidence studies estimated an age-standardized PD incidence of 14 per 100 000 in developed countries (Hirtz et al. 2007); this figure rose to 160 per 100 000 when the analysis was restricted to studies of elderly patients (Hirtz et al. 2007).

As with PD prevalence, PD incidence rates are very low under the age of 40 and rise sharply after the age of 60, attesting to the importance of age as a PD risk factor (Van Den Eeden et al. 2003). A similar drop in PD incidence figures are reported for the old age groups (Morens et al. 1996; Bower et al. 1999); however, there is some debate over whether this decline is real or due to underdiagnosis (Driver et al. 2009).

Comparison of PD incidence across different countries is hampered by differences in study methodology in the various publications (e.g. reporting on crude incidence v. population-adjusted incidence). Most European studies report overall incidence estimates between 9 and 22 per 100 000 (Taba and Asser 2003; Linder et al. 2010), whereas the corresponding estimates for Asian populations range from 1.5 to 17 per 100 000 (Wang et al. 1991; Morioka et al. 2002). Only a single study report on PD incidence in Africa, estimating the incidence in North-East Libya at 4.5 per 100 000 (Ashok et al. 1986). Few epidemiological studies consider incidence differences among ethnic populations within the same study group. In a study of a multi-ethnic Californian population, PD incidence was highest in Hispanic individuals, followed by non-Hispanic White, Asian and Black individuals (Van Den Eeden et al. 2003). Given the scarcity of incidence data for non-White populations, conclusive ethnic differences in PD incidence are a matter of debate.

1.3 NEUROPATHOLOGY OF PD

The primary neuropathological hallmark of PD is the loss of neuromelanin-containing dopaminergic neurons in the substantia nigra pars compacta (SNpc), which forms an integral part of the basal ganglia motor circuit. The neuronal loss characteristic of PD is illustrated in Figure 1.1. Such degeneration of neurons of the nigrostriatal pathway depletes the basal ganglia of dopamine, resulting in the distinguishing motor features of PD (Hornykiewicz 2008). Neuronal loss in the SNpc is most pronounced in the ventrolateral tier of neurons, which project to the striatum. Accompanying this loss is an increase in microglial activation and astrocytosis and a decrease in neuromelanin pigmentation in the affected area (Teismann and Schulz 2004). The extent of neuron loss in the SNpc has been shown to correlate well with the severity of many of the motor features of PD (Vingerhoets et al. 1997). It is estimated that, by the time of the first appearance of motor symptoms, approximately 40-60% of dopaminergic neurons of the SNpc have been lost, leading to an 60-80% reduction in nigrostriatal dopamine (Fearnley and Lees 1991; Halliday et al. 1996). Extrapolation of such findings suggests a preclinical phase of PD with progressively worsening SNpc degeneration of about 5 years (Greffard et al. 2006).

While the biggest emphasis is consistently placed on degeneration of the nigrostriatal pathway, it should be noted that PD-associated degeneration is not restricted to the SNpc. Dopaminergic and nondopaminergic neuronal loss can be found in the locus ceruleus, dorsal nuclei of the vagus, raphe nuclei, nucleus ambiguus, nucleus basalis of Meynert and several other areas of the brainstem (Braak and Braak 2000). The recognition of this extranigral pathology in PD is important for the proper management of the non-motor symptoms of PD, which usually do not respond well to treatment with the dopamine precursor levodopa or dopamine agonists (Chaudhuri and Odin 2010).

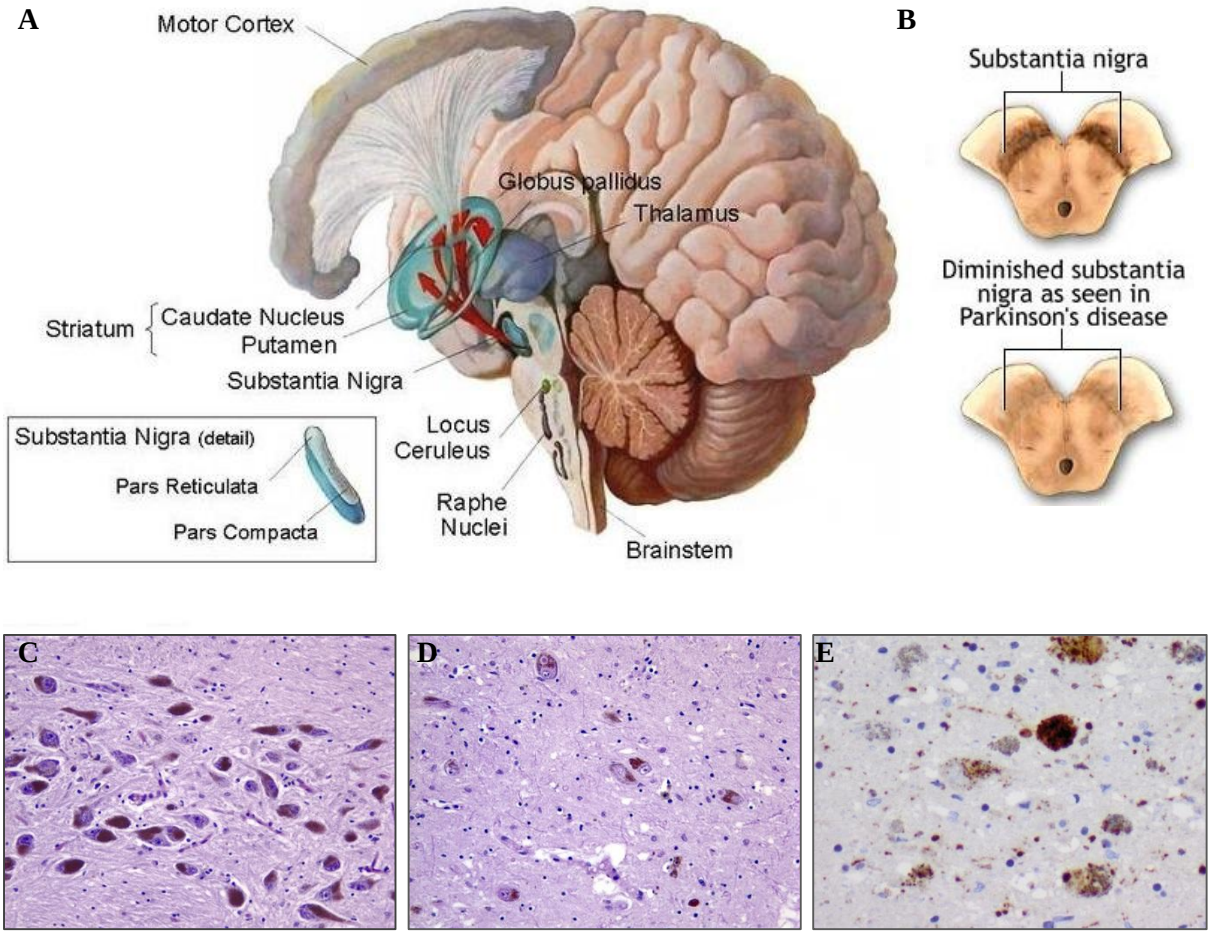

Figure 1.1 Neuropathology of Parkinson's disease. A, brain regions and neuronal pathways affected by PD. The principal affected pathway is the dopaminergic neurons of the nigrostriatal pathway (red arrows) whose cell bodies are located in the substantia nigra pars compacta (SNpc). These neurons project to the basal ganglia and synapse at the striatum (both the caudate nucleus and the putamen). Degeneration of the nigrostriatal pathway in PD leads to a dopamine deficit resulting in dysregulation of the basal ganglia. **B**, depigmentation (loss of neuromelanin) in PD-affected SNpc due to the loss of dopaminergic neurons. Illustrated are transverse sections through the superior colliculus of an unaffected individual (top) and a PD patient (bottom). **C**, histology of unaffected SNpc showing many pigmented neurons. **D**, histology of PD-affected SNpc showing severe loss of pigmented cells. **E**, immunohistochemical labeling of Lewy bodies (LBs) in a PD-affected SNpc. Immunostaining with an α-synuclein antibody reveals dark-staining intraneuronal inclusions. (Figures adapted from http://neuropathology-web.org). Abbreviations: LB, Lewy body; PD, Parkinson's disease; SNpc, substantia nigra pars compacta.

In addition to the loss of dopaminergic neurons, a defining hallmark of PD is the presence of intraneuronal inclusions, or Lewy bodies (LBs), in the surviving neurons of affected brain regions. LBs are spherical, eosinophilic, cytoplasmic aggregates which consist of a heterogeneous mixture of over a hundred various proteins (Wakabayashi et al. 2013). The main component of LBs is aggregated α-synuclein protein; α-synuclein antibodies are routinely used for the immunohistochemical detection of LB pathology during post-mortem diagnosis (Figure 1.1E). Considerations of the distribution of LB

pathology has led Braak et al. (2003) to propose that LB formation and neurodegeneration is not random but spreads along interconnected brain regions in a regular pattern as PD progresses. This six-stage pathological process begins at induction sites with degeneration of the olfactory bulb and the lowest parts of the brainstem, spreads rostrally up the brainstem to the raphe nuclei and locus ceruleus and progresses to encompass the SNpc. Later stages of disease involve LB pathology in the paralimbic regions and thalamus, spreading to the prefontal motor cortex and finally the entire neocortex at the terminal stages. Several studies have confirmed the validity of the Braak staging system, although it remains a subject of much debate and roughly 15% of PD patients do not conform to the proposed pattern (Kalaitzakis et al. 2008; Parkkinen et al. 2008). It has been suggested that many of the non-motor features of PD are related to the earlier Braak stages (Langston 2006).

1.4 CLINICAL FEATURES OF PD

PD is classically characterized by four cardinal motor features: bradykinesia, tremor at rest, rigidity and postural and gait impairment. However, each of these symptoms are not always present in every patient diagnosed with PD, as PD symptoms vary considerably with the diverse profiles and lifestyles of patients (Jankovic 2008). Motor features have traditionally defined the disorder, possibly because they are visually recognizable to even untrained observers. Nonetheless, various non-motor symptoms are frequently present in PD patients, including autonomic dysfunction, cognitive and psychiatric disturbances, sensory abnormalities and sleep disorders. Recent years have seen an increased interest in the non-motor features of PD not only because their presence aid in PD diagnostic purposes, but also because of the severe reduction in quality of life that these features bring about in PD patients, often necessitating specialized care (Lim et al. 2009; Gallagher et al. 2010).

1.4.1 Motor symptoms

1.4.1.1 *Bradykinesia*

Bradykinesia, or slowness of movement, is the most characteristic and disabling symptom of PD, and encompasses problems in planning, initiating and executing movement. It is characterized by the progressive loss of speed or amplitude during the execution of a motor action. Bradykinesia initially presents as difficulties with fine motor tasks, such as handwriting or tying up shoelaces, as well as slow movement and reaction times (Berardelli et al. 2001). Other manifestations of bradykinesia include loss of spontaneous movements, reduced arm swinging while walking, loss of facial expression (hypomimia) and decreased blinking, speech impairment and drooling resulting from swallowing difficulties (Bagheri et al. 1999).

1.4.1.2 *Rigidity*

Rigidity manifests as increased muscle tone resulting in stiffness and resistance to movement in joints. Passive movement of the limbs often results in ratchet-like movements, especially when related to an underlying tremor. This rigidity is present throughout the range of movement, and is increased by voluntary movements of the contralateral limb (Rodriguez-Oroz et al. 2009). Rigidity is often associated with pain, especially of the neck and shoulders; a painful shoulder is a frequent first presenting motor symptom of PD, although this often goes undiagnosed (Stamey et al. 2008)

1.4.1.3 *Resting tremor*

Tremor at rest is the most recognizable feature of PD, and is the first symptom in approximately 70% of PD patients (Hughes et al. 1993). Resting tremor is the rhythmic and involuntary movement of a body part that is not associated with any voluntary activity. The hands are most commonly affected, but tremor can also affect the lips, chin, legs and trunk; hand tremors are often described as "pill-rolling", involving a supination-pronation movement (Deuschl et al. 2000). Resting tremor is usually asymmetric at onset and worsens under stress or heightened emotion. Characteristically, resting tremor ceases with voluntary action and during sleep.

1.4.1.4 *Postural and gait impairment*

Patients with PD usually adopt a stooped posture with neck and trunk flexion due to the loss of postural reflexes (Jankovic 2008). The characteristic gait of PD patients is slow with short shuffling steps; turning around requires multiple small steps. Parkinsonian gait can also involve gait freezing, a sudden gait impediment where patients feel as if their feet are "glued to the floor" (Giladi et al. 1997). Postural instability refers to the gradual development of impaired balance, and usually only presents late in disease progress. Postural instability and gait abnormalities are the most common causes of falls among PD patients and significantly contribute to the risk of hip fractures (Williams et al. 2006).

1.4.2 Non-motor symptoms

1.4.2.1 *Autonomic dysfunction*

Autonomic dysfunction is a common non-motor feature of PD and encompasses orthostatic hypotension, urinary dysfunction, erectile dysfunction and constipation. Orthostatic hypotension is reported in approximately 35% of PD patients and presents as dizziness, nausea, drowsiness and loss of consciousness (Low 2008). As such, orthostatic hypotension significantly increases the risk of falls (Matinolli et al. 2009). Urinary dysfunction, in the form of urge incontinence, urinary urgency or high

frequency of urination, was found to affect between 50% and 70% of PD patients (Martinez-Martin et al. 2007). The same study found that erectile dysfunction affects 42% of patients. Constipation is a very common non-motor feature of PD, with a reported prevalence ranging from 40% to 80% of patients (Jost 1997; Khoo et al. 2013). Interestingly, constipation predates onset of the first noticeable motor symptoms of PD in about half of PD patients, whereas other signs of dysautonomia such as orthostatic hypertension and urinary dysfunction are late features of PD (Pellicano et al. 2007).

1.4.2.2 *Cognitive and psychiatric disturbances*

Neuropsychiatric abnormalities are common and disabling non-motor features of PD. Cognitive decline is a near universal feature of PD, and results in impairment of problem-solving, planning and learning abilities (Barone et al. 2011). The prevalence of dementia has been estimated at 30% (Aarsland et al. 2005), with PD patients being at a six-fold increased risk of dementia (Aarsland et al. 2001). Other psychiatric disturbances such as depression, anxiety, apathy, obsessive-compulsive behavior and psychosis are also commonly seen in PD patients (Bernal-Pacheco et al. 2012). Psychosis, usually in the form of paranoid delusions and hallucinations, has a reported prevalence as high as 50% in PD patients (Fénelon 2008) and is a significant factor leading to the need for full-time care in a nursing home (Aarsland et al. 2000). Depression affects around 35-50% of PD patients and can be present years before the manifestation of motor symptoms (Lieberman 2006).

1.4.2.3 *Sensory abnormalities*

Sensory symptoms, including olfactory dysfunction and unexplained painful sensations, are frequently present in patients diagnosed with PD. Painful sensations, manifesting as tingling, burning, neuralgia or diffuse pain are experienced by approximately 50% of PD patients (Tinazzi et al. 2006). A prominent sensory symptom of PD is loss of smell, or hyposmia, which affects up to 90% of PD patients (Ponsen et al. 2004) and has been associated with degeneration of the olfactory bulb (Pearce et al. 1995). Hyposmia is often present at diagnosis of PD and does not appear to progress over the course of disease. Idiopathic hyposmia is correlated with an increased risk of developing PD and may therefore be an early preclinical sign of PD (Ross et al. 2008a).

1.4.2.4 *Sleep disorders*

Sleep disturbances, such as excessive daytime sleepiness, frequent awakenings, sleep attacks and insomnia, were previously ascribed to anti-parkinsonian medications (Ondo et al. 2001), but are now recognized as integral features of the disease (Maass and Reichmann 2013). Particularly common is rapid eye movement (REM) sleep behavioral disorder (RBD), which is present in approximately 40%

of PD patients (Schenck and Mahowald 2002). This disorder is characterized by the loss of motor inhibition during REM sleep, leading to the often violent acting-out of dreams which frequently results in injury. The occurrence of RBD often predates the onset of motor symptoms by up to a decade, and RBD is a significant risk factor for the development of PD (Iranzo et al. 2006). RBD, along with hyposmia, constipation and depression, are some of the earliest symptoms of neurodegeneration in PD, and are considered to be prodromal non-motor symptoms of a pre-parkinsonian state (Pellicano et al. 2007).

1.5 DIAGNOSIS OF PD

Proper diagnosis of PD is important for patient counseling and treatment, and is essential for clinical research. A definitive PD diagnosis requires the histological confirmation of LB pathology in the substantia nigra, which can only be done post-mortem (Gibb and Lees 1988a).

Although patient diagnosis can be informed by radiological imaging, including ^{18}F-dopa positron emission tomography (PET), diagnosis is most often based on clinical criteria. Diagnostic criteria have been developed by the UK Parkinson's Disease Society Brain Bank which is routinely used for the accurate and objective diagnosis of PD; the use of these criteria typically delivers a diagnostic accuracy of around 90% (Hughes et al. 2001). A diagnosis of PD is made based on the presence of bradykinesia and at least one other motor symptom in the patient, and the absence of symptoms or history indicative of an alternative diagnosis (Appendix I).

1.6 PROGNOSIS OF PD

Life expectancy is significantly reduced in PD patients, with reported mortality ratios of 1.3-2.5 in comparison to age-matched controls, regardless of the duration of the disease (Herlofson et al. 2004; Driver et al. 2008). The duration from disease onset to death typically ranges from 7-14 years; however, this varies widely between patients. There is little evidence that levodopa treatment of PD decreases disease mortality (Macleod et al. 2014). Increased mortality of PD patients has been associated with an older age at onset, the male sex, and the presence of cognitive decline and dementia (de Lau et al. 2014). In contrast to the general population, the leading cause of death of PD patients is pneumonia (Beyer et al. 2001)

1.7 TREATMENT OF PD

PD is an incurable and progressive disorder. Nonetheless, various avenues are available for the alleviation and management of PD symptoms. Such symptomatic treatment can substantially improve functional capacity and quality of life of patients diagnosed with PD.

1.7.1 Pharmacological treatment of PD

1.7.1.1 *Levodopa*

The major pharmacological approach to PD treatment is dopamine replacement therapy, of which levodopa remains the most widely used and efficacious treatment (Schapira et al. 2009). Orally administered levodopa (L-DOPA; L-3,4-dihydroxyphenylalanine) crosses the blood-brain barrier and is metabolized to dopamine in the central nervous system (CNS) by DOPA-decarboxylase. Levodopa may also be metabolized in the peripheral nervous system resulting in side effects such as nausea, stiffness and dyskinesia (involuntary movements). Hence, levodopa is commonly administered in combination with a peripheral DOPA-decarboxylase inhibitor, such as carbidopa or benserazide, to prevent metabolism of levodopa outside of the CNS. While levodopa treatment results in marked and sustained benefits for PD patients for several years, many patients eventually develop dyskinesias, dystonia and debilitating fluctuations in treatment response. Such levodopa-induced effects are more frequent with early age of disease onset, prolonged levodopa treatment and higher doses of levodopa (Ku and Glass 2010).

1.7.1.2 *Dopamine agonists*

Dopamine agonists mimic the effect of levodopa by binding to dopamine receptors in the basal ganglia. They are the preferred first-line medication for younger patients, who are at a higher risk of levodopa-associated motor complications. However, dopamine agonists are more commonly associated with adverse effects such as nausea, dizziness, hallucinations and impulse control disorders, which may necessitate a change of treatment strategy (Antonini et al. 2009).

1.7.1.3 *MAO-B inhibitors*

Monoamine oxidase-type B (MAO-B) inhibitors such as selegiline or rasagiline increase the availability of dopamine in the striatum by limiting dopamine breakdown at the synaptic cleft. They offer milder therapeutic effects than levodopa or dopamine agonists, but they are typically better tolerated (Riederer and Laux 2011). MAO-B inhibitors used in conjunction with levodopa may reduce levodopa-associated motor fluctuations (Rascol et al. 2005; Olanow et al. 2009). Ultimately, the

choice of which pharmacological agent to prescribe for PD treatment depends largely on the characteristics and needs of the patient, as well as the preferences of the clinician, as each class of medication has its strengths and weaknesses.

1.7.2 Deep brain stimulation

While dopamine replacement therapy can be greatly effective at managing the symptoms of PD at the earlier stages of treatment, patient response to such medication almost invariably becomes less effective and predictable over time (Schapira et al. 2009). Patients who are responsive to levodopa but experience debilitating motor fluctuations or dyskinesias may be surgically treated with deep brain stimulation (DBS) (Okun 2012). This technique involves the placement of one or more electrodes in the brain which target specific basal ganglial nuclei, most commonly the subthalamic nucleus or the globus pallidus. The electrodes are connected to an insulated lead which passes through a burr hole in the skull and subcutaneously connects to an impulse generator implanted in the anterior chest wall. This delivers electrical stimuli to the brain in order to modulate neural activity in the basal ganglia. The effects of DBS can mitigate parkinsonian symptoms, especially tremor, and reduce the adverse effects of levodopa therapy. PD patients that undergo DBS may experience sustained clinical improvement for over ten years (Castrioto et al. 2011). However, DBS is very costly and has several adverse effects, including risk of infection, intracranial hemorrhage, seizures and a wide array of neuropsychiatric effects (Parsons et al. 2006).

1.8 PD RISK FACTORS

The great majority (~90%) of PD cases are sporadic and idiopathic, as they have no identifiable cause. Substantial progress has been made over the last two decades in the discovery of several causative monogenic mutations that induce familial PD; however, only a small percentage (~10%) of patients with sporadic PD has known genetic underpinnings. It is hoped that, ultimately, the genetic or non-genetic factors that either cause or increase the risk of developing PD will be identified for the majority of sporadic PD cases.

1.8.1 Intrinsic risk factors

1.8.1.1 *Age*

Age is the most significant risk factor for PD. As discussed in Section 1.2, the disorder is rare before the age of 50 years, after which both the prevalence and incidence of PD increase sharply with increasing age. Rare cases of juvenile PD (onset before the age of 20 years) have been reported, with

a clinical presentation similar to sporadic PD. Early onset PD (EOPD), with disease onset before the age of 50 years, increases the probability that genetic causes are involved (Schrag and Schott 2006).

While the association of aging with increasing PD incidence might seem self-evident, the underlying mechanism by which aging promotes the development of PD remains unclear. In fact, other neurodegenerative disorders such as Huntington's disease and amyotrophic lateral sclerosis (ALS) have earlier ages at onset than PD. It is assumed that some intrinsic age-dependent factors, or the accumulation of age-related damage, predispose older individuals to develop PD (Reeve et al. 2014).

1.8.1.2 *Gender*

The incidence of PD is higher in men than in women, as a meta-analysis of seven incidence studies reports an increased relative risk (RR) of 1.49 for men (Wooten et al. 2004). A similar meta-analysis of a separate set of studies reports a male to female ratio of 1.46 (Taylor et al. 2007). However, Taylor et al. found that this ratio is inconsistent across different study groups, with higher male-female ratios being reported in older study populations as well as a weaker association with gender in Asian populations (Taylor et al. 2007). The reasons for this male preponderance are not known, but it may be related to different environmental and occupational exposures associated with the "male lifestyle", the neuroprotective effects of estrogen in women (Inestrosa et al. 1998) or recessive susceptibility genes on the X chromosome.

1.8.2 Environmental risk factors

Many reports have implicated environmental factors in the development of PD. It was discovered in 1983 that the accidental exposure to 1-methyl-4-phenyl-1,2,3,6-tetrahydropyridine (MPTP), a by-product of illicit heroin production, leads to a levodopa-responsive parkinsonian disorder with symptoms largely indistinguishable from PD (Langston et al. 1983). MPTP induces parkinsonism when its active metabolite MPP^+ is transported into neurons by the dopamine transporter and inhibits the mitochondrial electron transport chain (ETC), which ultimately leads to degeneration of dopaminergic neurons. This discovery was heralded as proof of principle that exposure to environmental toxins may cause PD, or at least increase the risk of developing PD.

The identification of environmental risk factors for PD is mostly based on epidemiological approaches; such studies are prone to several kinds of bias. As such, the multitude of studies of the association of various environmental factors with risk of PD are often equivocal and inconclusive (de Lau and Breteler 2006; Kieburtz and Wunderle 2013).

1.8.2.1 *Cigarette smoking*

Many epidemiological studies have demonstrated a reduced risk for developing PD among cigarette smokers. A large meta-analysis of 48 studies encompassing 20 countries found a pooled RR of 0.6 for smokers compared to non-smokers (Hernán et al. 2002). In addition, most of these studies showed a dosage effect of smoking on PD risk, as people who have been smoking for a longer total period of time have an even lower risk of developing PD. Several possible mechanisms for the neuroprotective effects of smoking have been suggested; it is thought that nicotine may stimulate dopamine release, act as an antioxidant, or modulate MAO-B activity in the brain (Quik et al. 2012). On the other hand, several non-causal explanations have been proposed for the observed protective relationship between smoking and PD. Such explanations include the possibility that the increased mortality of smokers lowers their age-related risk of PD, or that early loss of smell and other sensory abnormalities of subclinical PD reduce the likelihood of smoking.

1.8.2.2 *Caffeine*

Similarly to cigarette smoking, caffeine intake decreases the risk of developing PD. A meta-analysis of thirteen studies found a significantly lowered RR of 0.7 for coffee drinkers (Hernán et al. 2002). The protective agent in coffee is thought to be caffeine, as no association had been found for other coffee components and risk of PD while non-coffee sources of caffeine did demonstrate such an effect (Ross et al. 2000). While both men and women coffee drinkers experience a decreased risk of PD, this decrease is less pronounced in women (Palacios et al. 2012); the protective effect of caffeine appears to be attenuated by the use of estrogen replacement in postmenopausal women (Ascherio et al. 2003). Caffeine binds antagonistically to adenosine A_2 receptors, which may protect against dopaminergic degeneration. In fact, caffeine administration improves motor deficits in a mouse model of PD (Xu et al. 2010).

1.8.2.3 *Pesticides and herbicides*

The discovery of the PD-inducing effect of MPTP, described above, spurred extensive research into the possible epidemiological effects of exposure to pesticides and other environmental toxins. While such studies consistently found a positive association between pesticide exposure and PD development, the association was only statistically significant in about half of these studies (Lai et al. 2002). A recent meta-analysis of retrospective case-control studies calculated a pooled odds ratio (OR) of 1.5 for lifetime pesticide exposure, although a significant degree of heterogeneity was seen between studies (Allen and Levy 2013). In particular, the herbicide paraquat and insecticide rotenone are frequently associated with an increased risk of developing PD (Kamel et al. 2007; Tanner et al.

2011). Paraquat and rotenone, like MPTP, are potent mitochondrial ETC inhibitors, and cause dopaminergic neurodegeneration in animal models (Betarbet et al. 2000). However, current epidemiological evidence is not sufficient to unequivocally establish a causal link between exposure to specific pesticides and increased risk for PD.

1.8.3 Genetic risk factors

Until 1997, the involvement of genes and genetic risk factors in the etiology of PD was contentious; indeed, PD used to be considered a classical "nongenetic" disorder (Lincoln et al. 2003). Large cross-sectional twin studies consistently found a lack of disease concordance in monozygotic twins, which argued against heritability (Piccini et al. 1999; Tanner et al. 1999; Wirdefeldt et al. 2004). Even though 10-30% of PD patients report a first-degree relative also affected by PD (Sveinbjörnsdottir et al. 2000; Rocca et al. 2004), the observed familial aggregation of this disorder was usually attributed to shared environmental exposures.

Nevertheless, the last two decades has seen the successful application of genetic linkage analysis, genetic association studies and genomic sequencing to pedigrees of PD-multi-affected families. Such approaches have identified the genetic underpinnings of several familial forms of PD. To date, a total of six genes (*SNCA*, *LRRK2*, *VPS35*, *parkin*, *PINK1* and *DJ-1*) have been robustly confirmed to harbor causal mutations for monogenic parkinsonism clinically similar to PD, with autosomal dominant (AD) or autosomal recessive (AR) modes of inheritance. Another gene (*EIF4G1*) has been associated with AD-PD, but its status as an authentic PD gene is currently unconfirmed. A further seven genes (*ATP13A2*, *PLA2G6*, *FBXO7*, *DNAJC6*, *SYNJ1*, *SCA2* and *SCA3*) have been associated with atypical parkinsonism, demonstrating one or more non-PD features in addition to parkinsonism. The genes implicated in monogenic PD or parkinsonism are summarized in Table 1.1. Several genetic variants have also been identified as strong risk factors for PD. The genes, mutations and polymorphisms implicated in PD will be briefly discussed.

1.8.3.1 *Autosomal dominant PD*

1.8.3.1.1 *α-Synuclein* (*SNCA*)

Genetic studies of PD first began with the identification of a pathogenic missense mutation in the *SNCA* gene (OMIM 163890), causing AD-PD (Polymeropoulos et al. 1997). Patients with *SNCA* mutations typically present with EOPD with a good response to levodopa treatment in the initial stages of disease; however, progression of the disease is rapid with a high prevalence of

Table 1.1 Genes implicated in monogenic PD or parkinsonism

Gene	Map locus	Inheritance	Phenotype	Pathology	Mutations	Reference(s)
SNCA	4q21-22	AD	EOPD	Diffuse LBs	5 point mutations, whole gene duplications/triplications	Polymeropoulos et al. (1997)
LRRK2	12q12	AD	Classical PD	Pleomorphic, mostly typical LBs	7 pathogenic mutations from ~70 missense variants	Paisán-Ruiz et al. (2004); Zimprich et al. (2004)
VPS35	16q11	AD	Classical PD	Unknown	1 missense mutation	Zimprich et al. (2011); Vilariño-Güell et al. (2011)
EIF4G1	3q27	AD	Classical PD	Unknown	2 missense mutations	Chartier-Harlin et al. (2011)
Parkin	6q25-27	AR	EOPD	Nigral degeneration, mostly without LBs	~170 point mutations, exonic rearrangements	Kitada et al. (1998)
PINK1	1p35-36	AR	EOPD	Typical LBs (one case only)	~50 point mutations, rare large deletions	Valente et al. (2004)
DJ-1	1p36	AR	EOPD	Unknown	~15 point mutations, large deletions	Bonifati et al. (2003)
ATP13A2	1p36	AR	Juvenile onset, atypical parkinsonism	Ceroid lipofuscinosis (one case only)	5 point mutations	Ramirez et al. (2006)
PLA2G6	22q13	AR	Juvenile onset, atypical parkinsonism	Typical LBs	2 missense mutations	Paisán-Ruiz et al. (2009)
FBXO7	22q12-13	AR	Juvenile onset, atypical parkinsonism	Unknown	3 point mutations	Shojaee et al. (2008); Di Fonzo et al. (2009)
DNAJC6	1p31	AR	Juvenile onset, atypical parkinsonism	Unknown	1 nonsense mutation, 1 large deletion	Edvardson et al. (2012); Köroğlu et al. (2013)
SYNJ1	21q22	AR	Juvenile onset, atypical parkinsonism	Unknown	1 missense mutation	Krebs et al. (2013); Quadri et al. (2013)
SCA2	12q24	AD	Atypical parkinsonism	Unknown	CAG repeat expansion	Gwinn-Hardy et al. (2000)
SCA3	14q32	AD	Atypical parkinsonism	Nigral degeneration	CAG repeat expansion	Gwinn-Hardy et al. (2001)

Abbreviations: AD, autosomal dominant; AR, autosomal recessive; *ATP13A2*, *ATPase type 13A2*; *DJ-1*, *Daisuke-Junko 1*; *EIF4G1*, *eukaryotic translation initiation factor 4 gamma 1*; EOPD, early-onset Parkinson's disease; *FBXO7*, *F-box only 7*; LBs, Lewy bodies; *LRRK2*, *leucine-rich repeat kinase 2*; p, short chromosomal arm; PD, Parkinson's disease; *PINK1*, *phosphatase and tensin homolog (PTEN)-induced kinase 1*; *PLA2G6*, *phospholipase A2 group VI*; q, long chromosomal arm; *SCA2*, *spinocerebellar ataxia type 2*; *SCA3*, *spinocerebellar ataxia type 3*; *SNCA*, *α-synuclein*; *SYNJ1*, *synaptojanin 1*; *VPS35*, *vacuolar protein sorting 35*.

dementia and severe autonomic dysfunction. Atypical features such as cortical myoclonus may also be present. Neuropathologically, *SNCA*-induced PD results in prominent and extensive LB pathology of the substantia nigra, hypothalamus and cerebral cortex, often incorporating limbic and glial pathology (Gwinn-Hardy et al. 2000).

Mutations in *SNCA* are rare. To date, only five different *SNCA* point mutations as well as whole gene duplications and triplications have been described (Bonifati 2014). *SNCA* duplications have been reported in approximately 1% of families with AD-inherited PD (Ibáñez et al. 2009); whereas triplications and point mutations are exceedingly rare and have only been found in a handful of families worldwide. Point mutations include the A53T, A30P and E46K missense mutations, and two novel missense mutations, H50Q and G51D, have only recently been described (Appel-Cresswell et al. 2013; Lesage et al. 2013). Point mutations in *SNCA* are highly penetrant, whereas a reduced penetrance for whole gene duplications of 30-40% has been described for some families (Nishioka et al. 2006). *SNCA* duplications have also been found in sporadic PD cases (Ahn et al. 2008). Interestingly, a dosage effect is seen for such gene amplifications, as each additional *SNCA* copy leads to an earlier onset, faster disease progression and a more severe phenotype (Fuchs et al. 2007; Ross et al. 2008b).

SNCA encodes the 140-amino acid (aa) cytosolic protein α-synuclein. This protein is abundantly expressed in the brain and forms a major component of LBs in PD neuropathology (Spillantini et al. 1997). It is thought that α-synuclein plays a role in synaptic plasticity and synaptic vesicular trafficking (Lundblad et al. 2012; Scott and Roy 2012). While this protein is predominantly natively unfolded, its amino (N)-terminal region adopts an amphipathic, α-helical structure when associated with lipid membranes (Ulmer et al. 2005). The identified *SNCA* missense mutations, all of which cluster within the N-terminal region of α-synuclein, reduces its lipid affinity and promotes the formation of stable, β-sheet-rich toxic oligomers, protofibrils and fibrils (Bertoncini et al. 2005). Hence, it is thought that elevated or mutated α-synuclein contributes to disease via a toxic gain of function, whereas LBs may represent a cell-protective mechanism to sequester toxic α-synuclein aggregates (Olanow et al. 2004).

1.8.3.1.2 *Leucine-rich repeat kinase 2* (*LRRK2*)

Mutations in the *LRRK2* gene (OMIM 609007) have been associated with both AD familial PD and apparently sporadic PD and, to date, constitute the most common genetic cause of PD (Paisán-Ruiz et al. 2004; Trinh and Farrer 2013). *LRRK2* mutation carriers present with parkinsonism that is largely clinically indistinguishable from idiopathic, late onset PD, with homozygous carriers presenting with a similar clinical phenotype to heterozygous carriers (Aasly et al. 2005; Lesage et al. 2005). The associated range of disease onset age is broad and includes patients with early and late onset. The

majority of autopsied PD patients with *LRRK2* mutations demonstrate typical LB pathology, but pure dopaminergic degeneration without LBs, and degeneration with neurofibrillary tangles, have also been described (Wider et al. 2010).

Seven disease-causing *LRRK2* missense mutations (N1437H, R1441H, R1441C, R1441G, Y1699C, G2019S, I2020T) have been found to date, whereas the pathogenicity of other sequence variants in this gene are currently unclear (Bonifati 2014). *LRRK2* mutations are found in approximately 10% of families with AD-PD. By far the most common and best studied is the G2019S mutation, occurring in approximately 1% of sporadic European cases, 20% of Ashkenazi Jewish patients and up to 40% of patients from North African Arab-Berber descent (Lesage et al. 2006; Healy et al. 2008; Thaler et al. 2009). The high frequencies of G2019S seen in apparently sporadic PD cases can be attributed to the age-related and ethnic-specific incomplete penetrance of this mutation. The penetrance can be as low as 30% at the age of 60 years, increasing to 75% penetrance at 80 years, while varying significantly between different population groups (Healy et al. 2008).

It is still unclear how mutations in *LRRK2* contribute to PD. The LRRK2 protein is a large, 2527-aa cytosolic protein with GTPase and kinase domains and multiple protein-protein interaction domains. It has been implicated in cellular signaling cascades, membrane trafficking, autophagy and mitochondrial function (Lewis and Alessi 2012). Mutations in the GTPase domain (R1441C, R441G, R441H) disrupt GTPase activity, whereas mutations in the kinase domain (G2019S, I2020T) increase the kinase activity of LRRK2 (West et al. 2005; Lewis et al. 2007). Hence, it is thought that mutated LRRK2 can promote cellular dysfunction via a disruption or exaggeration of normal function, or a gain of abnormal function (Dächsel et al. 2010).

1.8.3.1.3 *Vacuolar protein sorting 35* (*VPS35*)

In 2011, two groups independently reported the same D620N mutation in the *VPS35* gene (OMIM 601501) as a novel cause of AD-PD (Vilariño-Güell et al. 2011; Zimprich et al. 2011). Of note, this was the first PD gene to be identified using a next-generation sequencing (NGS)-based exome sequencing approach. Patients with mutated *VPS35* present with typical PD, albeit with a slightly earlier onset age, with a good response to levodopa therapy. The associated neuropathology of *VPS35*-linked PD remains unknown.

The D620N mutation was originally found to segregate with disease in families of Swiss and Austrian origin, respectively, and has now been described in several additional large families of various ethnicities (Ando et al. 2012; Lesage et al. 2012a; Sharma et al. 2012). These studies have reported a prevalence for this rare mutation of approximately 0.5-1% in AD-PD cases. It has also been described

in sporadic cases, suggesting a reduced penetrance for this mutation. Despite intensive screening, additional pathogenic mutations in the *VPS35* gene have not been found to date.

VPS35 is a subunit of the retromer cargo-recognition complex, which is involved in the cellular recycling of membrane proteins. It is thought to play a role in the sorting of acid hydrolases to lysosomes, retrograde transport between endosomes and the trans-Golgi network, developmental Wnt signaling, apoptosis and mitophagy (Chen et al. 2010a; Harterink et al. 2011; McGough and Cullen 2011). While it is currently unclear how the D620N mutation affects the function of the retromer complex or how this contributes to PD, future research on VPS35 in the brain is likely to provide valuable insights.

1.8.3.1.4 *Eukaryotic translation initiation factor 4 gamma 1* (*EIF4G1*)

The *EIF4G1* gene (OMIM 600495) has recently been implicated as an AD PD-inducing gene, as the R1205H missense mutation has found to segregate within a large French family (Chartier-Harlin et al. 2011). Further genetic screens identified this mutation, as well the A502V mutation, in a few additional families. However, subsequent studies failed to replicate these results convincingly, and the two mutations have been found in several unaffected control individuals (Lesage et al. 2012b; Schulte et al. 2012; Nishioka et al. 2014). Therefore, the status of *EIF4G1* as a PD gene is currently contentious and further clarifying studies are warranted.

1.8.3.2 *Autosomal recessive PD*

1.8.3.2.1 *Parkin*

Parkin (OMIM 602544) was the second PD-causing gene to be identified, and the first gene known to cause AR-PD (Kitada et al. 1998). Mutations in *parkin* are the most common cause EOPD, reported to account for up to 50% of familial EOPD cases and 15% of sporadic cases (Lücking et al. 2000). Some patients with *parkin* mutations have a disease onset even in childhood (juvenile PD). In addition to an early onset, *parkin*-induced PD is clinically characterized by a slow disease progression and an excellent and prolonged response to levodopa. Prominent dystonia and hyperreflexia are frequently observed, whereas cognitive decline and severe autonomic dysfunction are very rare non-motor features.

The neuropathology of *parkin*-associated cases was initially thought to lack LBs, but recent reports have described α-synuclein positive LB pathology in a minority of cases (Pramstaller et al. 2005; Miyakawa et al. 2013). In contrast to idiopathic PD, neurodegeneration is largely confined to the

substantia nigra and locus ceruleus, which suggests that the pathology of *parkin*-induced PD does not conform to the Braak staging of PD (Ahlskog 2009; Doherty et al. 2013).

A large number and wide spectrum of *parkin* mutations have been described, including point mutations, small deletions and whole exon rearrangements. As *parkin* is the focus of the present study, the molecular genetics of this gene will be discussed in more detail in Section 1.12.

The parkin protein functions as an E3 ubiquitin ligase, conjugating ubiquitin to various substrate proteins (Shimura et al. 2000). Ubiquitination of such parkin substrates may result in the ubiquitin proteasome system (UPS)-mediated degradation of the protein, or alteration of substrate protein activity, function, translocation or signaling (Kahle and Haass 2004). As such, parkin is involved in many diverse cellular pathways, including protein degradation, mitochondrial health, cellular signaling, stress responses, tumor suppression and innate immunity. Pathogenic parkin mutations abolish or reduce its ubiquitin ligase activity, supporting a loss-of-function disease mechanism (Dauer and Przedborski 2003). The loss of parkin function might result in the accumulation/dysregulation of non-ubiquitinated parkin substrates, thereby contributing to cellular stress and neurodegeneration (McNaught and Olanow 2003). A detailed review of the parkin protein and the cellular pathways it has been implicated in will follow in Sections 1.14-1.16.

1.8.3.2.2 *Phosphatase and tensin homolog (PTEN)-induced kinase 1* (*PINK1*)

Mutations in *PINK1* (OMIM 602544) are associated with AR familial EOPD (Valente 2004). The frequency of PINK1 mutations varies considerably across different ethnic groups, and it is estimated to account for 1-8% familial EOPD cases (Bonifati et al. 2005; Klein et al. 2005; Kilarski et al. 2012). The clinical phenotype of *PINK1*-induced PD appears to be similar to *parkin*-PD, although psychiatric symptoms may be more prevalent among patients with *PINK1* mutations. To date, only one autopsy of a patient with *PINK1* mutations has been reported; this patient demonstrated nigral degeneration with LB-positive pathology comparable to idiopathic PD (Samaranch et al. 2010).

Over 50 missense mutations, nonsense mutations, frameshifts and, rarely, large deletions have been described for *PINK1* (Kawajiri et al. 2011). Point mutations are near equally distributed across the eight exons. While only approximately 25% of the described *PINK1* mutations are nonsense mutations, more than 40% of patients carry a mutation that is truncating. Rare whole exon deletions in PINK1 have been described in a few families worldwide (Li et al. 2005; Cazeneuve et al. 2009). *PINK1* mutations are also a rare cause of sporadic EOPD (Tan et al. 2006).

PINK1 is a 581-aa cytosolic protein kinase that can be localized to the mitochondria. While the function of this protein is not fully understood, it has been implicated in mitochondrial homeostasis and mitophagy (Koh and Chung 2012). The majority of reported PINK1 mutations are loss-of-

function mutations which disrupt its kinase domain; this supports the importance of PINK kinase activity in the pathogenesis of PD.

1.8.3.2.3 *Daisuke-Junko-1* (*DJ-1*)

The third gene found to cause AR familial EOPD is the *DJ-1* gene (OMIM 602533) (Bonifati et al. 2003). Mutations in *DJ-1* are rare and only account for approximately 1% of familial EOPD cases (Pankratz et al. 2006). While the clinical phenotype of *DJ-1* mutation carriers has only been studied in a limited number of cases, it appears to be clinically indistinguishable from *PINK1*. The pathology of patients with *DJ-1* mutations remains unknown, as no autopsies of cases with *DJ-1* mutations have been reported yet.

About ten different *DJ-1* point mutations and large exonic deletions have been described (Tan and Skipper 2007). The best studied point mutation in *DJ-1* is L166P, which destabilizes the DJ-1 protein resulting in its rapid proteasomal degradation (Miller et al. 2003).

DJ-1 is a potent cellular sensor of oxidative stress. It is highly expressed in the brain where it adopts a dimeric structure (Macedo et al. 2003). In the presence of oxidative stress, DJ-1 is translocated to the mitochondrial membrane (Zhang et al. 2005). Although the precise cellular function of this protein is unknown, it has been implicated in neuroprotection against oxidative stress, mitochondrial dysfunction and dopamine toxicity (Wang et al. 2012a; Lev et al. 2013). Mutated DJ-1 protein is typically misfolded, unstable and rapidly degraded, suggesting that *DJ-1* mutations contribute to PD by depleting the cellular levels of this protein (Malgieri and Eliezer 2008).

1.8.3.3 *Atypical parkinsonism*

1.8.3.3.1 *ATPase type 13A2* (*ATP13A2*)

Mutations in the *ATP13A2* gene (OMIM 610513) cause an AR atypical parkinsonism termed Kufor-Rakeb syndrome (Ramirez et al. 2006). This syndrome is clinically characterized by juvenile-onset, levodopa-responsive parkinsonism with rapid disease progression, pyramidal signs, dementia and supranuclear gaze palsy. While the pathology of *ATP13A2* remains unknown, magnetic resonance imaging (MRI) of patients with *ATP13A2* mutations suggest accumulation of metals in the brain (Santoro et al. 2011).

Mutations in *ATP13A2* are exceedingly rare and, to date, eleven different pathogenic mutations have been described in only a handful of families (Crosiers et al. 2011). Intriguingly, *ATP13A2* mRNA is highly expressed in the substantia nigra of patients with classical late-onset PD (Ramirez et al. 2006).

The gene encodes a large transmembrane lysosomal protein of the P-type ATPase family. While the exact function of this protein is unclear, it is thought to be involved with the transport of metal cations from the cytosol into the lysosome.

However, a recent study found that a mutation in *ATP13A2* caused pathologically-confirmed neuronal ceroid-lipofuscinosis (Bras et al. 2012). Similar pathology was reported in a canine model of mutated *ATP13A2* (Farias et al. 2011). This would suggest that *ATP13A2*-linked parkinsonism is a disorder distinct from atypical PD and cast doubt on the status of *ATP13A2* as a *de facto* PD gene; however, additional studies are warranted.

1.8.3.3.2 *Phospholipase A2, group VI* (*PLA2G6*)

Mutations in the *PLA2G6* (OMIM 603604) were initially described as the cause of infantile neuroaxonal dystrophy and idiopathic neurodegeneration with brain iron accumulation, a severe neurodegenerative disorder that bears no resemblance to PD (Morgan et al. 2006). However, *PLA2G6* mutations were later found in families presenting with adult-onset, levodopa-responsive parkinsonism with prominent dystonia and pyramidal signs (Paisán-Ruiz et al. 2009; Sina et al. 2009). Other pathogenic mutations in *PLA2G6* were also found in additional families with a similar atypical PD phenotype (Paisán-Ruiz et al. 2010).

MRI of patients with *PLA2G6* mutations demonstrate broad neurodegeneration but generally no abnormal iron deposition, which is a defining feature of infantile onset cases of *PLA2G6* mutations (Paisán-Ruiz et al. 2009; Sina et al. 2009). While evidence of the pathology of *PLA2G6* is very limited, patients with *PLA2G6* mutations demonstrate widespread α-synuclein-positive LB pathology in the substantia nigra and the cortex, suggesting a possible mechanistic link with typical PD (Gregory et al. 2008; Paisán-Ruiz et al. 2010). Nevertheless, the role of *PLA2G6* in PD remains controversial.

1.8.3.3.3 *F-box only protein 7* (*FBXO7*)

FBXO7 (OMIM 605648) is implicated in a recessive form of early-onset parkinsonism with pyramidal features. Mutations in *FBXO7* were initially identified in an Iranian kindred; pathogenic mutations were later found in several other unrelated families with a similar clinical phenotype (Shojaee et al. 2008; Di Fonzo et al. 2009).

Whereas the neuropathology of *FBXO7* mutations is unknown, the FBXO7 protein is a known component of LBs of patients with typical PD (Zhao et al. 2013). This protein is implicated in the UPS and localizes to the nucleus. Patients with mutations in *FBXO7* demonstrate a dramatic depletion

of FBXO7 (Zhao et al. 2011b). This suggests that the protein has neuroprotective properties, but the extent to which FBXO7 is involved in typical PD is unclear.

1.8.3.3.4 *Auxilin* (*DNAJC6*) and *synaptojanin 1* (*SYNJ1*)

Two newly-identified PD-related genes, *DNAJC6* (OMIM 608375) and *SYNJ1* (OMIM 604297) have recently been discovered as novel causes of AR juvenile parkinsonism. An exome sequencing approach combined with genome-wide heterozygosity mapping identified mutations in *DNAJC6* in a Palestinian family (Edvardson et al. 2012). These findings were later confirmed in a Turkish family (Köroğlu et al. 2013). With regards to *SYNJ1*, the same pathogenic mutation was independently reported to cause early-onset parkinsonism in families of Iranian and Italian ancestry, respectively (Krebs et al. 2013; Quadri et al. 2013).

DNAJ1 encodes neuronally-expressed auxilin, and *SYNJ1* encodes synaptojanin 1. Both these proteins play important and related roles in the recovery and recycling of synaptic vesicles (Montesinos et al. 2005). This is of significant interest as other PD genes, including *SNCA*, *LRRK2*, *VPS35* and *parkin*, have been implicated in synaptic vesicle dynamics. Further genetic and functional studies of *DNAJ1* and *SYNJ1* and their relation to PD are warranted.

1.8.3.3.5 *Spinocerebellar ataxia type 2* (*SCA2*) and *spinocerebellar ataxia type 3* (*SCA3*)

Mutations in the *SCA2* gene (OMIM 183090) cause an inherited ataxia syndrome with extrapyramidal symptoms, including levodopa-responsive parkinsonism (Gwinn-Hardy et al. 2000), whereas *SCA3* (OMIM 109150) mutations result in Machado-Joseph disease with negligible ataxia and parkinsonism accompanied by peripheral neuropathy, dystonia and spasticity (Gwinn-Hardy et al. 2001). Mutations in both *SCA2* and *SCA3* are due to CAG trinucleotide repeat expansions in their respective coding regions. *SCA2* mutations are particularly common in some Asian populations where it accounts for approximately 5% of familial parkinsonism (Lu et al. 2004).

While the physiological function of the *SCA2* gene product ataxin-2 is currently unclear, ataxin-3 is a well-characterized de-ubiquitinating enzyme acting within the UPS (Burnett et al. 2003). Interestingly, ataxin-3 is known to interact with parkin, where ataxin-3-mediated de-ubiquitination regulates parkin activity (Durcan et al. 2011). Furthermore, mutant but not wild-type ataxin-3 promotes the autophagic degradation of parkin (Durcan and Fon 2011).

1.8.3.4 *Genetic susceptibility factors*

Despite the considerable progress made in the identification of genes responsible for monogenic PD and parkinsonism described above, mutations in the known PD genes account for only 5%-10% of PD cases. Monogenic models of PD are therefore inadequate to explain common, typical PD, which may result from complex gene-gene and/or gene-environment interactions. This stimulated the search for genetic susceptibility factors that alters the risk for, instead of causing, PD.

1.8.3.4.1 *SNCA*

Much of the earlier work on the identification of susceptibility variants was done using a candidate gene approach, which found an association between alleles at the *REP1* dinucleotide repeat length polymorphism in the *SNCA* promoter region and sporadic PD (Krüger et al. 1999). Several follow-up studies were performed to verify this association, which delivered equivocal results. Nevertheless, a large collaborative meta-analysis provided a clear association between the *REP1* susceptibility allele and a 1.4 fold increased risk of PD (Maraganore et al. 2006). Functional studies suggest that the *REP1* risk allele is associated with an increased expression of *SNCA* in a transgenic mouse model (Cronin et al. 2009). Other polymorphisms in *SNCA* besides the *REP1* polymorphism have also been implicated as susceptibility variants for sporadic PD, particularly at the 3' end of the gene, but further studies are needed to confirm their relevance (Mueller et al. 2005; Mizuta et al. 2006a; Myhre et al. 2008)

1.8.3.4.2 *LRRK2*

The G2385R variant in *LRRK2* was initially described as a pathogenic mutation in a Taiwanese family with PD (Mata et al. 2005). However, subsequent studies found that this variant is a relatively common polymorphism in the Asian population, where it is strongly associated with the risk of PD (Di Fonzo et al. 2006; Tan et al. 2007). This finding was confirmed by several studies as well as a large meta-analysis, which associated the G2385R allele with a two-fold increased risk of PD in the Chinese and Japanese populations (Tan 2007). A similar magnitude of risk effect has been reported for another *LRRK2* variant, R1628P, also in Asian populations (Ross et al. 2008c). However, this risk variant has does not have as much supportive evidence as G2385R (Ross et al. 2011).

1.8.3.4.3 *Microtubule-associated protein tau* (*MAPT*)

Common variability in *MAPT* (OMIM 157140) has been associated with several neurodegenerative diseases of which the pathological hallmark is the deposition of tau protein in neurofibrillary tangles. Rare pathogenic mutations in *MAPT* cause frontotemporal dementia with parkinsonism linked to

chromosome 17 (FTDP-17), whereas common *MAPT* variants have been robustly associated with an increased risk of progressive supranuclear palsy (PSP), Alzheimer's disease and, more recently, PD (Spillantini and Goedert 2013). Two common *MAPT* haplotypes, H1 and H2, are present in European populations. The H1 haplotype has been associated with an increased risk of developing PD, with an OR of approximately 1.3 (Skipper et al. 2004; Fung et al. 2006; Zabetian et al. 2007). The elevated risk promoted by the H1 haplotype can be attributed to an increased *MAPT* expression (Myers et al. 2007; Tobin et al. 2008). It is not clear how tau is involved in PD, as tau-positive neurofibrillary tangles are rare in PD cases. Nevertheless, the genetic association between *MAPT* variability and PD risk has been robustly confirmed in several studies.

1.8.3.4.4 *Glucocerebrosidase* (*GBA*)

Mutations in the *GBA* gene (OMIM 606463) cause AR Gaucher's disease, a lysosomal storage disorder. Initial reports found that patients with Gaucher's disease may present with PD more frequently than expected (Neudorfer et al. 1996; Tayebi et al. 2003). This keen observation led to the discovery that single heterozygous *GBA* mutations increases the risk of PD approximately seven-fold in the Ashkenazi Jewish population (Aharon-Peretz et al. 2004). This finding has been generalized to the worldwide PD population in a large meta-analysis which confirmed that single *GBA* mutations increase the risk of PD five-fold; *GBA* mutations were present in 15% of Ashkenazi Jewish PD patients, 3% of non-Ashkenazi Jewish patients, compared to 3% and <1% in unaffected controls, respectively (Sidransky et al. 2009).

The clinical phenotype of PD associated with a *GBA* risk allele is similar to sporadic PD, except for a slightly younger age at onset and a greater rate of cognitive disturbances, with typical LB pathology being present at autopsy. While it is not fully understood how *GBA* mutations increases the risk of PD, it is thought to relate to abnormal lysosomal function (Swan and Saunders-Pullman 2013).

1.8.3.4.5 *Genome-wide association studies*

A large number of genome-wide association studies (GWAS) have now been performed in order to identify low-penetrance risk alleles that are undetectable through conventional linkage approaches. These GWAS have independently verified common variants in *SNCA*, *LRRK2* and *MAPT* as risk factors for PD, in addition to the candidate gene approaches described above (Pankratz et al. 2009a; Satake et al. 2009; Simón-Sánchez et al. 2009; Edwards et al. 2010). The largest and best-powered GWAS, which included over 12 000 cases and 21 000 controls, provided evidence of association for sixteen independent loci (*MAPT*, *SNCA*, *LRRK2*, *HLA-DRB5*, *BST1*, *GAK*, *PARK16*, *FGF20*, *ACMSD*, *STK39*, *MCCC1/LAMP3*, *SYT11*, *CCDC62/HIP1R*, *STX1B*, *STBD1* and *GPNMB*)

(International Parkinson's Disease Genomics Consortium (IPDGC) and Wellcome Trust Case Control Consortium 2 (WTCCC2) 2011). Alleles at each of these loci represent only minor risk or protective factors, conferring 1.1 to 1.4 fold increases in risk and 0.97 to 0.7 decreases in risk, respectively. When viewing all sixteen risk variants collectively, individuals with the highest burden of risk alleles are at a three-fold increased risk of developing PD in comparison to individuals with the lowest burden of risk alleles. However, it is important to note that the biological relevance of most of the associated variants is unknown, and functional studies will be needed to assess GWAS-identified loci as *bona fide* susceptibility factors.

1.9 PATHWAYS TO NEURODEGENERATION

It is evident from the above-discussed literature that PD has a complex etiology with various contributing genetic and non-genetic factors. The identification of genes that induce familial PD has greatly advanced our understanding of the underlying molecular pathology of PD, whereby neuronal homeostasis is vulnerable to different genetic, cellular and environmental factors that independently or concurrently cause cell death over time (Sulzer 2007). Such factors appear to converge on common pathways to neurodegeneration, such as the accumulation of misfolded proteins, impairment of protein degradation pathways, and mitochondrial dysfunction (Figure 1.2).

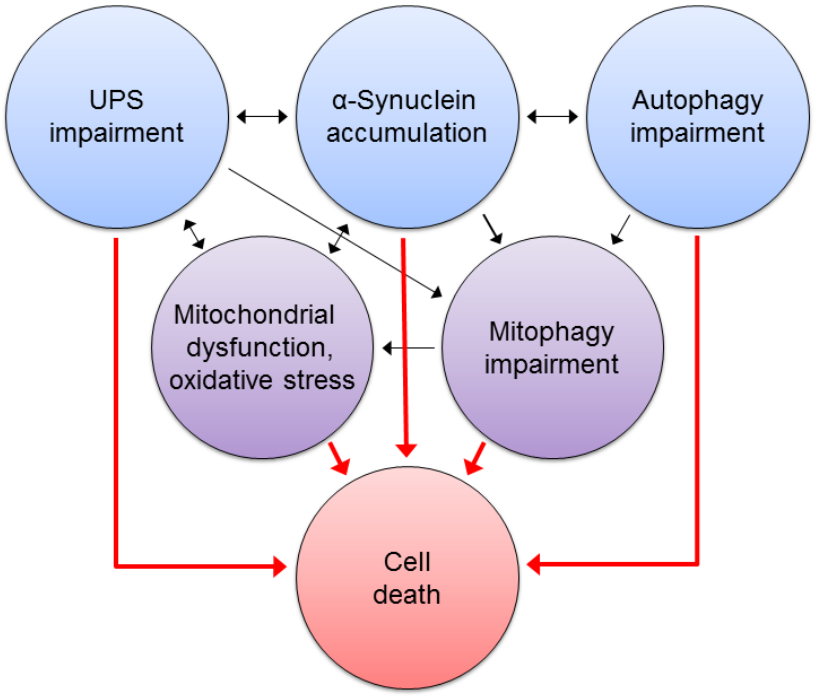

Figure 1.2 Pathways to neurodegeneration. An intersecting network of pathways, each of which are vulnerable to cellular stress from genetic susceptibility, environmental exposures or age-accumulated damage, independently or concomitantly impair neuronal homeostasis and contribute to neurodegeneration. Figure adapted from Valente et al. (2012). Abbreviations: UPS, ubiquitin proteasome system.

1.9.1 α-Synuclein accumulation

α-Synuclein has long been viewed as a key player in the pathology of PD. Not only was *SNCA* the first conclusive demonstration of a genetic defect leading to PD, but misfolded and aggregated α-synuclein protein is the main constituent of LB inclusions. LBs, the main pathognomonic feature of PD, are present in the brain tissue of both rare *SNCA* mutation carriers and common sporadic PD cases. Furthermore, GWAS consistently report *SNCA* variants as common risk factors for PD (Simón-Sánchez et al. 2009; Edwards et al. 2010); α-synuclein may therefore provide a unifying link between familial and sporadic PD.

It is generally accepted that enhanced α-synuclein protein levels, beyond a certain threshold, contribute to neurodegeneration, as familial *SNCA* duplications and triplications demonstrate a dose-dependent relationship of α-synuclein load with PD phenotype (Fuchs et al. 2007; Ross et al. 2008b). In fact, transgenic delivery of α-synuclein to the SNpc is sufficient to induce PD-like dopaminergic neuronal degeneration and inclusion formation in primates (Eslamboli et al. 2007). Accumulating α-synuclein levels promote its misfolding and subsequent oligomerization, aggregation and fibrillization (Giasson et al. 1999; Wood et al. 1999; Masliah et al. 2000). α-Synuclein oligomerization is also promoted by PD-causing *SNCA* missense mutations (Conway et al. 2000). The pathological aggregation propensity of α-synuclein is furthermore increased by various post-translational modifications, including nitrosylation and hyper-phosphorylation, as well as by dopamine adducts, which may contribute to the selective vulnerability of dopaminergic neurons in PD (Venda et al. 2010).

Misfolded and aggregated α-synuclein may have various cytotoxic effects. For example, it was found that the overexpression of α-synuclein in animal models induced mitochondrial defects (Song et al. 2004; Martin et al. 2006), and that α-synuclein oligomers and aggregates disrupt the UPS (Snyder et al. 2003; Lindersson et al. 2004). Moreover, α-synuclein oligomers interact with the PD-associated protein GBA to disrupt lysosomal function (Mazzulli et al. 2011). Aggregated α-synuclein impairs microtubule-based subcellular transport, leading to synaptic dysfunction (Sheng and Cai 2012). Hence, α-synuclein accumulation and aggregation may disrupt neuronal homeostasis beyond the cell's ability to recover, thereby inducing apoptotic cell death.

Interestingly, accumulating evidence suggest that α-synuclein may spread from cell to cell, where the transfer of misfolded oligomers and aggregates from affected to unaffected neighboring cells induce the toxic conversion of natively-folded proteins. Such an aggregate nucleation or seeding event results in the misfolding and recruitment of endogenous α-synuclein that presumably would not have misfolded in the absence of such a protein seed. This process is akin to the templated misfolding of

prion proteins, and has been called the "prion hypothesis" of aggregation propagation, which may be a common feature of many neurodegenerative diseases (Jucker and Walker 2013).

Several studies have reported the successful *in vitro* seeding of soluble α-synuclein after the internalization of recombinant α-synuclein in cell cultures, resulting in LB-like intracellular inclusions (Danzer et al. 2009; Desplats et al. 2009; Luk et al. 2009; Volpicelli-Daley et al. 2011). α-Synuclein aggregates have also been seen to propagate between co-cultured cells (Hansen et al. 2011). Perhaps the most striking examples of *in vivo* transfer and seeding of α-synuclein are reports of autopsies performed on PD patients who had received striatal grafts of fetal neuronal tissue 11-16 years earlier. Remarkably, LB pathology was found not only in the brains of the PD patients, but also in the implanted grafts (Kordower et al. 2008; Li et al. 2008, 2010). Such α-synuclein transfer was also seen in mouse models, where the intracerebral injection of brain extracts affected by LB pathology into young, unaffected transgenic mice resulted in the formation of α-synuclein aggregates and neurodegeneration (Luk et al. 2012; Mougenot et al. 2012). Significantly, intracerebral injection of mice with pure recombinant α-synuclein fibrils had the same effect as inoculation with brain homogenates of aged mice. Indeed, a dose-dependent effect was seen between the amount of recombinant α-synuclein and the acceleration of pathology. Synthetic α-synuclein fibrils are therefore sufficient to both induce LB pathology and to propagate disease *in vivo*.

In a nutshell, the propagation and cell-to-cell transfer of α-synuclein aggregates provides a molecular pathway whereby PD pathology spreads within the nervous system from a highly localized initiating event to more distal brain regions, following a cascade of protein dysregulation and cellular stress.

1.9.2 Defective protein clearance pathways

The counterpart toxic mechanism to pathological protein accumulation is defective protein degradation. Two important cellular pathways are responsible for the degradation and clearance of excess, misfolded or damaged proteins within the cell: the UPS and autophagy-lysosomal pathway (ALP). These two pathways mediate proper protein quality control in order to maintain cellular homeostasis; impairment of these pathways is implicated in neurodegeneration.

Early indications of the involvement of the UPS in PD came from the discovery that proteins in LBs are highly ubiquitinated (Kuzuhara et al. 1988; Lennox et al. 1989), and that LBs are composed of numerous UPS components, including proteasomal subunits, ubiquitinating and de-ubiquitinating enzymes and proteasome activators (Lowe et al. 1990; Kwak et al. 1991; Ii et al. 1997). Furthermore, the PD-causing gene parkin was found to be an E3 ubiquitin ligase, a component of the UPS (Shimura et al. 2000). Biochemical analyses of post-mortem brain tissue revealed reduced proteasomal activity in the SNpc of PD patients in comparison to age-matched controls (McNaught and Jenner 2001;

McNaught et al. 2003). Such results are similar to gene expression studies of PD brains, which found significantly downregulated expression of several proteasomal subunit genes in the SNpc (Grünblatt et al. 2004; Bukhatwa et al. 2010).

Studies using *in vitro* and *in vivo* models also support the involvement of the UPS in PD. These studies demonstrated that exposure to the parkinsonism-inducing toxin MPTP resulted in a marked decrease in proteasomal activity (Fornai et al. 2005; Zeng et al. 2006; Caneda-Ferrón et al. 2008). Treatment with proteasomal inhibitors induced reproducible nigral degeneration in rodent models (Vernon et al. 2010; Xie et al. 2010). Finally, transgenic mice expressing a conditional deletion of a proteasomal regulatory subunit in dopaminergic cells demonstrated severe proteasomal deficits in the SNpc, as well as progressive neurodegeneration and LB-like inclusion formation, underscoring the importance of the UPS in PD (Bedford et al. 2008).

The other major protein clearance pathway, the ALP, has also been implicated in PD. Early post-mortem studies saw accumulation of autophagic vacuoles in the SNpc of PD patients (Anglade et al. 1997), whereas more recent studies found altered levels of autophagy-related proteins in PD brains (Alvarez-Erviti et al. 2010; Li et al. 2011a; Tanji et al. 2011). Important genetic evidence in support of the involvement of the ALP in PD are mutations in the PD susceptibility gene *GBA*, encoding a lysosomal enzyme, and parkinsonism-inducing mutations in *ATP13A2*, a lysosomal transmembrane protein. Furthermore, *parkin* and *PINK1* are part of the signaling pathway that controls mitophagy, a specialized autophagic pathway that eliminates damaged mitochondria.

Impairment of the UPS and ALP may contribute to cellular dysfunction. For example, UPS dysfunction may result in proteolytic stress due to the accumulation and aggregation of excess and misfolded proteins in the cytosol. α-Synuclein in particular has been shown to accumulate and aggregate in cells treated with proteasomal inhibitors (Rideout et al. 2001; Rideout and Stefanis 2002). Similarly, treatment with autophagy inhibitors promoted the toxic oligomerization of α-synuclein (Klucken et al. 2012), whereas lysosomal dysfunction increased cell-to-cell transfer of α-synuclein aggregates (Alvarez-Erviti et al. 2011). Many studies have demonstrated impairment of both the UPS and ALP by mutant or excessive normal α-synuclein (Petrucelli et al. 2002; Snyder et al. 2003; Cuervo et al. 2004). The reciprocal interaction between α-synuclein and protein clearance pathways posits an interesting vicious cycle, whereby increasing accumulation of α-synuclein impairs UPS and ALP function, which further exacerbates α-synuclein accumulation.

1.9.3 Mitochondrial dysfunction and oxidative stress

The important role of mitochondrial dysfunction in the pathogenesis of PD is evident from observations that exposure to mitochondrial complex I inhibitors, such as MPTP and rotenone,

induces parkinsonism (Langston et al. 1983). Furthermore, there are many reports of mitochondrial complex I deficits in PD patients, along with high burdens of somatic mitochondrial DNA (mtDNA) mutations in SNpc neurons (Schapira et al. 1989; Janetzky et al. 1994; Bender et al. 2006a). The mitochondrial involvement in PD is also strongly supported by genetic evidence, as the AR familial PD genes *parkin*, *PINK1* and *DJ-1* are known to be involved in the maintenance of mitochondrial health. Whereas parkin and PINK1 act in concert to promote the autophagic clearance of damaged mitochondria (Clark et al. 2006; Exner et al. 2007), DJ-1 is involved in mitochondrial protection against reactive oxygen species (ROS) (Canet-Avilés et al. 2004).

Mitochondrial dysfunction mainly manifests as deficits in ATP production and elevated oxidative stress in the form of mitochondria-generated ROS. Such increased ROS production can instigate oxidative mtDNA damage, protein oxidation and lipid peroxidation, resulting in further damage of cellular organelles and triggering a vicious cycle of mitochondrial dysfunction and oxidative stress (Henchcliffe and Beal 2008). Furthermore, the impairment of cellular clearance pathways such as mitophagy may result in the deleterious accumulation of oxidatively damaged mitochondria. As physiological ROS also plays a part in intracellular signaling, heightened ROS generation may moreover disrupt important signaling cascades (Turrens 2003).

Besides the key function of mitochondria in energy metabolism, mitochondria are also involved in Ca^{2+} homeostasis, cellular signaling, apoptosis and the inflammatory response (Newmeyer and Ferguson-Miller 2003). It is likely that these processes are also involved in neurodegeneration to various extents, although it is not currently clear whether these mitochondria-associated pathways are a cause or consequence of canonical mitochondrial dysfunction.

While recent years has seen a lot of progress in understanding mitochondrial biology and the many cellular functions mitochondria are involved in, it is still unclear why mitochondria play such a pivotal role in neurodegeneration and PD (Exner et al. 2012; Corti and Brice 2013). The selective vulnerability of SNpc dopaminergic neurons to mitochondrial dysfunction might be due to the extremely long, unmyelinated, highly branched axons, multitude of synapses and low mitochondrial mass of these neurons (Liang et al. 2007; Matsuda et al. 2009; Bolam and Pissadaki 2012). Interestingly, common features between SNpc neurons and non-dopaminergic neurons that also undergo degeneration in PD include highly dense axonal arborization, pacemaker activity, high bioenergetic demands, elevated oxidative stress and heightened Ca^{2+} buffering stress (Sulzer and Surmeier 2013). It can be speculated that such characteristics collectively make certain neuronal populations particularly vulnerable to mitochondrial dysfunction, proteolytic stress, and a loss of cellular homeostasis.

1.10 THERAPEUTIC IMPLICATIONS OF VITAMIN K_2

The investigation of cellular and molecular pathways that contribute to neurodegeneration in PD has opened up new avenues for potential therapeutic approaches. Such neuroprotective approaches might prevent or treat neurodegeneration by targeting possible pathological processes such as α-synuclein accumulation, impairment of the UPS or ALP, or mitochondrial dysfunction. Potential neuroprotective agents would be a welcome addition to currently-available treatment options, based on levodopa-replacement strategies, which only provides symptomatic treatment for PD patients without addressing the underlying neuropathology.

As mitochondrial dysfunction is implicated in both sporadic and familial PD, mitochondria are attractive targets for potential neuroprotective agents, and several such strategies are currently under investigation. Such compounds aimed at enhancing mitochondrial function include coenzyme Q10, a mitochondrial ETC enhancer and antioxidant, and creatine, a compound that elevates cellular ATP generation (Bender et al. 2006b; Storch et al. 2007; Salama et al. 2013). A particularly interesting potential therapeutic compound is vitamin K_2, which has emerging roles in brain function and health (Beulens et al. 2013). As this dissertation will be investigating vitamin K_2 as a potential PD therapeutic modality, relevant information and exciting new findings on vitamin K_2 will be discussed.

Vitamin K_2 (menaquinone) is a generic term for a number of structurally related compounds that are characterized by a methylated naphthoquinone ring and an aliphatic side chain of varying numbers of isoprene residues (Shearer and Newman 2008). The best studied and most common form of vitamin K_2 in the body is menaquinone-4 (MK-4) (Beulens et al. 2013). Whereas most vitamin K_2 homologs are synthesized by intestinal bacterial flora, MK-4 is of note for being metabolized from dietary vitamin K_1 (phylloquinone) in tissues such as the brain, pancreas and kidney (Okano et al. 2008). This *in situ* synthesis of MK-4 is catalyzed by the recently-discovered UbiA prenyltransferase domain containing protein 1 (UBIAD1) enzyme (Nakagawa et al. 2010). Unless otherwise stated, all mentions of vitamin K_2 in this dissertation will refer to the MK-4 form of vitamin K_2.

Vitamin K_2 has a well-established function in blood coagulation, via its essential role as a cofactor for γ-glutamyl carboxylase. This cofactor activity is required for the posttranslational modification and activation of numerous proteins, including most blood-clotting factors and proteins involved in bone metabolism (Vermeer 1990). Vitamin K_2 has more recently been implicated in several other, γ-glutamyl carboxylase-independent functions; these functions do not appear to extend to non-MK-4 forms of Vitamin K_2. For example, vitamin K_2 was found to be involved in the transcriptional regulation of the steroid and xenobiotic nuclear receptor (SXR) (Azuma et al. 2009) and in the activation of protein kinase A (PKA) signaling (Ichikawa et al. 2007). Vitamin K_2 has been shown to inhibit vascular calcification (Saito et al. 2007; Beulens et al. 2009) and to reduce the risk of coronary

heart disease (Geleijnse et al. 2004). Furthermore, vitamin K_2 treatment elevated testosterone production in rats in a dose-dependent manner, implicating K2 in steroidogenesis (Ito et al. 2011).

Several studies have suggested that K2 has anti-tumor properties. Treatment with vitamin K_2 reduced proliferation and induced apoptosis in myeloid leukemia cell lines (Yaguchi et al. 1997), gastric cancer cell lines (Tokita et al. 2006) and colorectal cancer cell lines (Ogawa et al. 2007). These effects are also seen in a therapeutic context, as vitamin K_2 supplementation has been reported to suppress the development of hepatocellular carcinoma in at-risk patients (Habu et al. 2004), and to reduce the recurrence of hepatocellular carcinoma after resection (Mizuta et al. 2006b). While the mechanism of these anti-cancer properties is not fully understood, it has been suggested that vitamin K_2 reduces cell proliferation via inhibition of the transcription factor NF-κB, which suppresses the expression of the cell-cycle protein cyclin D1 (Ozaki et al. 2007). Moreover, vitamin K_2 was shown to induce autophagy and apoptosis simultaneously in leukemia cells, via an unknown mechanism (Yokoyama et al. 2008). These findings suggest that vitamin K_2 may be a promising anti-cancer compound.

An unexpected and stimulating finding, and of particular relevance to PD, is the demonstration that vitamin K_2 can act as an electron carrier in the mitochondrial ETC. Vos et al. (2012) used a genetic approach to identify the *Drosophila* homolog of mammalian *UBIAD1*, the gene responsible for vitamin K_2 synthesis, as a genetic modifier of *PINK1*. Heterozygosity for *UBIAD1* mutations strongly enhanced the mitochondrial defects seen in PINK1 mutant flies, such as reduced ATP production and loss of mitochondrial membrane potential, and these defects could be rescued by overexpressing *UBIAD1*. Overexpression of *UBIAD1* could similarly rescue the mitochondrial phenotype of *parkin* mutant flies. Interestingly, supplementing the diet of *PINK1* and *parkin* mutant flies with vitamin K_2 improved ETC efficiency and alleviated the mitochondrial defects of these mutants in a dose-dependent manner. Intriguingly, vitamin K_2 is a known electron carrier in bacterial membranes (Haddock and Jones 1977). Vos et al. (2012) convincingly demonstrated that vitamin K_2 can also facilitate electron transport in the mitochondrial ETC in eukaryotic cells, and suggested that this novel function of vitamin K_2 drives the phenotypic rescue seen in *PINK1* and *parkin* mutant *Drosophila*. While the rescue effect of vitamin K_2 on mitochondrial dysfunction has to date only been demonstrated in *Drosophila*, it would be interesting to see whether such pro-mitochondrial effects are also seen in human cell models with *PINK1* and *parkin* mutations. As such, vitamin K_2 may be a promising therapeutic compound in the treatment of PD.

PART TWO: PARKIN

Indubitably, the identification of genes and genetic factors that contribute to PD development has greatly improved our understanding of the molecular etiology underlying this disease, as exemplified by the multitude of studies discussed above. While many important questions remain unanswered, such studies often illuminate new avenues of research that may provide valuable insights into PD pathology. Particularly interesting amongst the known PD genes is *parkin*, as *parkin* mutations are the most common cause of familial EOPD (Lücking et al. 2000). Furthermore, parkin is noteworthy for been implicated in a wide array of cytoprotective pathways and processes, which often converge to promote proper cellular function and health.

This dissertation aims to further current knowledge on the role of parkin in PD. For that reason, a review of the established literature on parkin will follow.

1.11 GENETIC STRUCTURE OF *PARKIN*

The *parkin* gene (OMIM 602544; alternative symbols *PARK2, PRKN*) was first identified by Kitada et al. (1998), who used positional cloning to find the pathogenic locus of AR juvenile PD in a consanguineous Japanese family. This landmark publication mapped *parkin* to chromosomal position 6q25.2-q27 and described the gene as spanning more than 500 kilobases (kb). A further study determined that parkin consists of twelve exons and spans a genomic region of 1380 kb, which makes *parkin* one of the largest genes in the human genome (Asakawa et al. 2001). The considerable size of *parkin* is due to the large *parkin* intronic regions; the largest intron, intron 1, spans 284 kb alone.

Parkin lies in a head-to-head orientation with the parkin co-regulated gene (PACRG) (OMIM 608427) on the opposite DNA strand (Asakawa et al. 2001; West et al. 2003). These two genes share a common 5' flanking promoter region spanning 198 basepairs (bp). The 5' promoter region has no apparent TATA or CAAT box elements, but it does contain transcription factor SP1-binding sites, an AP4-binding site, a MYC-binding site and CG- and CpG-rich regions, which allow for the regulation of *parkin* and *PACRG* (West et al. 2003).

Interestingly, *parkin* is one of eight genes that lie within the fragile chromosome site FRA6E, one of the most active common fragile sites in the human genome (Cesari et al. 2003). This location of the parkin gene, in combination with its very large introns, makes *parkin* particularly prone to instability and deletions. The location of *parkin* within FRA6E suggests that it may be a candidate tumor suppressor gene (Cesari et al. 2003); this interesting association of *parkin* with cancer will be further discussed in Section 1.16.5.

1.12 MOLECULAR GENETICS OF *PARKIN*

1.12.1 Pathogenic mutations

Mutations in *parkin* are the most frequent known cause of EOPD. Initial reports identified *parkin* mutations in approximately 50% of patients of European descent with familial cases of EOPD, as well as 15% of sporadic EOPD cases (Lücking et al. 2000; Periquet 2003). Mutations in *parkin* were also reported to be common in EOPD patients from various other ethnic backgrounds (Hedrich et al. 2004). Later, more comprehensive studies reported frequencies of *parkin* mutations in EOPD patients ranging from 1% to 10% across various populations (Kann et al. 2002; Choi et al. 2008; Sironi et al. 2008; Mellick et al. 2009; Koziorowski et al. 2010). The frequency of *parkin* mutations decreases significantly with increasing age at onset of disease. This is exemplified by a study of 100 unrelated sporadic EOPD patients, which found parkin mutations in 77% of patients with PD onset before the age of 20 years, 26% of those between 20 and 30 years and only 3% of patients with onset between 30 and 45 years (Lücking et al. 2000). *Parkin* mutations are rare in cases with onset later than 50 years of age (Klein et al. 2003). It can therefore be said that the frequency of *parkin* mutations is a function of onset age: the earlier the onset, the higher the frequency.

Over 170 different mutations in *parkin* have been reported to date, including missense mutations, nonsense mutations, splice site mutations, small insertions/deletions (indels) and large whole exon deletions, duplications and triplications, across various ethnic groups (Nuytemans et al. 2010; Corti et al. 2011). A comprehensive list of the *parkin* mutations reported in the literature can be found in the PD Mutation Database (PDmutDB, http://www.molgen.ua.ac.be/PDmutDB). The exonic locations of a subset of the reported mutations are illustrated in Figure 1.3.

Approximately 50% of pathogenic *parkin* mutations are exonic rearrangements which cannot be detected by sequencing approaches alone (Hedrich et al. 2001). This speaks to the importance of performing exon dosage analysis in addition to exon sequencing when screening for mutations in *parkin*. Rare *parkin* deletions that extend into the 5' region of *PACRG* have also been reported (Lesage et al. 2007). The clinical phenotype of patients harboring such composite *parkin-PACRG* deletions is indistinguishable from the typical *parkin*-associated phenotype.

Haplotype analyses have been performed in order to determine the origin of certain commonly found *parkin* mutations (Periquet et al. 2001; Hedrich et al. 2004). In general, whole exon rearrangements are thought to represent independent and recurrent events, whereas missense mutations, found in families of different geographic areas, may result from a common founder.

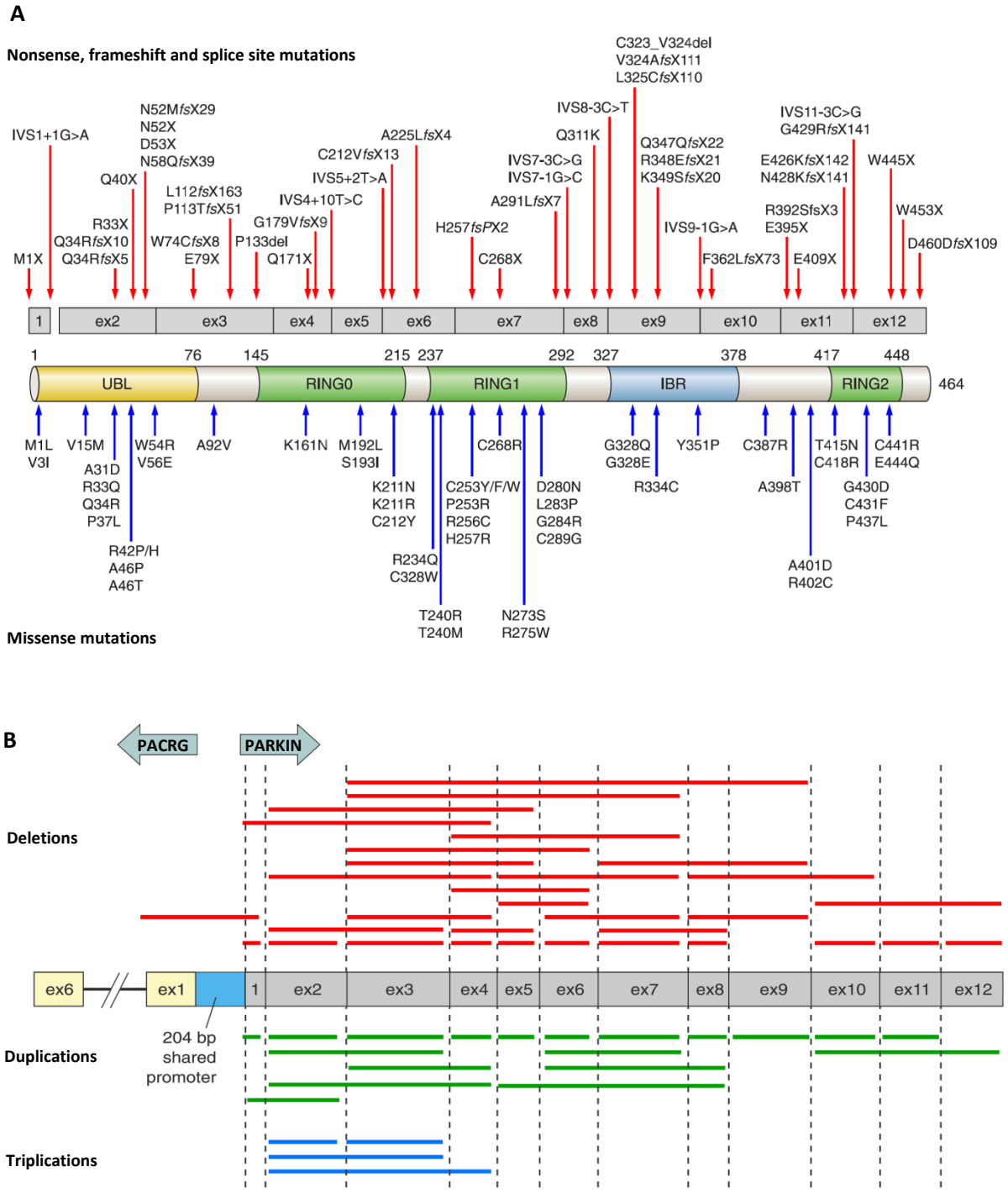

Figure 1.3 Schematic representations of the positions of the various pathogenic sequence mutations and copy number variations in *parkin*. A, the positions of pathogenic nonsense, missense, frameshift and splice site mutations in the *parkin* CDS and parkin protein domains. Only mutations reported in the homozygous or compound heterozygous state are shown. Numbers above the protein schematic indicate the amino acid boundaries of each domain. **B**, the positions of exonic rearrangements, including deletions, duplications and triplications, in the *parkin* CDS. A deletion affecting both *parkin* and *PACRG* is also shown. Figure adapted from Corti et al. (2011). Abbreviations: bp, basepairs; CDS, coding sequence; del, deletion; ex, exon; fs, frameshift; IBR, in-between RING; IVS, intervening sequence; RING, really interesting new gene; *PACRG*, *parkin co-regulated gene*; UBL, ubiquitin-like.

In accordance with the recessive inheritance of *parkin*, both alleles of parkin need to harbor mutations in order to cause disease. These biallelic mutations may be in either homozygous or compound heterozygous states. Most of the exon dosage mutations, indels and nonsense mutations are loss-of-function mutations, as they result in significant structural disruption of the protein coding sequence (CDS) or premature termination of the transcript. On the other hand, the many missense mutations in *parkin* rely on evidence from functional studies with regards to their pathogenicity.

1.12.2 The role of heterozygous variants

In some PD patients, only a single heterozygous *parkin* mutation is present. It has been suggested that such heterozygous mutations may act as risk factors for the development of late onset typical PD; however, this view is quite controversial. Interest in heterozygous mutation carriers was fuelled by early observations of multi-affected families carrying *parkin* mutations. In such families, EOPD patients harbored homozygous or compound heterozygous *parkin* mutations, whereas some of their relatives who developed later-onset PD had single heterozygous *parkin* mutations (Farrer et al. 2001; Foroud et al. 2003). Furthermore, heterozygous *parkin* mutations identified in PD patients were not found in unaffected controls (Hedrich et al. 2002; Schlitter et al. 2006; Sun et al. 2006).

These observations were criticized for the significant confounding effects of ascertainment bias. Moreover, the abovementioned studies only screened control subjects for the variants found in the PD patients, and may therefore have missed heterozygous variants present in controls but not patients. Later studies reported similar rates of heterozygous mutations among unaffected controls as PD patients (Kay et al. 2007). A comprehensive screen for *parkin* mutations in 1700 control subjects found exonic rearrangements in 1% of unaffected controls and heterozygous missense variants in 3% of controls (Kay et al. 2010). Interestingly, all of the exonic rearrangements identified in controls were found in exons 1-4, and no such rearrangements were seen in exons 5-12 which encode for functionally critical domains. Kay et al. (2010) found that heterozygous *parkin* mutations were not associated with an increased risk of PD. Single *parkin* mutations may therefore be incidental in PD patients and unrelated to disease; however, further large-scale studies are necessary. On the other hand, it is interesting to note that functional neuroimaging studies, such as ^{18}F-dopa PET imaging, have reported presynaptic dysfunction of striatal neurons in asymptomatic heterozygous *parkin* mutation carriers (Scherfler et al. 2004; Pavese and Brooks 2009; Guo et al. 2011). This would add support to a role of heterozygous parkin mutations as susceptibility factors for PD. It is hoped that future studies can resolve this contentious issue conclusively.

1.13 *PARKIN* EXPRESSION AND LOCALIZATION

1.13.1 *Parkin* transcript expression

Parkin is expressed as a 4,5 kb transcript comprising of a 1395 bp open reading frame (ORF) (Kitada et al. 1998). This transcript is expressed in most human tissues with a particularly high expression in the heart, skeletal muscle and brain, including the substantia nigra (Figure 1.4).

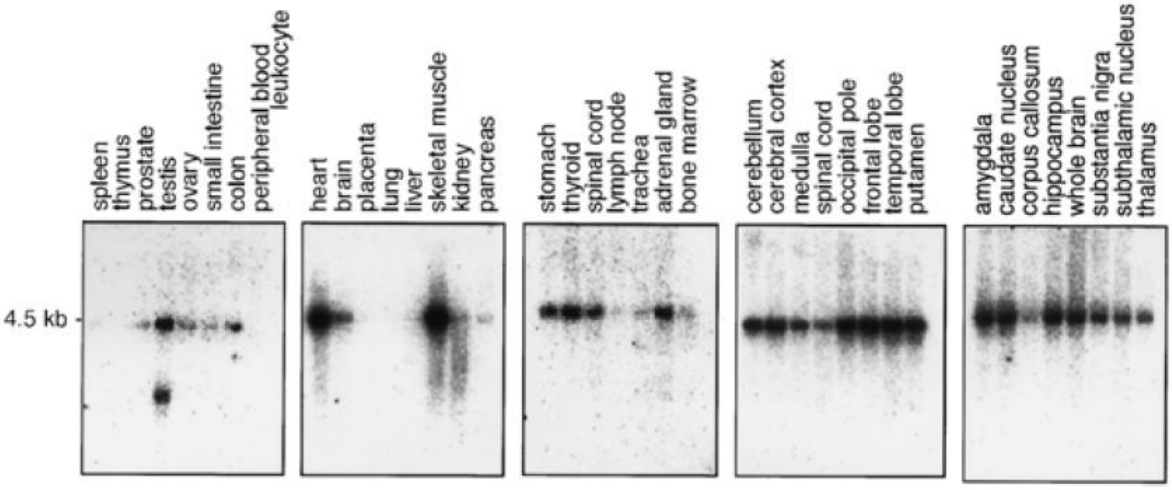

Figure 1.4 Expression profile of the *parkin* gene. Northern blot analysis of *parkin* gene expression in various human tissues. Gene expression in various regions of the adult human brain is shown in the two rightmost panels. Figure adapted from Kitada et al. (1998). Abbreviations: kb, kilobases.

Several alternatively spliced isoforms of *parkin* have been described. For example, isoforms lacking exon 4 or exon 5 are expressed in the brain (Kitada et al. 1998; Sunada et al. 1998; Tan et al. 2005). The pathogenic relevance of such splice variants is unclear; the ratio of exon 4 splice isoform to full-length parkin is higher in sporadic PD patients in comparison to unaffected controls (Tan et al. 2005). Differential expression of *parkin* isoforms in various tissues have been described, which may reflect regulation of tissue-specific parkin activity. For example, a *parkin* splice variant lacking exons 3-5 is the most abundant *parkin* transcript in peripheral lymphocytes, whereas full-length *parkin* is the predominant transcript in the brain (Sunada et al. 1998).

1.13.2 Parkin subcellular localization

Various approaches have been employed to study the subcellular localization of parkin, the 465-aa, 52 kDa protein product of the *parkin* gene. When considering fractionation studies, both endogenous and

overexpressed tagged parkin is found mainly in the cytosol, although parkin also co-fractionates with the outer mitochondrial membrane (OMM), Golgi apparatus, synaptic vesicles and postsynaptic membranes (Shimura et al. 1999; Kubo et al. 2001; Fallon et al. 2002; Darios et al. 2003). Ultrastructural investigation of overexpressed parkin in adult mouse brain tissue demonstrated that parkin associated with the OMM, the endoplasmic reticulum (ER), cytoplasmic vesicles, the outer nuclear membrane and the nuclear matrix (Stichel et al. 2000).

Other studies used immunocytochemistry to investigate endogenous parkin localization in various cultured cell lines. Such approaches corroborated the mainly cytosolic presence of parkin and also found that it co-localizes with actin filaments and the cytoskeleton, the ER, plasma membrane, cytoplasmic vesicles, Golgi apparatus (Huynh et al. 2000; Zarate-Lagunes et al. 2001). Furthermore, several studies reported the association of endogenous parkin with the mitochondria and OMM under native conditions (Kuroda et al. 2006; Rothfuss et al. 2009). This is in contrast to other studies which found that parkin is recruited from the cytosol to the OMM only upon chemically-induced mitochondrial depolarization (Narendra et al. 2008; Matsuda et al. 2010; Rakovic et al. 2010). Nonetheless, the latter studies should not been interpreted as proof of absence of parkin in mitochondria under native conditions, as they merely demonstrated the substantial increase in the mitochondrial fraction of parkin protein under stress conditions.

Subcellular localization studies using overexpressed, tagged proteins should be interpreted with caution as they are susceptible to artefacts. For example, the transgenic overexpression of parkin greatly increases its relative proportion of mitochondrial-bound protein (Narendra et al. 2010a). This speaks to the value of using endogenous protein for *in vivo* studies of parkin localization and function.

1.14 PARKIN IS AN E3 UBIQUITIN LIGASE

Early studies of parkin demonstrated that the protein has ubiquitin ligase enzymatic activity, and hence identified parkin as an E3 ubiquitin ligase (Imai et al. 2000; Shimura et al. 2000; Zhang et al. 2000). This implicated parkin as a member of the UPS, the major cellular pathway for the degradation of soluble intracellular proteins. As an oversimplification, it can be said that the UPS consists of two major steps: the ubiquitination of E3-bound protein substrates (Section 1.14.1) followed by the proteasome-dependent degradation of ubiquitinated substrates (Section 1.16.2.1). It is E3 enzymes, such as parkin, that confer the substrate specificity of the UPS. Parkin-mediated ubiquitination is also involved in proteasome-independent processes such as protein trafficking, mitophagy, cell signaling and apoptosis.

1.14.1 Ubiquitination

The process of ubiquitin conjugation requires the concerted, sequential action of three enzymes: an E1 activating enzyme, an E2 conjugating enzyme and an E3 ubiquitin ligase (Hershko and Ciechanover 1998). In brief, an ubiquitin monomer is activated by an E1 enzyme in an ATP-dependent manner, which results in the conjugation of the now adenylated C-terminal glycine (Gly76) of ubiquitin to a cysteine residue of E1 via a high-energy thiolester bond. Activated ubiquitin is then transferred from E1 to an active-site cysteine residue of an E2 enzyme, forming a similar thiolester linkage. The E1 enzyme dissociates, and E2 interacts with a substrate-bound E3 enzyme. This results in the transfer of adenylated ubiquitin to the ε-amino group of an internal lysine residue of the substrate protein, conjugating ubiquitin to the substrate via an isopeptide bond.

The above-described process results in the conjugation of a single ubiquitin monomer to a substrate protein, termed mono-ubiquitination. Mono-ubiquitination of substrates is involved with the regulation of endocytosis, histone modification and protein sorting (Osley et al. 2006; Clague et al. 2012). However, as ubiquitin itself contains seven lysine residues, chains of ubiquitin molecules can be formed by the conjugation of the C-terminal glycine of an activated ubiquitin to a lysine residue of another ubiquitin, termed poly-ubiquitination. Such poly-ubiquitination, resulting in a chain of at least four monomers, is required for protein degradation. The best studied poly-ubiquitin chain is K48 (conjugation of ubiquitin to lysine 48 of substrate ubiquitin), which targets proteins for degradation via the proteasome (Chau et al. 1989; Thrower et al. 2000). K63 poly-ubiquitin chains are involved in various proteasome-independent functions such as signal transduction, DNA repair, apoptosis and autophagy (Chan and Hill 2001; Chen and Sun 2009). Hence, the fate of an ubiquitinated protein is dependent on both the mode of ubiquitination (mono- or poly-ubiquitination) and the type of chain linkage. However, the wealth of recent studies suggest that cellular ubiquitin signaling, whether degradative or non-degradative, is significantly more complicated than previously appreciated (Komander and Rape 2012; Kravtsova-Ivantsiv and Ciechanover 2012).

Early studies of parkin demonstrated that it associates with the UbcH7 and UbcH8 E2 enzymes to mediate K48 poly-ubiquitination, thereby targeting substrates for proteasome-dependent degradation (Kahle and Haass 2004; Rankin et al. 2011) (Section 1.16.2.1). Consistent with parkin's involvement in the UPS, parkin's UBL domain can directly associate with several subunits of the proteasome: Rpn1, Rpn10, Rpt5, Rpt6 of the 19S regulatory particle and the α4 subunit of the 20S core particle (Sakata et al. 2003; Tsai et al. 2003; Dächsel et al. 2005). Hence, parkin is able to mediate the translocation of its substrates to the proteasome and so promote their degradation.

Surprisingly, parkin is also capable of mediating proteasome-independent ubiquitination of protein substrates such as mono-ubiquitination (Fallon et al. 2006; Hampe et al. 2006; Joch et al. 2007) and K63 poly-ubiquitination (Doss-Pepe et al. 2005; Lim 2005) via interactions with the E2 complex

UbcH13/Uev1a. Parkin furthermore self-regulates its ubiquitin ligase activity via auto-ubiquitination (Chaugule et al. 2011). Parkin is therefore a multifunctional ubiquitin ligase (Lim et al. 2006).

1.14.2 The structure of parkin protein

Until recently, all E3 ubiquitin ligases were divided into three structural classes: RING (Really Interesting New Gene) ligases, U-Box ligases and HECT (Homologous to E6 C-Terminus) ligases. These differed with respect to the mechanism of ubiquitin transfer to substrates. RING and U-Box ligases do not possess catalytic activity, but act as scaffolds to facilitate the direct transfer of ubiquitin from E2 to the substrate, whereas HECT ligases accept activated ubiquitin from E2 and subsequently catalyze the enzymatic transfer of ubiquitin to the substrate. Parkin belongs to the RING Between RING (RBR) set of E3 ligases, originally thought to be a subclass of RING E3s (Eisenhaber et al. 2007). However, recent studies demonstrated that RBR ligases function like RING/HECT hybrids: they associate with E2 via a Zn^{2+}-binding RING domain (like RING E3s), but transfer ubiquitin directly to substrates via a catalytic cysteine residue (like HECT E3s) (Wenzel et al. 2011). RBR ubiquitin ligases such as parkin consist of three consecutive domains: RING1, in between RING (IBR) and RING2. Parkin also contains an ubiquitin-like (UBL) domain at its N-terminal end. Recently, a third RING domain unique to parkin was identified N-terminally of RING1 and named RING0 (Hristova et al. 2009).

Remarkably, the natively folded structure of parkin was only elucidated as recently as 2013, when four groups independently published the crystal structure of the parkin's characteristic RBR domains (Riley et al. 2013; Spratt et al. 2013; Trempe et al. 2013; Wauer and Komander 2013); one of the groups also reported the structure of full-length parkin at a lower resolution (Trempe et al. 2013). Despite the different crystallization approaches used, the reported parkin structures are highly similar and very insightful (Figure 1.5).

The studies found that the C-terminal RING1, IBR and RING2 domains are not an isolated structural unit, but are intertwined with the UBL and RING0 domains to form a compact structure that is folded back onto itself, reminiscent of a coiled snake (Dove and Klevit 2013). Interestingly, two regions that are critical for parkin's ligase activity, the catalytic site in RING2 and the E2 binding site in RING1, are occluded. This validates other studies which suggested an inactive, auto-inhibited state for native parkin (Chaugule et al. 2011; Chew et al. 2011). Parkin's auto-inhibition is due to the hydrophobic interfacing of RING0 with RING2, which buries the catalytically vital cysteine residue (Cys431) in RING2, and the binding of the newly-discovered repressor element of parkin (REP) to RING1, which obstructs the E2 docking site in RING1.

Parkin's crystal structure also confirmed that RING0, RING1, IBR and RING2 each bind two Zn^{2+}-ions as previously predicted (Hristova et al. 2009); however, the topologies of the folded RING domains differed significantly (Dove and Klevit 2013). RING1 is the only *bona fide* RING domain, as it adopts a canonical structure and coordinates its Zn^{2+}-ions in a cross-brace pattern. In opposition to RING1, RING2 and IBR adopt similar folding topologies with Zn^{2+}-binding cysteine residues arranged sequentially. RING0 coordinates Zn^{2+} in a hairpin structure, assuming a characteristic fold that has been previously called the unique parkin (UP) domain (Hampe et al. 2006).

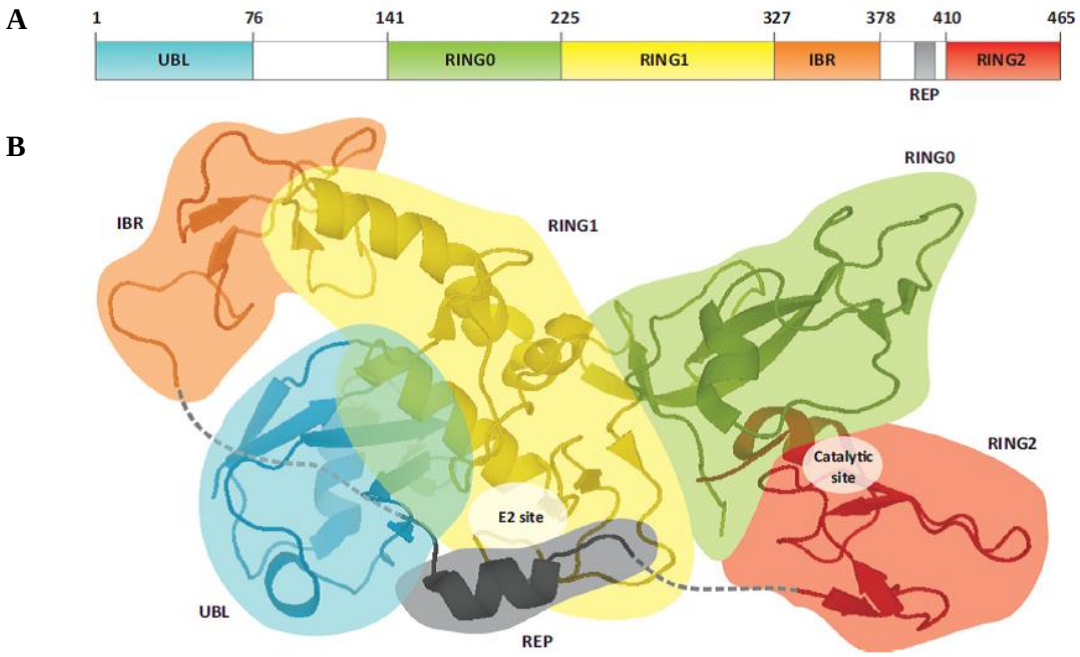

Figure 1.5 Schematic representation of parkin protein structure. A, the domain architecture of parkin. Numbers above the protein schematic indicate the amino acid boundaries of each domain. **B**, representation of the crystal structure of parkin. Parkin forms a compact structure with multiple domain interfaces; each domain is colored according to the diagram in **A**. Parkin is natively inactive and auto-inhibited, as two critical sites are inaccessible. The catalytic site in RING2 is obstructed by RING0, and the E2 binding site in RING1 is occluded by REP. Adapted from Winklhofer (2014). Abbreviations: IBR, in-between RING; RING, really interesting new gene; REP, repression element of parkin; UBL, ubiquitin-like.

As stated, the enzymatic active site of parkin is located in RING2 and centered on the Cys431 residue. Several authors noted the close proximity of His433 and Glu444 to Cys431, which may form a catalytic triad whereby the pK_a of Cys431 is lowered and the residue rendered highly reactive (Riley et al. 2013; Spratt et al. 2013). It is perhaps this high reactivity which necessitates the auto-inhibition of parkin activity.

However, several important questions remain unanswered. It is still unclear how posttranslational modifications and/or binding of interacting proteins switch parkin from an inactive to an active state, or how structurally dynamic the protein is. Indeed, the active sites of E2s and parkin's Cys431 are separated by a distance of approximately 50Å; parkin therefore needs to undergo significant conformational rearrangements to permit ubiquitin transfer. The recent advances in the understanding of parkin's structure will greatly inform further research into its regulation and function.

1.14.3 Pathogenic mutations affect parkin's ubiquitin ligase activity

The structure of soluble, natively folded parkin (Section 1.14.2) provides valuable insights into how pathogenic parkin mutations may result in parkin dysfunction. As such, parkin mutations can conceivably impact on parkin function in four major ways: affecting parkin stability and solubility; decreasing parkin ligase activity; affecting protein-protein interactions with E2s, adaptor proteins, regulatory proteins or substrates, and increasing parkin ligase activity. Mutations that disrupt Zn^{2+}-binding or other important structural residues may destabilize the tertiary structure of parkin, which would result in the loss of functional parkin. Such destabilized protein may also form aggregates, with potentially cytotoxic results. Parkin's ligase activity can be abrogated by pathogenic mutations in its catalytic site (e.g. C431F) or E2 binding site (e.g. T240R). Mutations that disrupt parkin substrate recognition or binding would also result in a decrease in parkin ligase activity; however, it is still unclear how or through which domain parkin binds its substrates. Lastly, mutations that abolish parkin auto-inhibition would result in an increase of ligase activity. This may be mediated by pathogenic mutations at the interfaces of RING0 and RING2 (e.g. T183A) or REP and RING1 (e.g. A398T) (Riley et al. 2013; Spratt et al. 2013; Trempe et al. 2013; Wauer and Komander 2013).

Spratt et al. (2013) noted that regulatory auto-ubiquitination of parkin occurs only in *cis*, not in *trans*, providing an interesting molecular explanation for the recessive nature of parkin mutations. If a heterozygous mutation destabilizes or inactivates the protein, only the mutant protein loses its function without affecting the wild-type copy. On the other hand, a heterozygous mutation that disrupts parkin auto-inhibition and subsequently increases its ligase activity, produces a mutant protein that auto-ubiquitinates itself in *cis* without affecting the wild-type copy. This would result in the selective degradation of the mutant protein, leaving the unaffected copy intact. Therefore, either homozygous or compound heterozygous mutations are necessary for the complete loss of parkin function.

The complexity and interconnectedness of parkin's structure make accurate predictions of a particular mutation's effect difficult. This can be appreciated when considering that pathogenic mutations have been described in all five domains, rather than clustering in its catalytic domain; hence, mutations in any part of parkin can disrupt multiple intertwined domains on several levels.

1.15 PARKIN INTERACTORS

Numerous proteins have been observed to interact with parkin to date, which are listed in Table 1.2. Such protein-protein interactions have been detected via established biochemical approaches, including yeast two-hybrid (Y2H), co-immunoprecipitation (co-IP) and affinity purification followed by mass spectrometry analysis (AP-MS). Interestingly, there are now several examples of previously-identified parkin interactors that cannot be reconciled with the recent elucidation of parkin structure. For example, many studies originally reported the interaction of UbcH8 (an E2 ubiquitin-conjugating enzyme) with parkin's RING2 domain (Imai et al. 2000; Zhang et al. 2000; Olzmann et al. 2007); recent findings that RING2 is not a canonical RING domain and lacks the conserved residues required for E2 recruitment cast significant doubt on such an interaction (Spratt et al. 2013).

The identified parkin interactors can be grouped in five non-exclusive categories (Table 1.2): proteins that interact with parkin as part of the ubiquitination machinery, parkin substrates which are ubiquitinated by parkin, parkin interactors without current evidence of ubiquitination, interactors which translocate parkin to various cellular organelles or events, and interactors which regulate parkin ligase activity either via direct association or by chemical modifications. Many of the identified parkin interactors will be discussed in subsequent sections in relation to the cellular functions of parkin.

Table 1.2 Reported protein-protein interactions with parkin

Interactor	Official symbol*	Detection method(s)	Reference(s)
Components of ubiquitination machinery			
CASK	CASK	Co-IP	Fallon et al. (2002)
Cullin-1	CUL1	Co-IP	Staropoli et al. (2003)
Ubc7	UBE2G1	Co-IP	Imai et al. (2000); Shimura et al. (2000)
UbcH5c	UBE2D3	Co-IP	Joch et al. (2007); Shin et al. (2011)
UbcH6	UBE2E1	Co-IP	Shin et al. (2011)
UbcH7	UBE2L3	Co-IP	Imai et al. (2000); Wenzel et al. (2011)
UbcH13	UBE2N	Co-IP	Doss-Pepe et al. (2005); Olzmann et al. (2007)
Ubiquitin	UBC	Co-IP	Shimura et al. (2000); Zhang et al. (2000)
Uev1a	UBE2V1	Co-IP	Doss-Pepe et al. (2005)
Interactors which are ubiquitinated			
Aβ	APP	Co-IP; co-localization	Rosen et al. (2010); Lonskaya et al. (2013)
Ataxin-2	ATXN2	Co-IP	Huynh et al. (2007)
Bax	BAX	Co-IP	Johnson et al. (2012)
β-Catenin	CTNNB1	AP-MS	Rawal et al. (2009)
CISD1	CISD1	AP-MS	Okatsu et al. (2012)
Cyclin E	CCNE1	Co-IP	Staropoli et al. (2003)
DAT	SLC6A3	Co-IP	Jiang et al. (2004)
DMT1	SLC11A2	Co-IP	Roth et al. (2010)

Interactor	Official symbol*	Detection method(s)	Reference(s)
Drp1	DNM1L	Co-IP	Wang et al. (2011a)
Eps15	EPS15	Co-IP	Fallon et al. (2006)
ERRα	ESRRA	Co-IP	Ren et al. (2011)
ERRβ	ESRRB	Co-IP	Ren et al. (2011)
ERRγ	ESRRG	Co-IP	Ren et al. (2011)
FAF-1	HFAF1	Co-IP	Sul et al. (2013)
FBP1	FBP1	Co-IP	Ko et al. (Ko 2006);
Fbw7β	FBXW7B	Co-IP	Staropoli et al. (2003); Ekholm-Reed et al. (2013)
GBA	GBA	Co-IP	Ron et al. (2010)
Hexokinase 1	HK1	Co-IP; AP-MS	Okatsu et al. (2012); Sarraf et al. (2013)
IKKγ	IKBKG	Co-IP	Henn et al. (Henn et al. 2007)
LIM kinase 1	LIMK1	Co-IP	Lim et al. (2007)
Miro	RHOT1	Co-IP	Wang et al. (2011b)
Mitofusin 1	MFN1	Co-IP; AP-MS	Glauser et al. (2011); Sun et al. (2012)
p38	AIMP2	Co-IP	Corti et al. (2003); Ko et al. (2005)
Pael-R	GPR37	Y2H; Co-IP	Imai et al. (2000)
PARIS	ZNF746	Co-IP	Shin et al. (2011)
Parkin	PARK2	Co-IP	Shimura et al. (2000); Chaugule et al. (2011)
PDCD2	PDCD2	Co-IP	Fukae et al. (2009)
Phospholipase c-γ1	PLCG1	Co-IP	Dehvari et al. (2009)
PICK1	PICK1	Co-IP	Joch et al. (2007)
RanBP2	RANBP2	Co-IP	Um et al. (Um et al. 2006)
Septin 4	ARTS	Co-IP	Choi et al. (2003); Kemeny et al. (2012)
Septin 5	SEPT5	Y2H; Co-IP	Zhang et al. (2000)
SIM2	SIM2	Co-IP	Okui et al. (2005)
αSp22	SNCA	Co-IP	Choi et al. (2001); Shimura et al (2001);
Synaptotagmin XI	SYT11	Y2H; Co-IP	Huynh et al. (2003)
Synphilin-1	SNCAIP	Y2H; Co-IP	Chung et al. (2001); Bandopadhyay et al. (2005)
TOMM70A	TOMM70A	Co-IP; AP-MS; FRET	Okatsu et al. (2012); Bertolin et al. (2013)
TRAF2	TRAF2	Co-IP	Henn et al. (2007); Chung et al. (2013)
α-Tubulin	TUBA	Co-IP	Ren et al. (2003)
β-Tubulin	TUBB1	Co-IP	Ren et al. (2003)
γ-Tubulin	TUBG1	Co-IP	Zhao et al. (2003)
VDAC1	VDAC1	Co-IP; AP-MS	Okatsu et al. (2012); Sun et al. (2012)
Interactors which are not ubiquitinated			
Actin	ACTA1	AP-MS	Kim and Son (2000)
Ambra1	AMBRA1	Co-IP; AP-MS	Van Humbeeck et al. (2011)
Arrestin-1	ARRB1	Co-IP	Ahmed et al. (2011)
Bcl-2	BCL2	Co-IP	Chen et al.(2010b)
CHIP	STUB1	Co-IP; AP-MS	Imai et al. (2002)
DJ-1	PARK7	Co-IP	Moore et al. (2005); Xiong et al. (2009)
HHARI	ARIH1	Co-IP	Parelkar et al. (2012)
Hsc70	HSPA8	Co-IP	Imai et al. (2002); Imai et al. (2003)
HSJ1a	DNAJB2A	Co-IP	Imai et al. (2002)

Interactor	Official symbol*	Detection method(s)	Reference(s)
Hsp70	HSPA4	Co-IP; AP-MS	Imai et al. (2002); Tsai et al. (2003)
Hsp90	HSPA1	Co-IP	Imai et al. (2003)
Mitofusin 2	MFN2	Co-IP; AP-MS	Glauser et al. (2011); Sun et al. (2012)
Mortalin	HSPA9	Co-IP	Yang et al. (2011)
NME2	NME2	AP-MS	Okatsu et al. (2012)
p62	SQSTM1	Co-localization	Narendra et al. (2010b)
PACRG	PACRG	Co-IP	Imai et al. (2003)
PCNA	PCNA	Co-IP	Kao et al. (2009)
PIK3C3	PIK3C3	Co-IP	Choubey et al. (2014)
PS-α4	PSMA4	Y2H; Co-IP	Dächsel et al. (2005)
Rpn1	PSMD2	Co-IP	Um et al. (2010)
Rpn10	PSMD4	Co-IP	Sakata et al. (2003); Uchiki et al. (2009)
Rpt5	PSMC3	Co-IP	Um et al. (2010)
Rpt6	PSMC5	Co-IP	Tsai et al (2003); Um et al. (2010)
Tau	MAPT	Co-IP	Petrucelli et al. (2004)
TDP-43	TARDBP	Co-IP	Hebron et al. (2013)
TOMM40	TOMM40	FRET	Bertolin et al. (2013)
VDAC2	VDAC2	AP-MS	Okatsu et al. (2012); Sun et al. (2012)
VDAC3	VDAC3	AP-MS	Okatsu et al. (2012); Sun et al. (2012)
Interactors which mediate parkin translocation			
AF-6	MLLT4	Co-IP	Haskin et al. (2013)
Beclin 1	BECN1	Co-IP	Choubey et al. (2014)
HDAC6	HDAC6	Co-IP; AP-MS	Jiang et al. (2008); Hebron et al. (2013)
Klokin 1	CHPF	Y2H; Co-IP	Kuroda et al. (2012)
Interactors which regulate parkin activity			
14-3-3η	YWHAH	Co-IP	Sato et al. (2006)
Ataxin-3	ATXN3	Co-IP	Durcan et al. (2011); Bai et al. (2013)
BAG5	BAG5	Co-IP	Kalia et al. (2004)
C-Abl	ABL1	Co-IP	Ko et al. (2010); Imam et al. (2011)
Casein kinase-1	CSNK1A1	Co-IP	Yamamoto et al. (2005)
Cdk5	CDK5	Co-IP	Avraham et al. (2007)
HtrA2	HTRA2	Co-IP	Park et al. (2009)
LRRK2	LRRK2	Co-IP	Smith et al. (2005)
NAC1	NACC1	Co-IP	Korutla et al. (2014)
NEDD8	NEDD8	Co-IP; AP-MS	Choo et al. (2012); Um et al. (2012)
Nrdp1	RNF41	Y2H; Co-IP	Zhong et al. (2004)
p32	C1QBP	Co-IP	Li et al. (2011c)
PINK1	PINK1	Co-IP	Sha et al (2009); Shiba et al. (2009);
Protein Kinase A	PKA	Co-IP	Yamamoto et al. (2005)
Protein kinase C	DYT10	Co-IP	Yamamoto et al. (2005)
SUMO-1	SUMO1	Co-IP	Um & Chung (2006)

*Refers to the HGNC approved gene symbol. Adapted from the BioGRID database (http://thebiogrid.org). Abbreviations: AP-MS, affinity purification mass spectrometry; Co-IP, co-immunoprecipitation; FRET, Förster resonance energy transfer; Y2H, yeast two-hybrid.

1.16 CELLULAR FUNCTIONS OF PARKIN

A wide array of neuroprotective functions of parkin has been described. Such neuroprotection is aimed against numerous sources of cellular stress that may result in cell death, including proteotoxic stress, mitochondrial stress, excitotoxicity and pro-apoptotic stimulation (Corti et al. 2011; Rankin et al. 2011; Exner et al. 2012). In fact, several studies have reported that *parkin* is transcriptionally upregulated during periods of cell stress. The neuroprotective functions of parkin can be broadly grouped into three mechanisms: maintaining proper protein degradation, promoting mitochondrial function and health, and modulating proteasome-independent ubiquitin signaling in pro- and anti-apoptotic pathways. Parkin has also been implicated in non-neuronal functions, such as tumor suppression and innate immunity, which will be briefly discussed.

1.16.2 Parkin and protein degradation

Early studies of parkin demonstrated that it can associate with the UbcH7 and UbcH8 E2 enzymes to mediate K48 poly-ubiquitination, thereby targeting substrates for proteasome-dependent degradation (Kahle and Haass 2004; Rankin et al. 2011). Loss of function of parkin may therefore result in the deleterious accumulation of such substrates, potentially contributing to neurotoxicity. While many parkin substrates have been identified to date (Table 1.2), there is little evidence that most of these substrates accumulate in the absence of functional parkin or that parkin modulates their levels in a proteasome-dependent manner *in vivo* (Periquet et al. 2005; Davison et al. 2009; Dawson and Dawson 2010). However, a handful of authentic parkin UPS substrates (cyclin E, AIMP2, FBP-1 and PARIS) demonstrate pathological relevance (Corti et al. 2003; Ko 2005, 2006; Shin et al. 2011); these interactions will be discussed in Section 1.16.2.2.

1.16.2.1 *The proteasomal degradation pathway*

Parkin plays important roles in protein quality control and turnover via the UPS. Therefore, the process whereby ubiquitinated substrates are degraded will be briefly discussed. Degradation of sufficiently poly-ubiquitinated substrates is mediated by a large multimeric protein complex called the 26S proteasome (Bedford et al. 2010). This structure consists of a 20S core particle which can be capped at one or both ends by the 19S regulatory particle. The 20S core particle is a hollow, barrel-shaped structure composed of 28 subunits organized into four heptameric rings. Whereas the two outer rings, comprised of seven α-subunits, enable docking of the 19S regulatory particles to the core particle, the two inner rings of seven β-subunits have potent proteolytic activities. The β1, β2 and β5 subunits of the 20S core possess peptidylglutamyl-like activity, trypsin-like activity and chymotrypsin-like activity, respectively.

Access to the 20S core particle is tightly regulated by the 19S regulatory particle, which recognizes, de-biquitinates and unfolds poly-ubiquitinated substrates through the concerted action of various ubiquitin-binding, de-ubiquitinating and ATPase-like subunits (Bedford et al. 2010). The unfolded, untagged protein is subsequently threaded through the catalytic core of the proteasome, where it is promptly degraded.

1.16.2.2 *Parkin targets substrates for degradation*

Several studies demonstrated that parkin regulates the steady-state levels of many (but not all) of its protein substrates via the UPS; the accumulation of such substrates may contribute to cytotoxicity and dopaminergic neurodegeneration. Parkin is able to act as a component of a multiprotein SCF (Skp1, Cullin-1, Roc1 and F-box protein)-like ubiquitin ligase complex via interactions with cullin-1 and fbw7β (Staropoli et al. 2003). As part of such a complex, parkin targets and promotes the degradation of the apoptosis-regulator cyclin E. Parkin deficiency in primary neurons potentiates the accumulation of cyclin E and resulting apoptosis in primary neurons experiencing kainite-induced excitotoxicity, whereas overexpressed parkin attenuated cyclin E accumulation in such a model of neuronal stress.

Transgenic mice that overexpress the authentic parkin substrate aminoacyl-tRNA synthase complex-interacting multifunctional protein-2 (AIMP2)/p38 present with age-dependent dopaminergic neuronal loss and accompanying motor features (Lee et al. 2013). Such accumulation of AIMP2 mediated cell death via a nuclear interaction between AIMP2 and poly(ADP-ribose)-polymerase-1 (PARP1), which resulted in the activation of PARP1 and accumulation of poly(ADP-ribose) molecules. Interestingly, the subsequent neurodegeneration was restricted to the ventral midbrain of such transgenic mice.

The accumulation of the parkin-interacting substrate (PARIS, ZNF746) is regulated by parkin in a neuronal cell model: overexpression of parkin results in reduced expression of PARIS, whereas downregulation of parkin expression results in PARIS upregulation (Shin et al. 2011). PARIS is a specific and key transcriptional repressor of peroxisome proliferator-activated receptor γ coactivator 1α (PGC-1α), an important mediator of mitochondrial biogenesis (St-Pierre et al. 2006; Ventura-Clapier et al. 2008). PARIS accumulation in a parkin deficient mouse model resulted in the selective degeneration of dopaminergic neurons (Shin et al. 2011).

During periods of oxidative stress, parkin ubiquitinates and mediates the degradation of F-box protein fbw7β (Ekholm-Reed et al. 2013). Fbw7β regulates the degradation of the mitochondrial pro-survival factor myeloid cell leukemia-1 (Mcl-1); hence, parkin indirectly promotes neuronal survival by maintaining Mcl-1 levels. Mcl-1 is downregulated when parkin is knocked down in primary neuronal

cell cultures, resulting in an acute sensitivity to oxidative stress. Pathogenic mutations in parkin may therefore result in dopaminergic cell death via unregulated Fbw7β-targeted degradation of Mcl-1.

Another study found that parkin mediates the degradation of the pro-apoptotic Fas-associated factor 1 (FAF1) in a neuronal cell line, where pathogenic parkin mutations resulted in the accumulation of FAF1 (Sul et al. 2013). Furthermore, FAF1 accumulated selectively in the substantia nigra of a MPTP-induced mouse model of PD, and the subsequent dopaminergic degeneration is attenuated in transgenic mice with diminished levels of FAF1.

1.16.3 Parkin and mitochondrial health

Compelling evidence of the mitochondrial involvement of parkin were obtained from *Drosophila* models of parkin deficiency. Such flies demonstrated prominent mitochondrial dysfunction, muscle degeneration and dopaminergic degeneration (Greene et al. 2003; Cha et al. 2005; Whitworth et al. 2005). Flies overexpressing mutated parkin showed similar neural degeneration and mitochondrial impairment as flies lacking in parkin (Wang et al. 2007). Interestingly, the abnormalities seen in parkin knockout flies closely resembled that of PINK1 knockout *Drosophila* models; furthermore, parkin overexpression rescued the pathological effects of PINK1 deficiency, but not *vice versa* (Clark et al. 2006; Park et al. 2006; Yang et al. 2006). These interesting observations spurred the discovery of a common PINK-parkin pathway acting upon mitochondria (Poole et al. 2008).

Narendra et al. (2008) found that carbonyl cyanide 3-chlorophenylhydrazone (CCCP)-induced mitochondrial depolarization of HeLa cells induced the recruitment of parkin at the OMM, where parkin promoted the sequestration and autophagic degradation of damaged mitochondria (mitophagy). Moreover, the mitochondrial translocation of parkin was found to be depended on PINK1, which accumulates at the OMM upon mitochondrial depolarization (Narendra et al. 2010a; Matsuda et al. 2010).In addition to recruiting parkin to the OMM, PINK1 is also involved in the activation of parkin-mediated mitophagy by phosphorylating parkin at Ser65 within parkin's UBL domain (Kondapalli et al. 2012; Shiba-Fukushima et al. 2012). The PINK1-mediated parkin recruitment is aided and regulated by several recently identified components, including translocase of outer membrane (TOM) member 7 (TOMM7) and hexokinase 2 (HK2) (Hasson et al. 2013; McCoy et al. 2014). At the OMM, activated parkin ubiquitinates mitofusins 1 and 2 (Mfn1 and Mfn2), voltage-dependent anion-selective channel protein 1 (VDAC1), CDGSH iron-sulfur domain-containing protein 1 (CISD1), hexokinase 1 (HK1) as well as members of the TOM complex (Gegg et al. 2010; Geisler et al. 2010; Yoshii et al. 2011; Okatsu et al. 2012). However, parkin likely ubiquitinates a wide variety of currently unknown proteins on the OMM in response to mitochondrial damage (Sarraf et al. 2013). The widespread

ubiquitination of OMM proteins results in the recruitment of the autophagy machinery and the autophagic clearance of damaged mitochondria, promoting cell survival (Chan et al. 2011b).

While the discovery of the important role of parkin in mitophagy in chemically-stressed cell models is very insightful, it is not clear to what extent impairment of this function is responsible for *in vivo* dopaminergic neuronal degeneration in cases of pathogenically mutated parkin. It was recently reported that the rate of mitochondrial protein turnover is reduced in parkin mutant *Drosophila*, supporting the role of parkin in mitophagy under normal physiological conditions (Vincow et al. 2013). The role of parkin-induced mitophagy in mouse models has yet to be demonstrated.

Parkin, together with PINK1, has also recently been implicated in a selective vesicular pathway for mitochondrial quality control (McLelland et al. 2014). This subtler pathway, distinct from canonical mitophagy, involves the selective sorting and transport of oxidized and damaged mitochondrial proteins in mitochondria-derived vesicles (MDVs), which then bypass autophagosomes and are delivered directly to lysosomes for degradation. McLelland et al. (2014) found that wild-type, but not mutant, parkin co-localized with MDVs in response to mild oxidative stress, and stimulated the formation of MDVs in an ubiquitin-dependent manner. It is thought that this vesicular pathway provides a mechanism for routine mitochondrial quality control, whereas mitophagy may be reserved for more severe mitochondrial damage.

While the numerous recent studies of parkin's role in mitophagy have garnered much attention, parkin is also implicated in other pathways promoting mitochondrial health. For example, parkin has been shown to promote mitochondrial biogenesis. Parkin associated with the mitochondrial transcription factor TFAM, enhancing TFAM-mediated transcription activity; conversely, parkin deficiency significantly decreased the level of mitochondrial-encoded mRNA (Kuroda et al. 2006a). Parkin was also found to directly bind mtDNA and to preserve mtDNA integrity in response to elevated ROS levels (Rothfuss et al. 2009). Moreover, parkin promotes mitochondrial biogenesis via its UPS-dependent regulation of the PARIS-PGC-1α pathway (Section 1.16.2.2).

Parkin is also involved in the regulation of mitochondrial fission and fusion, continuous processes that orchestrate a dynamic cellular network of mitochondria. These processes fine-tune the mitochondrial network in response to changes in cellular conditions, in order to promote proper mitochondrial function and health (Westermann 2010). The core machinery of mitochondrial fusion is composed of Mfn1, Mfn2 and optic atrophy protein 1 (OPA1), whereas fission is driven by dynamin-related protein 1 (Drp1). Parkin, together with PINK1, is thought to regulate mitochondrial fusion and fission via ubiquitination of Mfn1, Mfn2 and Drp1 in a common PINK1-parkin pathway (Gegg et al. 2010; Poole et al. 2010; Glauser et al. 2011; Wang et al. 2011a). Indeed, Drp1-dependent mitochondrial fragmentation is commonly reported in cell- and animal models of parkin deficiency (Deng et al. 2008; Lutz et al. 2009; Yu et al. 2011). Hence, parkin plays important roles in the promotion and

coordination of many aspects of mitochondrial health, including degradation of damaged mitochondria, mitochondrial biogenesis and mitochondrial dynamics. Dysregulation of the careful balance between these processes may significantly compromise mitochondrial health and contribute to neurodegeneration (Exner et al. 2012).

1.16.4 Parkin and cell death pathways

Various neuroprotective effects of parkin have been described that relate to apoptotic signaling. Parkin is involved in the regulation of the mitochondrial release of cytochrome c; there is an inverse relationship between cellular parkin levels and cytochrome c release and apoptosis (Darios et al. 2003; Berger et al. 2009). Parkin also physically interacts with the promoter region of *p53* and downregulates its transcription, which reduces caspase-3 activation (da Costa et al. 2009). Interestingly, this anti-apoptotic effect of parkin is not dependent on its ligase activity. In contrast, parkin ligase activity is required for its transcriptional attenuation of *MAO-A* and *MAO-B* (Jiang et al. 2006). MAO is a substantial source of ROS in dopaminergic neurons; parkin therefore indirectly reduces the generation of ROS.

Parkin associates with and stabilizes microtubules, where it protects neurons against microtubule-depolymerizing toxins by diminishing the activation of mitogen-activated protein kinases (MAPK) such as extracellular signal-related kinase (ERK), c-Jun N-terminal kinase (JNK) and p38 (Ren et al. 2009). The regulation of JNK activity by parkin was also seen in parkin *Drosophila* models (Cha et al. 2005). Parkin suppression of JNK and p38 activity was found to protect against tyrosinase-mediated neurotoxicity (Hasegawa et al. 2008). Furthermore, JNK signaling induces cyclooxygenase 2, a necessary step for neurodegeneration in a MPTP-induced mouse model of PD; suppression of this pathway may be another avenue for parkin-mediated neuroprotection (Hunot et al. 2004).

Parkin suppresses the trafficking of epidermal growth factor (EGF) receptor (EGFR) by ubiquitinating the adaptor protein Eps15 (Fallon et al. 2006). As ubiquitination of Eps15 interferes with its ability to bind and internalize EGFR, the absence of parkin resulted in accelerated EGFR degradation and reduced EGFR signaling via the phosphoinositide 3-kinase (PI(3)K)/Akt signaling cascade. Parkin therefore promotes PI(3)K/Akt pro-survival signaling (Fallon et al. 2006). In fact, transgenic delivery of constitutively active Akt protected against neurodegeneration in a drug-induced mouse model of PD (Ries et al. 2006). Parkin was also found to mediate neuroprotection via the activation of the IκB kinase/NF-κB pathway (Henn et al. 2007). Moreover, parkin was observed to ubiquitinate Bax in a way that abrogated the mitochondrial translocation of Bax and thus suppressed Bax's pro-apoptotic effects (Johnson et al. 2012). This effect was mediated by cytosolic parkin without the translocation of parkin to mitochondria under pro-apoptotic conditions, illustrating that the neuroprotective and mitochondrial functions of parkin are mediated through different mechanisms.

1.16.5 Parkin and cancer

As stated previously, the *parkin* genomic structure spans a large region of FRA6E, one of the most active common chromosome fragile sites in the human genome (Cesari et al. 2003). Such fragile sites are susceptible to chromosomal breaks and rearrangements and are implicated in oncogenesis. In fact, *parkin* copy number mutations are frequently reported in breast cancer (Shah et al. 2012), renal carcinoma (Toma et al. 2008), esophageal carcinoma (Gu et al. 2010), glioma (Yin et al. 2009), non-small cell lung cancer (Iwakawa et al. 2012), cervical cancer (Mehdi et al. 2011) and gastric cancer (Deng et al. 2012). Such genetic observations are supported by functional studies of parkin as a tumor suppressor; for example, heterozygous deletion of *parkin* accelerated the development of intestinal adenoma in transgenic mice expressing mutant APC, a regulator of Wnt signaling (Poulogiannis et al. 2010), whereas parkin knockout mice demonstrated enhanced hepatocyte proliferation and development of hepatic tumors (Fujiwara et al. 2008)

The mechanism of the tumor suppressor activity of parkin is not fully understood. As stated in Section 1.16.2.2, cyclin E is a substrate for parkin ubiquitination and subsequent proteasomal degradation. It is interesting to speculate that dysregulation of this important cell cycle regulator may contribute to oncogenesis, and several studies have found increased cyclin E levels in parkin-null cancer cell lines (Ikeuchi et al. 2009; Tay et al. 2010; Yeo et al. 2012). Parkin deficiency may also promote cancer via metabolic changes resulting from parkin-linked mitochondrial dysfunction. Tumor cells often demonstrate the Warburg effect, whereby the cells switch from mitochondrial energy production to anaerobic glycolysis, coupled with an increased glucose uptake and utilization (Van der Heiden et al. 2009). Parkin, a p53 target gene, mediates the role of the tumor suppressor p53 in glucose metabolism and the Warburg effect (Zhang et al. 2011); in fact, parkin deficiency was found to promote glycolysis and reduced mitochondrial respiration in human lung cancer cells, leading to the Warburg effect (Zhang et al. 2011).

1.16.6 Parkin and innate immune defense

Whereas parkin plays an important and much-studied role in mediating mitophagy (Section 1.16.3), a recent report implicated parkin in an additional autophagic pathway: the clearance of intracellular pathogens via the process of xenophagy (Manzanillo et al. 2013). This interesting finding supports genomic association studies which show that *parkin* polymorphisms, resulting in decreased *parkin* expression, are associated with increased susceptibility to intracellular bacterial pathogens such as *Mycobacterium leprae* and *Salmonella typhi* (Mira et al. 2004; Ali et al. 2006). Manzanillo et al. (2013) demonstrated that parkin is required for the ubiquitin-mediated xenophagy of *Mycobacterium tuberculosis* in macrophages, where parkin ubiquitinates an unknown membrane protein on phagosomal vesicles containing ingested *M. tuberculosis*, thereby targeting the phagosome for

lysosomal degradation. Interestingly, it was found that both mouse and *Drosophila* models of parkin deficiency demonstrate increased susceptibility to various intracellular bacterial pathogens, suggesting that parkin may play an evolutionarily conserved role in eukaryotic innate immune responses (Manzanillo et al. 2013).

1.17 THE PRESENT STUDY

It is evident from the above-discussed literature that PD has a complex etiology with various contributing genetic and non-genetic factors. The identification of genes that induce familial PD has greatly advanced our understanding of PD pathogenesis; however, much of the etiology and pathobiology of the disease remain unclear. It is hoped that further investigation of PD-associated proteins, and the molecular pathways they form part of, would lead to new insight and direction in PD research.

This dissertation focusses specifically on the role of parkin, and the study is divided into three parts. The **first part** comprises a molecular genetic screen for *parkin* mutations in South African PD patients. While the genetic basis of PD has been extensively characterized in North American, European and Asian populations, very little is known of the molecular etiology of PD in sub-Saharan Africa (Blanckenberg et al. 2013). Investigation of the genetic contribution to PD in South African patients may be particularly insightful given the unique genetic heritage of the Black African, Afrikaner and mixed ancestry sub-populations of South Africa. As both *parkin* point mutations and exonic rearrangements are reported to be common causes of EOPD, the present study aimed to assess the contribution of *parkin* mutations to PD in South African populations by determining the frequency of both point mutations and exon rearrangements in all 12 *parkin* exons in a group of unrelated South African patients diagnosed with PD. A better understanding of the molecular genetics of *parkin* in a South African context may assist in risk stratification, diagnosis and counseling of South African PD patients.

The **second part** of the study entails an identification and investigation of novel parkin-interacting proteins. Although many substrates of parkin's E3 ligase activity have been identified in the literature, it is anticipated that novel, pathologically-relevant parkin substrates remain to be discovered. The benefit of identifying parkin substrates is well illustrated by the recognition of PARIS, AIMP2, Fbw7β and other proteins as authentic, pathologically-relevant parkin substrates, as described in preceding sections. The current study aimed to identify novel parkin-interacting proteins by using the RBR region of parkin as bait in a yeast two-hybrid (Y2H) library screen. This functionally important RBR region contains substrate binding sites for a variety of known parkin substrates, including PARIS, AIMP2 and Fbw7β; it is therefore appropriate for use in a Y2H library screen for novel

interactors. As the identified parkin interactions may constitute UPS-mediated regulation and degradation of a parkin substrate, it is hypothesized that the absence of functional parkin would result in an accumulation of such substrates, eventually leading to cellular toxicity.

The **third part** of this dissertation involves the functional effects of parkin deficiency in a cell model and a pilot study of the possible rescue effect of vitamin K_2 treatment. Initially, it was aimed to employ RNA interference (RNAi) to create a parkin knockdown neuronal cell model, in order to determine the effect of the absence of parkin on each parkin interactor's level of expression. Subsequently, dermal fibroblasts obtained from patients with parkin-null mutations were used as a parkin deficient cell model. The effect of the absence of parkin on various cellular parameters such as cell viability and proliferation, mitochondrial respiration rate, mitochondrial membrane potential and mitochondrial network integrity was determined. It was then investigated whether the treatment with the recently identified potential therapeutic agent vitamin K_2 would ameliorate the effect of absence of parkin on such cellular parameters. While it was previously demonstrated that the treatment of parkin-knockout *Drosophila* with vitamin K_2 rescued the mitochondrial defects seen in this fly model (section 1.9.4), it would be worthwhile to investigate whether similar effects would be seen in a human neuronal cell model. Such evidence would add weight to the potential use of vitamin K_2 as a therapeutic agent for PD patients with *parkin* mutations.

To summarize, the present study had the following objectives:

1. Determine the frequencies of both *parkin* missense mutations and exonic rearrangements in a group of 229 unrelated South African patients diagnosed with PD, by means of high resolution melt (HRM) analysis and multiplex ligation-dependent probe amplification (MLPA) analysis, and verification by DNA sequencing.
2. Identify potentially novel interactors of the RBR region of parkin using a Y2H approach.
3. Verify selected putative parkin interactors by means of *in vivo* 3D co-localization and co-immunoprecipitation assays.
4. Assess whether the protein expression levels of the verified parkin interactors are increased in a cellular model of parkin deficiency.
5. Investigate the effect of parkin deficiency on various cellular parameters by means of cell growth and viability assays, mitochondrial respiration assays, mitochondrial membrane potential assays and mitochondrial network morphology analyses.
6. Evaluate the effect of treatment with vitamin K_2 on aforementioned cellular parameters.

Hence, results generated by this study would stimulate further discussion about parkin and parkin-interacting proteins, as well as their potential relevance in cellular stress, neurodegeneration and PD.

CHAPTER TWO: MATERIALS AND METHODS

TABLE OF CONTENTS **PAGE**

CHAPTER TWO: MATERIALS AND METHODS

PART ONE: MOLECULAR ANALYSIS OF *PARKIN*

The first part of this dissertation entails a molecular genetic investigation of the *parkin* gene in the context of PD in South African patients. As such, the genetic contribution of parkin mutations to PD pathology was assessed by determining the frequency of mutations in all 12 exons of *parkin* in a group of South African patients diagnosed with PD (Section 2.2). Point mutations and small insertions/deletions were detected by performing HRM analysis (Section 2.6) and automated DNA sequencing (Section 2.7), whereas whole exon rearrangements were identified by MLPA analysis (Section 2.8). Furthermore, reverse-transcription PCR (RT-PCR) was performed on lymphocytes of selected study participants (Section 2.5.5). Relevant and detailed information regarding the materials and methods used in this part of the study follows below.

2.1 ETHICAL CONSIDERATIONS

This study gained ethical approval from the Health Research Ethics Committee of Stellenbosch University, Cape Town, South Africa (Protocol number 2002/C059). Ethical approval was renewed annually during the course of this study. Written informed consent was obtained from all participants.

2.2 STUDY PARTICIPANTS AND BLOOD COLLECTION

The study group consisted of 229 unrelated PD patients, who were recruited from the Movement Disorders clinic at Tygerberg Hospital (Cape Town, South Africa) and the Parkinson's Association of South Africa. All patients recruited at Tygerberg Hospital underwent a standardized examination by a movement disorder specialist and were diagnosed with PD based on the UK Parkinson's Disease Society Brain Bank diagnostic criteria (Gibb and Lees 1988b). The majority of recruited patients demonstrated early disease onset (age at onset (AAO) <=50 years) and/or positive family history of PD. AAO and family history were determined via a questionnaire filled out by a trained research nurse, where a positive family history was defined as the self-reported presence of PD in a first- or second-degree relative. Patients with late onset PD (AAO > 60 years) were included in the study as *parkin* mutations had been found in both early and late onset PD patients (Sun et al. 2006).

Over 100 ethnically-matched control samples were recruited from healthy, unrelated individuals of each relevant ethnic group; these control individuals had not been examined for PD symptoms by a

neurologist. No information regarding the ages of the control individuals was available as control samples were de-identified. While the 229 PD patients recruited for the genetic study were unrelated, patients that were found to harbor pathogenic parkin mutations following the genetic screen (Section 3.1.2) were subjected to a thorough family work-up by a research nurse. This included the procurement of blood samples from consenting family members, who were then screened for presence of the relevant *parkin* mutation(s). The genetic results of these family members of the 229 unrelated probands were not included in the analysis of parkin mutation frequency.

Blood samples were collected from each study participant by a trained phlebotomist using two 10ml Vacutainer® ethylene-diamine-tetra-acetic acid (EDTA) tubes (Becton Dickinson, Franklin Lakes, New Jersey, USA) for DNA extraction (Section 2.3). For selected study participants, blood samples were collected in two 2.5ml volumes in PAXgene™ Blood RNA tubes (PreAnalytiX, Hombrechtikon, Switzerland) for RNA extraction (Section 2.4).

2.3 DNA EXTRACTION FROM BLOOD

DNA was extracted from whole blood samples using a modification of the method described by Corfield et al. (1993). All DNA blood extractions were performed by Mrs. Ina le Roux.

Briefly, each EDTA-blood sample was transferred to a 50ml polypropylene tube and the sample brought to a final volume of 45ml with cold (4°C) cell lysis buffer (Appendix II). Samples were incubated on ice for 10min followed by centrifugation at 2800rpm for 10min at 10°C on an Eppendorf model 5810R centrifuge (Eppendorf, Hamburg, Germany), and the supernatant discarded. Pellets were resuspended in 20ml cell lysis buffer and the incubation and centrifugation steps repeated. The supernatant was discarded and volumes of 900µl Na-EDTA solution (Appendix II), 100µl of 10% SDS and 100µl proteinase K (Roche, Basel, Switzerland) added to the pellets, which were fully resuspended and incubated at 37°C overnight (16h).

Following the overnight incubation, volumes of 2ml ddH_2O, 500µl of 3M Na-Ac (Appendix II) and 2.5ml phenol-chloroform (Appendix II) were added to each tube. Tubes were incubated at 4˚C for 10min with shaking on an Orbit 300 shaker (Labnet, Edison, New Jersey, USA). The mixtures were transferred to separate 10ml glass tubes and centrifuged at 8000rpm for 12 min at 10°C in a Sorvall™ RC5B Plus centrifuge (Thermo Fisher Scientific, Waltham, Massachusetts, USA). Each aqueous phase was transferred to fresh glass tubes. A volume of 2.5ml chloroform-octanol (Appendix II) was added to each tube and the tubes centrifuged at 8000rpm for 10 min at 10°C in a Sorvall™ RC5B Plus centrifuge. Supernatants were then transferred to 15ml polypropylene tubes and a total of 5ml of ice-cold (-20°C) 96% ethanol added to facilitate DNA precipitation. The precipitate was transferred to a

1.5ml microcentrifuge tube containing 1ml of 70% ethanol. Samples were pelleted by centrifugation at 15 000rpm for 3min at room temperature in a Labnet Prism™ microcentrifuge (Labnet, Edison, New Jersey, USA). The supernatants were discarded and the 70% ethanol wash repeated. After centrifugation, pellets were air-dried at room temperature for approximately 30min.

Pellets were resuspended in the following manner: A volume of 200µl of 1X TE buffer (Appendix II) was added to each tube which were then incubated at 37°C overnight (16h) followed by further incubation at 4°C on a model HS100 rotating wheel (Labnet, Edison, New Jersey, USA) for three days. Subsequently, DNA concentration and purity was determined using a NanoDrop® ND-1000 spectrophotometer (Thermo Scientific, Waltham, Massachusetts, USA) and NanoDrop1000® software version 3.7.1 (Thermo Scientific, Waltham, Massachusetts, USA). Purified DNA samples were stored at -20°C until use.

2.4 BLOOD RNA EXTRACTION AND cDNA CONVERSION

Total RNA was extracted from whole blood samples collected in PAXgene™ Blood RNA tubes. RNA extraction was performed by using a PAXgene™ Blood RNA kit (PreAnalytiX, Hombrechtikon, Switzerland) according to manufacturer's instructions. Isolated RNA concentration and quality was subsequently measured with an Experion™ StdSens Analysis kit (Bio-Rad, Hercules, California, USA) on an Experion™ automated electrophoresis station (Bio-Rad, Hercules, California, USA). Only RNA samples with a RNA quality indicator (RQI) value above 8.0 (out of 10) were used in subsequent applications.

Following RNA isolation, the purified RNA was converted to complementary DNA (cDNA) by using a Quantitect® Reverse Transcription Kit (Qiagen, Hilden, Germany) as per manufacturer's instructions. cDNA concentration was determined using a NanoDrop® ND-1000 spectrophotometer and NanoDrop1000® software version 3.7.1. The cDNA samples were then stored at -20°C until use.

2.5 POLYMERASE CHAIN REACTION (PCR)

2.5.1 Oligonucleotide primer design and synthesis

Oligonucleotide primers were designed using published sequence data obtained from the Ensembl Genome Browser database (http://www.ensembl.org) or the NCBI GenBank database (http://www.ncbi.nlm.nih.gov). Primers were designed using Primer3 software version 4.0.0 (http://primer3.ut.ee) (Koressaar and Remm 2007) and were subsequently tested for primer-primer complementarity, self-complementarity and melting temperature compatibility using IDT

OligoAnalyzer® software version 3.1 (http://eu.idtdna.com/analyzer/Applications/OligoAnalyzer). Primer sequences were also submitted to the Basic Local Alignment Search Tool (BLAST) (http://www.ncbi.nlm.nih.gov/BLAST) in order to verify the specificity of the primer binding sites. All primers were synthesized using standard phosphoramidite chemistry at Integrated DNA Technologies (IDT, Coralville, Iowa, USA).

2.5.2 Primers for *parkin* exon screening

Primers were designed for the amplification of all twelve *parkin* exons. Primer design was based on *parkin* genomic DNA (gDNA) sequence data obtained from the NCBI GenBank database (accession number NT_007422). These primers were designed to amplify whole exonic sequences by annealing to sites in flanking intronic regions; these primer sequences are shown in Table 2.1.

2.5.3 Primers for reverse-transcription PCR (RT-PCR)

Primers were designed for the amplification of a 555bp fragment of the *parkin* CDS. These primers were designed to recognize cDNA sequences flanking *parkin* exons 3-4, which facilitated exon dosage analysis of exons 3-4 by means of RT-PCR (Section 2.5.5). Primer design was based on *parkin* cDNA sequence data obtained from the Ensembl Genome Browser database (Ensembl ID ENST00000366898). The primer sequences for the amplification of the *parkin* CDS fragment for RT-PCR are shown in Table 2.2.

2.5.4 PCR amplification

PCR amplification of all twelve *parkin* exons was performed in all 229 patients. This was done in order to screen for *parkin* sequence variants by means of HRM analysis (Section 2.6). In addition, PCR amplification was also performed as part of two-step RT-PCR analysis of selected study participants (Section 2.5.5).

In brief, PCR was performed in 25µl reactions in a 2720 Thermal Cycler (Applied Biosystems, Forster City, California, USA), with each reaction mixture containing 10ng template DNA, 20pmol of each primer (Tables 2.1 and 2.2), 1.5mM $MgCl_2$, 75µM dNTPs (Promega, Madison, Wisconsin, USA), 1X NH_4 reaction buffer (Bioline, London, UK) and 0.5 U BIOTAQ DNA polymerase (Bioline, London, UK). A total of 5% formamide was used for selected reactions (Table 2.1). PCR cycling conditions were as follows: an initial denaturation step at 94°C for 5min, 35 cycles consisting of denaturation at 94°C for 30sec, annealing at T_a for 30sec and extension at 72°C for 45sec, and a final extension at 72°C for 7min.

Table 2.1 Primer sequences for *parkin* exon screening

parkin exon	Primer	Sequence (5'-3')	T_a (˚C)	Additive
1	PARK2 1 F	GAACTACGACTCCCAGCAG	55	Formamide
	PARK2 1 R	CCCGTCATTGACAGTTGG		
2	PARK2 2 F	CACCATTTAAGGGCTTCGAG	55	Formamide
	PARK2 2 R	TCAGGCATGAATGTCAGATTG		
3	PARK2 3 F	TCTCGCATTTCATGTTTGACA	55	n/a
	PARK2 3 R	GCAGACTGCACTAAACAAACA		
4	PARK2 4 F	GCTTTTAAAGAGTTTCTTGTC	55	n/a
	PARK2 4 R	TTTCTTTTCAAAGACGGGTGA		
5	PARK2 5 F	GGAAACATGTCTTAAGGAGT	55	n/a
	PARK2 5 R	TTCCTGGCAAACAGTGAAGA		
6	PARK2 6 F	CCAAAGAGATTGTTTACTGTG	55	n/a
	PARK2 6 R	GGGGGAGTGATGCTATTTTT		
7	PARK2 7 F	CCTCCAGGATTACAGAAATTG	55	n/a
	PARK2 7 R	GTTCTTCTGTTCTTCATTAGC		
8	PARK2 8 F	GGCAACACTGGCAGTTGATA	55	n/a
	PARK2 8 R	GGGGAGCCCAAACTGTCT		
9	PARK2 9 F	TCCCATGCACTGTAGCTCCT	55	n/a
	PARK2 9 R	CCAGCCCATGTGCAAAAGC		
10	PARK2 10 F	CCAGCCAGAGGAATGAATAT	53	n/a
	PARK2 10 R	GGAACTCTCCATGACCTCCA		
11	PARK2 11 F	CCGACGTACAGGGAACATAAA	55	n/a
	PARK2 11 R	GGCACGTACAGGGAACATAAA		
12	PARK2 12 F	TCTAGGCTAGCGTGCTGGTT	55	Formamide
	PARK2 12 R	GCGTGTGTGTGTGTTTGA		

Abbreviations: 3', three-prime end; 5', five-prime end; A, adenine; C, cytosine; F, forward primer; G, guanine; n/a, not applicable; PARK2, *parkin* gene; R, reverse primer; T, thymine; T_a, annealing temperature.

Table 2.2 Primer sequences for RT-PCR

Gene	Primer	Sequence (5'-3')	T_a (˚C)
parkin (CDS)	PARK2 2i F	GGAGCTGAGGAATGACTGGA	60
	PARK 5i R	ATCATCCCAGCAAGATGGAC	

Abbreviations: 3', three-prime end; 5', five-prime end; A, adenine; C, cytosine; CDS, coding sequence; F, forward primer; G, guanine; PARK2, *parkin* gene; R, reverse primer; T, thymine; T_a, annealing temperature.

2.5.5 RT-PCR and analysis

RT-PCR was performed on cDNA obtained from lymphocytes of selected study participants found to harbor exonic rearrangements following MLPA analysis (Sections 2.4, 2.8 and 3.1.2). This was done in order to confirm the presence and determine the phase of the detected exonic rearrangements. Amplification was done as described in Section 2.5.4, using 1µl of synthesized cDNA as template and primers listed in Table 2.2. An aliquot of the PCR products were subsequently resolved on a 1% agarose gel (Section 2.10.1). In addition, PCR products were purified and subjected to automated DNA sequencing and sequence analysis (Section 2.7) in order to verify mutation status.

2.6 HIGH-RESOLUTION MELT (HRM) ANALYSIS

Amplified DNA fragments were screened for variants using HRM analysis. This approach quantitatively assessed the melting behavior of double stranded DNA (dsDNA) fragments. As melting behavior of dsDNA fragments is highly dependent on sequence length and content, altered melting behavior can be used as a proxy for DNA sequence changes (Reed et al. 2007).

Prior to HRM analysis, all twelve *parkin* exons were PCR amplified (Section 2.5.4) with the inclusion of 2µM of SYTO® 9 green fluorescent intercalating nucleic acid dye (Life Technologies, Carlsbad, California, USA) in PCR reaction mixtures. PCR setup employed an Eppendorf ep*Motion*™ 5070 automated pipetting system (Eppendorf, Hamburg, Germany) for liquid handling. HRM of PCR products was performed on a Rotor-Gene 6000 analyzer (Corbett Life Sciences, Mortlake, Australia) and Rotor-Gene 6000 software version 1.7.65 (Corbett Life Sciences, Mortlake, Australia). Melting profiles were acquired from 75ºC to 95ºC with a temperature ramp rate of 0.1˚C/sec. The denaturation profiles were subsequently normalized and compared to wild type control samples using the Rotor-Gene 6000 software. Samples demonstrating altered heat denaturation profiles following HRM analysis were subjected to automated DNA sequencing and analysis (Section 2.7).

2.7 AUTOMATED DNA SEQUENCING AND ANALYSIS

Automated DNA sequencing of PCR fragments was performed in order to characterize DNA sequence variants identified by HRM analysis (Section 2.6) and to verify the presence of exonic rearrangements identified by RT-PCR (Section 2.5.5). Selected PCR products were subjected to post-PCR clean-up in preparation of DNA sequencing. This was performed as follows: A total 0.5U each of Exonuclease I (Exo I) (Promega, Madison, Wisconsin, USA) and shrimp alkaline phosphatase (SAP) (Thermo Fisher Scientific, Waltham, Massachusetts, USA) was added to 8µl of PCR product in

a 200µl PCR tube. The mixture was incubated at 37˚C for 15min followed by heat-inactivation at 85˚C for 15min. Cleaned-up PCR products were stored at 4˚C until use.

Automated DNA sequencing of purified PCR products was performed at the Core Sequencing Unit of the Central Analytical Facility (CAF) of Stellenbosch University, Stellenbosch, South Africa using a BigDye® Terminator version 3.01 Cycle Sequencing kit (Applied Biosystems, Forster City, California, USA) on an ABI Prism™ 3100 automated sequencer (Applied Biosystems, Forster City, California, USA). Primers used in these sequencing reactions are listed in Tables 2.1 and 2.2.

DNA sequencing electropherograms obtained from automated DNA sequencing were analyzed using Bioedit Sequence Alignment Editor Software version 7.0.5 (Ibis Bioscience, Carlsbad, California, USA) (Hall 1999). PCR fragments were compared to DNA sequences deposited in the Ensembl Genome Browser database (http://www.ensembl.org) and the NCBI GenBank database (http://www.ncbi.nlm.nih.gov). All sequence variants were characterized according to established nomenclature (den Dunnen and Antonarakis 2000). Possible consequences of coding non-synonymous variants on parkin protein function were bioinformatically predicted with PolyPhen-2 software version 2.2.2 (http://genetics.bwh.harvard.edu/pph2) (Adzhubei et al. 2010) and MutationTaster software version 2.0 (http://www.mutationtaster.org) (Schwarz et al. 2010).

2.8 MULTIPLEX LIGATION-DEPENDENT PROBE AMPLIFICATION (MLPA) ANALYSIS

Exon rearrangements, resulting in exon dosage mutations, were detected by multiplex ligation-dependent probe amplification (MLPA) analysis. These assays were done by Dr. Rowena Keyser.

MLPA assays were performed using the P051 and the P052 Salsa® MLPA Parkinson probe sets (MRC Holland, Amsterdam, The Netherlands). Both kits included probes for all twelve *parkin* exons; true positive results needed to be detected in both kits. MLPA was performed using 150ng of gDNA according to manufacturer's instructions. MPLA products were analyzed on an ABI 3130x1 Genetic Analyzer (Applied Biosystems, Forster City, California, USA) using GeneScan™-500 LIZ® size standards (Applied Biosystems, Forster City, California, USA), with MLPA peaks visualized using GeneMapper® software version 3.7 (Applied Biosystems, Forster City, California, USA). Thereafter, peak height and area values were exported to a Microsoft Excel template. Data normalization and dosage calculations were performed according to manufacturer's instructions (MRC Holland, Amsterdam, The Netherlands). Dosage ratio values of 0.7-1.3 were considered to be normal (indicating the absence of exon rearrangements); values of 0.3-0.6 were indicative of heterozygous deletions, 1.4-1.6 of heterozygous duplications and a dosage ratio value ≥1.7 of triplications. Homozygous deletions were detected by the absence of a peak (dosage ratio value = 0.0).

PART TWO: PARKIN INTERACTORS

This second part of the dissertation deals with the identification, verification and investigation of parkin-interacting proteins. This entailed the identification of putative parkin interactors using Y2H methodology (Section 2.19), verification of selected putative interactions using *in vivo* 3D co-localization (Section 2.22) and co-immunoprecipitation (Section 2.24), as well the establishment of two cell models of parkin deficiency, a RNAi-mediated parkin knockdown neuronal model and a parkin-null primary fibroblast model, in order to study the effect of the lack of parkin on each interacting protein (Section 2.25).

2.9 POLYMERASE CHAIN REACTION (PCR)

2.9.1 Primers for generation of yeast two-hybrid (Y2H) construct

Oligonucleotide primers were designed for the specific amplification of the cDNA fragment encoding the C-terminal region of parkin (aa 223-465). Primer design was based on *parkin* cDNA sequence data obtained from the Ensembl Genome Browser database (Ensembl ID ENST00000366898). The primers incorporated restriction enzyme (RE) recognition sites at their respective 5' ends, which allowed for subsequent subcloning of PCR amplified inserts into the pGBKT7 vector (Section 2.13). The use of these RE sites was dependent on their presence in the multiple cloning site (MCS) of the pGBKT7 vector (appendix V) and their absence in the *parkin* insert sequence. In addition, primers incorporated universal "seat" sequences 5' to their respective RE sites to facilitate proper RE binding and digestion (Section 2.12). Primer design and synthesis is described in Section 2.5.1. The primer sequences for the amplification of the *parkin* insert for the generation of Y2H constructs are shown in Table 2.3.

Table 2.3 Oligonucleotide primer sequences for generation of Y2H construct

Primer	Sequence (5'-3')	T_a (°C)
PARK2 RBR F	ACTGCAGAA CATATG TCAGTAGCTTTGCACCTGATCG	57
PARK2 FL R	ACTGCAGAA GAATTC CTACACGTCGAACCAGTGG	

Sequences in black font represent gene-specific primer sequences that anneal to cDNA template during PCR amplification. Sequences in colored font represent sequences for cloning. Blue, universal enzyme seat; pink, *NdeI* recognition site; green, *EcoRI* recognition site. Abbreviations: 3', three-prime end; 5', five-prime end; A, adenine; C, cytosine; F, forward primer; FL, full length; G, guanine; PARK2, *parkin* gene; R, reverse primer; RBR, RING1-between RINGS-RING2; T, thymine; T_a, annealing temperature; Y2H, yeast two hybrid.

2.9.2 Primers for Y2H insert screening

Vector-specific oligonucleotide primers were designed for the amplification of vector inserts from the MCS of the Y2H vectors pGBKT7 (BD Biosciences, Clontech, Paulo Alto, California, USA) and pGADT7 (BD Biosciences, Clontech, Paulo Alto, California, USA). This was necessary for the DNA sequence identification of insert fragments by means of automated DNA sequencing and sequence analysis (Section 2.11). The vector sequences used in the design of the primers were obtained from the Clontech MATCHMAKER™ vector handbook (http://www.clontech.com). The sequences of these primers are shown in Table 2.4.

Table 2.4 Primer sequences for Y2H construct insert screening

Vector	Primer	Sequence (5'-3')	T_a (˚C)
pGBKT7	pGBKT7 F	TCATCGGAAGAGAGTAG	45
	pGBKT7 R	TCACTTTAAAATTTGTATACA	
pGADT7	pGADT7 outer F	CGATGATGAAGATACCCCACCAAA	57
	pGADT7 outer R	TCAAGTGAAGTTGACAGCTAGCAC	
	pGADT7 inner F	TAATACGACTCACTATAGGGCGAGC	59
	pGADT7 inner R	CGACGTCTACTTAGCATCTATGACTTT	

Abbreviations: 3', three-prime end; 5', five-prime end; A, adenine; C, cytosine; F, forward primer; G, guanine; R, reverse primer; T, thymine; T_a, annealing temperature; Y2H, yeast two hybrid.

2.9.3 Primers for construct integrity verification

Constructs used in establishing a Y2H bait culture (Section 2.19.2) were first subjected to automated DNA sequencing and DNA sequence analysis (Section 2.11). This was done in order to verify the integrity of the vector inserts. Primers used for these purposes are listed in Table 2.5.

Table 2.5 Primer sequences for construct integrity verification

Vector	Primer	Sequence (5'-3')
pGBKT7-*parkin*	pGBKT7 F	TCATCGGAAGAGAGTAG
(C-terminal region)	pGBKT7 R	TCACTTTAAAATTTGTATACA

Abbreviations: 3', three-prime end; 5', five-prime end; A, adenine; C, cytosine; C-terminal, carboxy-terminal; F, forward primer; G, guanine; R, reverse primer; T, thymine.

2.9.4 PCR amplification for generation of Y2H construct

PCR was used to amplify the C-terminal-encoding region of the *parkin* CDS from a fetal human brain cDNA library. Subsequently the cDNA fragment was cloned into the pGBKT7 Y2H vector (Section 2.13).

For amplification of this cDNA fragment, 50ng of a fetal human brain library (BD Bioscience, Clontech, Palo Alto, California, USA) was used as template in a 25µl reaction containing 20pmol of each primer (Table 2.3), 1.5mM $MgCl_2$, 75µM dNTPs (Promega, Madison, Wisconsin, USA), 1X NH_4 reaction buffer (Bioline, London, UK) and 0.5U BIOTAQ® DNA polymerase (Bioline, London, UK).

Amplification was performed in a ABI 2720 Thermal Cycler (Applied Biosystems Inc., Foster City, California, USA) under the following thermal cycling conditions: an initial denaturing step at 94˚C for 5min followed by 35 cycles consisting of denaturation at 94˚C for 45sec, annealing at T_a for 45sec and elongation at 72˚C for 1min. Cycling was followed by a final extension step at 72˚C for 10min. PCR amplification products were subsequently electrophoresed on a 1% agarose gel for verification (Section 2.10.1)

2.9.5 Bacterial colony PCR

Bacterial colony PCR was employed to rapidly identify transformed bacterial colonies containing recombinant pGBKT7 with a correctly ligated *parkin*-CDS insert. This was necessary as the Y2H constructs do not allow for blue-white colony screening.

A small quantity of a single bacterial colony was picked from an agar plate and used a DNA template in the PCR amplification. The same primers used for the generation of the Y2H construct (Table 2.3) were utilized for bacterial colony PCR, which followed identical PCR conditions and cycling parameters as described above (Section 2.9.4). PCR amplification products were subsequently electrophoresed on a 1% agarose gel for verification (Section 2.10.1). Successful bacterial colony PCR amplification using primers listed in Table 2.3 indicated correct ligation of the *parkin*-CDS insert into pGBKT7.

2.10 GEL ELECTROPHORESIS

2.10.1 Agarose gel electrophoresis

Agarose gel electrophoresis was performed in order to visualize successful PCR amplification (Section 2.9.4) and to confirm successful plasmid isolation (Section 2.17.2). Electrophoresis was performed as follows: a 1-2% agarose gel, depending on the size of the DNA fragment, containing 1µg/ml ethidium bromide was cast and submerged in 1X sodium tetraborate (SB) buffer (Appendix II). A total of 8µl of each PCR product was individually mixed with 2µl bromophenol blue loading dye (Appendix II) and loaded into separate wells. A 100bp molecular size marker (Promega, Madison, Wisconsin, USA) was co-electrophoresed with the DNA fragments in order to facilitate fragment size estimation. Electrophoresis followed at 240V for approximately 20min in 1X SB buffer. Subsequently, the samples were visualized and photographed in a SynGene UV gel documentation system (Synoptics Ltd., Cambridge, UK) using GeneTools software version 3.0.6 (Synoptics Ltd., Cambridge, UK).

Agarose gel electrophoresis was also employed to separate RE digested PCR fragments (Section 2.12) in order to excise the RE digested fragments for subsequent purification (Section 2.17.1). For these applications, a total of 24µl digested product was mixed with 6µl bromophenol blue loading dye resolved in a similar manner as described above. Samples were visualized by means of a long-wave 3UV transilluminator (UVP, Upland, California, USA) and the appropriate band was excised from the gel using a sterile scalpel blade. The excised band was subsequently purified using a Wizard® SV Gel and PCR clean-up kit (Promega, Madison, Wisconsin, USA) (Section 2.17.1).

2.10.2 Sodium dodecyl sulfate (SDS) polyacrylamide gel electrophoresis (SDS-PAGE)

SDS-polyacrylamide gel electrophoresis (SDS-PAGE) was used for the size-dependent separation of proteins either obtained from a whole cell extract (Section 2.23.1) or from immunoprecipitation (IP) or co-immunoprecipitation (co-IP) reactions (Section 2.24). SDS-PAGE was performed in 100x80x1mm 12% polyacrylamide gels containing 0.1% SDS (Appendix II) for selected applications. Alternatively, 4-15% Mini-Protean® TGX™ precast gels (Bio-Rad, Hercules, California, USA) were used. Samples to be resolved were mixed with an appropriate volume of 2X or 5X SDS loading buffer (Appendix II) and incubated at 95˚C for 10min. The samples were then centrifuged at 15 000rpm for 1min in a Labnet Prism™ microcentrifuge (Labnet, Edison, New Jersey, USA). Subsequently, samples were loading into separate gel wells and electrophoresed in 1X SDS running buffer (Appendix II) at 100V for 1.5 - 2h. When 4-15% Mini-Protean® TGX™ precast gels were used, electrophoresis followed at 150V for 45min. A total of 7µl of Spectra™ Broad Range Multicolor protein ladder (Thermo Scientific, Waltham, Massachusetts, USA) was co-electrophoresed with the

samples. Protein samples were then transferred to a polyvinylidene difluoride (PVDF) membrane (Section 2.10.3) for downstream western blotting (Section. 2.23).

2.10.3 Transfer of proteins from SDS polyacrylamide gels to PVDF membrane

Proteins separated by SDS-PAGE were electrophoretically transferred to a PVDF membrane, to be used during western blotting (Section 2.23). This was done using the iBlot™ Dry Blotting System (Life Technologies, Carlsbad, California, USA) along with iBlot™ PVDF Gel Transfer Stacks (Life Technologies, Carlsbad, California, USA), according to manufacturer's instructions.

Alternatively, proteins were transferred to a PVDF membrane following a wet transfer approach: After SDS-PAGE was completed, the gels were retrieved and briefly rinsed in ddH_2O by shaking for 5min on an Stuart® orbital shaker SSL1 (Bibby Scientific Ltd., Stone, Staffordshire, UK) at room temperature. The gel was then immersed in ice-cold transfer buffer (Appendix II) and left shaking for an additional 20min. During this time, a PDVF membrane (GE Healthcare Ltd., Little Chalfont, Buckinghamshire, UK) was prepared by activating the membrane in absolute methanol for 15sec followed by rinsing with ddH_2O for 5min. The membrane was then also soaked in ice-cold transfer buffer for 20min, along with six equal-sized Whatman papers and two sponges per membrane. A transfer stack was then assembled consisting of a sponge and three Whatman papers on either side of the stack, with the gel (on the anode side) and the activated membrane (on the cathode side) in the middle. The transfer stack was placed in a tank filled with transfer buffer and containing an ice pack, and electrophoresed at 100V for 1h with constant stirring. The stack was disassembled and the membrane briefly rinsed in ddH_2O prior to further use (Section 2.23.4).

2.11 AUTOMATED DNA SEQUENCING AND ANALYSIS

Automated DNA sequencing of construct inserts was performed in order to identify the insert sequence or to verify the insert sequence integrity. This was done at the Core Sequencing Unit of CAF at Stellenbosch University, Stellenbosch, South Africa using a BigDye® Terminator version 3.01 Cycle Sequencing kit on an ABI Prism™ 3100 automated sequencer. Vector-specific primers (Tables 2.4 and 2.5) were used for these sequencing reactions.

DNA sequencing electropherograms obtained from automated DNA sequencing were analyzed using Bioedit Sequence Alignment Editor Software version 7.0.5. The generated Y2H construct (Section 2.13) was analyzed to confirm insert integrity; this was done to verify that the correct reading frame of the vector, as well as the correct CDS of the insert, were maintained during cloning. Insert

sequences were compared to cDNA sequences deposited in the Ensembl Genome Browser database (http://www.ensembl.org).

DNA sequences of Y2H prey construct inserts were entered into BLAST and compared to cDNA and messenger RNA (mRNA) sequences in GENBANK using a BLASTn query (http://www.ncbi.nlm.nih.gov/BLAST) in order to identify the prey insert. Moreover, each insert DNA sequence was translated in the correct reading frame using DNAMAN™ Software version 4.1 (Lynnon Biosoft, Pointe-Claire, Canada), after which the corresponding protein sequences were analyzed using a BLASTp query (http://www.ncbi.nlm.nih.gov/BLAST). A list of the protein products of the prey insert was compiled, after which publicly available databases such as ExPASy http://www.expasy.org), GeneCards (http://www.genecards.org) and the Human Protein Atlas (http://www.proteinatlas.org) were used to obtain relevant information regarding the function and subcellular expression of the proteins.

2.12 RESTRICTION ENZYME DIGESTION

In order to facilitate cloning of the DNA fragment encoding the C-terminal region of *parkin* into the pGBKT7 Y2H shuttle vector, the PCR amplified fragment harbored restriction enzyme (RE) recognition sites on either end (Section 2.9.1; Table 2.3). The PCR fragments as well as the vector were separately double-digested with two RE's: *NdeI* and *EcoRI*.

Double digestion was performed as follows: a first digestion RE (*NdeI*) cocktail of final volume 20µl was prepared containing either 5µl purified vector (Section 2.17.2) or 15µl purified insert fragments (Section 2.17.1), 2U *NdeI* and 1X RE buffer supplied by the manufacturer (Fermentas, Burlington, Canada). The cocktail was incubated for 3h at 37˚C in a Scientific 9000 Series incubator (United Scientific, Cape Town, South Africa) followed by heat-inactivation for 15min at 65˚C. Digested products were then purified using the Wizard SV® Gel and PCR clean-up system (Section 2.17.1) and eluted in a volume of 30µl ddH_2O. Thereafter, a second RE digestion *(EcoRI)* cocktail of final volume 20µl was prepared containing 16µl purified *NdeI*-digested fragments, 2U *EcoRI* and 1X RE buffer (Fermentas, Burlington, Canada). The cocktail was incubated for 3h at 37˚C in a Scientific 9000 Series incubator (United Scientific, Cape Town, South Africa) followed by heat-inactivation for 15min at 65˚C. Digested products were then purified using the Wizard SV® Gel and PCR clean-up system (Section 2.17.1) and eluted in a volume of 50µl ddH_2O. Double-digested vector and insert fragment were subsequently used in the generation of Y2H constructs (Section 2.13).

2.13 GENERATION OF Y2H CONSTRUCT

The C-terminal region of *parkin* was cloned into the pGBKT7 shuttle vector in order to generate the Y2H bait construct. Both the PCR fragments (Section 2.9.4) and the pGBKT7 Y2H bait vector (Appendix V) were first double-digested with appropriate RE's (Section 2.12) in order to facilitate cloning of the insert sequence in the correct orientation.

The digested and purified vector was then subjected to calf intestinal alkaline phosphatase (CIP) treatment to dephosphorylate 5' ends of the linearized vector, which prevented self-ligation of the vector. This was not done to digested PCR fragments. CIP treatment was performed as follows: a cocktail of volume 50 µl was prepared containing 30µl double-digested and purified vector, 2U CIP and 1X CIP buffer supplied by the manufacturer (Promega, Madison, Wisconsin, USA). The cocktail was incubated for 30min at 37˚C in a Scientific 9000 Series incubator (United Scientific, Cape Town, South Africa) after which an additional 2U SIP was added to the cocktail. This was followed by further incubation for 30min at 37˚C and heat-inactivation for 20min at 65˚C. The vector was then purified using the Wizard SV® Gel and PCR clean-up system (Section 2.17.1.).

Thereafter, DNA ligation of double-digested PCR fragments and linearized vector was performed in order to generate the pGBKT7-*parkin* Y2H bait construct. Briefly, 1µl of CIP-treated vector was added to 1µl, 3µl or 5µl digested PCR fragments (Section 2.12). This was added to a cocktail of final volume 10µl additionally consisting of 5U T4 DNA ligase and 1X T4 DNA ligase buffer (Promega, Madison, Wisconsin, USA). The cocktail was incubated at 4˚C overnight (16h), after which 5µl of the ligation reaction was used in a bacterial plasmid transformation (Section 2.16.1).

Following retrieval of the generated construct by means of bacterial colony PCR (Section 2.9.5) and bacterial plasmid purification (Section 2.17.2), the construct was subjected to DNA sequencing and analysis to verify insert integrity (Sections 2.11). Only constructs in which the correct reading frame and insert CDS were maintained during cloning were used to transform the *S. cerevisiae* strain AH109 (Section 2.16.2).

2.14 BACTERIAL AND YEAST STRAINS

2.14.1 Bacterial strains

Escherichia coli (*E. coli*) strain DH5α (Appendix IV) was transformed in order to facilitate selection, amplification and purification of constructs. Transformed bacterial colonies were selected for their ability to grown on Luria-Bertani (LB) agar plates (Appendix II) containing the appropriate selection antibiotic. For selection of pGBKT7 constructs, kanamycin (5µg/ml) was used, while ampicillin

(25µg/ml) was used to select for pGADT7 constructs. Bacterial colony PCR was performed to identify colonies containing recombinant constructs (Section 2.9.5).

2.14.2 Yeast strains

The pGBKT7-*parkin* Y2H bait construct was transformed into *Saccharomyces cerevisiae* (*S. cerevisiae*) strain AH109 (Appendix IV). *S. cerevisiae* strain Y187 (Appendix IV) was pre-transformed with pGADT7 Y2H prey constructs by the manufacturer (BD Biosciences, Clontech, Palo Alto, California, USA). Both yeast strains AH109 and Y187 lack the nutritional genes *ADE2*, *HIS3*, *LEU2* and *TRP1* and are therefore unable to growth in synthetic defined (SD) media deficient in adenine (-Ade), histidine (-His), leucine (-Leu) and tryptophan (-Trp) (Appendix II). AH109 transformed with the pGKBT7 construct was selected based on the ability to grow in SD^{-Trp} media, while Y187 transformed with pGADT7 constructs were selected on the ability to grow in SD^{-Leu} media.

2.15 GENERATION OF BACTERIAL COMPETENT CELLS

In order to generate transformation-competent bacterial cells, the following procedure was performed: A 50µl aliquot of an *E. coli* DH5α frozen (-80˚C) glycerol stock was used to inoculate 10ml of antibiotic-free LB media (Appendix II). The culture was then incubated overnight (16h) at 37˚C while shaking at 200rpm in a YIH DER model LM-530 shaking incubator (Scilab Technology Co. Ltd., Taipei, Taiwan).

The following day, 1ml of the culture was used to inoculate 200ml antibiotic-free LB media in a 2L Erlenmeyer flask, which was incubated for 16-24h at room temperature while shaking at 70rpm on a Stuart® orbital shaker SSL1 (Bibby Scientific Ltd., Stone, Staffordshire, UK), until the culture reached mid-logarithmic (log) phase (OD_{600nm}= 0.4-0.6). The culture was then transferred to four 50ml polypropylene tubes and centrifuged at 3000rpm for 15min at 4˚C in a Beckman model TJ-6 centrifuge (Beckman Coulter, Pasadena, California, USA). The supernatant was discarded and the pellets resuspended in 4ml of ice-cold CAP buffer (Appendix II). This suspension was aliquoted in 200µl volumes into 2ml microcentrifuge tubes, which were left at 4˚C overnight before being transferred to -80˚C for long-term storage.

2.16 TRANSFORMATION OF PLASMIDS INTO BACTERIAL AND YEAST CELLS

2.16.1 Bacterial plasmid transformation

In preparation of a bacterial plasmid transformation, frozen (-80˚C) microcentrifuge tubes containing 200µl aliquots of competent *E. coli* DH5α cells (Section 2.15) were thawed on ice for approximately 30min. To this, 1µl of purified plasmid (Section 2.17.1) or 5µl ligation reaction (Section 2.13) was added and the tubes incubated on ice for a further 20min. The tubes were subsequently immersed in a Lasec 102 circulating water bath (Lasec Laboratory and Scientific Co. Ltd. Pty, Cape Town, South Africa) at 42˚C for 45sec. Tubes were removed from the water bath and left at room temperature for 2min. Thereafter, 1ml of antibiotic free LB media (Appendix II) was added to each tube and the cultures incubated at 37˚C for 1h while shaking at 200rpm in a YIH DER model LM-530 shaking incubator.

A total of 200µl of the culture was plated on LB agar plates containing the appropriate selection antibody (Appendix II). The remaining culture was centrifuged at 15 000rpm for 1min in a Labnet Prism™ microcentrifuge (Labnet, Edison, New Jersey, USA). The supernatant was discarded and the pellet resuspended in 200µl LB media, after which the concentrated culture was plated on LB agar plates containing the appropriate selection antibody. All plates were incubated, inverted, overnight (16h) at 37˚C in a model 239 CO_2 stationary incubator (Forma Scientific, Marietta, Ohio, USA). The following day, colonies were picked for bacterial plasmid purification (Section 2.17.2) or colony PCR (Section 2.9.5).

2.16.2 Yeast plasmid transformation

S. cerevisiae strains to be transformed were streaked from frozen (-80˚C) glycerol stocks onto yeast peptone dextrose adenine (YPDA) agar plates (Appendix II), which were then incubated at 30˚C for 3-4 days in a Sanyo MIR262 stationary ventilated incubator (Sanyo Electric, Moriguchi, Osaka, Japan).

Several large yeast colonies were picked with a sterile inoculation loop and suspended in 1ml ddH_2O in a 2ml microcentrifuge tube. The cells were centrifuged for 30sec at 15 000rpm in an Eppendorf model 5417C centrifuge and the supernatant discarded. The pellet was resuspended in 1ml of 100mM lithium acetate (LiAc) (Appendix II) and the suspension incubated at 30˚C for 5min in a Sanyo MIR262 stationary ventilated incubator. The cells were subsequently repelleted via centrifugation at 15 000rpm for 30sec in an Eppendorf model 5417C centrifuge and the supernatant discarded. The following reagents were added to the pellet in quick succession: 240µl of 50% polyethylene glycol (PEG), 36µl of 1M LiAc (Appendix II), 25µl of 2mg/ml heat-denatured and snap-cooled herring

sperm DNA (Promega, Madison, Wisconsin, USA), 10-20µl purified plasmid and ddH_2O to a final volume of 350µl. The sample was then thoroughly mixed by vortexing for at least 1min on a Snijders model 34524 press-to-mix vortex (Snijders Scientific, Tilburg, the Netherlands). After the pellet was fully resuspended, the sample was incubated at 42˚C for 25min in a Lasec 102 circulating water bath.

After incubation, the sample was centrifuged at 15 000rpm for 30sec in an Eppendorf model 5417C centrifuge and the supernatant discarded. The pellet was resuspended in 200µl ddH_2O and the suspension plated on appropriate agar selection plates (Appendix II). All plates were inverted and incubated at 30˚C in a Sanyo MIR262 stationary ventilated incubator for 3-4 days.

2.17 DNA ISOLATION AND PURIFICATION

2.17.1 DNA purification from agarose gels

In order to purify yeast plasmid preparations (Section 2.17.3), PCR amplified DNA products (Section 2.9.4) and RE digestion products (Section 2.12) a Wizard® SV Gel and PCR Clean-up Kit (Promega, Madison, Wisconsin, USA) was used according to manufacturer's instructions. Purified product was used for bacterial plasmid transformation (Section 2.16.1) or cloning experiments (Sections 2.12 and 2.13), or stored at 4˚C.

2.17.2 Bacterial plasmid purification

Bacterial plasmid purification was performed to obtain DNA constructs for subsequent yeast transformation (Section 2.16.2) and automated DNA sequencing and analysis (Section 2.11). A single transformed bacterial colony was picked from appropriate selection plates and used to inoculate 10ml of LB media containing the appropriate selection antibody (Appendix II) in a 50ml polypropylene tube. The tube was incubated overnight (16h) at 37˚C while shaking at 200rpm in a YIH DER model LM-530 shaking incubator.

The culture was then centrifuged at 3000rpm for 10min a Beckman model TJ-6 centrifuge. The supernatant was discarded and plasmid DNA extracted using a TOpure™ Plasmid Miniprep Kit (Gene Technologies, Hong Kong, China) according to manufacturer's instructions. Subsequently, DNA concentration and purity was determined using a NanoDrop® ND-1000 spectrophotometer and NanoDrop1000® software version 3.7.1. Additionally, an aliquot of the purified construct was electrophoresed on a 1% agarose gel (Section 2.10.1) to visually verify plasmid integrity.

2.17.3 Yeast plasmid extraction

Y2H constructs were extracted from diploid yeast colonies to be used in bacterial plasmid transformations (Section 2.16.1). A yeast colony was picked with a sterile inoculation loop and used to inoculate 1ml of SD media containing the appropriate dropout supplement (BD Biosciences, Clontech, Palo Alto, California, USA), which was thereafter incubated overnight (16h) at 30˚C while shaking at 150rpm in a Labnet 311DS shaking incubator (Labnet, Edison, New Jersey, USA).

The following morning, 4ml of YPDA media (Appendix II) was added to the culture, which was then incubated for an additional 4h at 30˚C with shaking at 150rpm. The culture was subsequently centrifuged at 3000rpm for 5min in a Beckman model TJ-6 centrifuge and the supernatant discarded by decanting. The pellet was resuspended in residual supernatant and transferred to a 2ml microcentrifuge tube. To this, 200µl of yeast lysis buffer (Appendix II), 200µl of phenol:chloroform:isoamyl alcohol 25:24:1 (PCI) (Sigma Aldrich, St. Louis, Missouri, USA) and 300mg sterile 450µm-600µm glass beads (Sigma Aldrich, St. Louis, Missouri, USA) were added. Yeast cells were then triturated by uninterrupted vortexing for 2.5min on a Snijders model 34524 press-to-mix vortex and centrifuged at 15 000rpm for 10min in an Eppendorf model 5417C centrifuge (Eppendorf, Hamburg, Germany) to facilitate phase separation. The upper aqueous phase was transferred to a sterile microcentrifuge tube and the plasmids purified as described in Section 2.17.1.

2.18 ASSESSMENT OF Y2H CONSTRUCTS

2.18.1 Phenotypic assessment of yeast strains

S. cerevisiae strains AH109 and Y187 were phenotypically assessed prior to being transformed with Y2H constructs (Section 2.16.2), in order to verify purity and viability of the strain. This was accomplished by streaking selected colonies grown on YPDA plates on selective plates lacking specific essential amino acids, i.e. SD^{-Trp}, SD^{-Leu}, SD^{-His}, SD^{-Ade} and SD^{-Ura} agar plates (Appendix II). All plates were then inverted and incubated at 30˚C in a Sanyo MIR262 stationary ventilated incubator for 3-4 days. Only untransformed colonies that were unable to grow on SD^{-Trp}, SD^{-Leu}, SD^{-His} and SD^{-Ade} plates but did grow on SD^{-Ura} plates were used in subsequent yeast transformations (Section 2.16.2).

An additional phenotypic assessment was done on transformed AH109 harboring the pGBKT7-*parkin* Y2H bait construct, in order to test for autonomous activation of Y2H reporter genes by the bait construct and to ensure that transformation did not alter the strain phenotype improperly. Only transformed AH109 colonies that were unable to grow on SD^{-Leu}, SD^{-His} and SD^{-Ade} plates but did grow on SD^{-Trp} and SD^{-Ura} plates were used in subsequent Y2H analysis (Section 2.19).

2.18.2 Yeast transformation toxicity test

An evaluation of yeast transformation toxicity was performed prior to Y2H analysis to determine whether the Y2H bait construct detrimentally affected the growth of *S. cerevisiae* strain AH109. To this end, a growth curve of AH109 transformed with the pGBKT7-*parkin* bait construct was generated and compared to a growth curve of AH109 transformed with non-recombinant pGBKT7. The two growth curves were set up in tandem under similar experimental conditions.

The two transformed strains were each inoculated in 1ml of SD^{-Trp} media in 50ml polypropylene tubes and growth to stationary phase for 24h at 30˚C while shaking at 200rpm in a Labnet 311DS shaking incubator. A 1:10 dilution in SD^{-Trp} media was made of both cultures, which were incubated for a further 24h at 30˚C while shaking at 200rpm in a Labnet 311DS shaking incubator. During this incubation period, 1ml aliquots of the cultures were taken and the OD_{600nm} measurements recorded at time points 0h, 2h, 4h, 6h, 8, and 24h. Linearized growth curves were established by charting the log of these measurements against time and the gradients of the two graphs, recombinant and non-recombinant transformed AH109, were compared. Significant differences in growth of the two transformed strains would preclude the use of the pGBKT7-*parkin* bait construct in Y2H analysis (Section 2.19).

2.18.3 Establishment of yeast mating efficiency

Small scale yeast matings were performed to evaluate the effect of the Y2H bait construct on *S. cerevisiae* strain AH109 mating efficiency. This was done by mating AH109, transformed with the pGBKT7-*parkin* bait construct, with the prey host strain Y187 transformed with non-recombinant pGADT7. A positive control mating was also performed between AH109 transformed with control construct pGBKT7-53 (containing murine p53) (BD Biosciences, Clontech, Palo Alto, California, USA) and Y187 transformed with non-recombinant pGADT7.

The various strains were plated on appropriate selection plates (AH109 transformed with pGBKT7-*parkin*; pGBKT7-53 = SD^{-Trp} plates; Y187 transformed with pGADT7 = SD^{-Leu} plates). All plates were inverted and incubated at 30˚C in a Sanyo MIR262 stationary ventilated incubator for 3-4 days. Singles colonies of both AH109 strains were separately picked and combined with Y187 colonies in 1ml YPDA media in a 2ml microcentrifuge tube, which were incubated overnight (16h) at 30˚C in a Labnet 311DS shaking incubator, shaking at 200rpm. After this incubation period, serial dilutions (1:10, 1:100, 1:1000 and 1:10 000) of the mating culture were plated onto SD^{-Leu}, SD^{-Leu} and $SD^{-Leu-Trp}$ plates and incubated inverted for 3-4 days at 30˚C in a Sanyo MIR262 stationary ventilated incubator. The colonies on each plate were counted and the yeast mating efficiency calculated (Appendix III).

2.19 YEAST TWO-HYBRID (Y2H) ANALYSIS

Y2H analysis was employed in the present study to identify physical interactions between two proteins. This methodology exploits the two functional domains of the *S. cerevisiae* galactose metabolism transcription factor GAL4, namely the GAL4 DNA binding domain (DNA-BD) and the GAL4 activation domain (AD). Whereas both domains are necessary for proper activation of the galactose metabolism gene *GAL* promoter, the modular nature of GAL4 allows for the two domains to function in proximity to each other without direct binding. Hence, the GAL4 DNA-BD and AD can be separately expressed from engineered constructs as fusion proteins and still activate the *GAL* promoter provided that the two domains indirectly reconstitute the GAL4 transcription factor (Keegan et al. 1986).

In Y2H, the protein fused to the DNA-BD is referred to as the bait protein (the C-terminal region of parkin in the present study) while the protein fused to the AD is referred to as the prey protein (members of a library of brain-expressed proteins in the present study). Co-transformation of bait- and prey-expressing Y2H constructs into yeast strains allows for possible physical interactions between bait and prey proteins to be evaluated: if binding takes place between the bait and prey fusion proteins, the GAL4 DNA-BD and AD is brought into sufficient proximity for the successful activation of the *GAL* promoter. Positive bait-prey interactions are then detected by transcription of downstream reporter genes. If no binding takes place between the bait and prey proteins, the reporter genes are not expressed; interaction detection is therefore based on observable changes in the yeast phenotype. Three reporter genes are utilized in the present study: the *HIS3* and *ADE2* nutritional reporter genes and the *MEL1* colorimetric reporter gene.

2.19.1 Adult human brain cDNA library

A Clontech MATCHMAKER™ adult human brain cDNA library, consisting of brain-expressed cDNA sequences cloned into the pGADT7 Y2H prey vector (Appendix V), was pre-transformed into *S. cerevisiae* strain Y187 by the manufacturer (BD Biosciences, Clontech, Palo Alto, USA) and used in a Y2H library screen. This library was constructed from mRNA isolated from normal, whole brains of eight male Caucasian individuals of ages 43-66 years. Cause of death of all eight individuals was sudden death. The cDNA was normalized prior to library construction to reduce the copy number of highly abundant CDNAs. The cDNA library inserts ranged in size from 700bp to 3kb, with an average insert size of 1.56kb.

2.19.2 Establishment of the bait culture

Four separate colonies of *S. cerevisiae* strain Y187 transformed with pGBKT7-*parkin* (Section 2.16.2) were picked using a sterile inoculation loop and used to inoculate four 200ml Erlenmeyer flasks each containing 50ml of SD^{-Trp} media, which were incubated overnight (16h) at 30˚C while shaking at 200rpm in a Labnet 311DS shaking incubator. The cultures were then transferred to four 50ml polypropylene tubes, centrifuged at 3000rpm for 10min in a Beckman model TJ-6 centrifuge and the supernatant discarded by decanting. The pellets were resuspended in residual supernatant and pooled to provide a final bait culture titer greater than 1×10^{10}, as confirmed by a hemocytometric cell count (Appendix III).

2.19.3 Library mating

In preparation of library mating, a 1ml aliquot of a frozen (-80˚C) pre-transformed Clontech MATCHMAKER™ adult human brain cDNA library (Section 2.19.1) was thawed at room temperature and, after brief mixing, a 10µl aliquot was set aside to establish a library titer (Section 2.19.4).

The bait (Section 2.19.2) and library cultures were combined in a 2L Erlenmeyer flask containing 45ml of 2X YPDA media (Appendix II), which was incubated overnight (16h) at 30˚C with gentle shaking at 50rpm in a YIH DER model LM510R shaking incubator (Scilab Technology Co. Ltd., Taipei, Taiwan).

The mating culture was then transferred to a 50ml polypropylene tube, centrifuged at 3000rpm for 10min in a Beckman model TJ-6 centrifuge and the supernatant discarded. The 2L Erlenmeyer flask was rinsed with 40ml of 2X YPDA media which was subsequently used to resuspend the pelleted culture. The mating culture was repelleted by centrifugation at 3000rpm for 10min in a Beckman model TJ-6 centrifuge and the supernatant discarded. This rinsing and centrifuging process was repeated once more, with the final pellet resuspended in 10ml of 0.5X YPDA (Appendix II). A 10µl aliquot of the mating culture was set aside for a control mating experiment (Section 2.19.5).

The total remaining volume of the mating culture was then plated on multiple (approximately 60) triple dropout (TDO) ($SD^{-Leu-Trp-His}$) plates (Appendix II) with a volume of 200µl used on each plate. All plates were inverted and incubated at 30˚C in a Sanyo MIR262 stationary ventilated incubator for 3 weeks.

2.19.4 Establishment of library titer

A 10µl aliquot of the adult brain cDNA library culture (Section 2.19.3) was serially diluted (1:10, 1:100, 1:1000 and 1:10 000), plated onto SD^{-Leu}, SD^{-Leu} and $SD^{-Leu-Trp}$ plates and incubated inverted for 3-4 days at 30˚C in a Sanyo MIR262 stationary ventilated incubator. The colonies on each plate were counted and the library titer calculated (Appendix III).

2.19.5 Control mating

A 10µl aliquot of the library mating culture (Section 2.19.3) was serially diluted (1:10, 1:100, 1:1000 and 1:10 000) and plated onto SD^{-Leu}, SD^{-Leu} and $SD^{-Leu-Trp}$ plates. All plates were incubated inverted for 3-4 days at 30˚C in a Sanyo MIR262 stationary ventilated incubator. The colonies on each plate were counted and used to calculate the yeast mating efficiency as well as the number of diploid clones screened (Appendix III).

2.19.6 Selection and screening for reporter gene activation

2.19.6.1 *Selection for nutritional reporter gene activation*

Diploid yeast colonies resulting from the library mating were grown on TDO ($SD^{-Leu-Trp-His}$) plates for three weeks (Section 2.19.3). The plates were monitored every four days and full-grown (diameter>2mm) colonies, capable of activating the *HIS3* nutritional reporter gene, were re-streaked onto TDO and quadruple dropout (QDO) ($SD^{-Leu-Trp-His-Ade}$) plates (Appendix II), which were incubated inverted at 30˚C in a Sanyo MIR262 stationary ventilated incubator for 5 days. Successful colony formation on QDO plates indicated the additional activation of the *ADE2* nutritional reporter gene.

Streaked colonies on TDO and QDO plates were phenotypically assessed for colony growth and color. Colony growth was visually categorized as very good (+++), good (++), weak (+) or no growth (-). Furthermore, only white (healthy) colonies were considered for further analysis, whereas red (dying or dead) colonies were excluded. Colonies growing on QDO plates were then transferred onto QDO plates containing 5-bromo-4-chloro-3-indolyl α-D-galactopyranoside (X-α-gal) (Section 2.19.6.2).

2.19.6.2 *Screening for colorimetric reporter gene activation*

In order to test for activation of the *MEL1* colorimetric reporter gene, in addition to activation of *HIS3* and *ADE2* nutritional reporter genes, diploid colonies were transferred from QDO plates to QDO plates containing the chromogenic substrate X-α-gal.

QDO-X-α-gal plates were prepared by evenly spreading 200µl of a 5mg/ml X-α-gal solution (Appendix II) (Sigma Aldrich, St. Louis, Missouri, USA) onto fresh QDO plates. Colonies grown on QDO plates (Section 2.19.6.1) were replicated onto Hybond N^+ nylon membranes (GE Healthcare Ltd., Little Chalfont, Buckinghamshire, UK) which were placed colony-side up onto QDO-X-α-gal plates. The plates were incubated at 30˚C in a Sanyo MIR262 stationary ventilated incubator for 24h. Activation of the *MEL1* reporter gene was subsequently evaluated by blue-white screening.

2.19.7 Prey plasmid isolation and purification from diploid yeast colonies

Diploid yeast colonies that were able to activate all three reporter genes, i.e. strong growth on QDO plates that turned blue on QDO-X-α-gal plates (Section 2.19.6), harbored bait and prey constructs expressing putatively interacting fusion peptides. Hence, the pGADT7 prey constructs were retrieved for prey insert identification (Section 2.11) and interaction specificity tests (Section 2.19.8).

Yeast constructs were extracted as described in Section 2.17.3 and subsequently transformed into competent *E. coli* DH5α cells (Section 2.16.1), which were plated on LB plates supplemented with ampicillin (25µg/ml). This allowed for selection of colonies harboring pGADT7. All plates were incubated inverted overnight (16h) at 37˚C in a model 239 CO_2 stationary incubator. The following day, colonies were picked for bacterial plasmid purification (Section 2.17.2).

2.19.8 Interaction specificity test

Direct Y2H tests were performed to determine whether the interactions seen in diploid yeast colonies (Section 2.19.6) were specific to the pGBKT7-*parkin* bait construct. Rescued prey constructs (Section 2.19.7) were each retransformed into *S. cerevisiae* strain Y187 (Section 2.16.2). Transformed Y187 colonies were individually mated with *S. cerevisiae* strain AH109 colonies transformed with one of four heterologous bait constructs: pGBKT7-*parkin*, non-recombinant pGBKT7, pGBKT7-53 and pGBKT-TTN (encoding the 11-repeat superdomain of human cardiac-expressed titin, a kind gift from Ms. Carol Todd).

Mating was performed by individually mixing Y187 prey-expressing colonies with each of the AH109 heterologous bait-expressing colonies on YPDA plates. The plates were then inverted and incubated overnight (16h) at 30˚C in a Sanyo MIR262 stationary ventilated incubator. The following morning, colonies were streaked onto TDO and QDO plates, which were incubated at 30˚C in a Sanyo MIR262 stationary ventilated incubator for 2 weeks. Colony growth and appearance was then evaluated for each mating pair. Only healthy (white) prey colonies that were able to grow on QDO plates when mated to pGBKT7-*parkin* bait colonies, but did not grow on QDO plates when mated to non-recombinant pGBKT7, pGBKT7-53 and pGBKT7-TTN bait colonies, were considered to

demonstrate specific bait-prey interactions. Prey constructs resulting in such interaction-specific colonies were considered to be putatively true parkin interactors, and the relevant pGADT7 prey constructs were subjected to automated DNA sequencing and analysis (Sections 2.9.3 and 2.11) to identify the parkin-interacting preys. These putative interactions, identified in a Y2H experimental setting, were further investigated in human cell lines in order to better approximate biologically-relevant cellular conditions (Section 2.20).

2.20 HUMAN CELL LINES

2.20.1 The SH-SY5Y cell line

Human derived neuroblastoma SH-SY5Y cell line was purchased from the European Collection of Cell Cultures (ECACC, Porton Down, Salisbury, UK). The originator cell line SK-N-SH was isolated from a bone marrow biopsy of a four-year old female with neuroblastoma, from which the derived cell line SH-SY5 was subcloned. The cell line was subcloned for a third time to produce the SH-SY5Y cell line (Biedler et al. 1978). SH-SY5Y cells are routinely used as *ex vivo* models of mature dopaminergic neurons, as SH-SY5Y cells exhibit dopamine-β-hydroxylase activity and express several dopaminergic markers (Ciccarone et al. 1989).

In the present study, SH-SY5Y cells were used for co-localization (Section 2.22), western blot (Section 2.23) and co-IP (Section 2.24) experiments. In addition, SH-SY5Y cells were transfected with small interfering RNA (siRNA) for use in RNA-interference (RNAi) experiments (Section 2.25).

2.20.2 Primary dermal fibroblast cell lines

Primary cells lines derived from individuals with disease are a useful tool to study disease-related cellular phenotypes. In particular, PD patient-derived dermal fibroblasts are widely used as cellular models of PD. The use of such explant cell lines is advantageous as it creates a model system with the predefined mutations and age-accumulated cellular damage of patients, while being minimally invasive to donor individuals (Auburger et al. 2012).

In the present study, primary dermal fibroblasts were obtained from three patients diagnosed with PD, hereafter referred to as patient 1 (P1), patient 2 (P2) and patient 3 (P3). All three patients harbored homozygous *parkin*-null mutations, which were identified as part of this study using MLPA analysis and confirmed with cDNA sequencing (Sections 2.5.5 and 2.7; Section 3.1.1). Three wild-type (WT) age- and gender-matched control individuals were also used in the present study: WT2, WT3 and WT4 (WT1, a male individual recruited for a previous study, was not included in the present study).

The three controls had no history of neurological disease, and were confirmed to be wild-type in regards to the parkin gene by means of DNA sequencing (Section 2.7). Relevant genotypic and phenotypic details of the three PD patients and three controls are summarized in Table 2.6.

Dermal fibroblasts were obtained from P1, P2, P3 and WT2 by means of skin punch biopsies (Section 2.21.1), whereas WT3 and WT4 fibroblast cell lines were purchased from Sciencell Laboratories (Sciencell, San Diego, California, USA).

Table 2.6 Genotypic and phenotypic characteristics of the five dermal fibroblast donors

Identifier	Parkin mutation	Gender	Ethnicity	AAO (years)	AAR* (years)	PD duration (years)
PD patients						
P1	Deletion exon 3-4 hom	Female	MA	27	39	12
P2	Deletion exon 4 hom	Female	AC	27	54	27
P3	Deletion exon 4 hom	Female	AC	27	52	25
Controls						
WT2	n/a	Female	AC	n/a	62	n/a
WT3	n/a	Female	C	n/a	56	n/a
WT4	n/a	Female	Unknown	n/a	44	n/a

*Refers to the age of the donor at the time of skin punch biopsy. Abbreviations: AAO, age at onset; AAR, age at recruitment; AC, Afrikaner Caucasian; C; Caucasian; hom, homozygous; MA, Mixed ancestry; n/a, not applicable; P, patient; PD, Parkinson's disease; WT, wild-type.

2.21 CULTURING OF CELL LINES

2.21.1 Isolation of dermal fibroblasts from skin punch biopsies

Primary dermal fibroblast cell lines were established by isolating dermal fibroblasts from skin punch biopsies from three PD patients with homozygous parkin-null mutations and one control individual. Skin punch biopsies were performed by a trained clinician at Tygerberg Hospital (Cape Town, South Africa), after which dermal fibroblast cell lines were established by Unistel Medical Laboratories (Pty) Ltd. (Cape Town, South Africa).

A 2mm x 2mm skin punch biopsy was taken from the inner upper arm and suspended in fibroblast culture media (Appendix II) in a 15ml polypropylene tube for transportation purposes. In a sterile tissue culture environment, a volume of 300µl per 1ml culture media of collagenase (Sigma Aldrich, St. Louis, Missouri, USA) was added to the suspended biopsy. The suspension was incubated for 1h at 37˚C, with manual agitation at regular intervals, after which the suspension was centrifuged at 1200rpm for 10min in a Sorval® GLC-6 general laboratory centrifuge (Separations, Johannesburg,

South Africa). The supernatant was discarded and the pellet resuspended in 5ml fibroblast isolation media (Appendix II), and the suspension transferred to a CellBind® T25 tissue culture flask (Corning Inc., Corning, New York, USA). Incubation followed at 37˚C in in a Farma thermosteri-cycle 5% CO_2 humidified incubator (Farma International, Miami, Florida, USA).

After four days of incubation, the culture media was decanted and 5ml fresh fibroblast isolation media added. The tissue culture flask was regularly checked for the formation of nest-like fibroblastic colonies. After confluency of approximately 70-80% was reached, the cells were subcultured as described below (Section 2.21.3).

2.21.2 Culture of cells from frozen stocks

Frozen (-196˚C, in liquid N_2) cell stocks were rapidly thawed by submerging the vial in a 37˚C water bath (Memmert, Schwabach, Germany). Immediately upon thawing, the exterior of the vial was sterilized with 70% ethanol and the toxic cryoprotectant, dimethyl sulfoxide (DMSO), was removed in the following manner: A total of 1ml of the appropriate pre-warmed culture media (Appendix II) was directly added to the thawed cell stock and the suspension transferred to a 12ml Greiner tube (Greiner Bio-one, Frickenhausen, Germany). An additional 5ml culture media was added to the suspension, after which it was centrifuged at 1000rpm for 2min in a Sorval® GLC-6 general laboratory centrifuge. The supernatant was discarded and the pellet resuspended in 5ml culture media, and the suspension transferred to a CellBind® T25 tissue culture flask. The flask was gently swirled to distribute cells evenly over the growth surface. Incubation followed at 37˚C in in a Farma thermosteri-cycle 5% CO_2 humidified incubator.

2.21.3 Subculturing of cells

Cell cultures were growth in a Farma thermosteri-cycle 5% CO_2 humidified incubator until a confluency of approximately 70-80% was reached (3-5 days for SH-SY5Y cells, 7-10 days for dermal fibroblasts). Cells were then subcultured: The growth media was removed from the adherent cells and the cell monolayer gently rinsed with 3ml sterile phosphate-buffered saline (PBS) (Lonza, Basel, Switzerland). A volume of 3ml trypsin (0.5g/L) (Lonza, Basel, Switzerland) was added to the cells, which was incubated at room temperature for 5min to facilitate detachment of cells from the growth surface. Subsequently 3ml of culture media was added to the cell suspension and mixed by gentle pipetting. The suspension was transferred to a 12ml Greiner tube and centrifuged at 1000rpm for 2min in a Sorval® GLC-6 general laboratory centrifuge. The supernatant was discarded and the pellet resuspended in 4ml culture media. This suspension was transferred either to four T25 CellStar® tissue culture flasks (Greiner Bio-one, Frickenhausen, Germany) each containing 5ml complete growth

media, or to a T75 or T175 CellStar® tissue culture flask (Greiner Bio-one, Frickenhausen, Germany) containing final volumes of 15ml or 25ml complete growth media, respectively.

2.21.4 Seeding cells onto coverslips

Cells to be labeled for *in vivo* co-localization analyses (Section 2.22) were grown on glass coverslips. This was done by placing sterile glass coverslips in CellStar® six well tissue culture plates (Greiner Bio-one, Frickenhausen, Germany) containing 3ml culture media (Appendix II) in each well. An aliquot of a cell suspension to be subcultured (Section 2.21.3) was used to perform a hemocytometric cell count (Appendix III). Thereafter, a volume of cell suspension containing approximately 50 000 cells was seeded per well in a drop-wise manner. Plates were incubated in a Farma thermosteri-cycle 5% CO_2 humidified incubator until a confluency of 60-70% was reached (1-2 days).

2.22 *IN VIVO* CO-LOCALIZATION

2.22.1 Fluorophores

Three-dimensional (3D) *in vivo* co-localization of putatively interacting proteins was performed in order to evaluate such interactions of endogenously-expressed proteins in a cellular environment. All co-localization experiments were done with SH-SY5Y cells grown on glass coverslips, where endogenous proteins were immunocytochemically labeled with fluorophore-conjugated secondary antibodies. This procedure is described below (Section 2.22.2), and information regarding the relevant fluorophores is detailed in Table 2.7.

Table 2.7 Excitation and emission spectra of fluorophores for co-localization experiments

Fluorophore	Excitation (nm)	Emission (nm)	Visible color
Alexa488	494	517	Green
Cy3	550	570	Red

Abbreviations**:** Alexa488, Alexa Fluor® 488; Cy3, cyanine 3; nm, nanometer.

2.22.2 Immunocytochemistry

SH-SY5Y cells were grown on glass coverslips in a CellStar® six well tissue culture plate until a confluency of 60-70% was reached (Section 2.21.4). Thereafter, the growth media was removed and the wells briefly rinsed with PBS. A total of 3ml of 4% paraformaldehyde (Appendix II) was added to

each well and the cells fixed at room temperature for 10min. Alternatively, cells to be stained with the γ-actin antibody were fixed with 3ml of ice-cold (-20˚C) absolute methanol at -20˚C for 10min. Each well was washed in PBS for 10min three times, with fresh PBS used for each wash. Coverslips were carefully removed from the six well plate and placed in a light-proof humidified chamber, after which the coverslips were blocked by incubation with 300µl of 1% bovine serum albumin (BSA)-PBS containing 0.1% Triton® X-100 (Sigma Aldrich, St. Louis, Missouri, USA) for 1h at room temperature. Cells fixed in absolute methanol were blocked in 1% BSA-PBS without Triton® X-100. Subsequently, 150µl of 1% BSA-PBS containing the relevant primary antibody/antibodies (Table 2.8) was added to each coverslip. The humidified chamber was sealed and incubated overnight (16h) at 4˚C.

Table 2.8 Antibody pairs and optimized dilution ratios for co-localization experiments

Antigen	Primary Ab	Manufacturer	Primary Ab Dilution Ratio	Secondary Ab	Secondary Ab Dilution Ratio
Parkin	Anti-parkin pAb	Abcam (ab15954)	1:50	DaR-Cy3	1:500
	Anti-parkin mAb	Cell Signaling (Park8)	1:100	DaM-Alexa488	1:500
SEPT5	Anti-sept5 pAb	Abcam (ab109294)	1:250	DaR-Cy3	1:500
SEPT9	Anti-MSF mAb	Abcam (ab38314)	1:100	DaR-Cy3	1:500
14-3-3η	Anti-14-3-3η pAb	Cell Signaling (#9640)	1:50	DaR-Cy3	1:500
γ-Actin	Anti-γ-actin mAb	Abcam (2A3)	1:1500	DaM-Alexa488	1:500
ATPAF1	Anti-ATPAF1 pAb	Abcam (AB107202)	1:500	DaR-Cy3	1:500

Manufacturer details: Abcam (Abcam, Cambridge, UK); Cell Signaling (Cell Signaling Technology, Cambridge, UK); Promega (Promega, Madison, Wisconsin, USA). Abbreviations: Ab, antibody; Alexa488, Alexa Fluor® 488; Cy3, cyanine 3; DaM, donkey anti-mouse; DaR, donkey anti-rabbit; mAb, monoclonal antibody; pAb, polyclonal antibody.

The following morning, the coverslips were washed in PBS for 10min three times. The coverslips were then incubated in the dark with 200ul of PBS containing the relevant secondary

antibody/antibodies (Table 2.8) for 90min at room temperature. After a series of three PBS washes, the coverslips were incubated with 200ul of a 1:5000 dilution Hoechst H-33342 nucleic acid stain (Sigma Aldrich, St. Louis, Missouri, USA) in PBS for 10min at room temperature in the dark. The coverslips were rinsed a final time with PBS for 10min, after which the coverslips were mounted on clean microscope slides with a 15µl aliquot of Mowiol mounting media (Appendix II). Slides were left in the dark overnight at room temperature and then stored at 4˚C until viewing (Section 2.22.3).

For each co-localization experiment, a set of immunocytochemical slides were prepared as described above, which included a secondary antibody negative control, a single-stained control for each of the two proteins under investigation and a double-stained experiment slide. The negative control was incubated with 1% BSA-PBS without any primary antibodies and both secondary antibodies for the primary and secondary antibody incubation steps, respectively. Similarly, single-stained controls were incubated with one primary antibody and one secondary antibody and double-stained experiments were incubated with both primary antibodies and both secondary antibodies. All slides were stained with Hoechst H-33342 nucleic acid stain for image orientation purposes.

2.22.3 Confocal microscopy and analysis

Fixed and stained cells were viewed at the Cell Imaging Unit of CAF at Stellenbosch University, Stellenbosch, South Africa. A Carl Zeiss LSM780 confocal microscope system (Carl Zeiss, Oberkochen, Germany) was employed to this end.

This system is equipped with a 488nm argon multiline laser, a 561nm red diode-pumped solid state laser and a 633 HeNe laser for excitation of the Alexa488 fluorophore, Cy3 fluorophore and Hoechst H-33342 nucleic acid stain, respectively. Fluorescence emission was detected using a 32-channel GaAsP PMT detector with quantum efficiency of 45%, a significant improvement on the 25% efficiency typically achieved by classic PMT detectors. Images were acquired an Alpha Plan-Apochromat 100X/1.4 DIC M27 oil-immersion objective and ZEN 2011 imaging software (Carl Zeiss, Oberkochen, Germany).

Images were acquired of each of the secondary antibody negative control, single-stained controls and double-stained co-localization experiments in triplicate, where two to three cells were imaged per replicate. The inclusion of a negative control facilitated correcting for background fluorescent staining, whereas single-stained controls provided fluorescent signal parameters for setting relevant co-localization thresholds. Importantly, image acquisition settings were kept constant for each set of experiment and controls. All images were acquired with Z-stacking, which facilitated signal acquisition and resolution in all three dimensions. This was done by acquiring images in multiple focal planes; Z-stacks consisted of 21 images taken at 0.25µm intervals in the optical plane. Hence,

each three-dimensional Z-stacked image was 58.02µm in length, 85.02µm in width and 5.25µm in depth. Images were evaluated for signal co-localization using co-localization scatter plots as well as visual images of co-localized pixels in each Z-stack plane, as generated by the ZEN 2011 imaging software.

2.23 WESTERN BLOTTING

2.23.1 Mammalian cell lysis

Cultured SH-SY5Y cells were lysed for subsequent use in western blot, co-IP and RNAi experiments (Sections 2.23, 2.24, 2.25.4). Similarly, cultured fibroblasts were lysed for western blot experiments (Sections 2.25.4).

Cell lysis was achieved in the following manner: Growth media was removed and the cell monolayer rinsed with PBS, after which an appropriate amount of pre-heated (37˚C) trypsin was added to the tissue culture vessel (T25, T75, T175 CellStar® tissue culture flasks or CellStar® six well tissue culture plates). The vessel was incubated at room temperature for 5-10min, after which cells were further dislodged with a cell scraper. The cell suspension was transferred to a 50ml polypropylene tube containing 10ml growth media. In the case of cells cultured in CellStar® six well tissue culture plates, similarly treated cells from separate wells were pooled in 50ml polypropylene tubes. The suspension was centrifuged at 3000rpm for 3min at 4˚C in an Eppendorf model 5810R centrifuge (Eppendorf, Hamburg, Germany) and the supernatant discarded. The pellet was resuspended in 1ml of PBS after which the suspension was transferred to a sterile 2ml microcentrifuge tube and repelleted by centrifugation at 5000rpm for 1min in a Labnet Prism™ microcentrifuge. The supernatant was discarded and the pellet resuspended in 50-300µl ice-cold passive lysis buffer (Appendix II), depending on pellet size. Cells were incubated on ice for 30min. Centrifugation at 15 000rpm for 15min at 4˚C in a UEC 13 microcentrifuge (UniEquip, Munich, Germany) followed, after which the supernatant was transferred to a sterile 1.5ml microcentrifuge tube.

All cell lysates were either used immediately for downstream applications or stored at -80˚C for future use. Prior to use, the protein concentration of the whole cell extract was determined via a Bradford assay (2.23.2).

2.23.2 Bradford protein concentration determination

Accurate measurements of cell lysate protein concentration were obtained by means of a Bradford assay prior to the use of the lysates in western blot, co-IP and RNAi experiments (Sections 2.23, 2.24, 2.25).

To generate a standard curve of protein concentrations, 10µl of a dilution range of BSA in PBS ranging from 0-1000µg/µl were loaded in duplicate into a luminometer 96 well plate. A volume of 1µl of each sample to be assayed was also loaded in duplicate. A total of 200µl Bradford protein reagent (Appendix II) was added to each well, and the protein concentration measured via absorbance at 595nm in a Synergy HT luminometer (BioTek Instruments Inc., Winooski, Vermont, USA) using KC4™ software version 3.4 (BioTek Instruments Inc., Winooski, Vermont, USA).

2.23.3 Western blot preparation

Western blots were performed in order to visualize proteins of interest either in whole cell lysates (Section 2.25.4) or pulled down as part of co-IP experiments (Section 2.24). Western blotting conditions, including the ratios of primary and secondary antibodies used to immunoblot proteins of interest, were first optimized. Optimal western blotting conditions are summarized in Table 2.9.

Cell lysates to be used were subjected to a Bradford assay to determine protein concentration (Section 2.23.2). Lysates were resolved using SDS-PAGE (Section 2.10.2) with a total of 50-100µg of protein loaded per well. Subsequently the resolved proteins were transferred to a PVDF membrane (Section 2.10.3).

2.23.4 Membrane blocking

The PVDF membrane, containing the resolved and transferred proteins, was blocked in order to prevent non-specific binding of antibodies to the membrane. This was achieved by submerging the membrane in blocking buffer consisting of either 5% fat free powder milk in tris-buffered saline with 0.1% Tween-20 (TBST) (Appendix II) or 3% BSA in TBST, depending on the protein on interest (Table 2.9). The membranes was incubated in blocking buffer for 1h at room temperate while shaking on a Stuart® SSL1 orbital shaker.

Table 2.9 Optimized western blot conditions

Antigen	Membrane Blocking	Primary Ab	Manufacturer	Primary Ab Dilution Ratio	Primary Ab Diluent	Secondary Ab	Secondary Ab Dilution Ratio	Secondary Ab Diluent	Expected Size (kDa)
Parkin	5% milk-TBST	Anti-parkin pAb	Abcam (ab15954)	1:500	0.5% milk-TBST	DaR	1:4000	5% milk-TBST	52
SEPT5	5% milk-TBST	Anti-sept5 pAb	Abcam (ab109294)	1:1000	5% milk-TBST	DaR	1:6000	5% milk-TBST	43
SEPT9	5% milk-TBST	Anti-MSF mAb	Abcam (ab38314)	1:750	5% milk-TBST	DaR	1:6000	5% milk-TBST	65
14-3-3η	5% BSA-TBST	Anti-14-3-3η pAb	Cell Signaling (#9640)	1:2000	TBST	DaR	1:4000	TBST	28
γ-Actin	5% milk-TBST	Anti-γ-actin mAb	Abcam (2A3)	1:20 000	5% milk-TBST	DaM	1:40 000	5% milk-TBST	42
ATPAF1	5% BSA-TBST	Anti-ATPAF1 pAb	Abcam (AB107202)	1:500	TBST	DaR	1:4000	TBST	36
GAPDH	5% milk-TBST	Anti-GAPDH mAb	Santa Cruz (FL-335)	1:2500	5% milk-TBST	DaR	1:8000	5% milk-TBST	36

Manufacturer details: Abcam (Abcam, Cambridge, UK); Cell Signaling (Cell Signaling Technology, Cambridge, UK); Promega (Promega, Madison, Wisconsin, USA), Santa Cruz (Santa Cruz Biotechnology, Dallas, Texas, USA). Abbreviations: Ab, antibody; BSA, bovine serum albumin; DaM, donkey anti-mouse; DaR, donkey anti-rabbit; kDa, kiloDalton; mAb, monoclonal antibody; pAb, polyclonal antibody; TBST, tris-buffered saline with 0.1% Tween-20.

2.23.5 Addition of primary antibody

After the membrane was blocked (Section 2.23.4), it was washed in TBST for 5min on a Stuart® SSL1 orbital shaker. A volume of 2-5ml of the appropriate primary antibody dilution (1:500-1:20 000) was prepared with the relevant antibody diluent (TBST, 0.5% milk in TBST or 5% milk in TBST) as listed in Table 2.9. The blocked membrane was immersed in the primary antibody solution in a plastic sleeve, which was then sealed and incubated overnight (16h) at 4˚C with shaking on an Orbit 300 shaker (Labnet, Edison, New Jersey, USA).

The following morning, the membrane was vigorously rinsed twice in TBST, followed by a 15 min wash in TBST and then three 5min TBST washes. TBST was discarded and fresh TBST added after each wash step.

2.23.6 Addition of secondary antibody

After the membrane has been adequately washed of excess primary antibody (Section 2.23.5), the membrane was incubated with a relevant HRP-conjugated secondary antibody (Santa Cruz Biotechnology, Dallas, Texas, USA): A volume of 5ml of the appropriate secondary antibody dilution (1:4000-1:40 000) was prepared with the relevant antibody diluent (TBST or 5% milk in TBST) as summarized in Table 2.9. The membrane was immersed in the secondary antibody solution in a plastic sleeve, which was then sealed and incubated for 1h at room temperature with shaking on a Stuart® SSL1 orbital shaker.

Following incubation, the membrane was vigorously rinsed twice in TBST, followed by a 15min wash in TBST and then three 5min TBST washes. TBST was discarded and fresh TBST added after each wash step.

2.23.7 Chemiluminescent visualization of membrane-bound proteins

Chemiluminescent detection of the protein of interest followed thorough removal of excess secondary antibody from the membrane (Section 2.23.6). In a darkroom, a 1:1 mixture of the two substrate components (SuperSignal® West Pico Stable Peroxide solution and the SuperSignal® West Pico Luminol/Enhancer solution) of a SuperSignal® West Pico Chemiluminescent Substrate kit (Thermo Scientific, Waltham, Massachusetts, USA) was prepared. This was added to the membrane which was incubated in the chemiluminescent substrate for 5min at room temperate. The membrane was then transferred to an autoradiography cassette and excess substrate removed by gently blotting with paper towels, after which the membrane was covered with a transparent plastic sheath. CL-Xposure™ autoradiography film (Thermo Scientific, Waltham, Massachusetts, USA) was placed in the cassette

and exposed for an appropriate amount of time (10sec-16h), depending to the strength of the chemiluminescent signal. The exposed film was developed in a Hyperprocessor™ automatic autoradiography film processor (GE Healthcare Ltd., Little Chalfont, Buckinghamshire, UK).

2.23.8 Stripping of membranes

For applications in which more than one protein of interest needed to be detected in the same lysate on a single membrane, such as the protein expression experiments (Section 2.25.4), either cutting or stripping of the membrane was employed. If the difference in expected sizes of the proteins to be detected was sufficiently large, the membrane was cut in two at the position halfway between the expected proteins, and each membrane section incubated with the appropriate primary antibody simultaneously (Section 2.23.5). Otherwise, the membrane was stripped and reprobed for each protein of interest sequentially, as described below.

Following the chemiluminescent visualization of the membrane (Section 2.23.7), the membrane was rinsed twice in TBST for 10min per rinse. It was then incubated in 10-20ml of stripping buffer (Appendix II) for 15min at room temperature with shaking on a Stuart® SSL1 orbital shaker, after which the stripping buffer was discarded and the membrane incubated in fresh stripping buffer for a further 15min at room temperature with shaking. Following incubation, the membrane was vigorously rinsed twice in TBST, followed by a 15min wash in TBST and then three 5min TBST washes. TBST was discarded and fresh TBST added after each wash step. The membrane was subsequently blocked (Section 2.23.4) and incubated with the appropriate primary antibody (Section 2.23.5).

2.24 CO-IMMUNOPRECIPITATION

Co-immunoprecipitation (co-IP) of endogenous proteins was performed as follows: Whole cell extracts were prepared (Section 2.23.1) and the protein concentration determined (Section 2.23.2). A total of 200-1000µg protein was then transferred to a 1.5µl microcentrifuge tube and the volume equalized to 200µl with fresh passive lysis buffer (Appendix II). A volume of 20µl Protein G agarose bead slurry (KPL, Gaithersburg, Massachusetts, USA) was added to the sample, which was incubated on a model HS100 rotating wheel (Labnet, Edison, New Jersey, USA) for 40min at 4˚C to pre-clear the lysates. Samples were centrifuged at 7000rpm for 1min at 4˚C in UEC 13 microcentrifuge and the supernatant transferred to a clean 1.5µl microcentrifuge tube. A total of 2µg of primary antibody directed against the protein to be immunoprecipitated was added to the lysate, which was incubated overnight (16h) at 4˚C on model HS100 rotating wheel.

The next morning, 60µl of Protein G agarose bead slurry was added to the lysate followed by further incubation on a model HS100 rotating wheel at 4˚C for 1h. Beads were collected by centrifugation at 7000rpm for 30sec at 4˚C in a UEC 13 microcentrifuge, and the supernatant carefully transferred to a clean 1.5µl microcentrifuge tube for western blot analysis (Section 2.23). The beads were then gently washed a total of four times in ice-cold passive lysis buffer, recollecting the beads via centrifugation after each wash. Finally, 30µl of 2X SDS loading dye (Appendix II) was added to the beads and the mixture boiled at 95˚C for 10min. Subsequently the sample was centrifuged at 15000rpm for 5min in a Labnet Prism™ microcentrifuge and the supernatant loaded onto a SDS-PAGE gel (Section 2.10.2) for use in western blot analysis (Section 2.23).

2.25 CREATION AND ANALYSIS OF PARKIN-DEFICIENT CELL MODELS

2.25.1 RNA-interference-mediated parkin knockdown

RNA-interference (RNAi) using siRNA was performed to bring about the targeted knockdown of parkin expression in cultured SH-SY5Y cells. This was done to evaluate the functional consequences of suppressed/absent parkin expression (Sections 2.25.4).

Four non-validated human siRNAs were purchased (Qiagen, Hilden, Germany); siRNA sequence information is listed in Table 2.10. Each siRNA was optimized and assessed for parkin knockdown efficiency and only siRNAs demonstrating sufficient parkin knockdown were used in subsequent experiments.

Table 2.10 siRNA sequences for parkin knockdown

siRNA name	Strand	siRNA sequence (5'-3')
Hs_PARK2_2	Sense	GUUUGUUCACGACCCUCAATT
	Antisense	UUGAGGGUCGUGAACAAACTG
Hs_PARK2_8	Sense	CCAUCUAUAUAAAUCGCAUTT
	Antisense	AUGCGAUUUAUAUAGAUGGAA
Hs_PARK2_9	Sense	GAGGAAAGUCACCUGCGAATT
	Antisense	UUCGCAGGUGACUUUCCUCTG
Hs_PARK2_10	Sense	GGCUCCACUGUAAAUUUAATT
	Antisense	UUAAAUUUACAGUGGAGCCAA

Abbreviations: 3', three-prime end; 5', five-prime end; A, adenine; C, cytosine; G, guanine; Hs, *Homo sapiens*; PARK2, *parkin* gene; siRNA, small interfering RNA; T, thymine.

SY-SY5Y cells were cultured as described (Section 2.21). An aliquot of a cell suspension to be subcultured (Section 2.21.3) was used to perform a hemocytometric cell count (Appendix III). Thereafter, a volume of cell suspension containing approximately 200 000 cells was seeded per well in a CellStar® six well tissue culture plate in a drop-wise manner. The plate was incubated in a Farma thermosteri-cycle 5% CO_2 humidified incubator until a confluency of 70-80% was reached (16h).

The following day, the culture media in each well was removed and replaced by 2.3ml of fresh complete culture media (Appendix II). For each transfection, a total of 0.6µl of 20µM siRNA stock was diluted in 98.2µl serum-free media (Appendix II) in a 200µl PCR tube, to which 12µl of HiPerFect transfection reagent (Qiagen, Hilden, Germany) was added. The tubes were incubated at room temperature for 10min to allow for siRNA complex formation. The transfection mixture was subsequently added to the cells in a drop-wise manner, resulting in a final concentration of 5nM siRNA per well. Plates were gently rocked to distribute the transfection mixture evenly over the cell monolayer and then incubated in a Farma thermosteri-cycle 5% CO_2 humidified incubator for 48h.

Concurrent to targeted siRNA transfections, cells were also transfected with a non-silencing control (NSC) siRNA (Qiagen, Hilden, Germany) as well as subjected to a mock transfection, i.e. a transfection mixture containing no siRNAs. The efficiency of siRNA-mediated parkin knockdown was subsequently evaluated on a mRNA level (Section 2.25.3) as well as a protein level (2.25.4).

2.25.2 Total RNA extraction and cDNA conversion

Total RNA was extracted from siRNA-transfected SH-SY5Y cells (Section 2.25.1). RNA extraction was performed by using a RNeasy Plus Mini Kit (Qiagen, Hilden, Germany) as per manufacturer's instructions. Isolated RNA concentration and quality was subsequently measured with an Experion™ StdSens Analysis kit on an Experion™ automated electrophoresis station. Only RNA samples with a RQI value above 8.0 were used for subsequent analyses.

Following RNA isolation, the purified RNA was converted to cDNA by using a Quantitect® Reverse Transcription Kit as per manufacturer's instructions. cDNA concentration was determined using a NanoDrop® ND-1000 spectrophotometer and NanoDrop1000® software version 3.7.1. The cDNA samples were then stored at -20°C until use.

2.25.3 Two-step quantitative reverse-transcription PCR (q-RT-PCR)

Real-time quantitation of cDNA obtained from siRNA-transfected SH-SY5Y cells (Section 2.25.1) was done using four IDT PrimeTime® Std qPCR assays targeting *parkin* as well as *GAPDH* (glyceraldehyde-3-phosphate dehydrogenase), *B2M* (β-2 microglobulin) and *RPL13A* (ribosomal

protein L13a) housekeeping genes (Integrated DNA Technologies, Coralville, Iowa, USA). Briefly, 100ng of cDNA was used as template in a 5µl reaction containing 1X Primetime® Std qPCR assay and 1X QuantiFast™ Multiplex PCR master mix (Qiagen, Hilden, Germany). All quantitation reactions were set up in triplicate and included cDNA-free negative control reactions. Reaction setup employed an Eppendorf ep*Motion*™ 5070 automated pipetting system (Eppendorf, Hamburg, Germany) for liquid handling.

Q-RT-PCR was performed on an ABI 7900HT Fast Real-Time PCR System (Applied Biosystems Inc., Foster City, California, USA) using SDS software version 2.3 (Applied Biosystems Inc., Foster City, California, USA) under the following cycling conditions: an initial denaturation step at 95ºC for 10min followed by 40 cycles consisting of denaturation at 95ºC for 15sec and annealing/extension at 60°C for 45sec.

Relative *parkin* mRNA expression was quantified with reference to the three housekeeping genes using normalization factor calculations based on the geometric mean of multiple housekeeping genes, as described by Vandesompele et al. (2002).

2.25.4 Protein expression analysis

In order to verify successful parkin knockdown on a protein level, siRNAs that demonstrated sufficient *parkin* mRNA knockdown following q-RT-PCR analysis (Section 2.25.3) were used to transfect SH-SY5Y cells as described in Section 2.25.2. Whole cell extracts were then prepared of the transfected cells and the protein concentrations determined (Sections 2.23.1 and 2.23.2). Equal quantities of parkin siRNA-treated and NSC-treated cell lysates were used for western blotting with an anti-parkin antibody (Section 2.23). Following the autoradiographical recording of membrane-bound parkin (Section 2.23.7), the membrane was stripped of antibodies and reprobed with an anti-GAPDH antibody (Section 2.23.8). Visualization of GAPDH content of each lysate served as a loading control to verify equal loading of all lysates.

The band intensities of parkin and GAPDH bands on the obtained autoradiograph film were quantified using ImageJ Software version 1.47 (http://imagej.nih.gov/ij) (Schneider et al. 2012), and the band intensities of parkin in siRNA and NSC-transfected cell lysate lanes were normalized to the corresponding band intensities of GAPDH in the same lanes. Relative parkin expression in siRNA-treated cells was quantified in reference to normalized parkin expression in NSC-transfected cells. A total of three replicate knockdown experiments were independently performed to evaluate the reliability of siRNA-mediated parkin knockdown. All differences in protein expression were statistically assessed by means of mixed-effects linear modeling, as described in Section 2.30.

Membranes containing lysates in which successful parkin knockdown was verified were stripped and reprobed for each of the parkin-interacting proteins (Section 2.23.8), in order to assess the effect of the lack of parkin on the protein expression of each parkin interactor. The band intensity of each parkin-interacting protein was normalized to GAPDH and the relative expression of each protein was quantified in parkin-siRNA-treated cells in reference to their expression in NSC-transfected cells, as described above.

The effect of the lack of parkin on the protein expression of each parkin interactor was also evaluated in parkin-null dermal fibroblasts (Section 2.20.2). Equal quantities of whole cell lysates of the patient-derived parkin-null fibroblast cell lines and wild-type control fibroblast cell lines were used for western blotting (Section 2.23). A single membrane was probed for each parkin-interacting protein, whereas probing for GAPDH served as a loading control. The relative expression levels of each protein of interest in parkin-null fibroblasts were quantified and assessed as described above.

PART THREE: PARKIN DEFICIENCY AND VITAMIN K_2

In the third and final part of this dissertation, parkin-null primary fibroblasts were used to assess the effect of parkin deficiency on several informative parameters of cellular health. This third part furthermore entails an evaluation of the effect of the potential PD therapeutic agent vitamin K_2 on such cellular parameters in parkin-deficient fibroblasts. It has been reported that vitamin K_2 supplementation alleviated mitochondrial defects in *PINK1* and *parkin* mutant *Drosophila* (Vos et al. 2012); the present study therefore investigated mitochondrial health in particular. To this end, four parameters of cellular function and health were assayed: cell viability after cytotoxic insult (Section 2.26), mitochondrial respiration (Section 2.27), mitochondrial membrane potential (Section 2.28) and the integrity of mitochondrial networks (Section 2.29).

2.26 CELL VIABILITY AND CELL GROWTH ASSAYS

Dermal fibroblast cell viability was assessed by means of colorimetric thiazolyl blue tetrazolium bromide (MTT) assays. MTT, a water-soluble yellow tetrazole, is reduced to insoluble purple formazan by NAD(P)H-dependent oxidoreductases in living cells. Formazan aggregates can then be dissolved by the addition of an appropriate solubilization buffer, and the resulting color change can be measured via spectrophotometry. As the formation of formazan is dependent on cellular metabolic rates, MTT assays can be used as sensitive gauges of viable cell number (Berridge et al 2005). MTT

assays are also valuable in the assessment of the cytotoxicity of various compounds (Meerloo et al. 2011).

The CyQUANT® assay, on the other hand, is based on the measurement of cellular DNA content via fluorescent dye binding. As cellular DNA content is tightly regulated, CyQUANT® assays can be used as indirect measurements of cell number. The extent of cell proliferation can then be gauged by the comparison of cell counts of cells treated with various compounds to untreated cells (Jones et al. 2001). As cell proliferation is considered to be one of the most sensitive indicators of overall cellular health (Abraham et al. 2008), CyQUANT® assays were performed alongside MTT assays in this study as two parallel measurements of viable cell number. These assays were used to investigate the effect of treatment with vitamin K_2 on cell viability and growth in parkin-null and wild-type fibroblasts, in the absence and the presence of cellular stress.

2.26.1 Optimization of vitamin K_2 concentration

In the present study, a MTT assay was initially performed to evaluate potential cytotoxic effects of the vitamin K_2 analogue menaquinone 4 (MK-4) on wild-type fibroblasts, in order to determine the optimal MK-4 concentration for subsequent experiments. Briefly, an aliquot of a cell suspension of WT2 fibroblasts to be subcultured (Section 2.21.3) was used to perform a hemocytometric cell count (Appendix III). Thereafter, a volume of cell suspension containing approximately 5000 cells was seeded per well in a Corning® Costar® 96-well flat-bottom tissue culture plate (Corning Inc., Corning, New York, USA). The plate was incubated at 37ºC in a Farma thermosteri-cycle 5% CO_2 humidified incubator overnight (16h).

The following morning, the culture media was removed and replaced with a dilution series of MK-4 in 200µl fresh culture media, with MK-4 concentrations ranging from 0-100µM MK-4 (Sigma Aldrich, St. Louis, Missouri, USA) (Appendix II). Each concentration was added to the wells in quadruplicate. The plate was returned to the Farma thermosteri-cycle 5% CO_2 humidified incubator and incubated for a further 24h. The next day, a MTT assay was performed as described in Section 2.26.3.

2.26.2 Preparation of fibroblasts for MTT and CyQUANT® assays

MTT and CyQUANT® assays were also employed to assess cell viability and proliferation of patient and wild-type fibroblasts after cytotoxic insult; this was performed with and without vitamin K_2 co-treatment. Fibroblasts were seeded into 96-well plates at a density of 5000 cells per well as described above (Section 2.26.1), with two 96-well plates being prepared in parallel for MTT and CyQUANT®

assays, respectively. The following morning, the culture media was removed and a volume of 200µl of each of four treatment solutions was added to appropriate wells. The four treatment solutions were: 0.1% (v/v) ethanol in culture media (for untreated cells; the addition of ethanol serves as a vehicle control), 40µM MK-4 solution in culture media (Appendix II), 10µM carbonyl cyanide m-chlorophenylhydrazone (CCCP) solution in culture media (Appendix II), and culture media containing both 40µM MK-4 and 10µM CCCP. Each treatment solution was added to the wells in quadruplicate. Incubation followed for 24h at 37ºC in a Farma thermosteri-cycle 5% CO_2 humidified incubator. In the present study, 10µM CCCP was used to induce cellular stress, as a similar concentration is routinely used in the literature to produce mitochondrial impairment and bring about parkin-selective mitophagy of damaged mitochondria (Narendra et al. 2008; Matsuda et al. 2010).

After the fibroblasts had been appropriately treated, the two 96-well plates were separately used for MTT and CyQUANT® assays, respectively (Sections 2.26.3 and 2.26.4). Each assay was performed in triplicate as three separate experimental runs.

2.26.3 MTT assay

MTT assays were performed as follows: The culture media was removed and the wells gently rinsed once with 200µl pre-warmed sterile PBS. A 1:10 dilution of MTT stock solution (Sigma Aldrich, St. Louis, Missouri, USA) (Appendix II) was made in pre-warmed PBS, which was added to the wells in volumes of 100µl. The plate was covered in aluminum foil and incubated at 37ºC in a Farma thermosteri-cycle 5% CO_2 humidified incubator for 4h. Subsequently, the MTT solution was carefully aspirated and a volume of 100µl acidified isopropanol (Appendix II) added to each well. Formazan aggregates were dissolved by trituration followed by incubation at 37ºC with shaking for 10min in a Hybaid Midi Dual 14 incubator (United Scientific, Cape Town, South Africa). The resulting coloration was measured via absorbance at 570nm in a Synergy HT luminometer using KC4™ software version 3.4. Background absorbance was simultaneously measured at 650nm and subtracted from absorbance at 570nm. Statistical significance was measured as described in Section 2.30.

2.26.4 CyQUANT® assay

CyQUANT® assays were performed using a CyQUANT® NF Cell Proliferation Assay Kit (Life Technologies, Carlsbad, California, USA), according to manufacturer's instructions. Briefly, the culture media was removed from the cells in a 96-well plate, and the wells gently rinsed once with 200µl pre-warmed sterile PBS. A volume of 100µl of 1X dye binding solution was added to each well. The plate was then incubated in the dark at 37ºC in a Farma thermosteri-cycle 5% CO_2 humidified incubator for 1h. The subsequent fluorescence intensity was measured in a Synergy HT

luminometer using KC4™ software version 3.4, with excitation at 480nm and emission detection at 530nm. Statistical analysis was performed as described in Section 2.30.

2.27 MITOCHONDRIAL RESPIRATION ANALYSIS

Measurements of mitochondrial respiration are strong indicators of the functional capacity of mitochondria, and of overall cellular health. While classical respirometric methods largely rely on the use of Clark oxygen electrodes, these approaches are not conductive to the simultaneous measurement of several samples, and require large quantities of cells. The Seahorse Extracellular Flux Analyzer overcomes these challenges by using a plate-based approach and fluorescence detectors to accurately measure cellular oxygen consumption (Ferrick et al. 2008). Furthermore, the Seahorse Analyzer allows for the sequential addition of pharmacological inhibitors to probe the function of individual components of the mitochondrial respiratory chain in a single experiment. This can then be expressed as various parameters of mitochondrial function, such as basal respiration, ATP coupling efficiency and spare respiratory capacity, which can be insightful gauges of mitochondrial health (Brand and Nicholls 2011).

The present study used a Seahorse Analyzer, located in the Mito Laboratory of North West University, Potchefstroom, South Africa, to investigate mitochondrial respiratory control in parkin-null and wild-type fibroblasts. Furthermore, the effect of vitamin K_2 treatment on mitochondrial respiration was determined. All mitochondrial respiration assays were kindly performed by Dr. Chrisna Swart.

2.27.1 Seahorse Analyzer assay

Mitochondrial respiration assays were done using a Seahorse XF96 Cell Mito Stress Test Kit (Seahorse Biosciences, North Ballerica, Massachusetts, USA), in accordance with manufacturer's instructions. Briefly, fibroblasts were seeded at a density of 22 000 cells per well in a 96-well Seahorse assay plate: cells that were to be treated with vitamin K_2 were seeded into 80µl of 40µM MK-4 solution in culture media (Appendix II), whereas cells that were not treated with vitamin K_2 were seeded into 80µl of 0.1% (v/v) ethanol in culture media. The plate was then incubated at 37˚C with 5% CO_2 for 24h.

The following day, a Seahorse XF96 Extracellular Flux Analyzer (Seahorse Biosciences, North Ballerica, Massachusetts, USA) and XF^e Wave software (Seahorse Biosciences, North Ballerica, Massachusetts, USA) was used to measure the oxygen consumption rate (OCR) of each well. A

period of 1h before the measurements were initiated, the culture media in each well was replaced with 150µl of Seahorse assay media supplemented with 1mM pyruvate, and the plate was incubated for 1h at 37˚C without CO_2. Then, a series of successive OCR measurements were performed, which consisted of three basal OCR measurements, three OCR measurements after the automated injection of 1µM oligomycin into each well, three OCR measurements after the injection of 1µM carbonyl cyanide p-trifluoromethoxyphenyl hydrazone (FCCP), and three final OCR measurements after the dual injection of 1µM rotenone and 1 µM antimycin A. Oligomycin was used to inhibit the mitochondrial F_1F_0-ATP synthase; FCCP is a protonphore used to depolarize the inner mitochondrial membrane, and rotenone and antimycin A were used to inhibit complex I and complex III, respectively. All four of these reagents were included in the Seahorse XF96 Kit, and the working concentrations of all four were optimized to identify their minimum effective concentration. Experimental treatments were performed on six wells of each plate as technical replicates. After all twelve OCR measurements were taken, the plate was saved and the relative DNA content in each well was measured using a CyQUANT® assay (Section 2.26.4).

2.27.2 Analysis of mitochondrial respiratory control

The Seahorse assays (Section 2.27.1) were analyzed using XF^e Wave software, according to manufacturer's instructions. All OCR measurements were normalized to cell number as determined by a CyQUANT® assay. These normalized OCR measurements were used to calculate various mitochondrial parameters: The minimum OCR after rotenone and antimycin A injection was interpreted as the OCR due to non-mitochondrial respiration, and this rate was subtracted from all other responses in order to isolate mitochondrial OCR. The basal mitochondrial OCR was defined as the third measurement under basal conditions (the last measurement prior to oligomycin injection, after non-mitochondrial OCR subtraction). The oligomycin response, indicative of the OCR due to the proton leak across the inner mitochondrial membrane, was defined as the minimum OCR after oligomycin injection. The decline in OCR after oligomycin injection is indicative of the OCR due to ATP synthesis, and the ratio of this decline to the basal OCR was expressed as the ATP coupling efficiency. The FCCP response was defined as the maximum OCR after FCCP injection, and the ratio of this response to the basal OCR was used to calculate the spare respiratory capacity. These parameters, as well as the overall OCR measurements, were statistically analyzed as described in Section 2.30.

2.28 MITOCHONDRIAL MEMBRANE POTENTIAL ANALYSIS

Maintenance of the mitochondrial membrane potential ($\Delta\psi_m$) is essential for the proper functioning and health of cells, particularly for cells with high energetic demands, and measurements of $\Delta\psi_m$ can be used as an indicator of the energization state and health of cellular mitochondria. In the present study, $\Delta\psi_m$ was assessed with the tetraethyl benzimidazolyl carbocyanine iodide (JC-1) cationic dye and flow cytometric methods. JC-1 exhibits potential-dependent accumulation in mitochondria, resulting in a fluorescence emission shift from 525nm (green) to 590nm (red). Therefore, loss of $\Delta\psi_m$ is detectable by the decrease in the red:green florescence emission ratio (Reers et al. 1995).

2.28.1 Preparation and staining of fibroblasts with JC-1

Differences in $\Delta\psi_m$ were assessed in patient and wild-type fibroblasts with and without vitamin K_2 treatment. This was done as follows: Fibroblasts cells were cultured in T25 CellStar® tissue culture flasks until a confluency of 70-80% was reached. Two additional wild-type fibroblast flasks were cultured for subsequent use as positive and unstained controls, respectively. The culture media was discarded and a volume of 5ml of 40µM MK-4 solution in culture media (Appendix II) was added to cells that were to be treated with vitamin K_2. Alternatively, cells that were not treated with vitamin K_2 were incubated in 0.1% (v/v) ethanol in culture media. The flasks were left to incubate for 24h at 37ºC in a Farma thermosteri-cycle 5% CO_2 humidified incubator.

Thereafter, the culture media was removed and the cell monolayer stained with 3ml pre-warmed 0.5µg/ml JC-1 solution (Life Technologies, Carlsbad, California, USA) (Appendix II); 3ml clean culture media was added to the unstained control. The positive control flask was co-treated with CCCP at a final concentration of 50µM. CCCP is a potent electron transport chain uncoupler; in the present study CCCP was used to artificially induce the loss of $\Delta\psi_m$. The cell monolayers were stained in the dark for 1h at 37ºC in a Farma thermosteri-cycle 5% CO_2 humidified incubator. Afterwards, the staining solution was removed and the stained cells briefly rinsed with pre-warmed sterile PBS. The cells were detached by trypsin treatment (Section 2.21.3) and each cell suspension transferred to a 12ml Greiner tube and centrifuged at 1000rpm for 2min in a Sorval® GLC-6 general laboratory centrifuge. The supernatants were discarded and the pellets resuspended in 1ml of pre-warmed PBS to give an approximate final concentration of 200 000-300 000 cells/ml.

2.28.2 Flow cytometry and analysis

JC-1 dye equilibration was allowed for 10min at room temperature, after which the stained cell suspensions were immediately analyzed at the Flow Cytometry Unit of CAF at Stellenbosch

University, Cape Town, South Africa. A BD FACSCalibur flow cytometer (Becton Dickinson, Franklin Lakes, New Jersey, USA) and BD CellQuest PRO software (Becton Dickinson, Franklin Lakes, New Jersey, USA) was employed to this end. The JC-1 fluorophore was excited with a 488nm argon-ion laser after which red and green emission were separately detected in the FL1 and FL2 channels, respectively, using standard PMT detectors. Debris and aggregates were gated out by establishing a population of interest based on forward scatter/side scatter (FSC/SSC) properties. Compensation between FL1 and FL2 was carefully adjusted in reference to the CCCP-treated positive control sample, according to the manufacturer's instructions. A total of 10 000 events were collected per sample per run, and each fibroblast culture was assessed by means of JC-1 staining and flow cytometry in three separate experiments. Statistical differences were assessed as described in Section 2.30.

2.29 MITOCHONDRIAL NETWORK ANALYSIS

Despite the classic depiction of mitochondria as rod-like, individual organelles, mitochondria are in fact engaged in a complex cellular network that constantly fuses and divides. The morphology of this mitochondrial network is carefully maintained by the dual processes of mitochondrial fission and fusion, which act to regulate mitochondrial integrity and function (Detmer and Chan 2007). Dysregulation of such mitochondrial dynamics, perceivable as mitochondrial swelling and fragmentation of the mitochondrial network, can be used as an informative marker of cellular and mitochondrial dysfunction (Burbulla et al. 2010). In the present study, the mitochondrial morphology of fibroblast cells was assessed by means of live-cell fluorescence microscopy, where the Mitotracker® Red CMXRos dye was used to visualize the mitochondrial network.

2.29.1 Preparation of fibroblasts for live-cell microscopy

Mitochondrial morphology was assessed in patient and wild-type fibroblasts with and without vitamin K_2 treatment. This was done as follows: An aliquot of a cell suspension to be subcultured (Section 2.21.3) was used to perform a hemocytometric cell count (Appendix III). Thereafter, a volume of cell suspension containing approximately 3000 cells was seeded per well in a Nunc® Lab-Tek® 8-well chamber slide (Thermo Scientific, Waltham, Massachusetts, USA). The chamber slide was incubated at 37ºC in a Farma thermosteri-cycle 5% CO_2 humidified incubator overnight (16h).

The following morning, the culture media was removed and a volume of 200µl of 40µM MK-4 solution in culture media (Appendix II) was added to wells containing cells that were to be treated with vitamin K_2. Alternatively, cells that were not treated with vitamin K_2 were incubated in 0.1%

(v/v) ethanol in culture media. The chamber slide was returned to the Farma thermosteri-cycle 5% CO_2 humidified incubator and incubated for a further 24h.

2.29.2 Live-cell fluorescence microscopy and analysis

Fluorescence image acquisition was performed at the Cell Imaging Unit of CAF at Stellenbosch University, Stellenbosch, South Africa. An Olympus IX-81 motorized inverted fluorescence microscope (Olympus Biosystems GmbH, Tokyo, Japan), equipped with a F-view-II cooled CCD camera (Soft Imaging Systems, Berlin, Germany), and Cell^R software (Olympus Biosystems GmbH, Tokyo, Japan) was employed to this end.

Staining and imaging of the cultured cells was performed with each well of the chamber slide separately, in order to reduce photobleaching of the dye as well as dye-induced cytotoxicity. Briefly, the culture media was removed from the well to be stained, after which 100µl of a 100nM solution of Mitotracker® Red CMXRos (Life Technologies, Carlsbad, California, USA) in pre-warmed culture media was added to the well. The chamber slide was placed on the viewing deck of the Olympus IX-81 microscope inside a live-cell environmental chamber, where it was incubated for 5min at 37ºC and 5% CO_2 before viewing. Fluorescence was excited through a 572nm excitation filter, and fluorescence emission collected at 599nm using a UBG triple-bypass emission filter cube and an Olympus Plan AP N 60X/1.42 oil-immersion objective. All images were acquired as Z-stacks, with 7-12 image frames per stack and increments of 0.26-0.3µm between frames. A total of six images were taken per sample per experimental run, after which the next sample was separately stained and imaged. Each sample was stained and imaged in quadruplicate.

Following image acquisition, the images were deconvoluted using the Cell^R software in order to remove out-of-focus fluorescent signal. The Z-stack was then exported as a maximum intensity projection in TIFF file format for further processing and analysis. Clearly visible cells were individually analyzed using ImageJ Software version 1.47 (http://imagej.nih.gov/ij) with an average of 40 cells analyzed per sample across all experimental runs. Image analysis was performed as follows: Raw images were binarized by conversion to 8-bit image format and optimized by manual contrast adjustment to reduce non-specific fluorescent signal. The individual morphological characteristics of the mitochondria within a given cell, such as area, perimeter, and major and minor axes, were measured by the ImageJ software. These parameters were used to calculate and describe the morphological characteristics of the mitochondrial network of the cell, including the aspect ratio (ratio between the major and minor axes of the ellipse equivalent to the mitochondrion) and the form factor (defined as $\frac{\text{perimeter}^2}{4\pi \times \text{area}}$). The aspect ratio is consistent with mitochondrial length, whereas form

factor is a quantification of the degree of branching of the mitochondrial network. Statistical analyses were performed as detailed below (Section 2.30).

2.30 STATISTICAL ANALYSIS

All statistical analyses were performed by Prof. Lize van der Merwe. The freely-available program R, a language and environment for graphics and statistical computing (http://www.r-project.org), and R packages *nlme* and *effects* were used for statistical modeling and graphics (Fox 2003; R Core Team 2012; Pinheiro et al. 2014).

General linear modeling was used for pairwise comparisons of outcomes between individual fibroblast cell lines. When grouped patient-derived and wild-type fibroblasts were compared, a mixed-effects linear model was used, with groups as fixed effects. Here, adjustments were made for the effect that the observations on a specific cell line will be correlated. Separate experimental runs were modeled as random effects. All effect sized, confidence intervals and *p*-values were derived from the results of the specific models. All results corresponding to a *p*-value of <0.05 were described as statistically significant. Results were not adjusted for multiple testing because it has been suggested that corrections, such as Bonferroni, are too conservative when several associations are tested in the same group of individuals (Perneger 1998). Results may therefore be considered hypothesis-generating, where functional explanations of observed statistical differences may support the plausibility of such results.

For analysis of the protein expression levels (Section 2.25.4), the relative densitometry measurements (for each fibroblast lysate) for a given protein of interest in a given experimental run, were adjusted for differences in relative densitometry of the loading control (GAPDH) in the corresponding lysates, for the particular experimental run. Differences in protein expression between individual fibroblast cell lines were assessed by means of a general linear model, whereas mixed-effects linear modelling was used to compare grouped patient vs. grouped wild-type control fibroblasts. Here, effect plots were generated for the interaction between protein level and group identity (whether patient or wild-type).

All assessments of the effects of treatments, whether with CCCP (Section 2. 26) or with MK-4 (Sections 2.26-2.29) required a statistical interaction term in the general linear models (for assessments within individual fibroblast cell lines) or in the mixed-effects linear models (for assessments within groups). Where appropriate, a 2^2 factorial design was used to model effects of treatment on various outcomes. For analysis of mitochondrial network morphology (Section 2.29.2), all outcome distributions were transformed (taking the natural logarithm) in order to approach normality, as the untransformed distributions of form factor and aspect ratio were positively skewed.

CHAPTER THREE: RESULTS

TABLE OF CONTENTS PAGE

CHAPTER THREE: RESULTS

3.1 *PARKIN* MUTATION SCREENING

Our research group has previously reported on a molecular analysis of *parkin* in 91 South African PD patients (Bardien et al. 2009), as well as exon dosage analysis of these patients (Keyser et al. 2009). The present study expands on that work by the screening of an additional 138 South African PD patients. The results reported here are on the combined total of 229 patients.

3.1.1 Characteristics of the study group

Relevant demographic and clinical data of the study group is summarized in Table 3.1. The mean AAO of the PD patients was 54.4 ± 12.1 years, ranging from 17-80 years. The majority (132/229; 57.6%) of the study participants either had EOPD (defined as an AAO <=50 years) or a positive family history of PD. The study group was ethnically heterogeneous, consisting of 71.2% (163/229) Caucasian, 19.7% (45/229) Mixed ancestry, 7.4% (17/229) Black and 1.7% (4/229) Indian patients. Amongst the Caucasian patients, 41.7% (68/163) were of Afrikaner descent, a uniquely South African population known to have undergone a genetic bottleneck during the 19th century (Le Saux et al. 2002). The Mixed ancestry ethnic group refers to a uniquely admixed population with genetic contributions from indigenous African, European, Malagasy, Indian and South-East Asian populations (Patterson et al. 2009). The Black patient group consisted of Xhosa-speaking individuals from the South African Nguni ethnic group; indigenous Sub-Saharan African populations, such as the Nguni, exhibit complex evolutionary histories and remarkable degrees of genetic diversity (Tishkoff et al. 2009). The South African Indian subpopulation is mostly descended from indentured workers brought to South Africa in the 19th century.

Table 3.1 Demographic and clinical characteristics of 229 South African PD patients

	Total N = 229
AAO, mean ± SD, (range)	54.4 ± 12.1 years (17-80 years)
AAO<=50	82 (35.8%)
Family history of PD	81 (35.4%)
AAO <= 50 years and/or family history of PD	132 (57.6%)
Males	145 (63.3%)
Families with consanguinity	2
Ethnicity	
Caucasian	163 (71.2%)
Mixed ancestry	45 (19.7%)
Black	17 (7.4%)
Indian	4 (1.7%)

Abbreviations: AAO, age at onset; N, sample size; PD, Parkinson's disease; SD, standard deviation.

3.1.2 *Parkin* variants identified in South African PD patients

The study participants were screened for mutations in *parkin*, using HRM to detect point mutations and small insertions/deletions (Section 2.6) and MLPA to detect exonic rearrangements (Section 2.8). In total, this study identified seven patients with homozygous or compound heterozygous mutations in *parkin* in the 229 South African PD patients (Figure 3.1, Table 3.2).

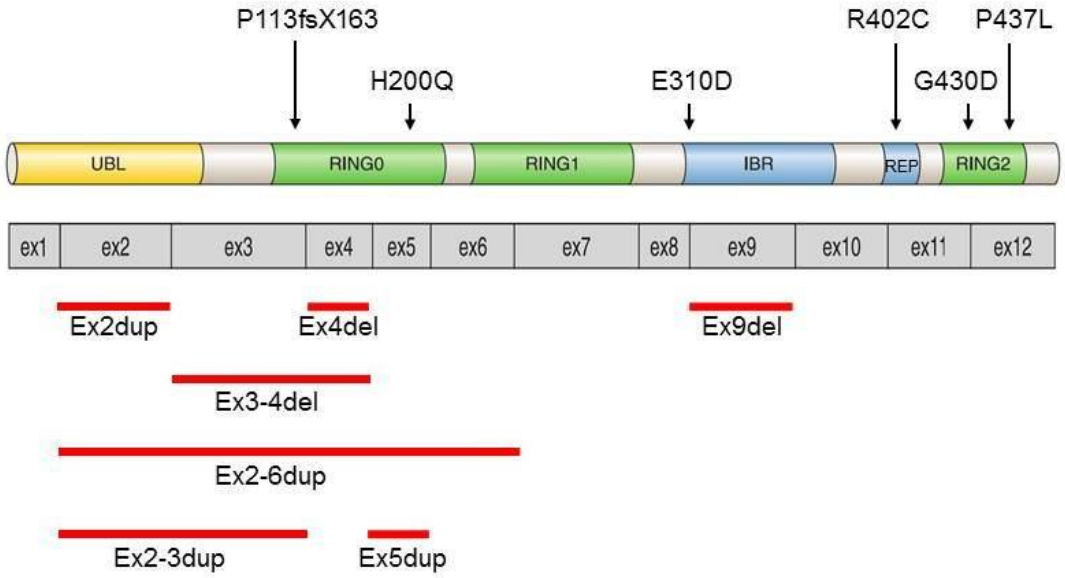

Figure 3.1 Schematic representation of *parkin*, with locations of mutations and sequence variants identified in this study indicated. The top figure represents the parkin protein sequence, with functional domains as indicated. The bottom figure represents the *parkin* coding sequence, where exon rearrangements are indicated by red lines representing their locations and sizes. Abbreviations: Del, deletion; dup, duplication; ex, exon; IBR, in-between RING; UBL, ubiquitin-like; UP, unique parkin.

The patient labeled ID 1 (henceforth referred to as patient 1), a Black male with an AAO of 45 years, was found to harbor compound heterozygous mutations: a duplication of exon 2 and a deletion of exon 9. The same mutations were found in an affected female sibling; both siblings had an early AAO (<50 years) and presented with typical tremor predominant PD. The exon dosage mutations were detected by MLPA analysis; however, the presence of these mutations was not confirmed via RT-PCR analysis on the proband's lymphocytes as the patient was lost to follow-up. Interestingly, patient 1, along with patient 107, is one of only three cases of *parkin* mutations in Black Sub-Saharan African patients reported to date, with the third being a Zambian PD patient (Yonova-Doing et al. 2012; Blanckenberg et al. 2013).

Table 3.2 Putative and established mutations identified in *parkin* in 229 South African PD patients

Patient ID	Ethnicity	AAO (years)	Family History	Mutation status	In controls	Protein domain	PolyPhen-2 prediction	MutationTaster prediction	Study*
Compound heterozygous/ homozygous mutations									
1	Black	45	Yes	Duplication exon 2 het + Deletion exon 9 het	ND ND	UBL IBR			Keyser et al. 2009
16	Caucasian	27	Yes	Deletion exon 4 hom	ND	RING0			Bardien et al. 2009
23	Mixed ancestry	27	No	Deletion exon 3-4 hom	ND	RING0			Bardien et al. 2009
105	Caucasian	25	Yes	P113fsX163 het + Deletion exon 3 het	ND ND	RING0 RING0			Present study
107	Black	56	No	G430D (G**G**C > G**A**C) het (rs191486604) + Deletion exon 4 het	0/106 ND	RING2 RING0	Probably damaging	Disease causing	Present study
108	Caucasian	27	No	G430D (G**G**C > G**A**C) het + Deletion exon 4 het	0/106 ND	RING2 RING0	Probably damaging	Disease causing	Present study
121	Caucasian	48	Yes	Duplication exon 2-6 het + Duplication exon 5 het	ND	UBL; RING0 RING0			Present study
Heterozygous variants									
11	Caucasian	37	No	R402C (**C**GT > **T**GT) het (rs55830907)	0/100	REP	Probably damaging	Polymorphism	Bardien et al. 2009
21	Caucasian	42	No	E310D (GA**G** > GA**C**) het (rs72480423)	0/110	IBR	Benign	Disease causing	Bardien et al. 2009
31	Caucasian	56	No	Duplication exon 2 het	ND	UBL			Keyser et al. 2009
61	Caucasian	55	Yes	H200Q (CA**C** > CA**G**) het (rs72480421)	0/106	RING0	Possibly damaging	Polymorphism	Bardien et al. 2009
91	Mixed ancestry	50	No	Duplication exon 2-3 het	ND	UBL; RING0			Keyser et al. 2009
126	Mixed ancestry	49	Yes	Deletion exon 4 het	ND	RING0			Present study
133	Caucasian	54	No	P437L (C**C**G > C**T**G) het (rs56092260)	0/110	RING2	Probably damaging	Disease causing	Present study
217	Mixed ancestry	61	No	Deletion exon 3-4 het	ND	RING0			Present study

*Mutation status was reported in various publications: Bardien et al. (2009), Keyser et al. (2009) and the present study (Haylett et al. 2012). Abbreviations: AA0, age at onset; het, heterozygote; hom, homozygote; IBR, in between RING domain; ND, not determined; PD, Parkinson's disease; RING, RING-finger motif; UBL, ubiquitin-like domain.

A homozygous exon 4 deletion was found in patient 16, a Caucasian female with an early AAO of 27 years. Her affected sibling has the same homozygous exon 4 deletion. Both the proband and her sibling presented with typical PD features as well as dystonia. RNA was obtained from the patient and her sibling and RT-PCR used to confirm the presence of these mutations; this is illustrated in Figure 3.2A and B. Furthermore, dermal fibroblasts were obtained from this patient and her affected sibling by means of a skin biopsy (Section 2.21.1) for subsequent studies. The results emanating from such functional studies will be described later in this dissertation.

Patient 23 also has an early AAO (27 years), but was not aware of any family history of PD. The homozygous exon 3-4 deletion of patient 23 was confirmed by RT-PCR and sequencing analysis (Figure 3.2C). The patient presented with mild dyskinesia, tremor and dystonia of her left leg, and responded well to levodopa therapy. Dermal fibroblasts were obtained from this patient for use in functional studies of the homozygous *parkin* exon 3-4 deletion.

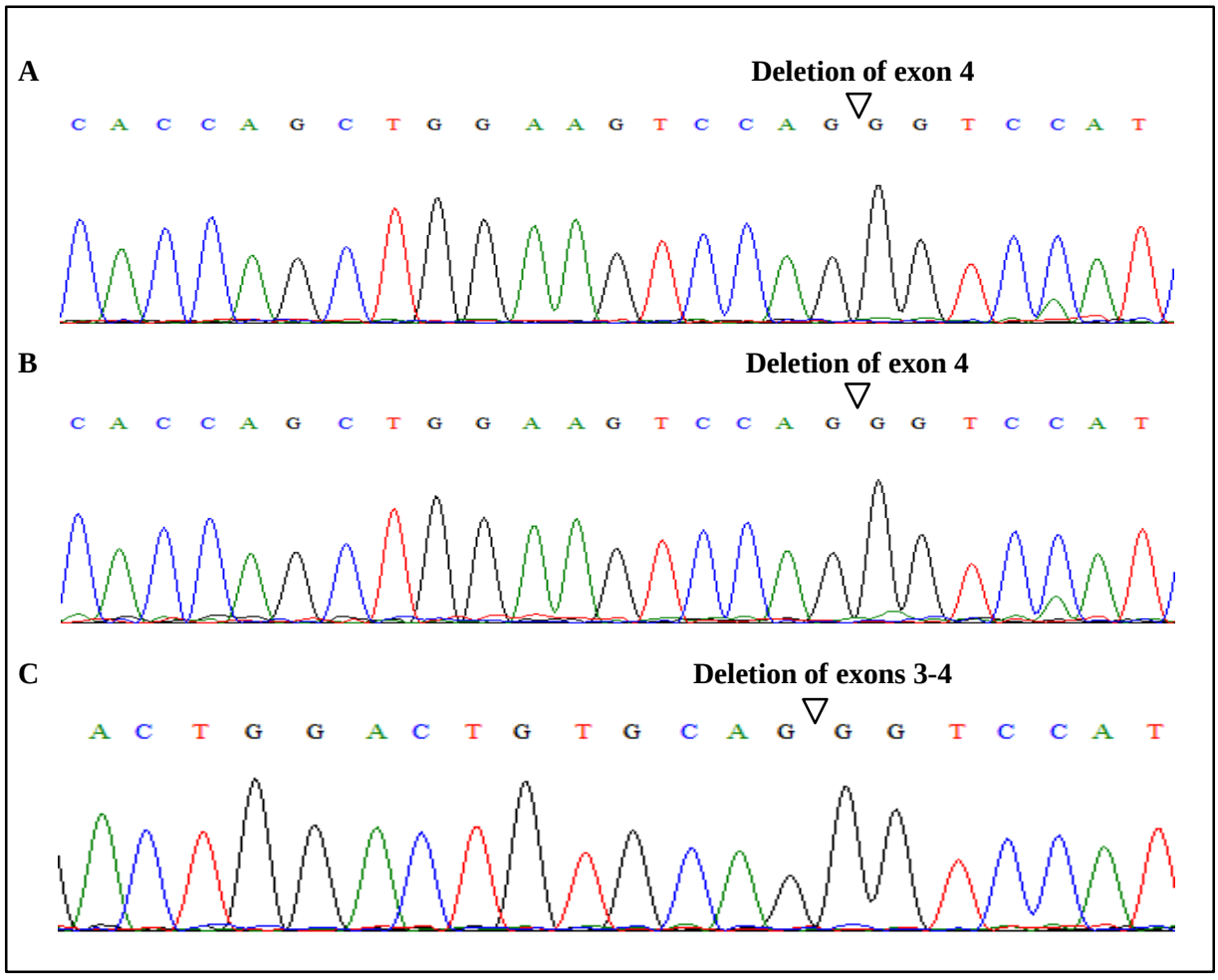

Figure 3.2 DNA sequence analysis of RT-PCR products which verify the presence of deletions in *parkin*. Positions of the deletions are indicated. **A**, patient 16 with homozygous whole exon 4 deletions. **B**, the affected sibling of patient 16, also with homozygous whole exon 4 deletions. **C**, patient 23 with homozygous whole exon 3-4 deletions.

In one patient (patient 105) a heterozygous 40bp deletion in *parkin* exon 3 resulting in a frameshift mutation (P113fsX163; c.337_376del) was found. The patient's other allele was found to harbor a heterozygous deletion of exon 3, which was confirmed with RT-PCR and sequencing analysis. This patient presented with gradual onset of dystonia in the legs, followed by onset of mild features of PD nine years later at the age of 25 years. This individual has Irish ancestry on both his maternal and paternal side, which is consistent with previous reports of this 40bp *parkin* exon 3 deletion (Lincoln et al. 2003).

Interestingly, two unrelated patients (patient 107 and 108), of different ethnic backgrounds (Black and Caucasian, respectively) each harbored identical compound heterozygote mutations; a heterozygous G430D and a whole exon 4 deletion. DNA samples from family members of the patients could not be obtained, which precluded haplotype analysis to determine the relatedness of the patients. The two patients, patient 107 and 108, have an AAO of 56 and 27 years, respectively. Both patients presented with typical tremor predominant PD; prominent left arm dystonia was seen in patient 107. The finding of parkin mutations in a patient with an AAO > 50 years justifies the inclusion of patients with older AAO's in our setting.

Patient 121 was found to harbor a compound heterozygous mutation consisting of an exon 2-6 duplication on one allele and an exon 5 duplication on the other allele. This female Caucasian patient reported family history of PD and has an AAO of 48. The patient presented with typical features of PD, with good levodopa responsiveness and occasional hypotension.

In addition to these seven PD patients with homozygous or compound heterozygous *parkin* mutations, heterozygous missense variants (H200Q, E310D, R402C, P437L), and various exonic deletions and duplications were found in a further eight patients but currently the pathogenicity of these single heterozygous variants are unclear (Table 3.2). In cases where only a single *parkin* mutation was detected, all twelve *parkin* exons were subjected to direct sequencing (Section 2.7) in order to verify the absence of a second mutation. All of the point mutations were detected only in the patients under study, being absent in over 100 control chromosomes. It should however be noted that heterozygosity for a deletion or duplication encompassing more than one exon could in fact be due to compound heterozygosity for two different exon rearrangements acting in *trans*. This may be the case for patient 91 (involving exons 2 and 3) and patient 217 (exons 3 and 4). Further clarifying studies could be performed on these individuals in order to determine the phase of the exon rearrangements; this could not be done in the present study as neither RNA from the patient nor DNA from family members were available for RT-PCR or haplotype analysis, respectively.

3.1.3 *Parkin* polymorphisms identified in South African PD patients

In addition to mutations, numerous polymorphisms were detected in *parkin* (Table 3.3). Sequence variants were designated as polymorphisms if the variant was located in a non-coding region, resulted in a silent substitution (P37P, C238C, L261L, A397A and R402R), had been previously described as a polymorphism (A82E) or if the variant was observed in ≥1% of ethnically-matched control chromosomes (Q34R, S167N, M192L, R334C, V380L and D394N). All of the polymorphisms detected in our study had been previously described. Interestingly, the S167N and M192L polymorphisms had been previously described as pathogenic variants (Satoh and Kuroda 1999; Hedrich et al. 2002); however, the high frequencies of these sequence variants found in control chromosomes from South African individuals (7.9% and 6.7%, respectively; Table 3.3) make it unlikely that they are of pathogenic relevance.

Table 3.3 Polymorphisms identified in the *parkin* gene in 229 South African PD patients

Sequence variant	Ethnicity of patient(s) with variant	Frequency in controls* (%)
5'UTR -258T > G	Caucasian, Mixed ancestry and Black	14.0 (Caucasian) 18.0 (Mixed ancestry)
5'UTR -227A > G	Caucasian and Mixed ancestry	ND
5'UTR -89C > T	Caucasian	ND
IVS1 +42C > T	Mixed ancestry	ND
Q34R (C**A**G > C**G**G)	Mixed ancestry	3.2
P37P (CC**G** > CC**A**)	Mixed ancestry and Black	ND
IVS2 +10C > T	Mixed ancestry	0
IVS2 +20delC	Mixed ancestry	4.8
IVS2 +25T > C	Mixed ancestry and Black	ND
IVS2 +35G > A	Caucasian and Mixed ancestry	ND
IVS2 +62G > A	Mixed ancestry	ND
IVS3 -20T > C	Caucasian	ND
A82E (C**G**A > G**A**A)	Caucasian	0
S167N (A**G**C > A**A**C)	Caucasian and Mixed ancestry	7.9
M192L (**A**TG > **C**TG)	Mixed ancestry	6.7
C238C (TG**C** > TG**T**)	Black	ND
L261L (TT**A** > TT**G**)	Black	ND
IVS7 -68C > G	Caucasian	ND
IVS7 -35G > A	Caucasian and Black	ND
IVS8 +43A > G	Mixed ancestry and Black	ND
IVS8 +48C > T	Caucasian and Black	ND
IVS8 -21_-17del	Mixed ancestry	ND
R334C (**C**GC > **T**GC)	Mixed ancestry and Indian	2.0 (Mixed ancestry)
V380L (**G**TA > **C**TA)	Caucasian, Mixed ancestry and Black	27.2 (Caucasian)
D394N (**G**AT > **A**AT)	Caucasian, Mixed ancestry, Black and Indian	6.0 (Caucasian)
A397A (GC**C** > GC**T**)	Mixed ancestry	ND
R402R (CG**T** > CG**C**)	Mixed ancestry and Black	ND
3'UTR *16G > A	Mixed ancestry	ND
3'UTR *94A > G	Caucasian	ND
3'UTR *103C > T	Black	ND

*Frequency was only determined for exonic, non-synonymous variants. Abbreviations: del, deletion; IVS, intervening sequence; ND, not determined.

Possible heterozygous whole exon 5 deletions of *parkin* had been detected in two patients; however, this putative deletion was only detected by the P051 MLPA probe set and not by the P052 set. Further investigation revealed that the two patients with ostensible whole exon 5 deletions were in fact heterozygous for the M192L polymorphism. The presence of this polymorphism disrupts the binding site of a probe in the P051 MLPA kit, resulting in a false positive result (Figure 3.3). This exemplifies the benefit of using two different MLPA kits to reduce the risk of false positives, and only exon dosage mutations in *parkin* that were independently detected by both MLPA kits were considered as true positive results.

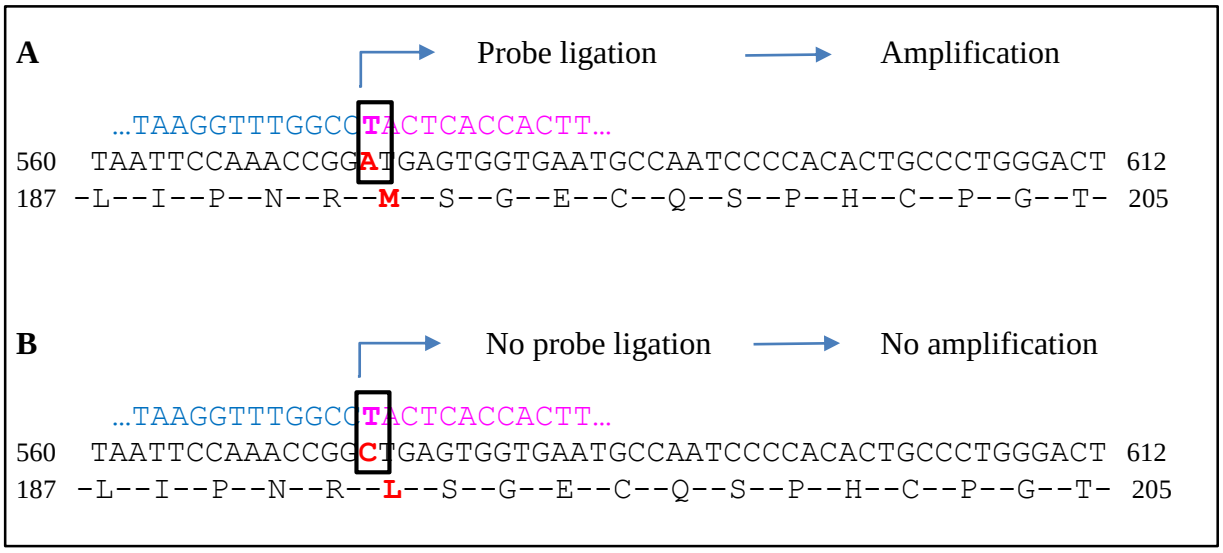

Figure 3.3 The M192L *parkin* polymorphism disrupts the binding site of a P051 MLPA probe. The partial *parkin* CDS and the encoded amino acid sequence are listed in black font. The position of the c.574A>C; M192L polymorphism is illustrated in **red** font. Partial sequences of the two halves of the 366bp P051 MLPA probe (probe 02177-L24889) are indicated in blue and pink. **A**, *parkin* sequence harboring the major allele (A) of the M192L polymorphism. The two halves of the MLPA oligonucleotide probe anneal adjacent DNA sequences. This allows for oligonucleotide probe ligation, MPLA primer binding and successful amplification, which would indicate the presence of exon 5. **B**, *parkin* sequence harboring the minor allele (C) of the M192L polymorphism. The pink half of the MLPA probe does not properly anneal at the ligation site (black box); hence, no oligonucleotide probe ligation or amplification takes place. This would falsely indicate the absence of exon 5.

3.2 IDENTIFICATION AND VERIFICATION OF PARKIN INTERACTORS

In order to further current knowledge on the role of parkin in health and disease, a focus of the present study was to use a Y2H approach to identify novel parkin-interacting proteins (Section 3.2.1). Such putative interactors were verified under biologically-relevant conditions using two *in vivo* approaches: 3D co-localization and co-IP (Section 3.2.3). The effect of the lack of parkin on each interacting protein was also evaluated in cellular models of parkin deficiency (Section 3.2.4)

3.2.1 Parkin Y2H analysis

3.2.1.1 *Generation of parkin Y2H bait construct*

The pGBKT7-*parkin* Y2H bait construct was successfully cloned as described in Section 2.13. The construct was subjected to DNA sequencing and sequence analysis, which confirmed that both the correct reading frame and insert sequence integrity had been retained throughout the cloning process.

3.2.1.2 *Phenotypic assessment of yeast strains*

The pGBKT7-*parkin* Y2H bait construct was used to transform *S. cerevisiae* strain AH109. This transformed strain, as well as untransformed AH109 and Y187 host strains, was assessed for their ability to grow on various nutritionally-deficient selection plates. Untransformed AH109 and Y187 were able to grow on SD^{-Ura} plates, but did not grow on SD^{-Trp}, SD^{-Leu}, SD^{-His} and SD^{-Ade} plates. This confirmed the viability and purity of the untransformed strains. AH109 transformed with pGBKT7-*parkin* was able to grow on SD^{-Ura} and SD^{-Trp} plates, but did not grow on SD^{-Leu}, SD^{-His} and SD^{-Ade} plates, which confirmed that the phenotype of AH109 was retained following transformation. Additionally, this verified that the *HIS3* and *ADE2* reporter genes were not autonomously activated by expression of the bait protein. Phenotypic assessment of yeast strains is summarized in Table 3.4.

Table 3.4 Phenotypic assessment of *S. cerevisiae* strains

Nutritional selection plate	AH109	Y187	AH109 transformed with pGBKT7-*parkin*
SD^{-Ura}	++	++	++
SD^{-Trp}	-	-	++
SD^{-Leu}	-	-	-
SD^{-His}	-	-	-
SD^{-Ade}	-	-	-

Abbreviations: ++, growth; -, no growth; -Ade, lacking adenine; -His, lacking histidine; -Leu, lacking leucine; -Trp, lacking tryptophan; -Ura, lacking uracil; SD, synthetic defined.

3.2.1.3 *Yeast transformation toxicity test*

Prior to Y2H analysis, a toxicity test was performed to determine whether the Y2H bait construct detrimentally affected the growth of *S. cerevisiae* strain AH109 (Section 2.18.2). To this end, a growth curve of AH109 transformed with the pGBKT7-*parkin* bait construct was generated and compared to a growth curve of AH109 transformed with non-recombinant pGBKT7 (Figure 3.4). It was determined that the bait construct had no significant effect of the growth of AH109, as evidenced by the similar gradients of the pGBKT7-*parkin* growth curve (gradient = 0.0241) and the non-recombinant pGBKT7 growth curve (gradient = 0.0256).

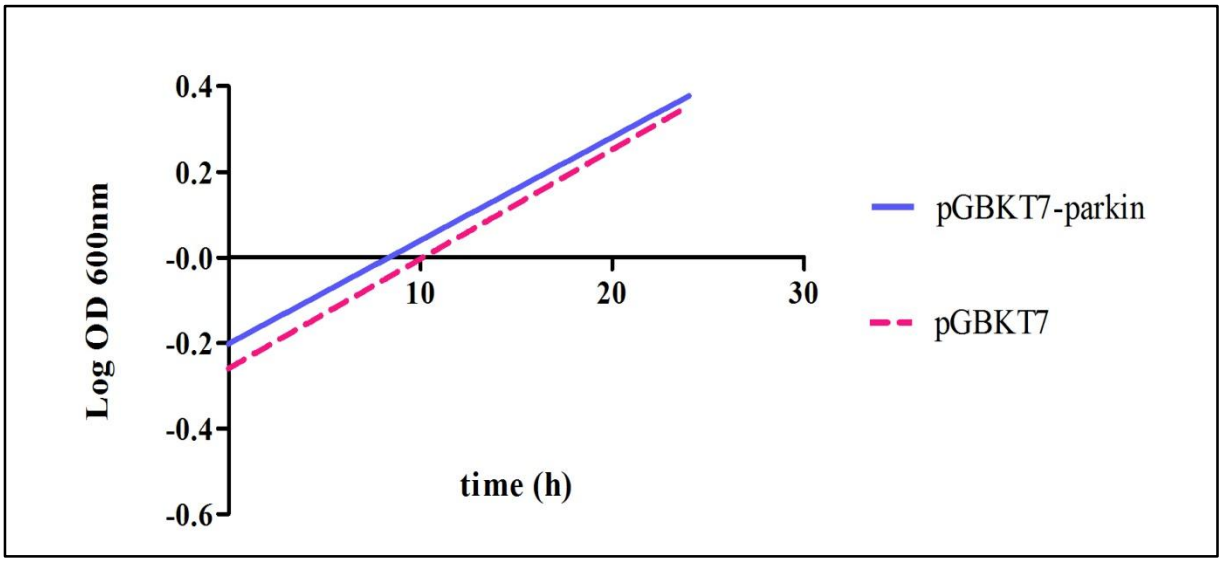

Figure 3.4 Linearized growth curves of *S. cerevisiae* strain AH109 transformed with pGBKT7-*parkin* and non-recombinant pGBKT7. Similar growth rates of AH109 transformed with pGBKT7-*parkin* and non-recombinant pGBKT7 demonstrated that pGBKT7-*parkin* did not adversely affect the growth of AH109. Abbreviations: Log, logarithm; nm, nanometer; OD, optical density.

3.2.1.4 *Mating efficiency determination*

Prior to Y2H analysis, *S. cerevisiae* strain AH109 transformed with pGBKT7-*parkin* bait construct was mated with Y187 transformed with non-recombinant pGADT7 (Section 2.18.3). An additional assessment of AH109 transformed with pGBKT7-*53* and mated with Y187 transformed with non-recombinant pGADT7 served as a positive control mating. It was concluded that the bait construct did not adversely affect the mating efficiency of AH109 (Table 3.5). During Y2H analysis a further small-scale mating assessment was performed. AH109 transformed with pGBKT7-*parkin* bait construct was mated with Y187 transformed with the pGADT7-cDNA library (Section 2.19.5). This delivered an actual Y2H mating efficiency of 11.6%, which is well above the minimum mating efficiency of 2% recommended by the MATCHMAKER™ Y2H system manufacturer (Clontech, Palo Alto, California, USA).

Table 3.5 Effect of Y2H bait construct on *S. cerevisiae* AH109 mating efficiency

Mating pairs	Mating efficiency (%)
pGBKT7-*parkin*::AH109 X pGADT7::Y187	17.9
pGBKT7-*53*::AH109 X pGADT7::Y187	10.1
pGBKT7-*parkin*::AH109 X pGADT7-cDNA library::Y187	11.6

Abbreviations: Y2H, yeast two-hybrid.

3.2.1.5 *Parkin Y2H adult brain cDNA library screen*

The Y2H bait culture, *S. cerevisiae* strain AH109 transformed with pGBKT7-*parkin* bait construct, passed all of the abovementioned quality control assessments (Sections 3.2.1.1-3.2.1.4). The bait culture was therefore deemed adequate for use in a Y2H library screen. This was performed by mating the bait culture with the Y2H prey culture, *S. cerevisiae* strain Y187 transformed with the pGADT7-cDNA library (Section 2.19.3). It is estimated that approximately 1.8 x 10^7 cDNA clones were screened in this Y2H analysis (Section 2.19.5).

Diploid yeast colonies were assessed for their ability to activate the Y2H reporter genes (Section 2.19.6). A total of 505 diploid yeast colonies formed on TDO plates, indicating successful activation of the *HIS3* nutritional reporter gene by 505 clones. Such colonies were numbered, individually picked and plated onto QDO plates. These high-stringency media plates required activation of both *HIS3* and *ADE2* nutritional reporter genes for colony formation. A total of 245 clones formed colonies on QDO plates. These clones were selected for X-α-gal assays to evaluate their ability to activate the *MEL1* colorimetric reporter gene. Clones were subsequently classified into 107 primary clones and 138 secondary clones according to their color intensity in the X-α-gal assay as well as their robustness of growth on QDO plates. A representative subset of scored clones is listed in Table 3.6 to illustrate the assessment of *HIS3*, *ADE2* and *MEL1* reporter genes activation. A complete list of scored clones is available in Appendix VI.

Table 3.6 Representative subset of clones illustrating scoring of *HIS3*, *ADE2* and *MEL1* reporter genes activation

Clone ID	Growth on TDO (*HIS3* activation)	Growth on QDO (*ADE2* activation)	X-α-gal assay (*MEL1* activation)
1	++++	+++	Pale blue
2	+++	+	No blue
3	+++	-	-
4	++++	++++	Pale blue
5	**++++**	**++++**	**Dark blue**
6	++++	+++	Pale blue
7	+++	-	-
8	++++	++++	Medium blue
9	++	++	Medium blue
10	++++	-	-
11	+++	++	Pale blue
12	+++	-	-
13	+	-	-
14	**++++**	**+++**	**Dark blue**
15	++	-	-
16	+	-	-

Clones in **blue** font were designated as primary clones. Abbreviations: ++++, excellent growth; +++ fair growth; ++ weak growth; +, very weak growth; -, no growth; QDO, quadruple dropout (SD media lacking tryptophan, leucine, histidine and adenine); TDO, triple dropout (SD media lacking tryptophan, leucine and histidine); X-α-gal, 5-bromo-4-chloro-3-indolyl α-D-galactopyranoside.

The 107 primary clones were investigated for the specificity of their interactions with the pGBKT7-*parkin* bait construct (Section 2.20.8). Only clones that were able to grow colonies on TDO plates when mated to pGBKT7-*parkin*, but had no or negligent colony growth when mated to either of three heterologous bait constructs, were considered to demonstrate specific bait-prey interactions. An example of such a TDO plate is shown in Figure 3.5. A representative subset of evaluated primary clones indicating their interaction specificity is listed in Table 3.7. A complete list of evaluated clones is tabulated in Appendix VII. Of the 107 primary clones subjected to interaction specificity testing, a total of 64 clones demonstrated interactions specific to the parkin bait.

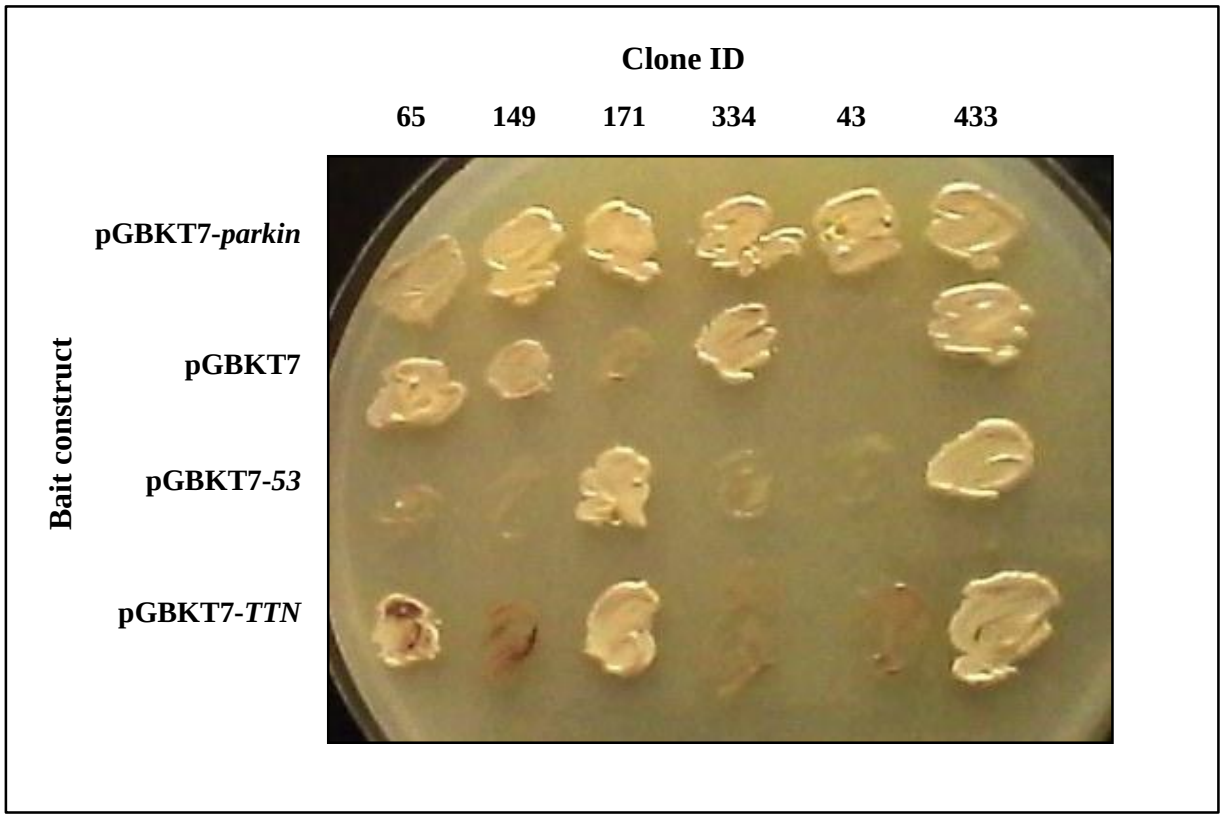

Figure 3.5 Interaction specificity testing using heterologous bait mating. Shown above are diploid yeast colonies resulting from six clones individually mated with four heterologous bait constructs and grown on a QDO plate for 7 days. Only clones that formed colonies when mated to pGBKT7-*parkin*, but did not form colonies when mated to non-recombinant pGBKT7, pGBKT7-*53* or pGBKT7-*TTN* were considered to demonstrate specific bait-prey interactions (clone 43 above). Abbreviations: QDO, quadruple dropout (SD media lacking tryptophan, leucine, histidine and adenine).

Table 3.7 Representative subset of clones scored for bait-prey interaction specificity

Clone ID	pGBKT7-*parkin*	pGBKT7	pGBKT7-*53*	pGBKT7-*TTN*
62	++++	+	+	-
64	++++	+	-	+
65	++++	++++	++++	+++
66	++++	+	+	+
69	++++	+	+	+
71	++++	++++	+++	++
75	++++	++++	+	+
90	++++	+++	+	+
100	++++	+	+	+
101	++++	-	-	+
102	++++	+	-	+
104	++++	+	++++	-
113	++++	+	+++	+
116	++++	+	++++	-
123	++++	++	+++	+++
140	++++	+	++++	+
141	++++	+	+	-
142	++++	+	+	+
147	++++	+	-	-
149	++++	+++	-	-
150	++++	-	+++	+
161	++++	+	+	+
162	++++	+	+++	+
164	++++	+	+	+
165	++++	+	+	+

Clones in **blue** font were considered to demonstrate specific parkin-bait interactions. All colonies were scored after 7 days on QDO plates. Abbreviations: ++++, excellent growth; +++ fair growth; ++ weak growth; +, very weak growth; -, no growth; QDO, quadruple dropout (SD media lacking tryptophan, leucine, histidine and adenine).

3.2.1.6 *Identification of putative parkin-interacting clones*

Each of the 64 clones that demonstrated parkin-specific interactions were subjected to automated DNA sequencing. The insert sequence as well the *in silico* translated sequence were then compared to known cDNA and protein sequences using the BLASTn and BLASTp queries, respectively (http://www.ncbi.nlm.nih.gov/BLAST). This delivered 29 unique clones encoding in-frame proteins, 16 duplicate clones (with identical insert sequences), and 19 clones with out-of-frame insert sequences (as dictated by the reading frame of the upstream GAL4-AD) that had no significant protein match when translated. The identities of the 64 investigated clones are listed in Table 3.8.

Table 3.8 Identification of putative parkin-interacting clones from the Y2H cDNA library screen

Clone ID	Identity	Genomic hit: BLASTn		Protein hit: BLASTp		Cellular localization	Domains
		Accession nr	E-value	Accession nr	E-value		
23; 321	*H. sapiens* exocyst complex component 4 (EXOC4)	NM_021807.3	0.00	NP_068579.3	2E-95	Cytoplasm	Sec8 exocyst complex component specific domain
43; 101; 161; 330; 377; 379	*H. sapiens* pre-mRNA cleavage complex 2 protein (Pcf11)	NM_015885.3	0.00	NP_056969.2	1E-85	Nucleus	CID domain
66	*H. sapiens* dehydrodolichyl diphosphate synthase (DHDDS)	NM_205861.2	6E-133	NP_995583.1	5E-41	Plasma membrane	Cis-isoprenyl diphosphate synthases
142	*H. sapiens* caldesmon 1 (CALD1)	NM_033140.3	0.00	NP_149131.1	2E-21	Plasma membrane; cytoskeleton	Caldesmon
147	*H. sapiens* fatty acid elongase 1 (ELOVL1)	NM_022821.2	1E-166	NP_073732.1	8E-13	Cytoplasm	GNS1/SUR4 family
165	*H. sapiens* coiled-coil domain containing 56 (CCDC56)	NM_001040431.1	0.00	NP_001035521.1	1E-56	Cytoplasm; mitochondria	Coiled-coil-56 superfamily
166	*H. sapiens* myelin basic protein (MBP)	NM_002385.2	0.00	NP_002376.1	2E-77	Cytoplasm; centrosome	Myelin MBP superfamily
188; 435; 437; 489; 494; 496	*H. sapiens* serine/arginine-rich splicing factor 3 (SRSF3)	NM_003017.4	0.00	NP_003008.1	6E-121	Nucleus but not nucleoli	RRM superfamily
204	*H. sapiens* transketolase (TKT)	NM_001064.3	0.00	NP_001055.1	3E-89	Cytoplasm	TPP enzyme PYR superfamily; transketolase C-terminal domain
208	*H. sapiens* protein-L-isoaspartate (D-aspartate) O-methyltransferase (PCMT1)	NM_005389.2	9E-59	NP_005380.2	5E-65	Cytoplasm	AdoMet-MTase superfamily

Clone ID	Identity	Genomic hit: BLASTn		Protein hit: BLASTp		Cellular localization	Domains
		Accession nr	E-value	Accession nr	E-value		
218	*H. sapiens* non-POU domain containing, octamer-binding (NONO)	NM_001145408.1	0.00	NP_001138880.1	4E-12	Nucleus but not nucleoli	NOPS_p54nrb superfamily; RRM1_p54nrb superfamily; RRM2_p54nrb superfamily
223	*H. sapiens* ArfGAP with RhoGAP domain, ankyrin repeat and PH domain 2 (ARAP2)	NM_015230.2	0.00	NP_056045.2	1E-48	Cytoplasm; cytoskeleton; focal adhesions	RhoGAP domain; 5 ankyrin and PH domain repeats; SAM domain of Arap1,2,3; ArfGap superfamily; Ras association domain; Sterile alpha motif
225; 277; 333 439	*H. sapiens* transmembrane protein 222 (TMEM222)	NM_032125.2	0.00	NP_115501.2	3E-112	Cytoplasm	DUF778 superfamily
242	*H. sapiens* A kinase (PRKA) anchor protein (yotiao) 9 (AKAP9)	NM_005751.4	0.00	NP_005742.4	8E-55	Golgi apparatus; vesicles; centrosome	Centrosomal targeting domain; DUF515 superfamily; Smc domain; SbcC domain
252	*H. sapiens* dehydrogenase/reductase (SDR family) member 7 (DHRS7)	NM_016029.2	0.00	NP_057113.1	1E-71	Nucleus but not nucleoli; cytoplasm	NADB-Rossmann superfamily; DltE domain
257	*H. sapiens* ATP synthase mitochondrial F1 complex assembly factor 1 (ATPAF1)	NM_022745.4	0.00	NP_073582.3	3E-87	Cytoplasm; mitochondria	ATP11 superfamily

Clone ID	Identity	Genomic hit: BLASTn		Protein hit: BLASTp		Cellular localization	Domains
		Accession nr	E-value	Accession nr	E-value		
258; 443	*H. sapiens* adaptor-related protein complex 3, sigma 1 subunit (AP3S1)	NM_001284.2	7E-173	NP_001275.1	1.00E-130	Cytoplasm	Clathrin adaptor S superfamily
259	*H. sapiens* calpain 3, (p94) (CAPN3)	NM_000070.2	5E-40	NP_775111.1	1E-67	Cytoplasm	EFh superfamily; EF-hand calcium binding motif; calpain-III superfamily
274	*H. sapiens* carboxypeptidase E (CPE)	NM_001873.2	1E-101	NP_001864.1	9E-20	Plasma membrane; cytoplasm; nucleus	Peptidase M14-like superfamily
276; 329	*H. sapiens* small nuclear ribonucleoprotein polypeptide N (SNRPN)	NM_003097.3	0.00	NP_073719.1	4E-75	Nucleus	Sm protein B superfamily
278	*H. sapiens* guanine nucleotide binding protein beta polypeptide 3 (GNB3)	NM_002075.2	0.00	NP_002066.1	4E-60	Plasma membrane; cytoplasm	WD40 domain
317	*H. sapiens* transformer 2 alpha homolog (Drosophila) (TRA2A)	NM_013293.4	0.00	NP_037425.1	1E-88	Nucleoli, vesicles	RRM superfamily
318	*H. sapiens* septin 9 (SEPT9)	NM_001113491.1	0.00	NP_001106963.1	2E-105	Cytoplasm; cytoskeleton	MCLC superfamily; CDC/septin GTPase family
319	*H. sapiens* actin, gamma 1 (ACTG1)	NM_001614.3	0.00	NP_001605.1	6E-23	Cytoskeleton	Actin
337	*H. sapiens* phosphoglucomutase 1 (PGM1)	NM_002633.2	0.00	NP_002624.2	1E-50	Cytoplasm; cytoskeleton	phosphoglucomutase superfamily

Clone ID	Identity	Genomic hit: BLASTn		Protein hit: BLASTp		Cellular localization	Domains
		Accession nr	E-value	Accession nr	E-value		
395	*H. sapiens* tyrosine 3-monooxygenase/tryptophan 5-monooxygenase activation protein, eta polypeptide (YWHAH)	NM_003405.3	0.00	NP_003396.1	8E-128	Cytoplasm	14-3-3 superfamily
423	*H. sapiens* nuclear receptor subfamily 1, group H, member 2 (NR1H2)	NM_007121.5	6E-39	NP_009052.3	5E-40	Cytoplasm; nucleus	NR-DBD superfamily
432	*H. sapiens* hepatocyte growth factor-regulated tyrosine kinase substrate (HGS)	NM_004712.3	0.00	NP_004703.1	2E-67	Cytoplasm; vesicles	VHS-ENTH-ANTH superfamily; ApoLp-III-like superfamily; Hrs-helical domain; FYVE domain
483	*H. sapiens* phosphoglycerate mutase 1 (PGAM1)	NM_002629.2	0.00	NP_002620.1	2E-54	Cytoplasm	Histidine phosphatase domain
141	PREDICTED: *H. sapiens* potassium voltage-gated channel, KQT-like subfamily, member 2 (KCNQ2)	XM_006723791	0.00	no significant similarity	-	-	-
198	*H. sapiens* postmeiotic segregation increased 2 pseudogene 4 (PMS2P4)	NR_046297.1	0.00	no significant similarity	-	-	-
48; 69; 100; 164; 372	*H. sapiens* chromosome 3 genomic contig - ubiquitin carboxyl-terminal hydrolase 4 (UCHL4)	NT_022517.18	0.00	no significant similarity	-	-	-

Clone ID	Identity	Genomic hit: BLASTn		Protein hit: BLASTp		Cellular localization	Domains
		Accession nr	E-value	Accession nr	E-value		
62	*H. sapiens* chromosome 20 genomic contig - double-stranded RNA-binding protein Staufen (STAU)	NT_011362.10	0.00	no significant similarity	-	-	-
64	*H. sapiens* chromosome 6 genomic contig - calcipressin-2	NT_007592.15	0.00	no significant similarity	-	-	-
102, 8	*H. sapiens* chromosome 2 genomic contig	NW_001838860.1	0.00	no significant similarity	-	-	-
174; 221	*H. sapiens* chromosome 1 genomic contig	NT_167186.1	0.00	no significant similarity	-	-	-
222	*H. sapiens* chromosome 5 genomic contig - BRCA1-A complex subunit (RAP80)	NT_023133.13	0.00	no significant similarity	-	-	-
14; 224	*H. sapiens* chromosome 4 genomic contig	NW_001838915.1	0.00	no significant similarity	-	-	-
436	*H. sapiens* chromosome 16 genomic contig - ADP-ribosylation factor-binding protein (GGA2)	NT_010393.16	0.00	no significant similarity	-	-	-
476	*H. sapiens* chromosome 18 genomic contig	NT_010859.14	0.00	no significant similarity	-	-	-
495	*H. sapiens* chromosome 12 genomic contig - TBC1 domain family member 30 (TBC1D30)	NT_029419.12	0.00	no significant similarity	-	-	-

Abbreviations: BLASTn, Basic Local Alignment Search Tool nucleotide; BLASTp, Basic Local Alignment Search Tool protein; Y2H, yeast two-hybrid; all domain abbreviations can be found in the conserved domain database (http://www.ncbi.nlm.nih.gov/ccd).

3.2.2 Selection of putative parkin interactors

Each of the 29 putative parkin interactors were investigated in publicly available databases such as ExPASy http://www.expasy.org), GeneCards (http://www.genecards.org) and the Human Protein Atlas (http://www.proteinatlas.org) in order to obtain relevant information regarding the function, tissue expression and subcellular expression of the proteins. Based on such information, four of the putative parkin interactors were prioritized for verification and further characterization: 14-3-3η, γ-actin, ATPAF1 and SEPT9. The selection of these four putative interactors does not exclude the other 25 as parkin-interacting candidates; however, due to time constraints, it was necessary to focus on interactors of plausible functional consequence. Each prioritized putative parkin interactor will be briefly discussed to highlight why they were selected for further analysis.

3.2.2.1 *14-3-3η*

The 14-3-3 eta (14-3-3η) protein, also referred to as tyrosine 3-monooxygenase/tryptophan 5-monooxygenase activation protein, eta polypeptide (YWHAH), is a member of the 14-3-3 protein family which mediates signal transduction by binding to phosphoserine-containing proteins. The 14-3-3 proteins are abundantly expressed in the brain, and are involved in the regulation of neuronal development and cell death (Takahashi 2003).

This protein has been previously shown to interact with parkin (Sato et al. 2006); 14-3-3η acts as a negative regulator of parkin activity by reducing parkin substrate affinity. The identification of a known parkin interactor by the Y2H library screen in this study supports the validity of this approach. Investigating the interaction between 14-3-3η and parkin might deepen our understanding of the regulation of parkin, which might be of interest in PD research.

3.2.2.2 *ATP synthase mitochondrial F1 complex assembly factor 1 (ATPAF1)*

Very little is known about ATPAF1; it is thought to be a soluble mitochondrial-associated protein that is required for the correct assembly of the α and β subunits of the F_1-ATP synthase (Wang and Ackerman 2000; Wang et al. 2001). This putative interactor was selected for further verification given parkin's important role in mitochondrial health, and ATPAF1 being the only mitochondrial-associated protein identified in the Y2H screen. While the nature and consequence of the interaction of parkin with ATPAF1 is unclear, disruption of this interaction could conceivably influence mitochondrial energetics. This may of relevance to PD and neurodegeneration (Petrozzi et al. 2007).

3.2.2.3 *γ-Actin*

The association between parkin and the cytoskeleton has been well established. Parkin associates with microtubules and promotes the ubiquitination and proteasomal degradation of α-tubulin and β-tubulin (Ren et al. 2003). It has also been demonstrated that parkin co-localizes with actin filaments in neuronal cells (Huynh et al 2000). Parkin is known to interact with LIM kinase-1, which phosphorylates cofilin, an actin depolymeration enzyme (Lim et al. 2007). It has also been shown that parkin overexpression reduces LIM kinase-1 induced actin filament accumulation, suggesting that parkin contributes to the regulation of actin accumulation. It would therefore be worthwhile to characterize this interaction of parkin and gamma-actin (γ-actin) further, particularly as the accumulation of actin has been associated with apoptosis and neurodegeneration (Gourlay and Ayscough 2005; Fulga et al. 2007).

3.2.2.4 *Septin 9 (SEPT9)*

Septins, including SEPT9, are GTPases that interact with the cytoskeleton and contribute to cellular processes such as cytokinesis, motility and cell polarity (Field and Kellogg 1999). Two members of the septin family, septins 2 (SEPT2) and 4 (SEPT4), were previously identified in neurofibrillary tangles and senile plaques in brains affected by Alzheimer's disease (Kinoshita et al. 1998). This supports the involvement of septins in neurodegeneration.

Parkin is known to interact with, ubiquitinate and promote the degradation of septin 5 (SEPT5; also known as CDCrel-1) (Zhang et al. 2000). A similar study found a further functional interaction between parkin and septin 4 (Choi 2003). Both septins 4 and 5 accumulate in the brains of patients with EOPD (Choi 2003; Shehadeh et al. 2009), suggesting an important functional relationship between parkin and septin proteins.

While SEPT9 has not been implicated in neurodegeneration to date, the putative parkin-SEPT9 interaction warrants further study, given the demonstrated role of septin proteins as parkin interactors. In addition, the interaction between parkin and SEPT5 will be used as a positive control in subsequent analyses, as SEPT5 is known to accumulate within cells in the absence of parkin.

3.2.3 Verification of four parkin interactors

When identifying putative protein interactions using the Y2H system, it is pivotal to distinguish between true interactions and false positive results. Such false positive interactions might arise due to several factors: proteins observed to interact in yeast do so as fusion proteins and not as their native forms; observed interactions occur in the yeast nucleus, which does not necessarily imitate the

subcellular localization of the proteins in neurons, or the observed interactions might be facilitated by the intracellular environment of the yeast cell (Serebriiskii et al. 2000; Guo et al. 2008). It is therefore important to perform experiments that verify the protein interactions in a setting that mimics the *in vivo* conditions as closely as possible.

For this reason, two further, independent approaches were used to verify the four putative parkin interactions in a human SH-SY5Y neuroblastoma cell line: three-dimensional *in vivo* co-localization (Section 3.2.3.1) and co-IP (Section 3.2.3.2). In addition to the four identified parkin interactions, the previously-described interaction of parkin with SEPT5 (Zhang et al. 2000) will be used as a positive control in these experiments.

3.2.3.1 *In vivo co-localization of parkin and putative parkin interactors*

Immunocytochemistry followed by confocal microscopy imaging of stained SH-SY5Y cells were used to investigate the *in vivo* co-localization of endogenously-expressed parkin and each of the putative parkin interactors (Section 2.22). Furthermore, Z-stacking was employed in order to acquire and resolve fluorescent signals in all three dimensions, encompassing the entire volume of the imaged cell.

The results of the co-localization analyses of each interacting pair are relayed in Figures 3.6 to 3.10. Each co-localization analysis was performed in triplicate (consisting of two to three imaged cells per replicate), of which one representative image of each interacting pair is shown in these figures. Illustrated in each figure is a single representative frame out of 25 frames collected in Z-stacks.

Each of Figures 3.6 to 3.10 consists of three fluorescent images: fluorescence acquired in the green channel (Panel A of each figure) and fluorescence acquired in the red channel (Panel B), where the green and red fluorescence correspond to the localization of each of the two proteins under investigation, and an overlay of the fluorescence acquired in the green, red and blue channels (Panel C), where Hoechst H-33342 nuclear staining (blue fluorescence) was employed for orientation purposes. Panel D of each figure illustrates a software-generated image of the subcellular co-localization of the protein pair, where yellow pixels indicate sites of co-localization. Co-localization is also diagrammatically represented as a scatter plot of the fluorescence acquired for each pixel (Panel E); green fluorescent intensity is plotted on the y-axis and red fluorescent intensity on the x-axis. Pixels with co-localizing green and red signals are represented in box 3 of the scatter plot (Panel E), where the threshold values for inclusion in box 3 were determined by the fluorescent intensity of single fluorophore-stained images of each protein of interest. Finally, each figure is accompanied by measures of the degree of co-localization as calculated by the imaging software (Panel F). The weighted co-localization coefficients of each color channel quantify the relative contribution of that

channel to the pixels of interest (ranging from 0 to 1.0); the overlap coefficient signifies the actual overlap of signals and represents the true degree of co-localization (ranging from 0 to 1.0), and the correlation R denotes the Pearson's correlation coefficient of intensity distribution between the two color channels (ranging from -1.0 to 1.0) (Zinchuk et al. 2007; Dunn et al. 2011).

Parkin and SEPT5

As can be seen in Figure 3.6A, SEPT5 is highly expressed in nuclei as well as the cytosol of SH-SY5Y cells. Parkin, on the other hand, is mainly localized to the cytosol, with little to no parkin staining observed in nuclei (Figure 3.6B). Parkin also demonstrates small punctuate staining behavior (e.g. upper left side of cell), which may represent the association of parkin with cellular organelles such as mitochondria (Narendra et al. 2008). Parkin and SEPT5 co-localize in the cytosol (Figure 3.6D), with the co-localization being particularly prominent in the uppermost neuronal projection of

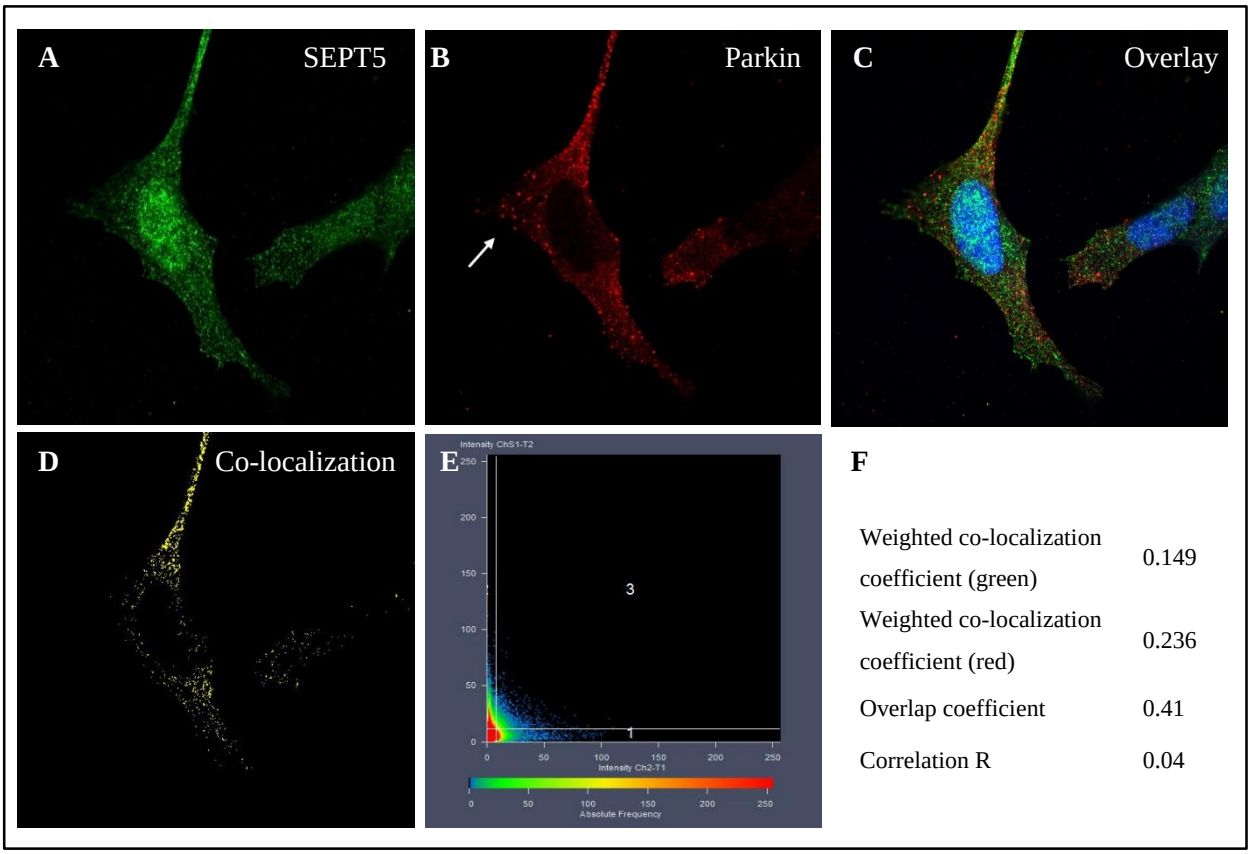

Figure 3.6 Florescent imaging and co-localization analysis of parkin and SEPT5. SH-SY5Y cells were immunocytochemically stained with primary antibodies directed against parkin and SEPT5 as well as appropriate fluorophore-conjugated secondary antibodies. **A**, localization of SEPT5 stained with Alexa488 (green). **B**, localization of parkin stained with Cy3 (red). Parkin punctae are indicated by a white arrow. **C**, overlay of red, green and Hoechst nuclear (blue) fluorescent signals. **D**, Co-localization of green and red signals. **E**, scatter plot of signal intensity in green and red channels, where pixels in box 3 represent co-localizing signals. **F**, quantitative measures of co-localization of parkin and SEPT5.

the imaged cell. The successful co-localization of parkin and SEPT5 is further reflected in the overlap coefficient of 0.41 (Figure 3.6F). While low values for the weighted co-localization coefficients of parkin (0.236) and SEPT5 (0.149) and the correlation R (0.04) were obtained, this is consistent with a model of transiently-interacting proteins, where only a small fraction of parkin is expected to be interacting with SEPT5 (and only a small fraction of SEPT5 with parkin) at a given time point.

Parkin and SEPT9

SEPT9 is observed throughout the cytosol and the nuclei (Figure 3.7A). Interestingly, SEPT9 adopts a fibrillar structure in the perinuclear area, which may be related to its function (Surka et al. 2002). The successful co-localization of parkin and SEPT9 is visually represented in Figure 3.7D, where the two proteins co-localize in the cytosol of SH-SY5Y cells. This co-localization is mainly in the central (but not nuclear) parts of the cells.

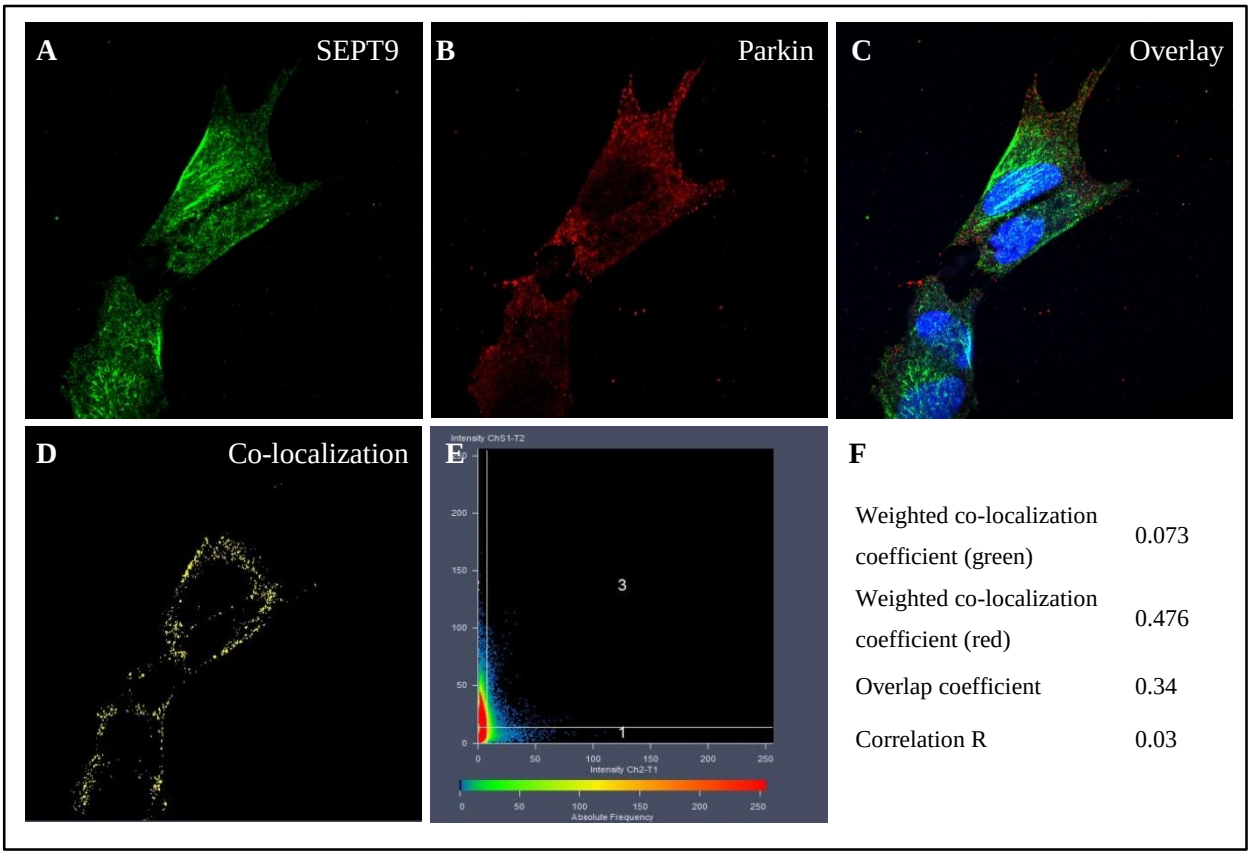

Figure 3.7 Florescent imaging and co-localization analysis of parkin and SEPT9. SH-SY5Y cells were immunocytochemically stained with primary antibodies directed against parkin and SEPT9 as well as appropriate fluorophore-conjugated secondary antibodies. **A**, localization of SEPT9 stained with Alexa488 (green). **B**, localization of parkin stained with Cy3 (red). **C**, overlay of red, green and Hoechst nuclear (blue) fluorescent signals. **D**, Co-localization of green and red signals. **E**, scatter plot of signal intensity in green and red channels, where pixels in box 3 represent co-localizing signals. **F**, quantitative measures of co-localization of parkin and SEPT9.

Parkin and ATPAF1

ATPAF1-positive staining was observed throughout the cytosol, as well as strong staining in the cell nuclei (Figure 3.8A). The regions of intense staining within nuclei are likely due to high expression of this protein within nucleoli. While cytosolic ATPAF1 is mostly dispersed in a diffuse fashion, some punctuate staining can be seen towards the left side of Figure 3.8A. Parkin "punctae" are clearly visible in the cytosol on these cells (Figure 3.8B). ATPAF1 and parkin co-localize somewhat irregularly in the cytosol (Figure 3.8D). No co-localization was found in the nuclei. Interestingly, some of the observed co-localization correspond to the aforementioned punctae (lower left area of Figure 3.8D), which may indicate the dual recruitment of these proteins to the same cellular locations.

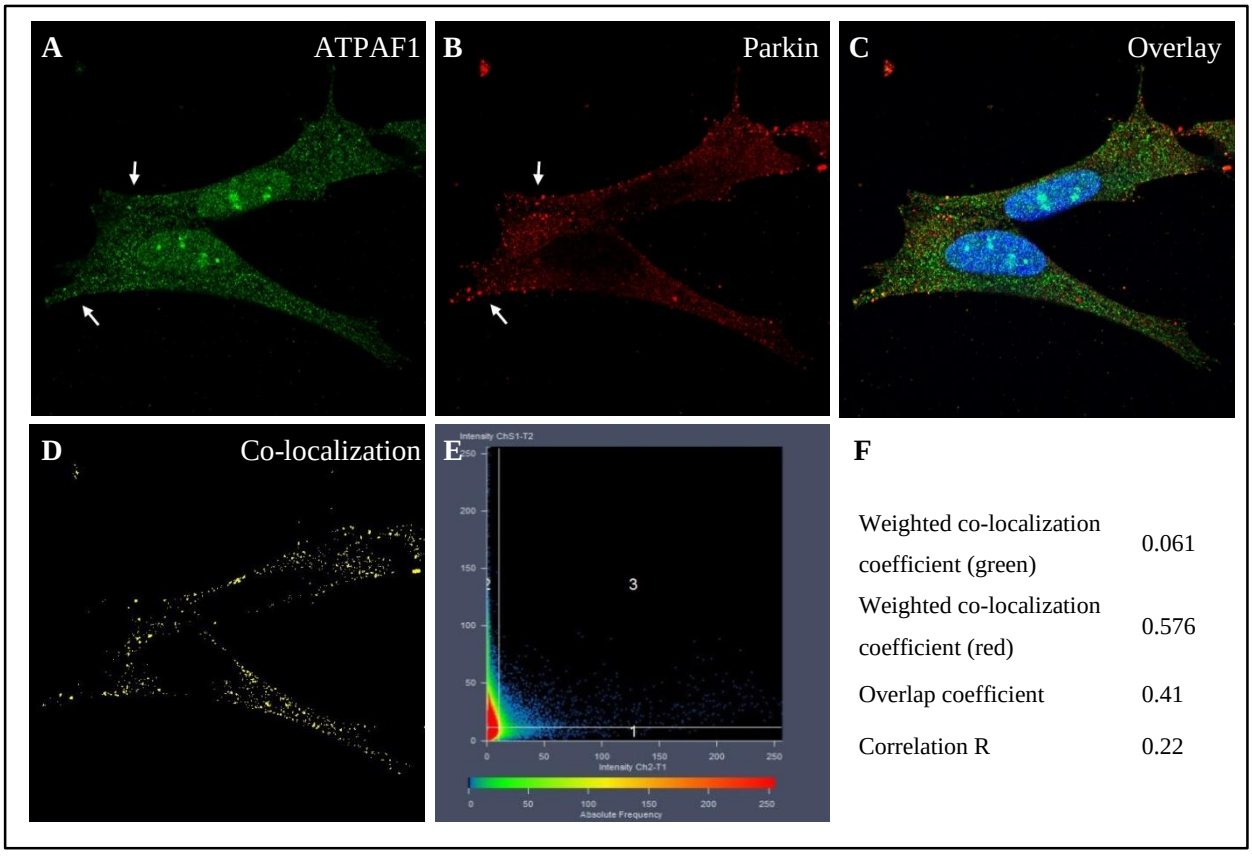

Figure 3.8 Florescent imaging and co-localization analysis of parkin and ATPAF1. SH-SY5Y cells were immunocytochemically stained with primary antibodies directed against parkin and ATPAF1 as well as appropriate fluorophore-conjugated secondary antibodies. Punctuate staining is indicated by white arrows. **A**, localization of ATPAF1 stained with Alexa488 (green). **B**, localization of parkin stained with Cy3 (red). **C**, overlay of red, green and Hoechst nuclear (blue) fluorescent signals. **D**, Co-localization of green and red signals. **E**, scatter plot of signal intensity in green and red channels, where pixels in box 3 represent co-localizing signals. **F**, quantitative measures of co-localization of parkin and ATPAF1.

Parkin and 14-3-3η

The 14-3-3η protein is found in the cytosol, nuclei and nucleoli (Figure 3.9A). Some co-localization of parkin and 14-3-3η is seen in cytosol, but not the nuclei, of SH-SY5Y cells (Figure 3.9D). The co-localization of these proteins is supported by the overlap coefficient of 0.41 (Figure 3.9F).

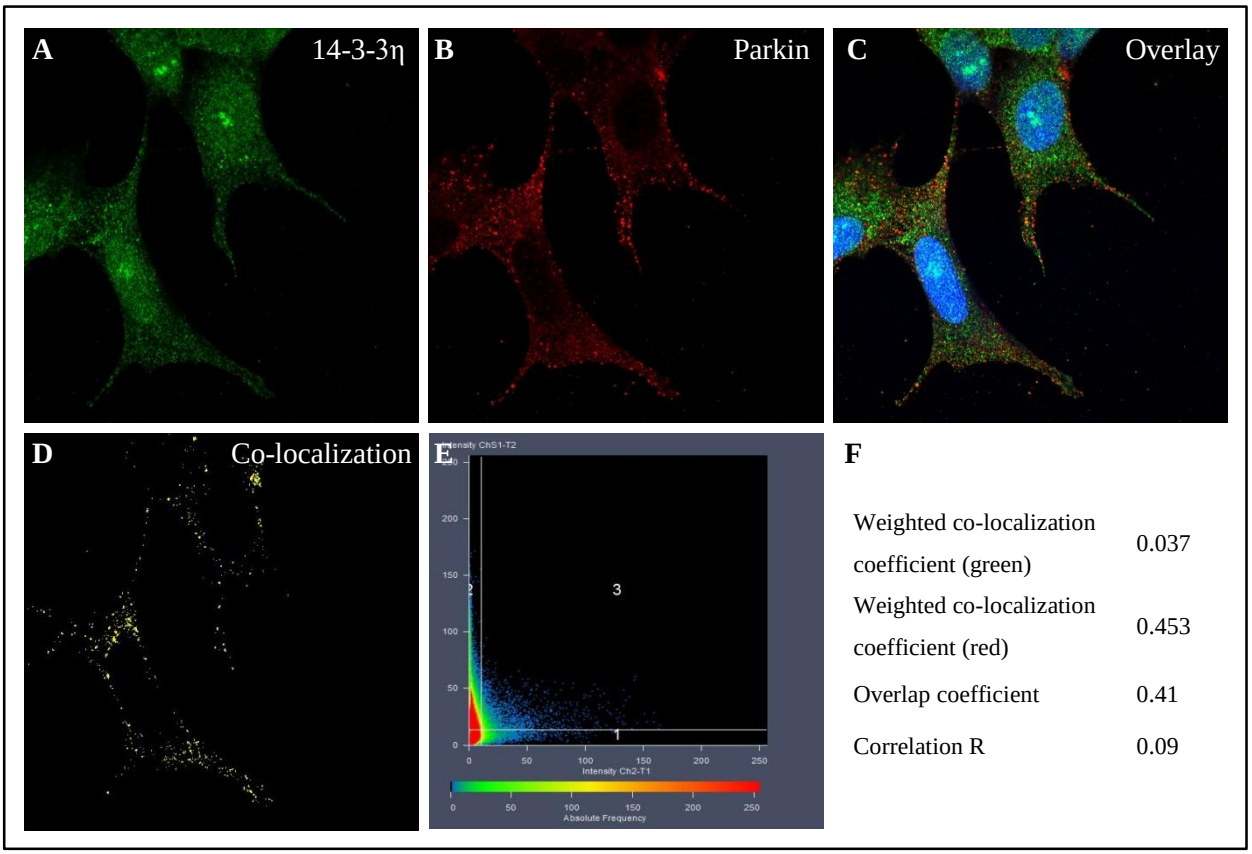

Figure 3.9 Florescent imaging and co-localization analysis of parkin and 14-3-3η. SH-SY5Y cells were immunocytochemically stained with primary antibodies directed against parkin and 14-3-3η as well as appropriate fluorophore-conjugated secondary antibodies. **A**, localization of 14-3-3η stained with Alexa488 (green). **B**, localization of parkin stained with Cy3 (red). **C**, overlay of red, green and Hoechst nuclear (blue) fluorescent signals. **D**, Co-localization of green and red signals. **E**, scatter plot of signal intensity in green and red channels, where pixels in box 3 represent co-localizing signals. **F**, quantitative measures of co-localization of parkin and 14-3-3η.

Parkin and cytoskeletal actin

It should be noted that the anti-γ-actin antibody used in this study is also likely to recognize the β-actin isoform (according to the manufacturer). This is due to the very high sequence similarity between these two cytoskeletal actin isoforms. Hence, it cannot be assumed that the results obtained here is specific to the γ-actin isoform only. This dissertation will therefore refer to cytoskeletal actin instead of γ-actin to reflect this distinction. In contrast with the other co-localization analyses, the cells that were stained for the co-localization analysis of parkin and γ-actin were fixed with methanol

instead of paraformaldehyde (Section 2.22.2). This was done as methanol fixation is better suited to preserving cytoskeletal fine-structure than paraformaldehyde, and was therefore appropriate for the imaging of actin. Actin demonstrated strong staining along the cytoskeletal filaments and the plasma membrane (Figure 3.10B). Interestingly, methanol-fixed parkin showed strand-like staining behavior in the cytosol which was not as evident in paraformaldehyde-fixed cells (Figure 3.10A). The substantial co-localization of parkin and cytoskeletal actin along actin filaments in the cytosol and along the plasma membrane is shown in Figure 3.10D.

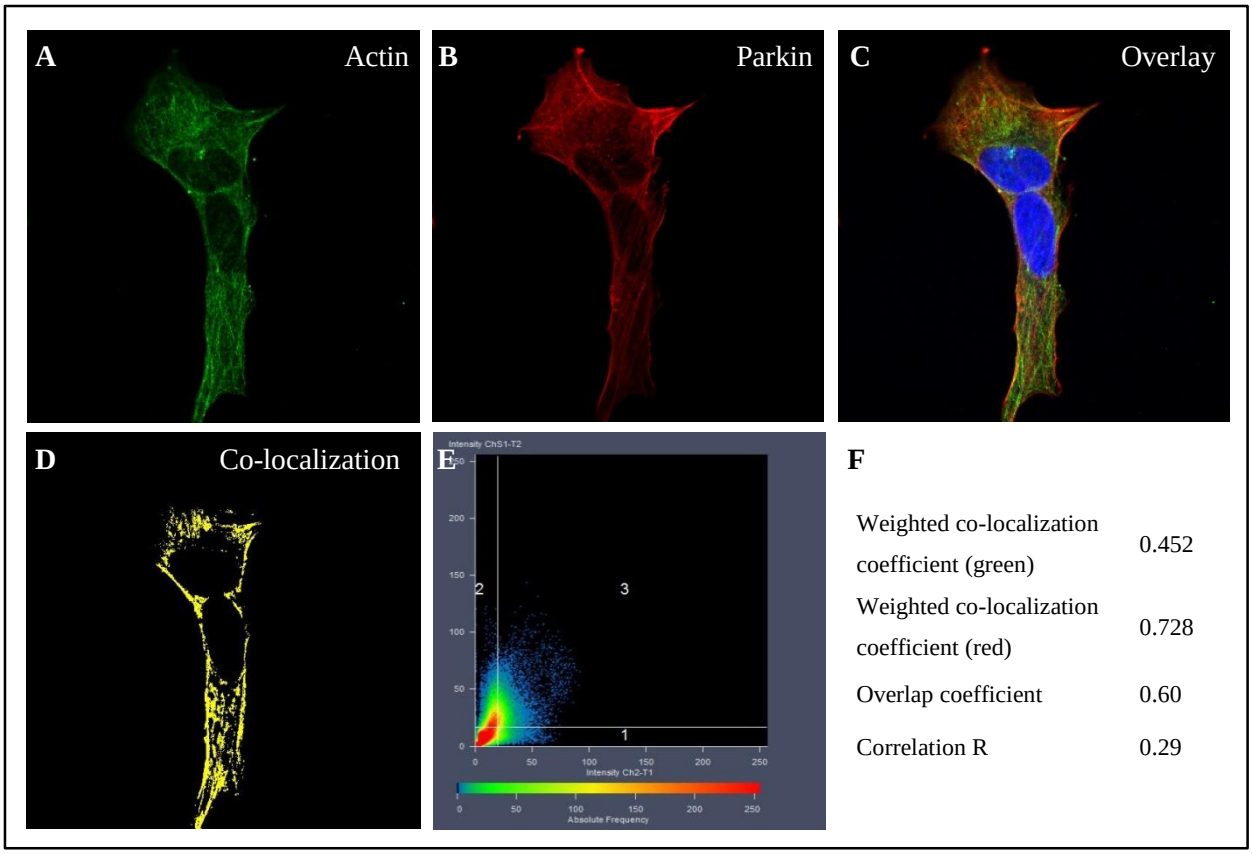

Figure 3.10 Florescent imaging and co-localization analysis of parkin and actin. SH-SY5Y cells were immunocytochemically stained with primary antibodies directed against parkin and γ-actin as well as appropriate fluorophore-conjugated secondary antibodies. **A**, localization of parkin stained with Alexa488 (green). **B**, localization of γ-actin (and β-actin) stained with Cy3 (red). **C**, overlay of red, green and Hoechst nuclear (blue) fluorescent signals. **D**, Co-localization of green and red signals. **E**, scatter plot of signal intensity in green and red channels, where pixels in box 3 represent co-localizing signals. **F**, quantitative measures of co-localization of parkin and actin.

In summary, all five of the putative parkin interactors (SEPT5, SEPT9, ATPAF1, 14-3-3η and cytoskeletal actin) that were investigated, co-localize with parkin to a sufficient degree; i.e. a significant fraction of each protein of interest was localized to the same subcellular localization as parkin. These co-localization analyses therefore support the plausibility of the putative protein interactions.

3.2.3.2 *Co-IP of parkin and putative parkin interactors*

While *in vivo* co-localization analyses provided evidence for the physical proximity of parkin and the putative parkin interactors in SH-SY5Y cells, further verification was needed to demonstrate physical interaction of these proteins. Co-IPs of each protein pair were therefore performed, where each endogenous protein was immunoprecipitated out of SH-SY5Y whole cell lysate (along with any interacting proteins), after which western blotting was used to test for the presence of the interacting partner (Sections 2.22 and 2.23).

Two control co-IPs were performed concurrent to each experiment: immunoprecipitation with an anti-hemagglutinin-tag (HA) antibody, and a protein G agarose control without any antibody. The use of these negative controls validated the specificity and authenticity of the obtained results.

The results of the co-IP experiments are shown in Figure 3.11. All five of the investigated parkin interactors (SEPT5, SEPT9, ATPAF1, 14-3-3η and γ-actin) were co-immunoprecipitated with parkin (Figure 3.11, left column). Reciprocally, parkin was co-immunoprecipitated with each of the proteins of interest (Figure 3.11, right column). No protein bands were visible in either of the two control lanes (labeled HA and Prot. G), demonstrating that the observed co-IPs are not spurious but the result of true interactions between parkin and the investigated parkin interactors.

Notably, in initial co-IP experiments involving parkin and SEPT9, it was found that, while parkin was present in a SEPT9 precipitate, the reciprocal co-IP of SEPT9 along with parkin could not be achieved (results not shown). This one-directional co-IP persisted during several repeat experiments. However, it was found that the use of a different anti-parkin antibody (Sigma-Aldrich, PRK8), which recognizes a different epitope on the parkin protein, did produce a successful co-IP of parkin and SEPT9 (Figure 3.11B, left column). This discrepancy could possibly be due to the binding site of SEPT9 on the parkin protein: binding of these two proteins may obscure the epitope for one anti-parkin antibody (preventing immunoprecipitation) without affecting the epitope of another antibody.

Initial co-IP of cytoskeletal actin along with parkin revealed binding of the anti-γ-actin antibody to proteins in both of the control lanes (results not shown). In order to overcome the non-specific binding of this antibody in this immunoprecipitation application, a different antibody raised against β-actin (Cell Signaling, #4970) was used to detect both β-actin and γ-actin isoforms in the parkin-immunoprecipitated lysate. According to the manufacturer, the β-actin antibody is not specific to the β-actin isoform only, due to the high homology of these isoforms (similar as to the γ-actin antibody). Probing with this β-actin antibody produced a positive and specific co-IP result (Figure 3.11E, left column).

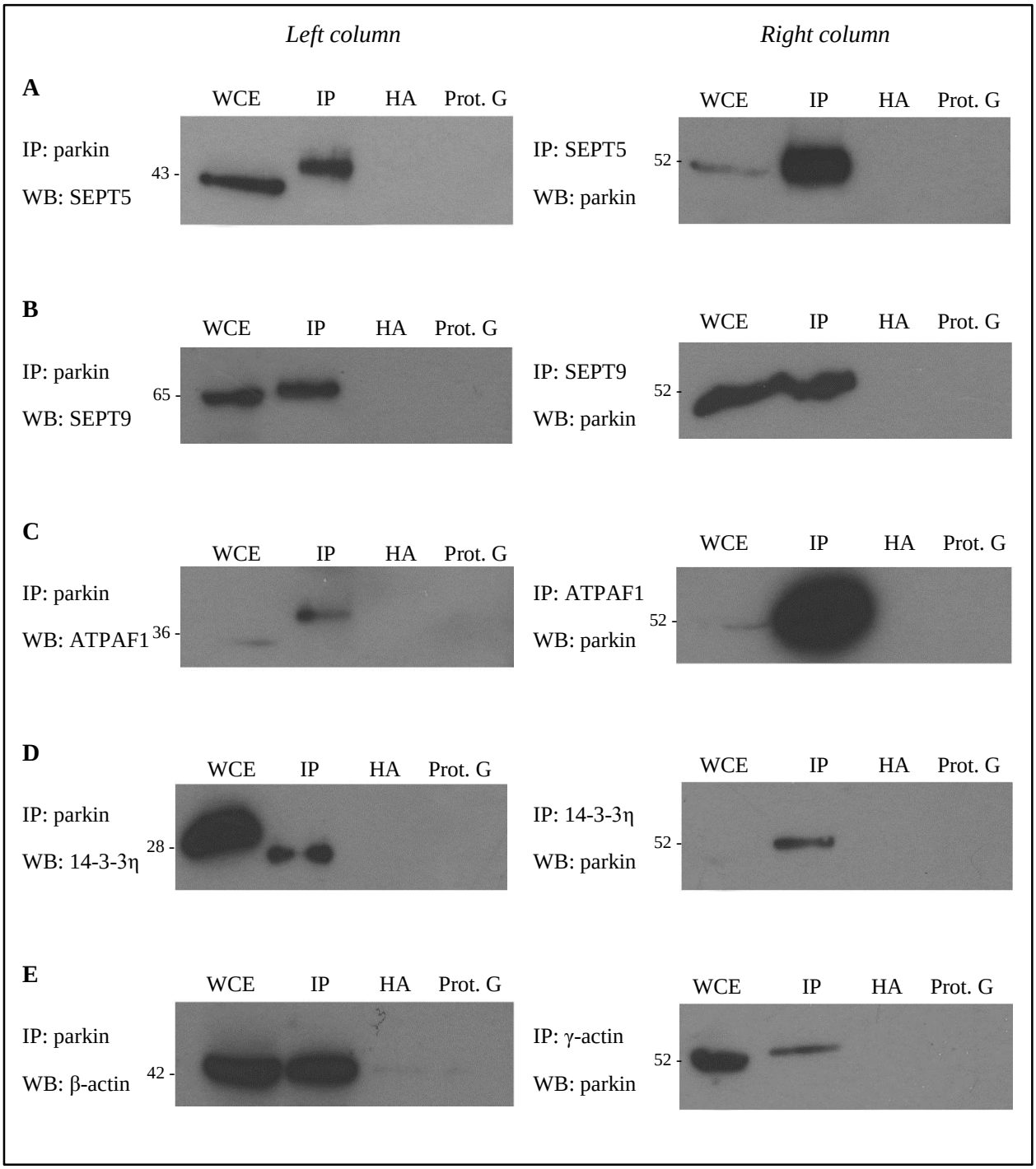

Figure 3.11 Co-IP of parkin and putative parkin interactors. Endogenous proteins were immunoprecipitated out of SH-SY5Y cell lysates and tested for the presence of the putative interactor via western blot. Reciprocal co-IPs were performed for each protein pair. Numbers on the right-hand side of western blots denote protein sizes (in kDa) Extra bands in **C** were removed for cosmetic effect. **A**, co-IP of parkin and SEPT5. **B**, co-IP of parkin and SEPT9. **C**, co-IP of parkin and ATPAF1. **D**, co-IP of parkin and 14-3-3η. **E**, co-IP of parkin and β/γ-actin. Abbreviations: co-IP, co-immunoprecipitation; HA, hemagglutinin-tag antibody control; IP, immunoprecipitation; kDa, kiloDalton; Prot. G, protein G agarose control; WB, western blot; WCE, whole cell extract.

As stated, the antibodies used could not distinguish whether parkin interacts with the γ-isoform only or with both the β- and γ-actin isoforms, but this uncertainty was overlooked given the extremely high sequence similarity (99%) and near-complete functional overlap of the two cytoskeletal actin isoforms. In fact, while the insert sequence of the Y2H clone used to identify γ-actin as a parkin-interacting protein (Section 3.2.1.6) had a higher nucleotide match with *ACTG1* (100% identity) than with *ACTB* (92% identity), the *in silico* translated sequence had a 100% identity to both actin isoforms (Figure 3.12). This strongly suggests that parkin interacts with the protein region common to both isoforms.

```
β-Actin      MDDDIAALVVDNGSGMCKAGFAGDDAPRAVFPSIVGRPRHQGVMVGMGQKDSYVGDEAQS   60
γ-Actin      MEEEIAALVIDNGSGMCKAGFAGDDAPRAVFPSIVGRPRHQGVMVGMGQKDSYVGDEAQS   60
ORF          ---------------------------------------------MGQKDSYVGDEAQS   14
                                                            **************

β-Actin      KRGILTLKYPIEHGIVTNWDDMEKIWHHTFYNELRVAPEEHPVLLTEAPLNPKANREKMT   120
γ-Actin      KRGILTLKYPIEHGIVTNWDDMEKIWHHTFYNELRVAPEEHPVLLTEAPLNPKANREKMT   120
ORF          KRGILTLKYPIEHGIVTNWDDMEKIWHHTFYNELRVAPEEHPVLLTEAPLNPKANREKMT   74
             ************************************************************

β-Actin      QIMFETFNTPAMYVAIQAVLSLYASGRTTGIVMDSGDGVTHTVPIYEGYALPHAILRLDL   180
γ-Actin      QIMFETFNTPAMYVAIQAVLSLYASGRTTGIVMDSGDGVTHTVPIYEGYALPHAILRLDL   180
ORF          QIMFETFNTPAMYVAIQAVLSLYASGRTTGIVMDSGDGVTHTVPIYEGYALPHAILRLDL   134
             ************************************************************

β-Actin      AGRDLTDYLMKILTERGYSFTTTAEREIVRDIKEKLCYVALDFEQEMATAASSSSLEKSY   240
γ-Actin      AGRDLTDYLMKILTERGYSFTTTAEREIVRDIKEKLCYVALDFEQEMATAASSSSLEKSY   240
ORF          AGRDLTDYLMKILTERGYSFTTTAEREIVRDIKEKLCYVALDFEQEMATAASSSSLEKSY   194
             ************************************************************

β-Actin      ELPDGQVITIGNERFRCPEALFQPSFLGMESCGIHETTFNSIMKCDVDIRKDLYANTVLS   300
γ-Actin      ELPDGQVITIGNERFRCPEALFQPSFLGMESCGIHETTFNSIMKCDVDIRKDLYANTVLS   300
ORF          ELPDGQVITIGNERFRCPEALFQPSFLGMESCGIHETTFNSIMKCDVDIRKDLYANTVLS   254
             ************************************************************

β-Actin      GGTTMYPGIADRMQKEITALAPSTMKIKIIAPPERKYSVWIGGSILASLSTFQQMWISKQ   360
γ-Actin      GGTTMYPGIADRMQKEITALAPSTMKIKIIAPPERKYSVWIGGSILASLSTFQQMWISKQ   360
ORF          GGTTMYPGIADRMQKEITALAPSTMKIKIIAPPERKYSVWIGGSILASLSTFQQMWISKQ   314
             ************************************************************

β-Actin      EYDESGPSIVHRKCF     375
γ-Actin      EYDESGPSIVHRKCF     375
ORF          EYDESGPSIVHRKCF     329
             ***************
```

Figure 3.12 Protein alignment of translated ORF sequence of Y2H clone 319 with actin isoforms. Protein sequence of clone 319 had a 100% identity to both the β- and γ-actin isoforms. *In silico* alignment was performed with CLUSTAL O 1.2.1 (http://www.ebi.ac.uk/Tools/msa/clustalo).

In summary, both *in vivo* co-localization and co-IP experiments demonstrated that the interaction of parkin with SEPT9, ATPAF1, 14-3-3η and cytoskeletal actin, originally identified in a Y2H library screen, are in fact true interactions.

3.2.4 Effect of parkin deficiency on protein levels of parkin interactors

The functional consequence of the verified interactions of parkin with SEPT9, ATPAF1, 14-3-3η and actin were investigated in cellular models of parkin deficiency. Given parkin's role in targeting many of its interactors for proteasomal degradation, the absence of functional parkin might result in the accumulation of such UPS-substrates. This loss-of-parkin-dependent accumulation has been demonstrated for many parkin substrates, including cyclin E (Staropoli et al. 2003), AIMP2 (Corti et al. 2003), PARIS (Shin et al. 2011) and FAF1 (Sul et al. 2013). Hence, accumulation of a parkin interactor in the absence of parkin would support the role of such an interactor as an authentic substrate for parkin K48-linked ubiquitination and proteasomal degradation. The previously described accumulation of SEPT5 (Zhang et al. 2000) will be used as a positive control in these experiments.

3.2.4.1 *In an RNAi-mediated parkin knockdown model*

The present study aimed to create an RNAi-mediated cell model of parkin deficiency, by using siRNA transfection to bring about the targeted knockdown of parkin in cultured SH-SY5Y cells. Of the four siRNA molecules tested, only two (Hs_PARK2_8 and Hs_PARK2_10) demonstrated an effect on parkin mRNA expression as determined by q-RT-PCR. Transfection with either of these siRNA molecules (henceforth referred to as siRNA's 8 and 10, respectively) decreased the expression of parkin mRNA by 50-55%, in comparison to cells transfected with a non-silencing control siRNA (Figure 3.13). This result was consistent across three separate experimental runs.

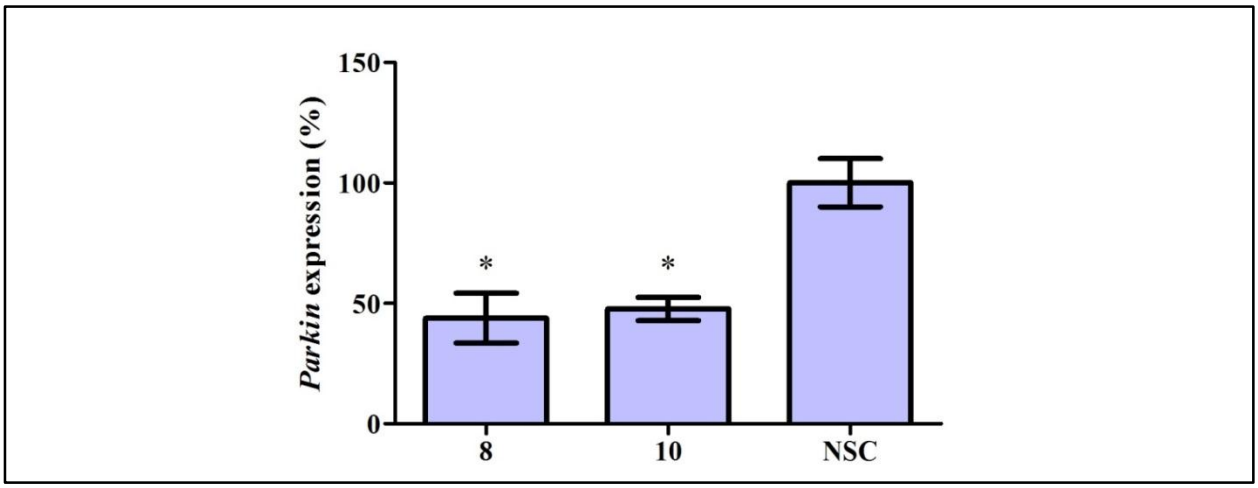

Figure 3.13 q-RT-PCR analysis of *parkin* mRNA expression following siRNA transfection. SH-SY5Y cells were treated with 5nM of siRNA's 8, 10 or a non-silencing control for 48h. *Parkin* mRNA expression was normalized to the expression of *GAPDH*, *B2M* and *RPL13A* reference genes. Relative mRNA expression is shown as mean ± SD, N=3. Asterisks indicate significance (p<0.05) upon unpaired t-testing (8: p=0.0025; 10: p=0.0012). Abbreviations: 8, Hs_PARK2_8 siRNA; 10, Hs_PARK2_10 siRNA; N, experimental runs; NSC, non-silencing control; SD, standard deviation.

When validating siRNA molecules for RNAi experiments, it is important to determine gene knockdown efficiency on both a mRNA and a protein level, as the optimal experimental conditions for protein knockdown may differ from that of mRNA knockdown (Shan 2010). Therefore, both siRNA's 8 and 10 were subjected to further knockdown efficiency validation via western blot.

Initial western blot experiments of siRNA-treated SH-SY5Y cells showed that neither siRNA molecule had an observable effect on parkin protein expression (results not shown). Consequently, siRNA transfection conditions were modified by increasing siRNA concentration from 5nM to 50nM, as well as by increasing siRNA treatment time from 48h to 72h. The siRNA concentration was increased in effort to improve siRNA transfection efficiency, whereas a longer incubation period may be necessary for parkin protein already expressed at the time of transfection to be degraded. Initial experiments showed that transfection of siRNA's 8 and 10 at these modified conditions resulted in 90% and 75% parkin knockdown, respectively (Figure 3.14A). However, multiple repeat experiments using the same transfection conditions failed to replicate these results consistently. Repeat transfections resulted in either only one of the siRNA's demonstrating sufficient knockdown of parkin (Figure 3.14B) or neither having a significant effect (Figure 3.14C).

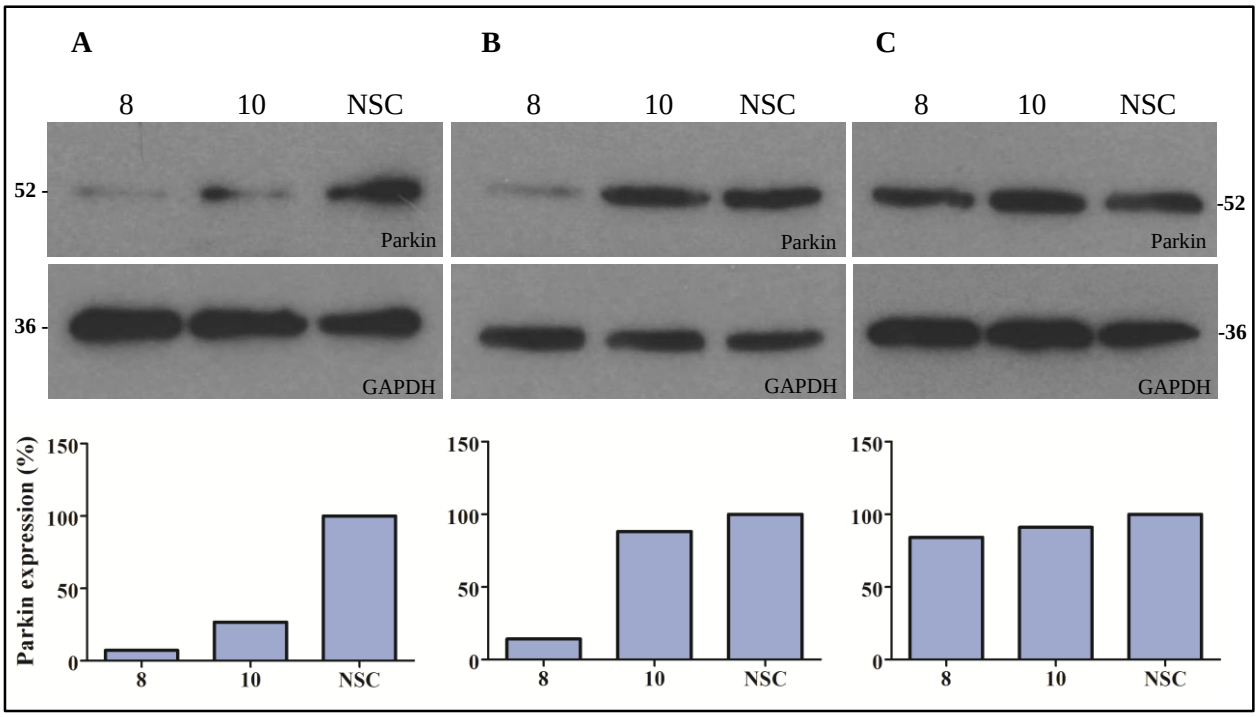

Figure 3.14 Parkin protein expression following siRNA transfection. SH-SY5Y cells were treated with 50nM of siRNA's 8, 10 or a non-silencing control (NSC) for 72h. Parkin expression (top lanes, 52 kDa) was normalized to GAPDH expression (bottom lanes, 36 kDa). Relative expression was calculated relative to NSC. Parkin knockdown efficiency of 8 and 10 was inconsistent across numerous experimental runs, with representative results illustrated here. **A**, successful knockdown by both siRNA's. **B**, successful knockdown by only one siRNA. **C**, unsuccessful knockdown by both siRNA's. Abbreviations: 8, Hs_PARK2_8 siRNA; 10, Hs_PARK2_10 siRNA; kDa, kiloDalton; NSC, non-silencing control.

Due to the inconsistency in knockdown ability at the protein level, it could not be confidently assumed that parkin is sufficiently knocked down following transfections with either of the two tested siRNA molecules. It is pivotal in downstream experiments that successful parkin knockdown can be implicitly assumed, as many of these downstream applications do not allow for parkin knockdown to be directly confirmed. For that reason, it was decided to use an alternative approach to investigate the functional effects of parkin deficiency.

3.2.4.2 *In fibroblasts from patients with parkin mutations*

Primary fibroblasts obtained from patients with *parkin* mutations are commonly used as cellular models of parkin dysfunction (Auburger et al. 2012). In particular, the use of fibroblasts with homozygous parkin mutations that grossly destabilize or truncate the protein, such as whole exonic deletions, provide cell models without any functional parkin (Mortiboys et al. 2008; Grunewald et al. 2010; Pacelli et al. 2011). Such parkin-null cell models are therefore valuable in the investigation of the functional effects of parkin deficiency, and will be employed in the present study as an alternative to RNAi-mediated parkin knockdown SH-SY5Y cells. While dermal fibroblasts may have several drawbacks in comparison to neuronal cells when studying neurodegeneration-related proteins, it is advantageous over RNAi-generated cell models in many regards. Of relevance to the current study, fibroblasts with predefined *parkin* mutations do not require repeated and transient genetic manipulation to bring about the loss of parkin. Parkin-mutant fibroblasts were therefore used as a robust and stable model of parkin deficiency.

Fibroblasts were obtained from three South African PD patients with parkin-null mutations, as identified by *parkin* mutation screening in this dissertation (Section 3.1.2), and who consented to skin punch biopsies. This included patient 23 with a homozygous exon 3-4 deletion (henceforth referred to as P1), as well as the affected sibling of patient 16 and the proband (patient 16), both with homozygous exon 4 deletions, which will be referred to as P2 and P3, respectively. P2, which was not included as a proband in the initial *parkin* genetic screen, has been examined by a movement disorder specialist. Three wild-type parkin fibroblast cell lines, namely WT2, WT3 and WT4, were used as age- and gender-matched controls. These samples were not re-labeled for the purposes of this study in order to ensure consistency of sample labeling in experiments by other members of our research team. All three patients were initially available for the current study. However, due to extensive microbial contamination of P1's fibroblasts, these cells had to be discarded and P1 was therefore not available for any of the functional studies in this dissertation.

The functional effect of parkin deficiency on the protein expression levels of each of the four parkin interactors was investigated in patient-derived and wild-type fibroblasts. Here, western blots and densitometry was used to assay the relative expression of each parkin interactor (Figure 3.15A-D).

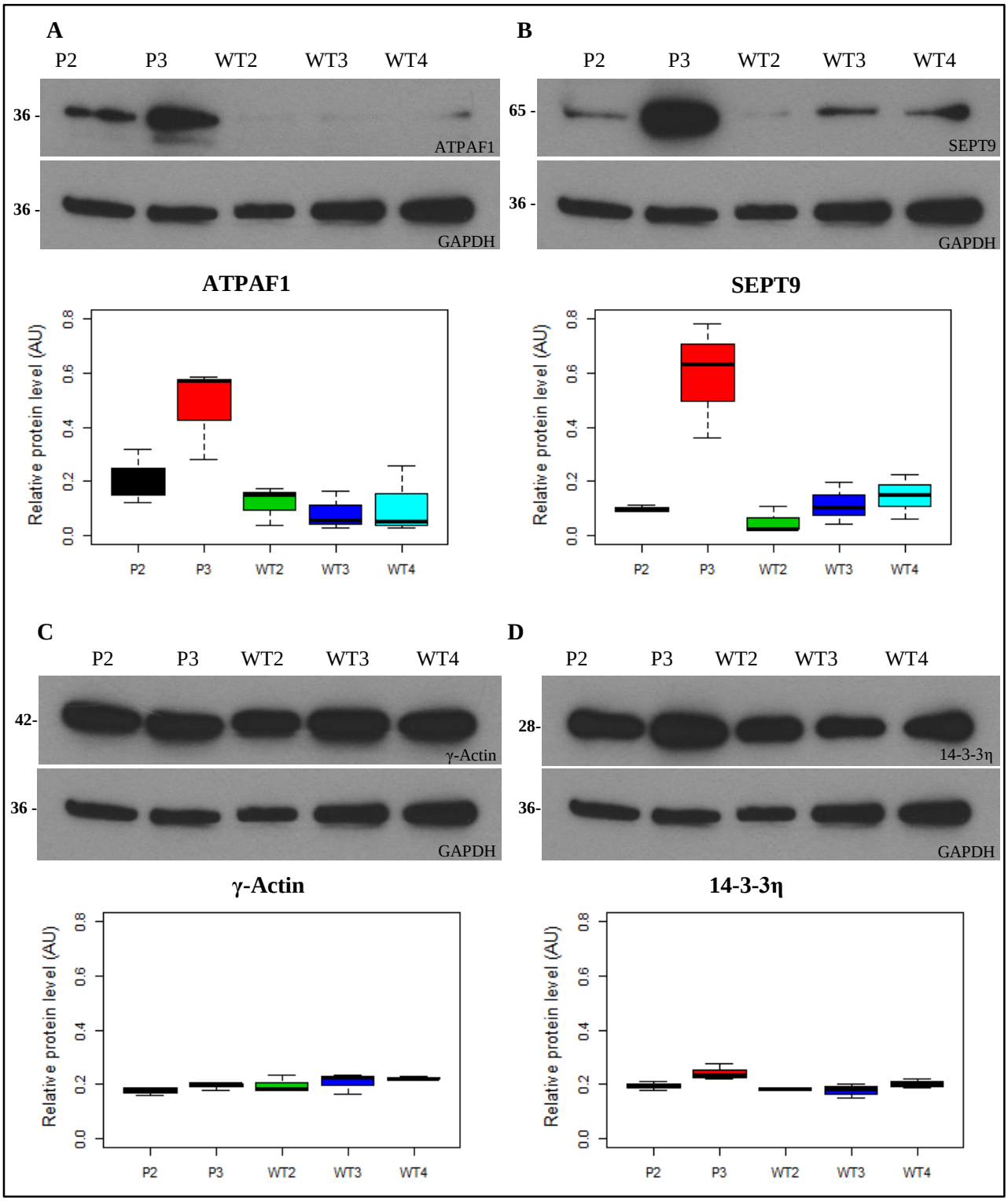

Figure 3.15 Protein expression levels of parkin interactors in patient-derived and control fibroblasts. Relative protein expression of (**A**) ATPAF1, (**B**) SEPT9, (**C**) γ-actin and (**B**) 14-3-3η was assayed with western blots in fibroblasts from patients with *parkin* mutations (P2 and P3) and wild-type controls (WT2, WT3, WT4). Expression of interactors (top lanes) was normalized to GAPDH expression (bottom lanes). Experiment was performed in triplicate (N=3) of which one representative western blot is shown for each interactor; all three replicate western blots can be found in Appendix VIII. Numbers on the side of western blots denote protein sizes (in kDa). Box-and-whisker plots depict relative protein densitometric measurements for three experimental runs. Abbreviations: AU, arbitrary units; kDa, kiloDalton; P, patient; WT, wild-type.

Each interactor was immunoblotted in three separate experimental runs in whole cell lysates from each of P2, P3, WT2, WT3 and WT4 cells. New lysates were obtained from three successive passages of each cell line for every experimental run. Lysates were simultaneously blotted for GAPDH expression, which served as a loading control and allowed for normalization of protein expression across different samples. Relative protein expression of each parkin interactor was calculated across all three experimental runs, as illustrated in Figure 3.15. As some variation was seen in protein expression levels among the three wild-type fibroblasts, relative protein levels were not scaled or expressed as a percentage of a given control.

For each parkin interactor, comparisons of grouped patient fibroblasts vs. grouped wild-type control fibroblasts were performed using mixed-effects linear modeling. Modeled effect sizes for each of the two groups are depicted in Figure 3.16.

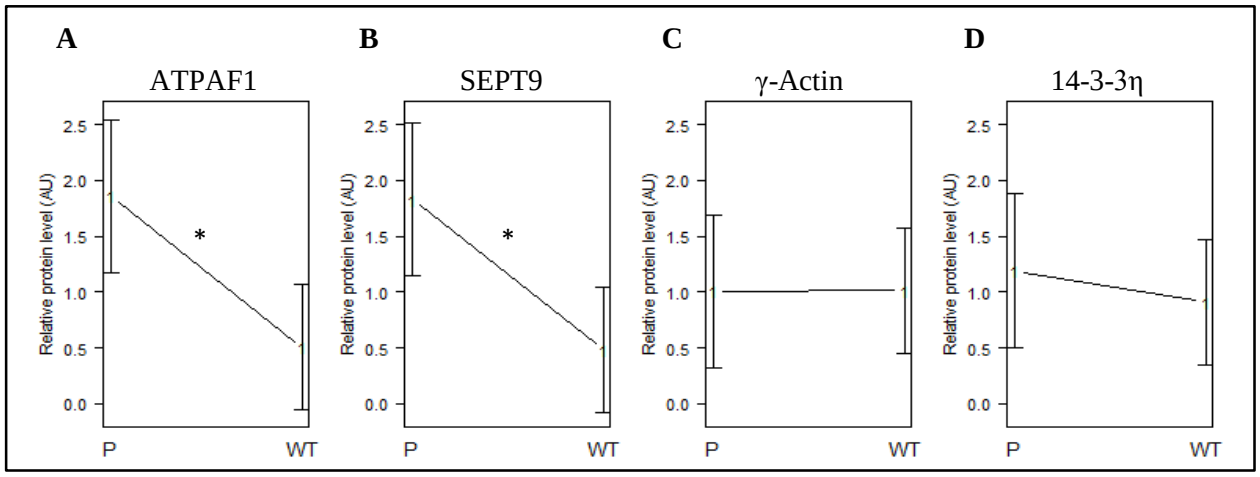

Figure 3.16 Mixed-effects linear modeling of protein expression levels in patients with *parkin* mutations and wild-type controls. Modeled effect sizes (differences between patients and controls) are shown with 95% confidence intervals (CI). Effect sizes with non-overlapping CI differ significantly ($p<0.05$) and are indicated by an asterisk. **A**, ATPAF1; **B**, SEPT9; **C**, γ-actin; **D**, 14-3-3η. Abbreviations: AU, arbitrary units; CI, confidence intervals; P, patient; WT, wild-type.

As can be seen in Figure 3.16A, ATPAF1 was found to strongly accumulate in patient-derived fibroblasts in comparison to wild-type controls ($p=0.0004$). Similarly, the protein expression levels of SEPT9 was marked higher in patients ($p=0.0003$; Figure 3.16). It should be noted that, for both proteins, little or no accumulation was seen in P2 (Figure 3.15). It is unclear why accumulation of ATPAF1 and SEPT9 was not seen in this one patient with *parkin* mutations. It should furthermore be noted that P2 and P3 are siblings, and the results obtained from this limited dataset should be interpreted with caution.

In contrast to the accumulation of ATPAF1 and SEPT9 in patients, the protein expression of cytoskeletal actin (as probed by a γ-actin antibody) was similar in patient-derived and wild-type fibroblasts ($p=0.8632$, Figure 3.16C). Hence, parkin deficiency had no observable effect on the

steady-state protein level of actin. Similarly, the protein expression of 14-3-3η was comparable between patients and wild-type controls (p=0.5099; Figure 3.16D).

Unfortunately, the previously described accumulation of SEPT5 (Zhang et al. 2000) could not be used as a positive control in these fibroblast models, as this protein is not expressed in fibroblasts to a detectable degree (Beites et al. 1999). Immunoblotting with an anti-SEPT5 antibody failed to detect this protein in fibroblast cell lysates (results not shown).

In summary, it was found that the parkin-null fibroblasts had substantially higher protein levels of both ATPAF1 and SEPT9 than the wild-type fibroblasts. This is consistent with a model wherein ATPAF1 and SEPT9 are authentic parkin substrates, which accumulate in the absence of parkin. While a marked accumulation of these two proteins was found in P3, their expression levels were similar in P2 in comparison to wild-type fibroblasts. It is interesting to consider that some unknown compensatory pathway may be suppressing the accumulation of these parkin substrates in the P2 fibroblast cell line. Importantly, actin and 14-3-3η did not accumulate in the parkin-null fibroblasts, which may suggest that the observed accumulation of ATPAF1 and SEPT9 is due to specific parkin-substrate interactions with these proteins.

3.3 FUNCTIONAL STUDIES IN A PARKIN-DEFICIENT CELLULAR MODEL

As two of the parkin-interacting proteins (ATPAF1 and SEPT9) were shown to accumulate in patient-derived fibroblasts, it was aimed to investigate the possible functional effects of such accumulation on cellular health. This protein accumulation may contribute to previously-described mitochondrial impairments in *parkin*-mutant fibroblasts (Mortiboys et al. 2008; Grunewald et al. 2010; Pacelli et al. 2011). Therefore, a range of experiments were undertaken in order to assess various aspects of cellular and mitochondrial function in a parkin-deficient cellular model. These included cell growth and viability assays (Section 3.3.1), mitochondrial respiration analysis (Section 3.3.2), $\Delta\psi_m$ analysis (Section 2.3.3) and mitochondrial network analysis (Section 2.3.4). Unless stated otherwise, all results refer to comparisons of grouped patient-derived vs. grouped wild-type fibroblasts. Graphical depictions of results obtained for individual fibroblast cell lines can be found in Appendix IX.

3.3.1 Cell growth and viability assays

Two complementary assays, a CyQUANT® assay of cell growth and a MTT assay of cell viability, were performed to determine whether the overall states of cellular health differed between patient-derived and wild-type fibroblasts (Section 2.26). These two assays were performed simultaneously in parallel plates, the results of which are shown in Figure 3.17.

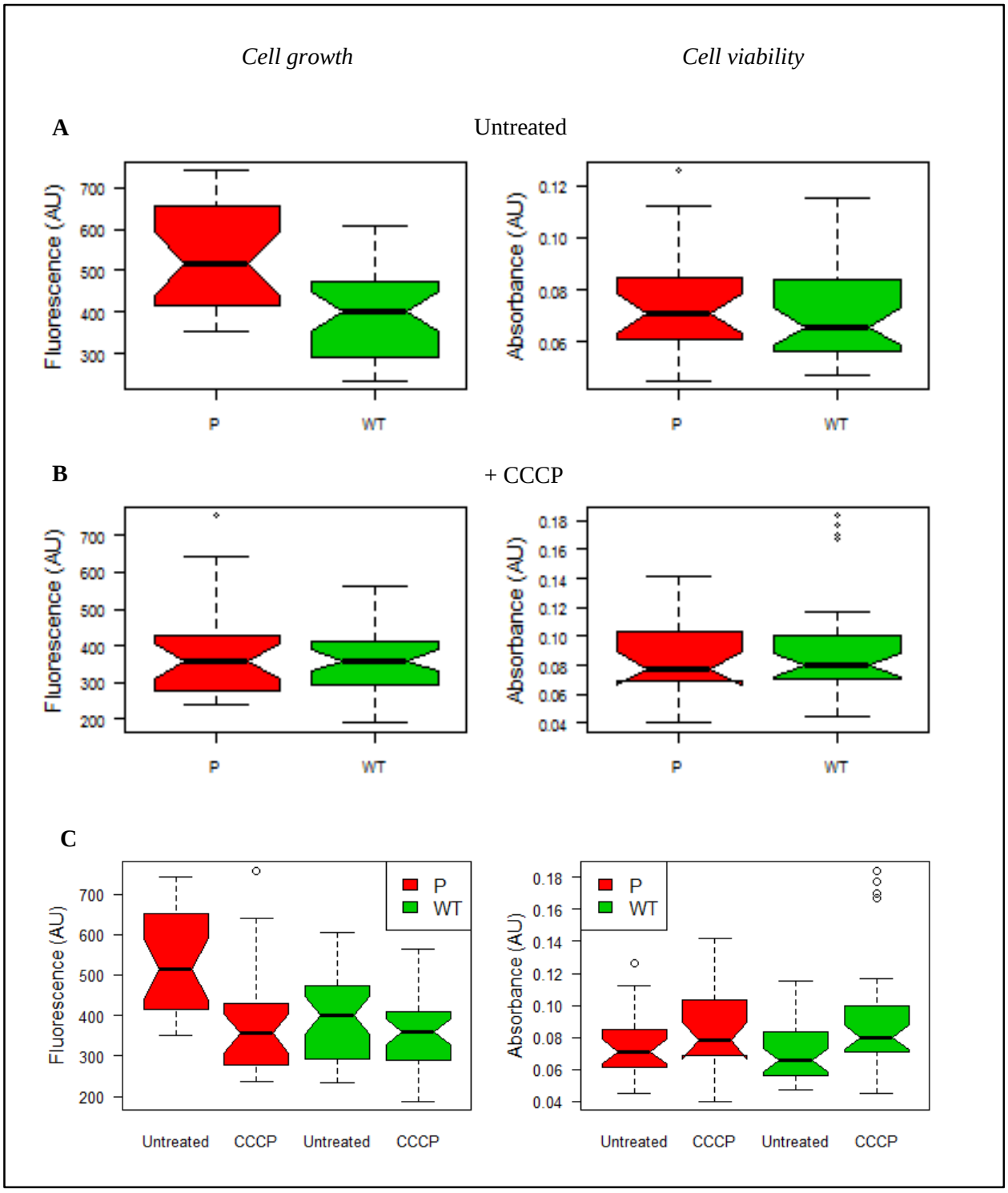

Figure 3.17 Cell growth and viability in patient-derived and wild-type fibroblasts under basal and CCCP-stressed conditions. Left panels represent cell growth as assessed by a CyQUANT® assay, whereas right panels represent cell viability as assessed by a MTT assay. Box-and-whisker plots depict grouped patients (P) and wild-type (WT) measurements for three experimental runs. **A**, cell growth and viability under basal (untreated) conditions. **B**, cell growth and viability after treatment with 10µM CCCP for 24h. **C**, comparison of cell growth and viability under basal and stressed conditions. Abbreviations: AU, arbitrary units; P, patient; WT, wild-type.

It was found that cell growth was significantly higher in patient-derived fibroblasts than controls under basal conditions (p=0.0001; Figure 3.17A, left panel). In contrast, cell viability was similar in all fibroblasts cell lines under basal conditions (p=0.7843; Figure 3.17A, right panel).

Cell growth and viability of the fibroblasts were also assessed under conditions of cellular stress, as any differences between patient-derived and wild-type cells may not be readily apparent under basal conditions. Here, the fibroblasts were treated with CCCP to induce mitochondrial impairment, and subsequent parkin recruitment to damaged mitochondria. It was found that both cell growth and cell viability were similar in all fibroblasts cell lines even after CCCP treatment (p=0.0922 and 0.7815, respectively; Figure 3.17B). However, a comparison of the effect of CCCP treatment within each fibroblast group (i.e. with and without cellular stress) demonstrated that the growth of patient-derived fibroblasts was significantly more suppressed by CCCP than the growth of wild-type fibroblasts (p=0.0013; Figure 3.17C, left panel). This is indicative of a heightened sensitivity to CCCP of patient-derived fibroblasts in comparison to wild-type fibroblasts.

In contrast, the cell viability was seemingly enhanced in all fibroblasts cell lines after treatment with the cytotoxic compound CCCP (p=0.0004; Figure 3.17C, right panel), but this effect was similar in patient-derived and wild-type fibroblasts (p=0.7226). This contradictory and perplexing result is best explained as an artefact of the MTT assay: it is possible that CCCP-treated cells reduce MTT to formazan at a greater rate than untreated cells not because they are more viable, but because CCCP artificially alters the rate of MTT reduction. Indeed, this high susceptibility to treatment-induced artefacts is a well-known limitation of the MTT assay (Berridge et al. 2005). The alternative scenario, i.e. increased cell viability in the presence of CCCP, contradicts the established cytotoxic properties of this mitochondrial depolarizing agent (Narendra et al. 2008).

3.3.2 Mitochondrial respiration analysis

Given the important role of parkin in maintaining mitochondrial health, it was decided to specifically compare *parkin*-mutant and wild-type fibroblasts in regards to various parameters of mitochondrial function. Therefore, rates of mitochondrial respiration were evaluated.

Respiration analyses were performed using a Seahorse Extracellular Flux Analyzer (Section 2.27). This allowed for a series of measurements to be taken of the oxygen consumption rate (OCR) of each fibroblast population, where pharmacological inhibitors were sequentially added to the cells in order to probe the function of individual components of the mitochondrial respiratory chain. All OCR readings were normalized to cell number, as determined by a CyQUANT® assay. The overall respiratory responses of all patient-derived and wild-type fibroblasts are illustrated in Figure 3.18A, from which several important respiratory parameters can be assessed (Figure 3.18B).

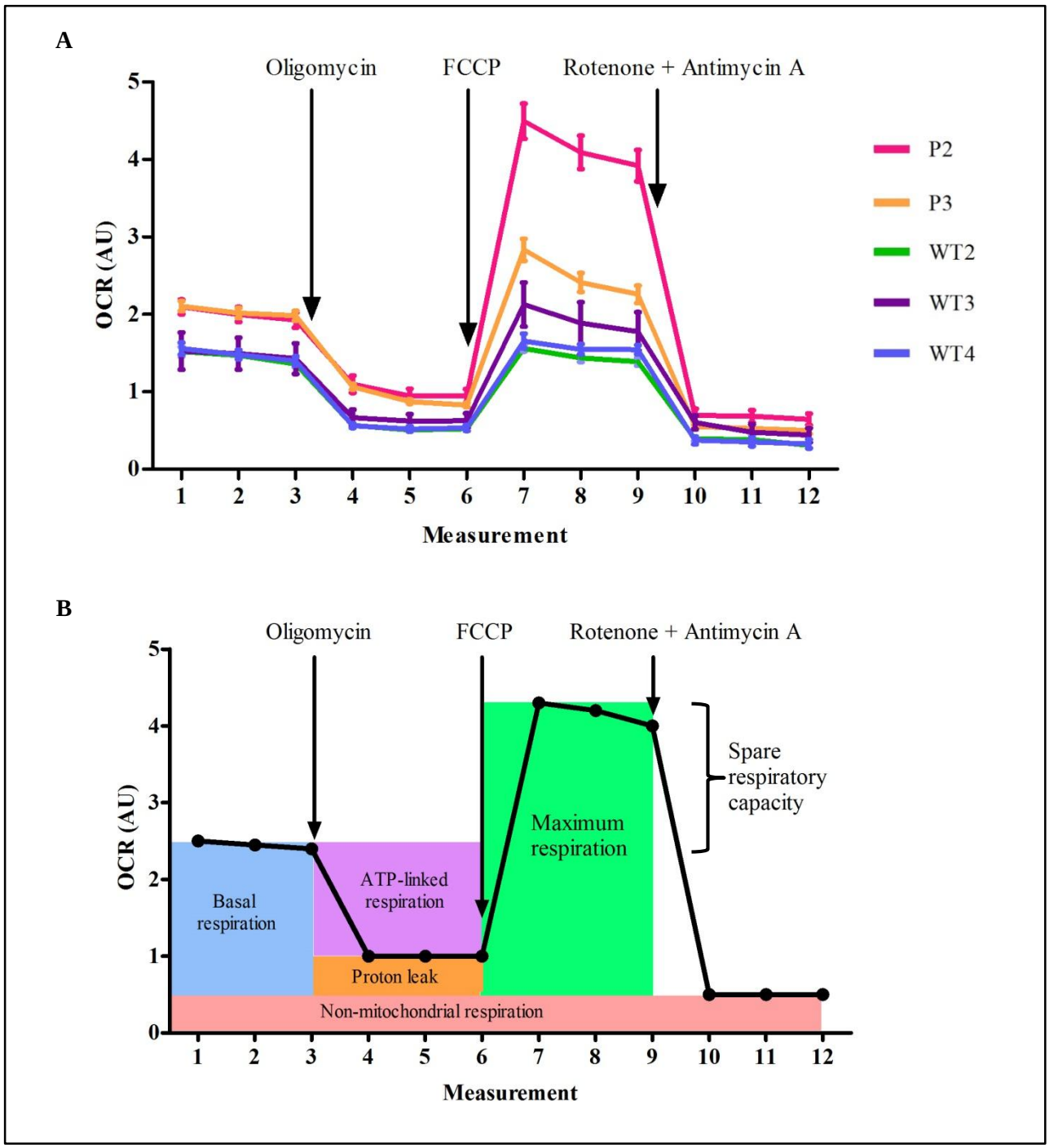

Figure 3.18 Respiratory flux profile of patient-derived and wild-type fibroblasts. Respiratory flux was determined with a Seahorse Extracellular Flux Analyzer by twelve consecutive measurements of oxygen consumption rate (OCR). Addition of ATP synthase inhibitor oligomycin, ETC uncoupler FCCP and complex I and III inhibitors rotenone and antimycin A are indicated. **A**, respiratory flux profiles of patient-derived and wild-type fibroblasts. Results are expressed as mean ± SEM. **B**, a representative respiratory flux profile indicating various parameters of respiratory control. These include: OCR due to non-mitochondrial respiration (rotenone/antimycin A response); basal mitochondrial OCR (basal measurement – rotenone/antimycin A response); ATP-linked OCR (basal measurement – oligomycin response); OCR due to proton leak (oligomycin response - rotenone/antimycin A response); ATP coupling efficiency (basal mitochondrial OCR / ATP-linked OCR); maximum OCR (FCCP response - rotenone/antimycin A response) and spare respiratory capacity (maximum OCR / basal mitochondrial OCR). Abbreviations: AU, arbitrary units, OCR, oxygen consumption rate; P, patient; SEM, standard error of the mea7n; WT, wild-type.

A comparison of these parameters in grouped *parkin*-mutant and wild-type control fibroblasts is given in Figure 3.19. As can be seen in Figure 3.19A, patient-derived fibroblasts had a higher mitochondrial respiration than wild-type fibroblasts under basal conditions (p=0.0355). This mitochondrial respiration is composed of two components: the oxygen consumption devoted to ATP synthesis, and the oxygen consumption required to overcome the natural proton leak across the inner mitochondrial membrane. The addition of the ATP synthase inhibitor oligomycin allowed for these contributory components to be isolated. While patient-derived fibroblasts had higher ATP-linked respiration than wild-type fibroblasts (p=0.0481; Figure 3.19B), the difference in proton leak between patient-derived and wild-type fibroblasts was more pronounced (p=0.0273; Figure 3.19C). In fact, a comparison of the ATP-coupling efficiency demonstrated that the patient-derived fibroblasts had a trend towards a lower coupling efficiency (≈80% OCR that is ATP-linked vs. ≈87% OCR that is ATP-linked in wild-type fibroblasts), but this trend did not reach statistical significance (p=0.0983; Figure 3.19D).

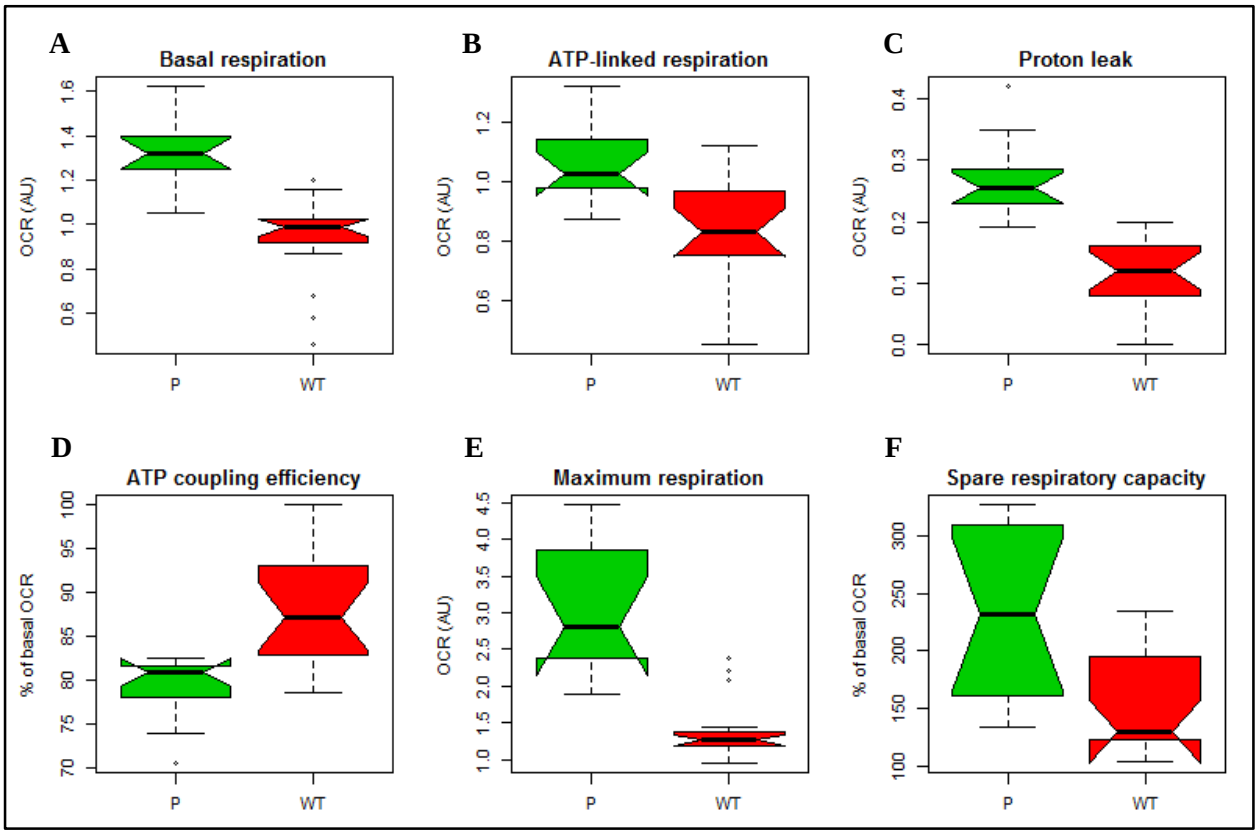

Figure 3.19 Parameters of respiratory control in patient-derived and wild-type fibroblasts. Box-and-whisker plots depict grouped patients (P) and wild-type (WT) values. **A**, basal mitochondrial OCR. **B**, ATP-linked OCR. **C**, OCR due to proton leak. **D**, ATP coupling efficiency (percentage OCR due to ATP synthesis). **E**, maximum OCR. **F**, percentage spare respiratory capacity. Abbreviations: AU, arbitrary units; OCR, oxygen consumption rate; P, patient; WT, wild-type.

The addition of the ETC-accelerator FCCP allowed for an estimation of the maximum, uncontrolled OCR. FCCP is an ionophore which directly transports protons across the inner mitochondrial membrane instead of via the ATP synthase proton channel. Hence, addition of FCCP collapses the $\Delta\psi_m$, leading to a rapid consumption of oxygen without the generation of ATP. The fold difference between this maximal uncontrolled OCR and basal OCR is indicative of the spare respiratory capacity of cells. The maintenance of some spare respiratory capacity is a major determinant of cellular health and survival, as it allows for increased ATP synthesis in times of high energetic demand (Nicholls 2009). This spare capacity is determined by several factors, including the functional capacity of the ETC. It was found that the patient-derived cells had a markedly higher maximum respiratory rate than control fibroblasts (p=0.0081; Figure 3.19E), whereas spare respiratory capacity was comparable between these two groups (p=0.2947; Figure 3.19F). However, it is important to note that significant differences were observed in these parameters between the two patient-derived fibroblast cell lines (Figure 3.20). Comparisons of P2 and P3 reveal that P2 had significantly higher maximum respiration (p=0.0016) and spare respiratory capacity (p<0.0001) than P3, whereas P3 was similar to wild-type fibroblasts in these regards.

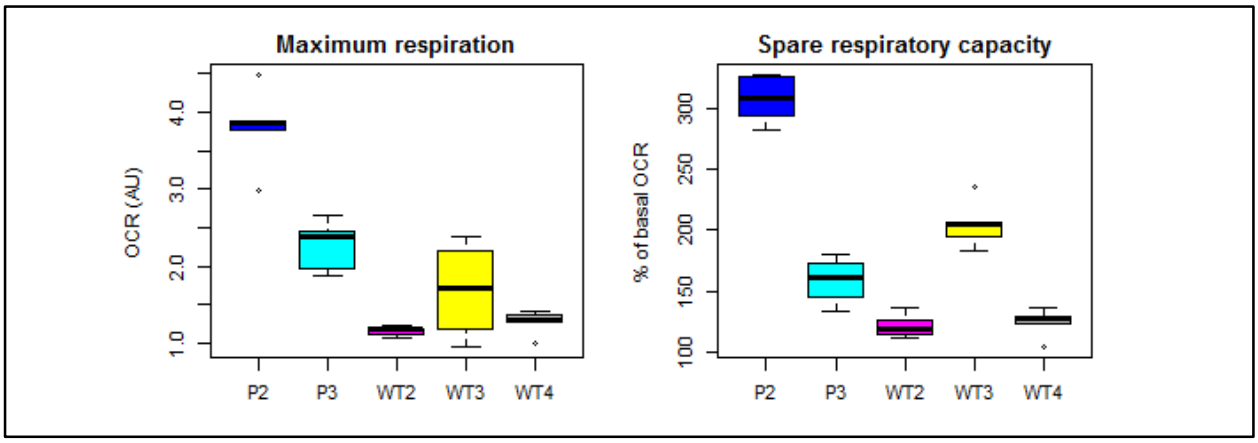

Figure 3.20 Maximum respiration and spare respiratory capacity in individual fibroblasts cell lines. Marked differences in the maximum respiration and spare respiratory capacity were observed between the two patient-derived fibroblast cell lines (P2 and P3). Abbreviations: AU, arbitrary units; OCR, oxygen consumption rate; P, patient; WT, wild-type.

3.3.3 Mitochondrial membrane potential ($\Delta\psi_m$) analysis

As $\Delta\psi_m$ is a central parameter of mitochondrial integrity, it was decided to assess $\Delta\psi_m$ in the *parkin*-mutant and wild-type fibroblasts. The fibroblasts were stained with the JC-1 potentiometric dye, and the green and red fluorescent emissions of each cell population were simultaneously measured by means of flow cytometry (Section 2.28). A representative experimental run of WT2 fibroblasts, as well as CCCP-treated depolarized WT2 is shown in Figure 3.21.

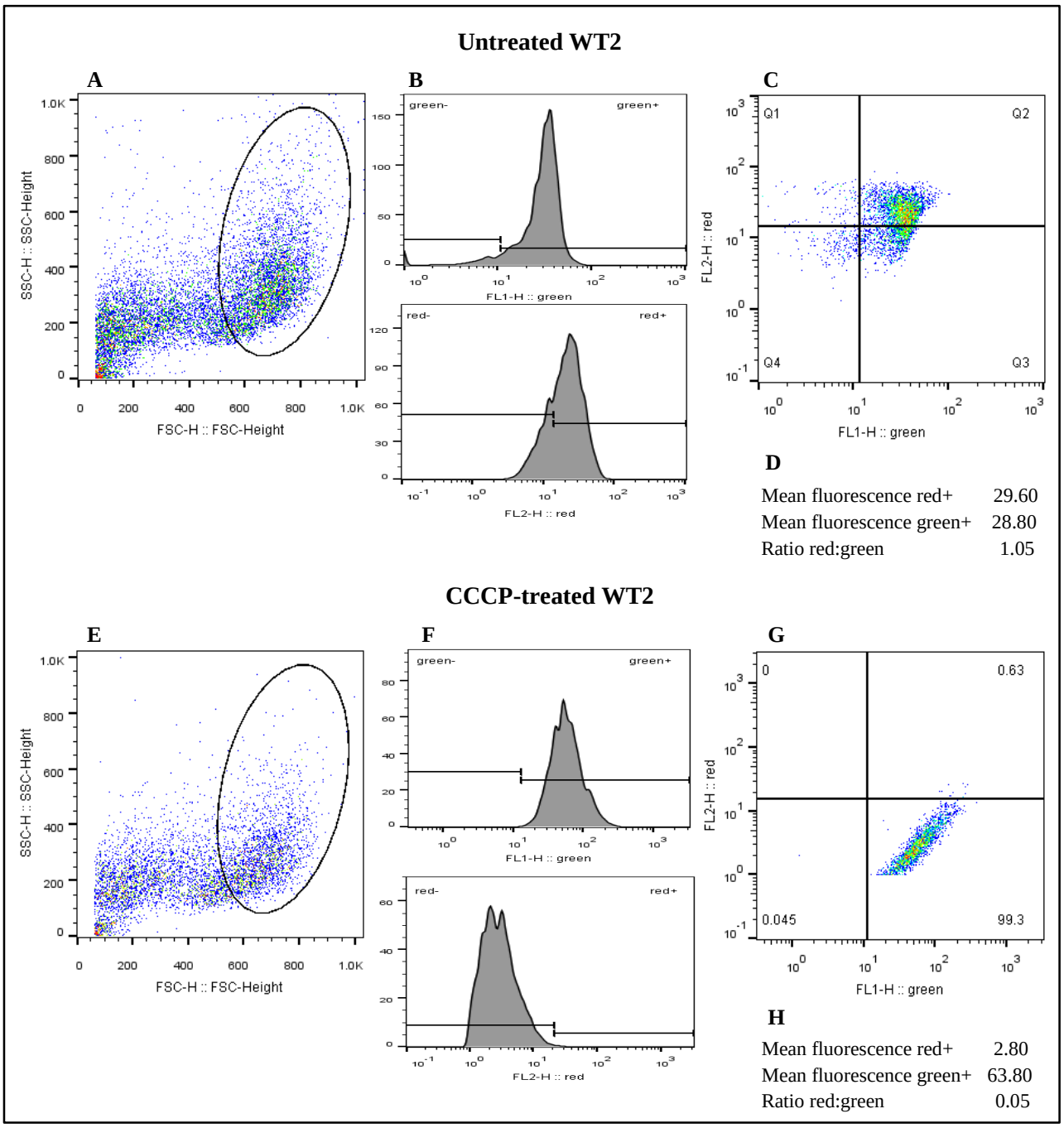

Figure 3.21 Bivariate flow cytometry analysis of JC-1 fluorescent emission in fibroblasts. **A-D**, representative experimental results of untreated WT2 fibroblasts. **E-H**, representative experimental results of CCCP-treated depolarized WT2 fibroblasts. For each JC-stained cell sample, several informative plots were generated. **A**, **E**, forward scatter/side scatter (FSC/SSC) plots. Debris and aggregates were gated out, with only the events enclosed in the black ovals analyzed further. **B**, **F**, fluorescent intensity histograms for green fluorescence (top panels) and red fluorescence (bottom panels). Fluorescent thresholds, as determined by fluorescence of unstained control cells, are demarcated by black bars. **C**, **G**, bivariate fluorescence depicted as logarithmic scatter plots, with fluorescent thresholds demarcated by crossbars. **D**, **H**, mean above-threshold green and red fluorescent intensities. These value were used to calculate the ratio of green:red fluorescent emission. Abbreviations: +, above threshold; -, below threshold; FSC/SSC, forward scatter/side scatter; WT, wild-type.

Each fibroblasts sample was assayed over three separate experimental runs, with 10 000 events collected per run. Differences in $\Delta\psi_m$ were detected by dissimilarities in red:green florescent emission ratios. The obtained red:green florescent emission ratios of the patient-derived and wild-type fibroblasts are graphically illustrated in Figure 3.22. No significant differences in Δψm were observed for parkin-derived and wild-type fibroblasts (p=0.1533).

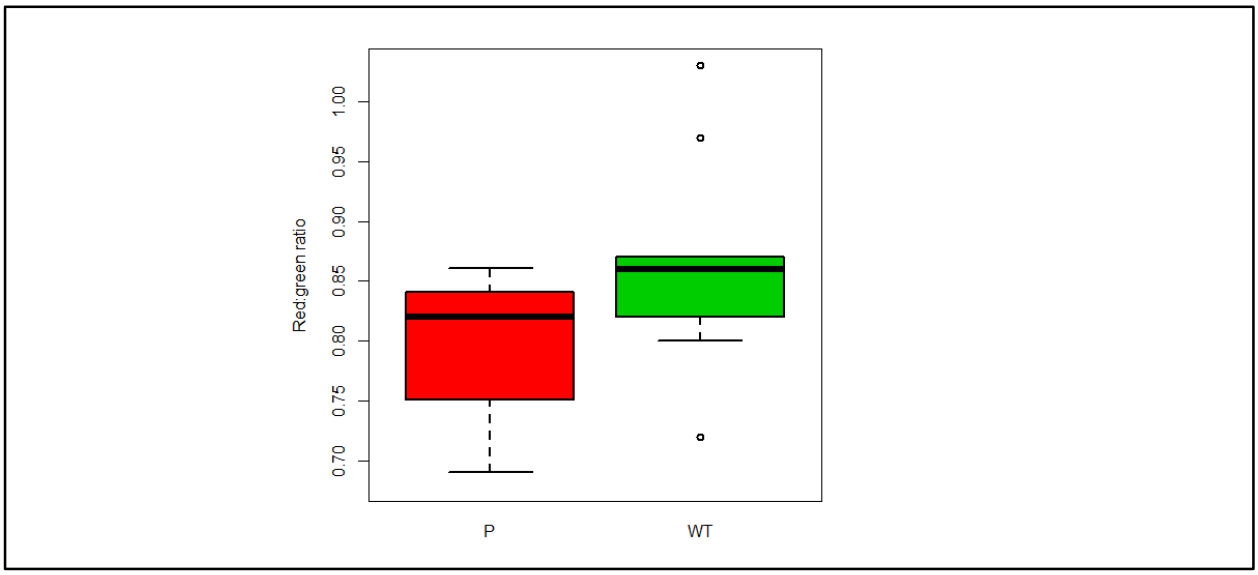

Figure 3.22 Relative $\Delta\psi_m$ of untreated patient-derived and wild-type fibroblasts. Relative $\Delta\psi_m$ was determined by JC-1 red:green fluorescent emission ratios. Similar $\Delta\psi_m$ was seen for patient-derived (P) and wild-type (WT) fibroblasts (p=0.3285). Abbreviations: $\Delta\psi_m$, mitochondrial membrane potential; P, patient; WT, wild-type.

3.3.4 Mitochondrial network analysis

As parkin is known to be involved in the regulation of mitochondrial dynamics, various parameters of mitochondrial morphology were assessed in the *parkin*-mutant and wild-type fibroblasts. This was done by means of live-cell microscopy and image analysis (Section 2.29). Approximately 40 cells were analyzed of each fibroblasts cell line, and representative images of P2 and WT2 fibroblasts are shown in Figures 3.23A and B, respectively. Each image was assessed in regards to two morphological parameters: the form factor (degree of mitochondrial branching) and the aspect ratio (degree of mitochondrial elongation). It was found that the form factor of patient-derived fibroblasts is significantly lower than that of wild-type controls (p=0.0306; Figure 3.23C). No significant differences were observed between the aspect ratios of patient-derived and wild-type fibroblasts (p=0.1654; Figure 3.23D).

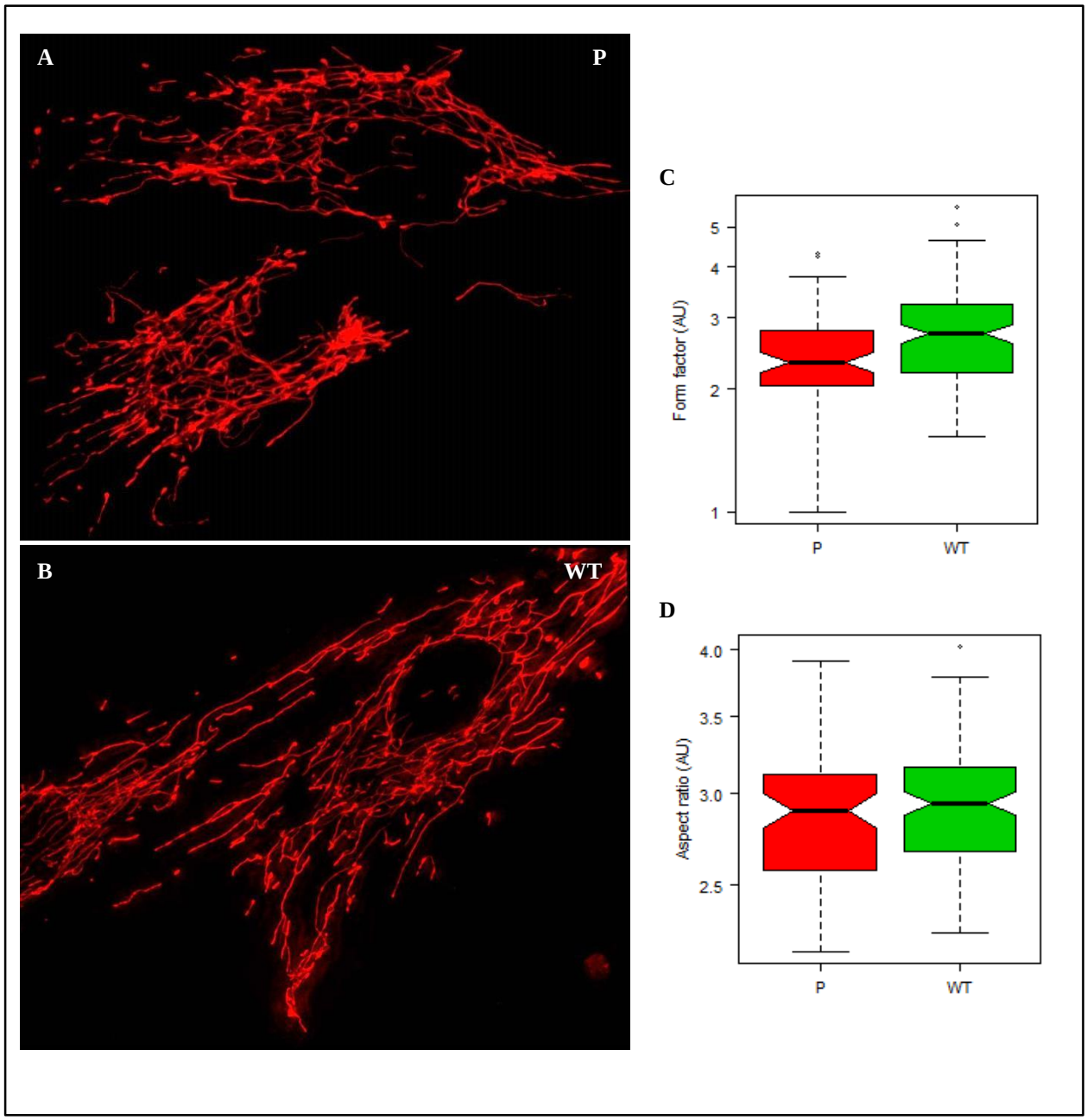

Figure 3.23 Mitochondrial network analysis of patient-derived and wild-type fibroblasts. Mitotracker Red and live-cell microscopy was used to visualize the mitochondrial network. **A**, **B**, representative images of patient and wild-type cells. All images were assessed in regards to the degree of mitochondrial branching (form factor) and degree of mitochondrial elongation (aspect ratio) The distribution of these parameters in grouped patient-derived and grouped wild-type fibroblasts are represented on logarithmic scale in box-and-whisker-plots, N=40. **C**, comparison of form factor, which was significantly lower in patient cells than wild-type cells (p=0.0306). **D**, comparison of aspect ratio, which was similar in patient and wild-type cells (p=0.1654). Abbreviations: AU, arbitrary units; N; cells analyzed; P, patient; WT, wild-type.

3.4 VITAMIN K_2 AS A POTENTIAL THERAPEUTIC MODALITY

It was recently reported that supplementing the diets of parkin-mutant *Drosophila* with vitamin K_2 alleviated the mitochondrial defects of these mutants in a dose-dependent manner (Vos et al. 2012). This exciting discovery may be of therapeutic value, as treatment with vitamin K_2 may similarly alleviate mitochondrial impairments in parkin-mutant human cells. Therefore, it was decided to perform a pilot study to investigate whether vitamin K_2 treatment can modulate the functional differences seen in parkin-null and wild-type fibroblasts.

3.4.1 Optimization of vitamin K_2 concentration

In the study by Vos et al (2012), mutant flies were placed on molasses medium supplemented with 1mM vitamin K_2, in the form of MK-4. It can be difficult to directly translate these supplementation conditions to appropriate working concentrations of MK-4 in cell culture. Hence, it was initially attempted to determine the effect of a range of MK-4 concentrations on the cell viability of wild-type fibroblasts (Section 2.26.1). It was determined that treatment with MK-4 did not significantly affect the cell viability of fibroblasts in the tested concentration range (0-100μM) after 24h of treatment (Figure 3.24).

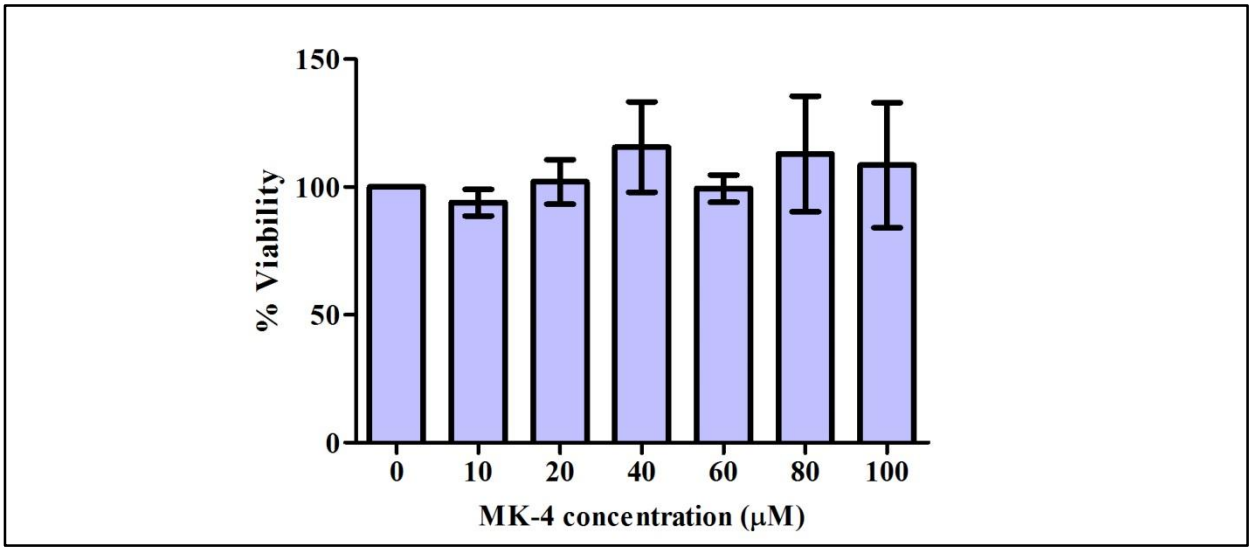

Figure 3.24 Effect of varying MK-4 concentrations on cell viability. A concentration range (0-100μM) MK-4 was added to WT2 fibroblasts for 24h, after which cell viability was assessed with a MTT assay. Untreated cells (0 μM MK-4) were supplemented with 0.1% ethanol as a vehicle control. All values are expressed as % viability in comparison to untreated cells (0 μM MK-4) ± SD, of four replicate readings. Abbreviations: MK-4, menaquinone 4 (vitamin K_2); SD, standard deviation; WT, wild-type.

As no apparent cytotoxic effects of MK-4 treatment were observed even at the highest tested concentration (100μM), it was decided to consult the established literature on effective working concentrations for MK-4 treatment in cell culture. The majority of these studies were investigating the anti-cancer properties of MK-4, and reported that significant functional effects of MK-4 treatment can been seen at concentrations of 30-50μM after 24h (Otsuka et al. 2004; Cao et al. 2009; Yao et al. 2012; da Silva et al. 2013). While MK-4 was similarly effective at concentrations higher than ≈40μM, the magnitude of the observed effects typically plateaued at higher concentrations. Furthermore, all concentrations higher than 10μM had pro-apoptotic effects when treated for longer than 48h (Cao et al. 2009). Hence, it was decided to use a MK-4 concentration of 40μM for 24h in this pilot study as an informed compromise between concentrations and incubation periods high enough to elicit effective cellular responses, but low enough to avoid non-specific effects and cytotoxicity.

3.4.2 Vitamin K_2 modulates cellular and mitochondrial parameters

In order to assess vitamin K_2 as a potential therapeutic compound, the *parkin*-mutant and wild-type fibroblasts were treated with MK-4. Various parameters of cellular and mitochondrial health were then evaluated by means of the same approaches discussed in Section 3.3, i.e. cell growth and viability assays, mitochondrial respiration analysis, $\Delta\psi_m$ analysis and mitochondrial network analysis. Where appropriate, the MK-4 treated cells were compared to "untreated" control cells, which were treated with a suitable vehicle control. All results demonstrate comparisons of treatment responses in grouped patient-derived vs. grouped wild-type fibroblasts. Graphical depictions of results obtained for individual fibroblast cell lines (before and after MK-4 treatment) can be found in Appendix IX.

It was found that cell growth was higher in patient-derived fibroblasts treated with MK-4 than in treated wild-type fibroblasts (p=0.0006; Figure 3.25A, left panel). However, this is likely a reflection of the higher cell growth rates of patient cells already seen under basal conditions (Section 3.3.1). In contrast, cell viability was similar in patients and controls treated with MK-4 (p=0.915; Figure 3.25A, right panel). When cells were simultaneously treated with MK-4 and the cellular stressor CCCP, both cell growth and cell viability were comparable between patient-derived and wild-type fibroblasts (p=0.1036 and p=0.6933, respectively; Figure 3.25B).

A comparison of the cellular responses to the different treatments employed in this study (untreated, CCCP, MK-4 and MK-4+CCCP) is shown in Figure 3.25C, where the results obtained for untreated and CCCP-treated fibroblasts were described in Section 3.3.1. It was found that overall response patterns to MK-4 treatment was very similar in patient-derived and wild-type fibroblasts when assessing cell growth (p=0.14; Figure 3.25C, top panel) and cell viability (p=0.4963; Figure 3.25C, bottom panel). Hence, 2^2 factorial modeling was used to analyze the global effects of MK-4 treatment

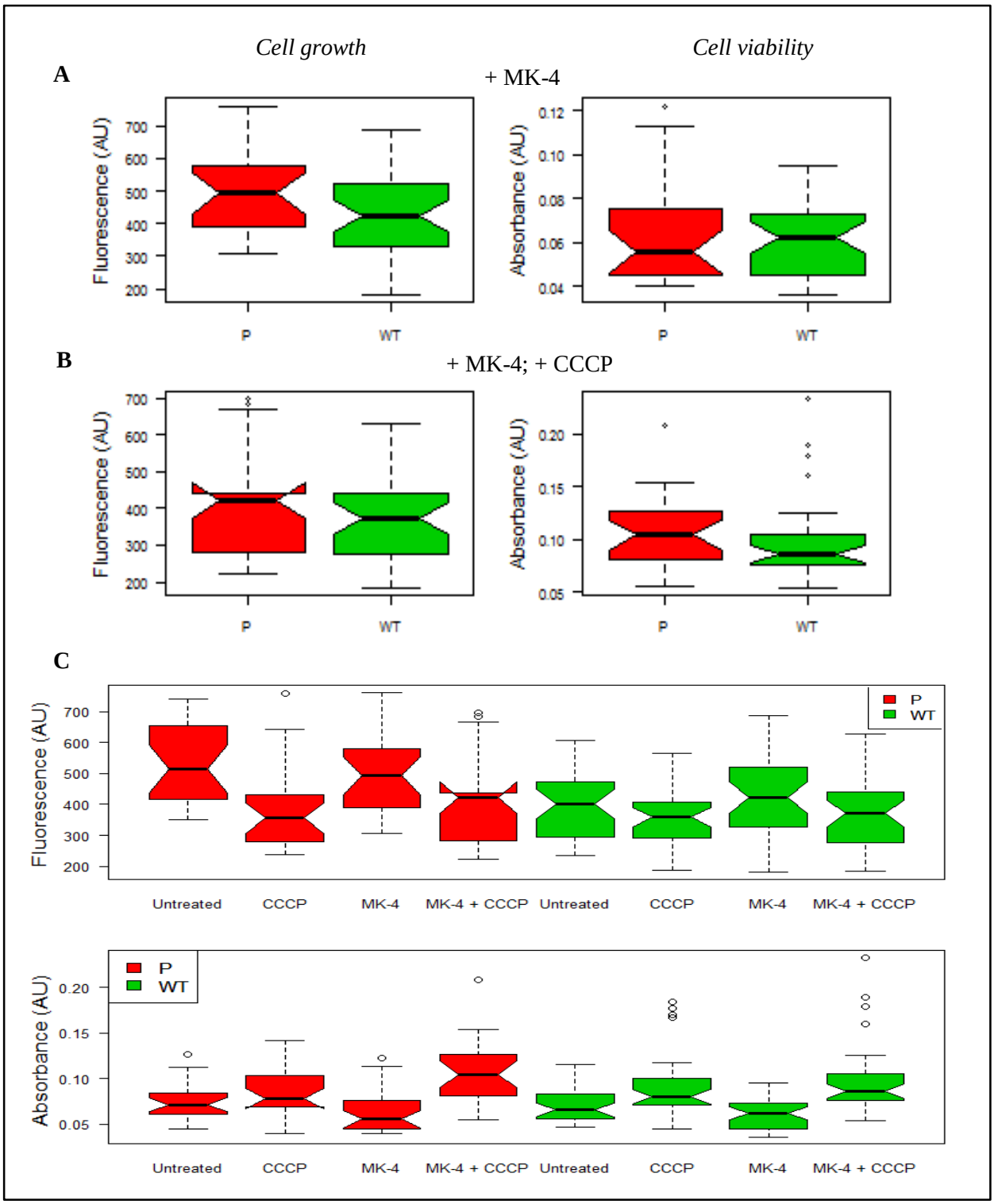

Figure 3.25 Cell growth and viability in patient-derived and wild-type fibroblasts after vitamin K_2 treatment. Left panels represent cell growth as assessed by a CyQUANT® assay, whereas right panels represent cell viability as assessed by a MTT assay. Box-and-whisker plots depict grouped patients (P) and wild-type (WT) measurements for three experimental runs. **A**, cell growth and viability after treatment with 40µM MK-4 for 24h. **B**, cell growth and viability after co-treatment with 40µM MK-4 and 10 µM CCCP for 24h. **C**, comparison of cell growth (top panel) and cell viability (bottom panel) of fibroblasts under various treatment conditions. Graphs depicting cell growth and viability of untreated and CCCP-treated fibroblasts can be found in Figure 3.17. Abbreviations: AU, arbitrary units; MK-4, menaquinone 4 (vitamin K_2); P, patient; WT, wild-type.

(on combined patient and wild-type cells), adjusting for correlations inside individual cell lines and experimental runs. It was found that treatment with MK-4 had no observable effect on cell growth in comparison to untreated fibroblasts (p=0.1531) or when co-administered with CCCP and compared to CCCP-only treated fibroblasts (p=0.5253). In contrast, MK-4 treatment was found to lower the cell viability of all treated cells in comparison to untreated fibroblasts (p=0.0014). Interestingly, MK-4 and CCCP co-treatment significantly increased measurements of cell viability in all fibroblasts (p=0.0001). Hence, MK-4 enhanced the previously mentioned MTT-artefact produced by CCCP treatment (Section 3.3.1); this artefact was not seen when MK-4 was used by itself. It is interesting to speculate that CCCP and MK-4 interact biochemically to artificially elevate the rate of MTT reduction, which does not occur in the absence of CCCP.

Several interesting effects on mitochondrial respiration were observed when patient-derived and wild-type fibroblasts were treated with MK-4, which are depicted in Figure 3.26.

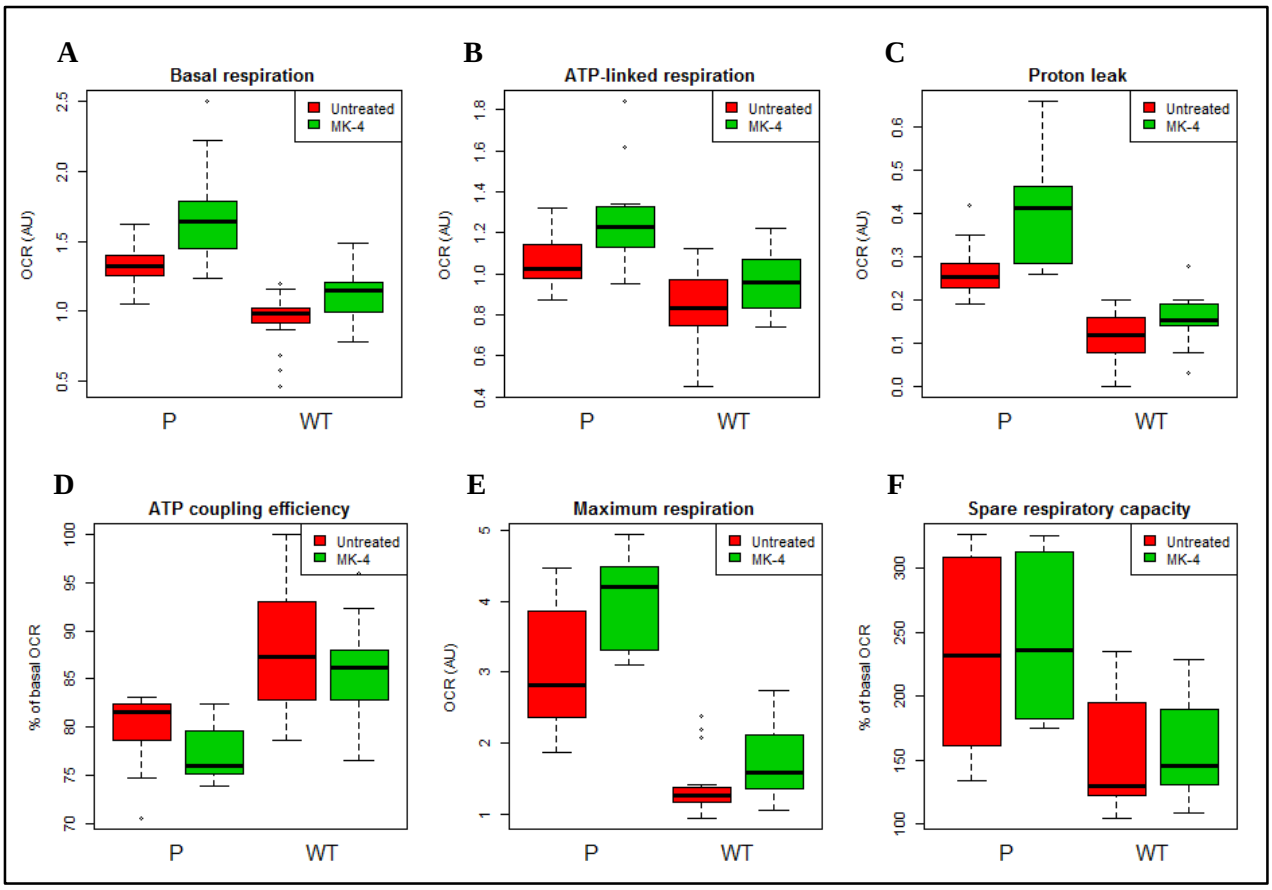

Figure 3.26 Parameters of respiratory control in patient-derived and wild-type fibroblasts after vitamin K_2 treatment. Fibroblasts were either treated with a vehicle control (0.1% ethanol) or 40µM MK-4 for 24h. Box-and-whisker plots depict grouped patients (P) and wild-type (WT) values. **A**, basal mitochondrial OCR. **B**, ATP-linked OCR. **C**, OCR due to proton leak. **D**, ATP coupling efficiency (percentage OCR due to ATP synthesis). **E**, Maximal OCR. **F**, Percentage spare respiratory capacity. Abbreviations: AU, arbitrary units; MK-4, menaquinone 4 (vitamin K_2); OCR, oxygen consumption rate; P, patient; WT, wild-type.

It was found that fibroblasts treated with MK-4 had increased basal mitochondrial respiration in comparison to untreated cells (p=0.0459; Figure 3.26A). Similarly, treatment with MK-4 increased the ATP-linked respiration (p=0.0465; Figure 3.26B), the oxygen consumption due to proton leakage (p=0.025; Figure 3.26C) and the maximum respiration (p=0.0331; Figure 3.26E) of all fibroblasts cell lines. When correcting for differences in basal mitochondrial respiration, if was found that MK-4 treatment did not significantly alter either the ATP coupling efficiency (p=0.0707; Figure 3.26D) or spare respiratory capacity (p=0.2495; Figure 3.26F).

Comparisons of patient-derived and wild-type fibroblasts in their responses to MK-4 treatment demonstrated that the increase in proton leak was more pronounced in patient-derived cells (p=0.0082). Similarly, the increase in maximum respiration was stronger in patient-derived cells (p=0.0105). The effect of MK-4 treatment on basal and ATP-linked respiration was found to be comparable between patient-derived and wild-type fibroblasts.

Potential effects on $\Delta\psi_m$ were similarly assessed after treatment with MK-4. As can be seen in Figure 3.27, no significant differences were found in the effect of MK-4 treatment on $\Delta\psi_m$ between patient-derived fibroblasts and wild-type fibroblasts. When all fibroblasts are viewed collectively, MK-4 treatment did not significantly alter the $\Delta\psi_m$ in comparison to untreated fibroblasts (p=0.3285).

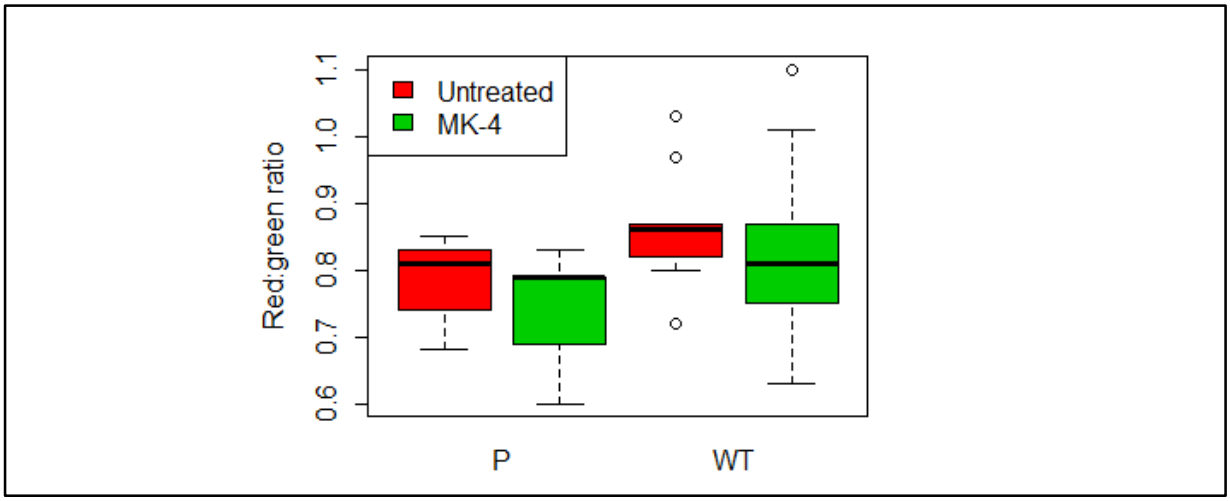

Figure 3.27 Relative $\Delta\psi_m$ of patient-derived and wild-type fibroblasts after vitamin K_2 treatment. Fibroblasts were either treated with a vehicle control (0.1% ethanol) or 40μM MK-4 for 24h**.** Relative $\Delta\psi_m$ was determined by JC-1 red:green fluorescent emission ratios. Similar $\Delta\psi_m$ was seen for treated and untreated patient-derived fibroblasts (p=0.3285), as well as for treat and untreated wild-type fibroblasts (p=0.3285). Abbreviations: $\Delta\psi_m$, mitochondrial membrane potential; MK-4, menaquinone 4 (vitamin K_2); P, patient; WT, wild-type.

Lastly, the mitochondrial networks of parkin-derived and wild-type fibroblasts were evaluated after treatment with MK-4. It was found that MK-4 treatment significantly increased the form factor of all fibroblast cell lines investigated (p<0.0001; Figure 3.28A). This effect on the form factor was observed in parkin-derived and wild-type fibroblasts; however, there was a non-significant statistical trend towards a more pronounced increase in the form factor in patients (p=0.0729). Moreover, the aspect ratio was increased in MK-4-treated cells (p<0.0001; Figure 3.28B); this was seen to a similar extent in parkin-derived and wild-type fibroblasts, irrespective of *parkin* mutation status (p=0.4091).

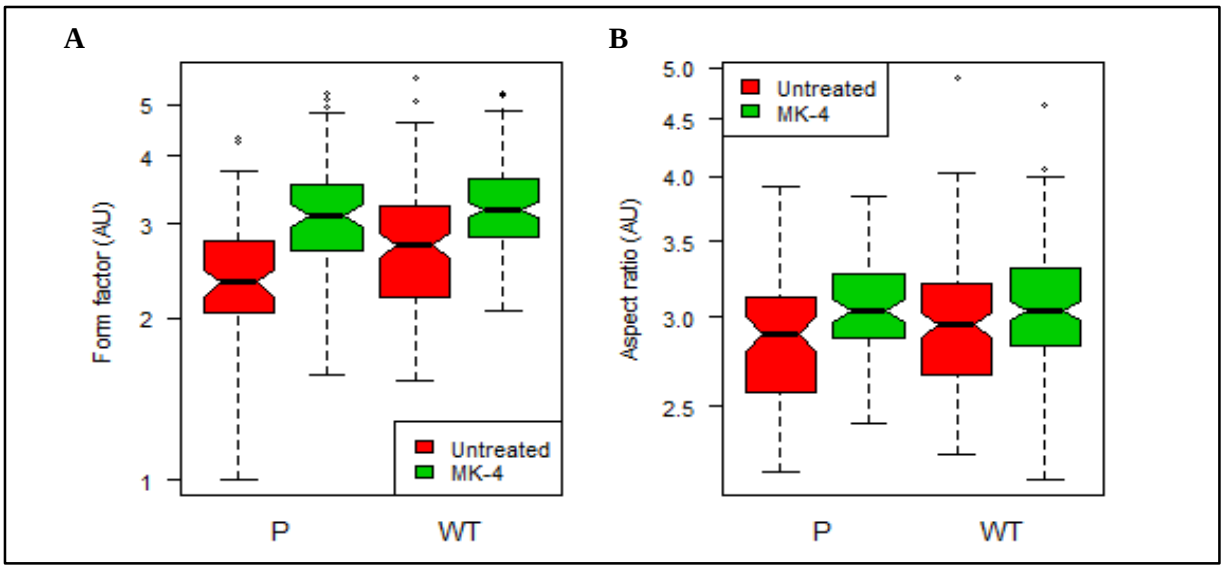

Figure 3.28 Mitochondrial network analysis of patient-derived and wild-type fibroblasts after vitamin K_2 treatment. Fibroblasts were either treated with a vehicle control (0.1% ethanol) or 40µM MK-4 for 24h**.** Mitotracker Red and live-cell microscopy was used to visualize the mitochondrial network. All images were assessed in regards to the degree of mitochondrial branching (form factor) and degree of mitochondrial elongation (aspect ratio) The distribution of these values are represented in box-and-whisker-plots, N=40. **A**, comparison of form factor. **B**, comparison of aspect ratio. Abbreviations: AU, arbitrary units; MK-4, menaquinone 4 (vitamin K_2); N; cells analyzed; P, patient; WT, wild-type.

In summary, treatment with vitamin K_2 (in the form of MK-4) modulated several parameters of mitochondrial health in interesting and unexpected ways. These effects were mostly seen to a similar extent in parkin-derived and wild-type fibroblasts (increased basal and ATP-linked respiration; increased aspect ratio), with some effects being more pronounced in *parkin*-mutant fibroblasts (increased oxygen consumption due to proton leak; increased maximum respiration; increased form factor). These interesting observations suggest functional interactions of vitamin K_2 with mitochondrial pathways, which should be investigated further in future studies.

CHAPTER FOUR: DISCUSSION

TABLE OF CONTENTS **PAGE**

CHAPTER FOUR: DISCUSSION

The present study undertook an investigation of the *parkin* gene and its protein product on various levels. Initially, it was found that mutants in *parkin* are infrequent in PD in South African PD patients. It was therefore sought to identify additional candidate PD genes by screening for protein interactors of parkin using a Y2H approach. This yielded a number of putative parkin interactors, of which four (ATPAF1, SEPT9, 14-3-3η and actin) were prioritized for verification and further study. Interestingly, two novel parkin interactors were found to accumulate in a cellular model of parkin deficiency. Additional investigation of cellular and mitochondrial dysfunction in these patient-derived fibroblast models demonstrated interesting and unanticipated effects, including possible compensatory increases in mitochondrial respiration. Moreover, the parkin-deficient cell model was used to evaluate vitamin K_2 as a potential therapeutic modality for PD.

4.1 *PARKIN* MUTATION SCREENING

The elucidation of genetic factors contributing to PD is of importance as such genetic factors may provide valuable insight into the etiology and molecular pathology of this disorder. However, while the molecular basis of PD has been extensively studied in numerous population groups over the last two decades, very little is known of the etiology of PD in Sub-Saharan African populations. In fact, a recent review of the available literature found only nine published studies on the genetics of PD in Sub-Saharan Africa (Blanckenberg et al. 2013). The majority (5/9) of these studies emanated from our research group focusing on South African PD patients, including results published from the present study (Haylett et al. 2012).

The investigation of the genetic etiology of PD in South African patients is of particular interest, given the diverse and distinctive genetic heritage of the population groups in this country. Hence, the present study aimed to investigate the contribution of *parkin* mutations to South African PD patients. Our research group had previously reported on a comparable molecular analysis of *parkin*, which concluded that *parkin* mutations are not a major cause of PD in the South African population (Bardien et al. 2009). While the previous study is of note as being the first report on the molecular etiology of PD in South African patients, the conclusions of the preliminary study were limited by a small sample size of only 91 study participants, and the fact that the contribution of *parkin* exon deletions and insertions was not determined. Therefore, the present study expands upon previous findings from our research group by the screening of an additional 138 South African PD patients, as well as by the inclusion of MLPA analysis to detect exonic rearrangements.

Only seven patients with homozygous or compound heterozygous *parkin* mutations were found in the study group of 229 South African PD patients (Section 3.1). A further eight patients were heterozygous carriers of a single *parkin* missense variant or exonic rearrangement, but the pathogenic relevance of such heterozygous variants are currently unclear.

The frequency of *parkin* mutations (3.1%; 7/229) in South African PD patients is low in comparison to previous reports of *parkin* mutation frequencies, with reported frequencies as high as 50% of EOPD patients with a family history of PD, as well as 15-20% of sporadic EOPD cases (Lücking et al. 2000; Periquet 2003; Hedrich et al. 2004). However, the reported *parkin* mutation frequencies vary significantly across different studies and study populations (Kann et al. 2002; Choi et al. 2008; Sironi et al. 2008; Mellick et al. 2009; Koziorowski et al. 2010). For example, homozygous or compound heterozygous *parkin* mutations were reported in as high as 25.4% of Mexican-mestizo EOPD patients (Camacho et al. 2012), whereas only 1.4% of EOPD patients from Queensland, Australia had *parkin* mutations (Mellick et al. 2009). It can be speculated that the parkin mutation frequency is dependent on the ethnicity on the study group, which is supported by the available literature (Djarmati et al. 2004). The low frequency of parkin mutations found in this study may therefore reflect the unique genetic heritage of the Black African, Afrikaner and Mixed ancestry sub-populations of South Africa.

The range of *parkin* mutation frequencies reported in the literature may be furthermore due to differences in study inclusion criteria. The present study also included PD patients with late onset PD, as *parkin* mutations had been previously reported in both early and late onset PD patients (Sun et al. 2006). In fact, this study identified a compound heterozygous *parkin* mutation in a patient with an AAO of 56 years (patient 107), which suggests that the conventional cut-off AAO of 50 years for *parkin* mutation screening is not recommended for the South African population. When considering only the 82 patients with EOPD, six (7.3%; 6/82) had homozygous or compound heterozygous *parkin* mutations, with a further four patients (4.8%; 4/82) carrying single heterozygous *parkin* variants. The majority of the EOPD patients included in the study (92.7%) therefore did not have *parkin* mutations. Surprisingly, no *parkin* mutations were found in one patient with juvenile onset PD, with an AAO of 17 years.

All five of the *parkin* missense variants (H200Q, E310D, R402C, G430D, P437L) as well as the *parkin* deletion (P113fsX163) identified in this study had been previously reported in the literature; however, the H200Q variant have only been reported by our research group to date (Bardien et al. 2009). While the pathogenic relevance of H200Q is unclear, this variant was found to be absent in 106 control chromosomes, and it is located in the functionally important RING0 domain. Functional studies of other parkin variants in the RING0 domain, such as K161N and K211N, found that such variants result in defective parkin auto-ubiquitination and protein interaction (Sriram et al. 2005; Hampe et al. 2006). The pathogenicity of the E310D variant is similarly uncertain; E310D was absent

in 110 control chromosomes in the present study. This variant was also absent in 526 control chromosomes in a published study of American PD patients (Pankratz et al. 2009b).

No functional studies of the R402C variant have been reported to date, and the pathogenicity of this variant remains equivocal. Functional studies of the P437L variant in RING2 reported that it markedly impairs parkin ubiquitination activity (Chen et al. 2010; Glauser et al. 2011); however, heterozygous P437L variants have been previously described in unaffected individuals and may therefore be a risk factor for, instead of a cause of, PD (Kay et al. 2007). On the other hand, the pathogenicity of the G430D mutation is well established in the literature. This mutation, affecting the catalytic site in RING2, has been shown to abrogate parkin ligase activity, impair its mitochondrial translocation, and reduce its neuroprotective capacity (Henn et al. 2007; Vives-Bauza et al. 2009; Koyano et al. 2013). Small deletions, such as P113fsX163, as well as the numerous exonic rearrangements reported in the present study, are likely to result in protein truncation due to the introduction of frameshifts; therefore, homozygous or compound heterozygous *parkin* mutations containing such deletions or insertions would result in the abolishment of parkin biological activity (Dawson and Dawson 2010).

In the present study, G430D was the only *parkin* missense mutation found in a compound heterozygous state; no homozygous *parkin* missense mutations were detected. It is currently unclear whether the four missense variants found only in a heterozygous state (H200Q, E310D, E402C, P437L) contribute to PD, as they may represent rare non-pathogenic *parkin* polymorphisms (Kay et al. 2007).

It can be concluded that *parkin* mutations are not a major cause of PD in South African patients. The 229 South African PD patients screened in the present study for *parkin* mutations were concurrently screened by our research group for mutations in other PD genes, including *SNCA*, *LRRK2*, *PINK1* and *DJ-1*, *VPS35* and *EIF4G1* (Keyser 2011; Blanckenberg et al. 2014; unpublished data). Overall, mutations in the known PD genes are rare in the South African PD population: of the 229 study participants, one (0.4%; 1/229) was found with a whole gene triplication of *SNCA*; six (2.6%; 6/229) with *LRRK2* mutations (five with G2019S and one with R1441C); and one patient with a homozygous *PINK1* mutation (Y258X) (Keyser 2011). When these results are combined with the results obtained in the present study, only fifteen (6.6%; 15/229) of the PD patients have mutations in a known PD gene. This is unexpected, given that the majority of the study participants had either EOPD or a known family history of PD. If only the 82 EOPD patients are considered, eight (9.8%; 8/82) have mutations in known EOPD genes (six patients with *parkin* mutations, one each with a *SNCA* triplication and *PINK1* mutation). Therefore, a total of 90.2% of the patients with a disease onset younger than 50 years do not have mutations in any of the known EOPD genes.

4.2 PARKIN INTERACTORS

In addition to a genetic investigation of *parkin*, the present study aimed to further current understanding of the cellular and physiological function of parkin. In this regard, a Y2H cDNA library screen was used to identify known and novel parkin-interacting proteins. It is speculated that such interactors may partake in the many cellular pathways parkin has been implicated in and, ultimately, the dysregulation or dysfunction of parkin interactors may contribute to neurodegeneration.

It is estimated that the present study screened approximately 1.8 x 10^7 cDNA clones from an adult human brain cDNA library, using the RBR region of parkin as bait (Section 3.2.1). Of these, a total of 64 clones were selected for their ability to successfully activate all three the Y2H reporter genes; such clones were considered to encode peptides that specifically interacted with the parkin bait protein under the Y2H experimental conditions.

4.2.1 Putative parkin interactors excluded from the present study

The clones were each bioinformatically analyzed in order to identify the in-frame cDNA clone and encoding peptide. Of the 64 clones, sixteen were discarded as duplicate clones, i.e. clones that encoded identical peptides. Such detection of duplicate bait-prey interactions was not unexpected, as each clone may be represented numerous times in the cDNA library, providing multiple opportunities for interactions with the parkin bait (Gietz 2006). A further nineteen clones had insert sequences that were not in-frame according to the reading frame dictated by the upstream GAL4-AD; therefore, when translated, these clones had no significant protein match in the NCBI database (http://www.ncbi.nlm.nih.gov). These nineteen out-of-frame clones were discarded as they encoded short, physiologically-irrelevant peptides. The high prevalence of such clones is a known and common limitation of cDNA libraries derived from oligo(dT)-primed cDNA, such as the Clontech MATCHMAKER™ cDNA library used in this study, where only one in six of all cDNA inserts are cloned in-frame with the GAL4-AD (Van Criekinge and Beyaert 1999).

The 29 in-frame cDNA clones with significant protein matches were investigated in publicly available databases in order to obtain relevant information regarding the subcellular expression and proposed function of the proteins. Based on such information, four of the putative parkin interactors were prioritized for further study, and will be discussed in Section 4.2.2. The remaining 25 candidate parkin-interacting proteins were not prioritized due to several reasons, which will be briefly discussed.

While parkin has been observed in many subcellular compartments, including the ER, cytoplasmic vesicles, mitochondria and the nucleus, endogenous parkin is predominantly localized to the cytosol (Section 1.13.2). Therefore, putative parkin interactors that are not likewise localized to the cytosol

were de-emphasized in the current study, as they are less likely to reflect physiologically-relevant interactions (Patil and Nakamura 2005). On the other hand, mitochondrial or mitochondrial-associated proteins were emphasized as being of particular interest, given parkin's role in the maintenance of mitochondrial function and health (Section 1.16.3).

Five of the 29 putative parkin interactors (representing sixteen of the 45 in-frame cDNA clones) are nuclear proteins. These proteins (PCF11, NONO, SNRPN, SRSF3 and TRA2A) were not prioritized for the present study as their cellular localization makes in less likely that they would interact with predominantly cytosolic parkin outside of the Y2H experimental environment. However, as limited parkin expression in the nucleus has been previously described (Shimura et al. 1999; Stichel et al. 2000), and parkin has been shown to have some nuclear-specific functions (da Costa et al. 2009; Duplan et al. 2013), it cannot at present be ruled out that some of these nuclear proteins are, if fact, authentic parkin interactors. Interestingly, all five of these proteins are involved in pre-mRNA splicing and processing, although parkin does not have a known RNA processing-related function. It is of note that the two putative interactors PCF11 and SRSF3 were repeatedly identified by six independent clones each, suggesting that their observed interaction with the parkin bait is less likely to be an artefact of the Y2H methodology (Parrish et al. 2006).

One other protein was identified by multiple (more than two) independent clones in the Y2H screen, namely TMEM222. The recurrent detection of such a presumed parkin-TMEM222 interaction via Y2H analysis is suggestive of the validity of this interaction. However, the putative parkin interactor was discarded as this protein is uncharacterized at present, and its biological function remains unknown. The uncharacterized protein DHRS7 was similarly excluded from further study. Conversely, another protein that was discarded from the study for being uncharacterized at the time, has lately been reported to be of potential relevance in neurodegeneration. This protein, CCDC56, was only recently characterized as a mitochondrial transmembrane protein and essential factor in cytochrome c oxidase (mitochondrial complex IV) biogenesis (Clemente et al. 2013). Given that mitochondrial respiratory dysfunction is a known pathological feature of parkin deficiency (Section 1.16.3), the identification of a putative interaction between parkin and CCDC56 may be of significant relevance to neurodegeneration, and future studies should aim to verify this protein interaction.

The remaining seventeen putative parkin interactors were not prioritized for verification; their biological function(s) are of unclear relevance to the known functions of parkin. These include several proteins involved in intracellular signaling (ARAP2, AKAP9, CALD1, GNB3 and NR1H2), various metabolic pathways (DHDDS, ELOVL1, PCMT1, PGAM1, PGM1, and TKT), vesicular trafficking and sorting (AP3S1, EXOC4, and HGS), prohormone processing (CPE), astrocyte plasticity and motility (CAPN3), and maintenance of the myelin sheath (MBP). While the detection of these putative parkin interactors with unclear functional relationships may be due to false positive Y2H

results (Mahdavi and Lin 2007), it cannot be ruled out that they reflect true, physiologically-relevant interactions with parkin. It is interesting to speculate that these candidate parkin interactions may illuminate previously unknown pathways to neurodegeneration. For that reason, these interactions should be verified in future studies in order to gain a more comprehensive understanding of the role of parkin in the cell.

4.2.2 Verified parkin interactors

Four of the parkin-interacting proteins originally detected in a Y2H screen were demonstrated to be authentic parkin interactors. Furthermore, it was shown that two of these interactors (SEPT9 and ATPAF1) accumulate in the absence of parkin, whereas parkin does not affect the steady-state protein level of the other two interactors (14-3-3η and actin) (Section 3.2.4.2). It should however be noted that this protein accumulation was not observed in one of the two parkin-mutant cell models, and that these preliminary findings need to be interpreted with caution. The following section will discuss what is known about the function of these parkin-interacting proteins, as well as hypothesize as to the possible biological significance of such interactions.

4.2.2.1 *ATPAF1*

The current study demonstrated a physical interaction of parkin with the ATPAF1 protein. Furthermore, it was found that ATPAF1 accumulated in the absence of parkin. Very little is known about ATPAF1; a PubMed literature search (http://www.ncbi.nlm.nih.gov/pubmed) using the keyword "ATPAF1" delivered just six published articles, while a search for Atp11p, the yeast homolog of ATPAF1, returned just thirteen results. Nevertheless, the discovery of a functional interaction between parkin and an assembly factor for an essential mitochondrial protein complex makes this an interesting protein to investigate further.

The mitochondrial F_1F_0-ATP synthase, also referred to as complex V, is located in the inner mitochondrial membrane. This multi-protein assembly consists of two physically and functionally coupled sectors: a catalytic F_1 enzyme complex and a membrane-imbedded F_0 ring-like channel. The electrochemical gradient generated by the ETC drives proton translocation from the inter-membrane space to the matrix through the F_0 channel. This is coupled to the rotation of F_0, which in turn induces conformational changes in F_1 that promotes the synthesis and release of ATP. This interesting mechanism has been well-studied (Boyer 1997; Senior et al. 2002).

The biogenesis of the mitochondrial ATP synthase has received considerably less attention. It is generally accepted to be a sophisticated process involving the coordinated activity of a number of

assembly factors, which drives the translocation, oligomerization and assembly of individual ATP synthase subunits to constitute functional ATP synthases (Ackerman and Tzagoloff 2005). The F_1 complex is comprised of five types of nuclear-encoded oligomeric subunits (α, β, γ, δ and ε), where the catalytic activity of F_1 is conveyed by the important hexameric assembly of three α- and three β-subunits (α_3:β_3). Biogenesis of F_1 requires two assembly factors: ATPAF1, which binds selectively to unassembled β-subunits of F_1, and ATPAF2, which associates with unassembled α-subunits (Wang and Ackerman 2000; Wang et al. 2001; Ackerman 2002). These two proteins act as substrate-specific molecular chaperones to stabilize unassembled α- and β-subunits by shielding their hydrophobic surfaces. This prevents the aggregation of α- and β-subunits prior to their assembly into a functional α_3:β_3 F_1 complex (Sheluho and Ackerman 2001). Binding of α- and β-subunits to their assembly factors is then appropriately relieved by the γ-subunit of the nascent F_1 complex (Ludlam et al. 2009). Separate assembly pathways are present for the assembly of the F_0-ATP synthase channel, as well as for the dimerization and oligomerization of fully assembled F_1F_0-ATP synthase complexes (Jonckheere et al. 2012). This mechanism of assembly factor-dependent biogenesis of mitochondrial ATP synthase is conserved in all eukaryotic lineages (Pícková et al. 2005).

Further studies found that the absence of either ATPAF1 or ATPAF2 not only resulted in their failure to assemble the F_1-ATP synthase complex, but lead to the accumulation of both α- and β-subunits within large aggregates in the mitochondrial matrix (Lefebvre-Legendre et al. 2005). This suggests that proper α_3:β_3 assembly is dependent on a balanced protein stoichiometry. While the functional effect of the opposite scenario, i.e. an overabundance of ATPAF1 over ATPAF2 or *vice versa*, has not been investigated, it could be speculated that this may also affect the proper assembly of the F_1-ATP synthase complex in some way.

A quantitative analysis of *ATPAF1* and *ATPAF2* mRNA expression revealed that these genes are expressed at very low levels in various tissues (Pícková et al. 2003). While this study did not investigate the protein expression of either ATPAF1 or ATPAF2, it is noteworthy that very low protein levels of ATPAF1 was seen in both SH-SY5Y cells (Section 3.2.3.2; Figure 3.11C) and wild-type fibroblasts (Section 3.2.4.2; Figure 3.15A) in the present study. Interestingly, Pícková et al. found a nearly constant *ATPAF1* mRNA level in all tissues investigated. This suggests that *ATPAF1* behaves like an housekeeping gene to provide constitutively low levels of this assembly factor.

Very few studies of the effect of altered *ATPAF1* expression have been published. A genetic association study found that sequence variation in *ATPAF1* is significantly associated with asthma and asthma severity (Schauberger et al. 2011). This study also showed that *ATPAF1* mRNA expression was markedly (50-fold) higher in bronchial biopsies from patients with asthma than controls, which validated the genetic association results. While the functional role of ATPAF1 as a novel asthma risk

factor is unclear, the authors speculated that it may involve altered ATP-signaling in bronchoconstriction. Another study highlighted *ATPAF1* as genetic modifier of prostate cancer (Schinke et al. 2014); it was found that *ATPAF1* mRNA is overexpressed in prostate cancer tissue.

The relevance of the parkin-ATPAF1 interaction to neurodegeneration is supported by recent studies suggesting that dysfunction of the mitochondrial ATP synthase specifically may contribute to parkin-linked PD. For example, a study by Kim et al. (2012) investigated the protective role of *Drosophila* glutathione *S*-transferase omega 1 (GSTO1) in a *Drosophila* model of PD. They found that overexpression of GSTO1 was able to rescue some of the phenotype of *parkin* mutants, including degeneration of dopaminergic neurons and muscle. Further investigation revealed that this rescue effect is dependent on the direct catalytic action of GSTO1 on its novel substrate, the β-subunit of F_1-ATP synthase.

The total protein expression of the β-subunit was unaffected in *parkin* mutant and wild-type flies; however, the level of GSTO1-mediated glutathionylation of the β-subunit was marked decreased in the *parkin* mutant (Kim et al. 2012). Kim et al. found that increased glutathionylation of the β-subunit was correlated with an improved mitochondrial F_1F_0-ATP synthase efficiency and elevated ATP levels, both of which were significantly decreased in *parkin*-mutant flies. Importantly, they also investigated the assembly level of F_1F_0-ATP synthase in *parkin* mutants. It was found that the level of correctly assembled F_1F_0-ATP synthase was markedly decreased in parkin mutants, and that this could be restored by upregulation of GSTO1. It is currently unclear how glutathionylation of the β-subunit improves ATP synthase assembly efficiency. While the investigators could not suggest why *parkin* mutants had defects in ATP synthase assembly in the first place, it could be hypothesized that the newly-discovered interaction of parkin with ATPAF1 contributes to this. In the absence of parkin, the dysregulation of ATPAF1 may lead to an impairment of the ATPAF1-driven β-subunit incorporation into the ATP synthase complex, which manifests as the altered ATP synthase assembly seen by Kim et al. To our knowledge, no other study specifically looked at impairment of ATP synthase assembly in parkin-deficient models, but it can be gathered from the above-described results that such impairment would contribute to altered cellular energetics and neurodegeneration.

Another insightful study investigated OGFOD1 (2-oxoglutarate and Fe^{2+}-dependent oxygenase domain containing protein 1), and implicated this protein as a pro-apoptotic factor (Saito et al. 2010). OGFOD1 knockout HeLa cells, i.e. cells deficient in OGFOD1, demonstrated a survival advantage upon exposure to ischemic stress. Further investigation of the pro-apoptotic mechanism of OGFOD1 revealed that OGFOD positively regulates *ATPAF1* mRNA expression: silencing of *OGFOD1* downregulated *ATPAF1* expression, whereas *ATPAF1* expression was enhanced by re-introduction of OGFOD1. Saito et al. speculated that this transcriptional activation of *ATPAF1* by OGFOD1 was

required for the promotion of cell death under ischemic conditions. In support of this, the overexpression of *ATPAF1* in *OGFOD1* knockout cells significantly increased ischemia-induced cell death compared to OGFOD1 knockout cells with endogenous expression of ATPAF1. This suggests that ATPAF1, acting downstream from OGFOD1, may participate in the ischemia-induced cell death pathway via an unknown mechanism (Saito et al. 2010).

To our knowledge, the above-mentioned study represents the only investigation of the functional consequences of ATPAF1 overexpression performed to date. The strong suggestion that it is elevated ATPAF1 which mediated the pro-apoptotic effects of OGFOD1 during ischemic stress is of special relevance to the present study. Parkin, as part of its pro-survival function, may monitor the protein expression of ATPAF1 in order to counteract OGFOD1-ATPAF1 pro-apoptotic signaling. It is revealing that the study of Saito et al. used HeLa cells as an experimental model; HeLa cells do not express any parkin due to a chromosomal deletion (Denison et al. 2003). Hence, their choice of the widely-used HeLa cell line may have unwittingly provided an appropriately parkin-free model where the effects of ATPAF1 expression would be amplified.

It is interesting to note that a recent exome sequencing study of 100 PD patients highlighted *OGFOD1* as a novel candidate risk gene for PD (Quadri et al. 2014). It could be speculated that the regulation of ATPAF1 protein expression by parkin (as seen in the present study), and *ATPAF1* mRNA expression by OGFOD1 (as seen by Saito et al.), may represent two alternative routes to a common pathogenic pathway in PD.

To summarize, the present study demonstrated that the mitochondrial F_1F_0-ATP synthase assembly factor ATPAF1 interacts with parkin, and that ATPAF1 accumulates in the absence of parkin. While there are very few functional studies on ATPAF1 available, it has been shown that impairment of F_1F_0-ATP synthase assembly is a feature of *parkin*-mutant *Drosophila* (Kim et al. 2012). Other studies have found that increased ATPAF1 is detrimental to cellular health. For example, upregulation of *ATPAF1* expression is involved in OGFOD1-ischemic cell death signaling (Saito et al. 2010); increased *ATPAF1* expression is also associated with asthma (Schauberger et al. 2011) and prostate cancer (Schinke et al. 2014). In light of these interesting findings, the interaction of parkin with ATPAF1 and its relevance to neurodegeneration should be investigated further.

4.2.2.2 *SEPT9*

The septins, a family of thirteen protein paralogs, are GTP-binding proteins with diverse roles in health and disease (Dolat et al. 2014). Septins form hetero-oligomeric complexes capable of assembling into higher ordered structures, including filaments and rings. As part of such non-polar filamentous structures, septins interact with both actin filaments and microtubules, and septins are

increasingly being recognized as an important and dynamic component of the cytoskeleton (Mostowy and Cossart 2012). A major function of septins is the control of cellular protein localization and trafficking, which contributes to the roles of septins in cytokinesis, cytoskeletal reorganization, cell motility, signaling cascades, vesicle trafficking and exocytosis (Peterson and Petty 2010).

Septins are of particular interest to neurodegeneration, as the accumulation of two septins, SEPT4 and SEPT5, has been implicated in the cytotoxic process underlying parkin-linked PD. SEPT5 was the first parkin substrate to be identified (Zhang et al. 2000), and was found to accumulate in the midbrain of PD patients with parkin mutations (Choi 2003). Overexpression of SEPT5 in both *Drosophila* and rats induced dopamine-dependent neurodegeneration (Dong et al. 2003; Muñoz-Soriano et al. 2012), suggesting that the accumulation of SEPT5 in the absence of functional parkin contributes to PD. SEPT5 interacts with both the exocyst complex and the SNARE protein syntaxin, implicating SEPT5 in the regulation of vesicle trafficking and exocytosis (Hsu et al. 1998; Beites et al. 1999). Hence, accumulation of SEPT5 may contribute to neurodegeneration by dysregulation of synaptic exocytosis.

SEPT4 is also a substrate of parkin (Choi 2003). Interestingly, the two distinct splice isoforms of SEPT4 (SEPT4_v1 and SEPT4_v2, also known as ARTS) have divergent functions in neurons. SEPT4_v1 has a neuroprotective role and directly interacts with α-synuclein to prevent its aggregation (Ihara et al. 2007). This isoform is abundantly found in LBs of PD patients (Ihara et al. 2003; Shehadeh et al. 2009). ARTS (Apoptosis-Related protein in the TGF-β Signaling pathway), on the other hand, is a mitochondrial pro-apoptotic protein (Larisch et al. 2000). While parkin interacts equally with both isoforms, only ARTS is ubiquitinated and targeted for degradation by parkin (Kemeny et al. 2012). Hence, only the ARTS isoform of SEPT4 accumulates in the absence of parkin, and promotes neurodegeneration by the activation of apoptotic signaling (Kemeny et al. 2012).

The present study demonstrated a novel interaction between parkin and SEPT9; furthermore, SEPT9 accumulated in parkin-null fibroblasts. Of all the septins, dysfunction of SEPT9 is the most convincingly linked to disease. Heterozygous mutations in *SEPT9* cause hereditary neuralgic amyotrophy, a rare form of neuropathy (Kuhlenbäumer et al. 2005), whereas *SEPT9* overexpression is found in diverse cancers, including breast, kidney, liver, lung, ovary, pancreas, etc. (Scott et al. 2005). *SEPT9* DNA methylation changes have been used as a biomarker in colorectal cancer (Grützmann et al. 2008), and MLL-SEPT9 fusion transcripts frequently occur in acute myeloid leukemia (Cerveira et al. 2011).

SEPT9 is near ubiquitously expressed in tissues; however, it has complex transcriptional pattern resulting in seven different protein isoforms (Kalikin et al. 2000). These isoforms are differentially expressed in body tissues: isoform 1 (SEPT9_v1) is detected in all tissues except the brain and thymus, while the other isoforms are expressed to varying degrees in the brain, among other tissues

(McIlhatton et al. 2001; Hall et al. 2005). SEPT9 isoforms are structurally very similar, differing only at their far N-termini while retaining identical GTPase domains and C-termini. Despite their similarity, some of the isoforms have diverging functions, and the altered expression of particular isoforms is linked to disease (Connolly et al. 2014).

It is noteworthy that, in the present study, the Y2H prey clone that demonstrated an interaction with the parkin bait (Section 3.2.1.6) did not encode the full SEPT9 peptide, but rather only for the region containing the GTPase domain and C-terminus of SEPT9 (Appendix X). This is not unexpected, as N-terminal domains are poorly represented in oligo(dT)-primed cDNA libraries such as the cDNA library used in this Y2H screen (Van Criekinge and Beyaert 1999). As the parkin bait interacted with a protein domain common to all SEPT9 isoforms, it can be concluded that the interaction is not isoform-specific, and that parkin can be expected to interact with whichever isoform is expressed in a particular cell type.

While several SEPT9 isoforms are expressed in the CNS, very little is known about the function of SEPT9 in the brain. To date, only one study have looked at SEPT9 protein expression and distribution in various brain tissues, in the context of SEPT9's possible role in traumatic brain injury in rats (Mao et al. 2013). This study found that SEPT9 is expressed in neurons, but not astrocytes or oligodendrocytes. SEPT9 protein expression (but not mRNA expression) was marked increased in neurons following traumatic brain injury, and that this increased expression was closely correlated with induction of caspase-3-mediated apoptosis. While these observations need to be investigated further, it is suggestive of a pro-apoptotic role for SEPT9 in neurons.

As stated, all septins form hetero-oligomers which polymerize into filaments. Despite this important property, the native assembly states and hetero-oligomerization partners of septins have only recently been investigated (Sellin et al. 2011). Current knowledge suggests that septins exist predominantly in the context of hexamers and octamers (Sellin et al. 2011). Importantly, all septin octamers contain SEPT9 at each terminus, which mediates octamer polymerization in a microtubule-dependent manner (Kim et al. 2011). Overexpression of SEPT9 alters the ratio of hexamers to octamers, and modulates the higher-order arrangement of septin filaments (Sellin et al. 2012). Hence, SEPT9 expression levels alter cellular septin assemblies in a stoichiometric manner, suggesting that its overexpression may impact on the functioning of most other septins, including septins enriched at the synaptic terminals. Septin filaments are particularly important for proper synaptic function at the synaptic terminal (Tsang et al. 2011); the important role of SEPT9 in septin filament assembly could conceivably disrupt the regulated functioning of these septins.

The identified interaction between parkin and SEPT9 could also have implications for oncogenesis, as both proteins have been implicated in cancer. SEPT9 positively regulates the hypoxic response

pathway, by interacting with and stabilizing hypoxia-inducible factor 1α (HIF-1α) (Amir et al. 2006). This activation of HIF-1α induces a diverse range of target genes, and plays a key part in the promotion of cell proliferation, tumor growth and angiogenesis (Semenza 2010). Cells overexpressing SEPT9 had enhanced HIF-1α activity and higher proliferation rates both *in vitro* and *in vivo* (Amir et al. 2009). Conversely, targeted knockdown of SEPT9 reduced HIF-1α expression, cell proliferation and tumorigenesis (Amir et al. 2010). Increased expression of SEPT9, possibly as a result of parkin dysfunction, therefore impairs cell cycle regulation and promotes oncogenesis via activation of the HIF-1α pathway. This interesting observation is in accordance with the established connection between parkin dysfunction and cancer (Section 1.16.5)

One is then faced with a conundrum: is increased SEPT9-HIF-1α signaling in the absence of parkin also relevant in neurodegeneration? After all, increased HIF-1α in the brain has a neuroprotective effect: HIF-1α promotes dopamine release (Witten et al. 2009) and protects against MPTP-induced neurotoxicity (Lee et al. 2009). Hence, parkin dysfunction in neurons could, paradoxically, have a pro-survival effect via the positive effect of SEPT9 accumulation on HIF-1α induction. This puzzle is solved by numerous studies showing that the interaction of SEPT9 with HIF-1α is restricted to the SEPT9_v1 isoform. In fact, the first 25 amino acids of SEPT9_v1, which are uniquely different from the other septin isoforms, were found to be critical for HIF-1α activation (Amir et al. 2009; Golan and Mabjeesh 2013). As this isoform is not expressed in the brain (McIlhatton et al. 2001; Hall et al. 2005), the SEPT9-HIF-1α effect is restricted to non-neuronal, mitotic tissues (Amir et al. 2006).

In summary, the identified functional interaction of parkin with SEPT9 may be of relevance to PD, given that two other members of the septin protein family have been implicated in parkin-associated neurodegeneration. Moreover, previous studies have established that dysregulated SEPT9 expression can have numerous pathological, tissue- and isoform-specific effects. While the cellular consequences of SEPT9 accumulation have not been specifically examined in neurons, previous reports suggest that it may have a pro-apoptotic effect. The accumulation of SEPT9 in the absence of parkin could conceivably impair neuronal function in several ways, as SEPT9 plays a pivotal role in regulating the assembly dynamics of many other septins. Finally, the interaction of parkin with SEPT9 may be of particular relevance to cancer research, and provide novel answers as to how parkin mutations increase susceptibility to various cancers.

4.2.2.3 *14-3-3η*

14-3-3 proteins are a family of highly conserved regulatory proteins ubiquitously expressed in cells; they are particularly abundant in the brain (Berg et al. 2003). To date, seven isoforms (β, γ, ε, ζ, η, θ and σ) have been identified, where each isoform is different in its cellular distribution, function and pathological relevance (Mhawech 2005). 14-3-3 proteins act as chaperones by binding to

phosphorylated serine sites of interacting partners. This binding may have several effects, whether augmenting or inhibiting the activity of the interactor, acting as an adaptor/scaffold for multi-protein assemblies, protecting the interactor from dephosphorylation, or regulation the subcellular localization of the interactor. In this manner, 14-3-3 proteins play important roles in the regulation and coordination of numerous diverse pathways, including intracellular trafficking, signal transduction, cell cycle control, cell survival and apoptosis (Mackintosh 2004).

14-3-3η, in particular, has been implicated in neuronal function and health. Polymorphisms in the 14-3-3η gene (*YWHAH*) are genetic susceptibility factors for both schizophrenia and bipolar disorder (Toyooka et al. 1999; Wong et al. 2003; Grover et al. 2009). Furthermore, *YWHAH* was found to be downregulated in a dopaminergic neuronal cell line during oxidative stress, suggesting that the loss of the chaperone activity of 14-3-3η contributes to the oxidative signaling underlying oxidative damage in dopaminergic neurons (Anantharam et al. 2007). Conversely, *YWHAH* was shown to be upregulated in primary cortical neurons during *in vitro* development, indicating a role of 14-3-3η in neuronal growth and differentiation (Chen et al. 2005). Moreover, transient overexpression of 14-3-3η in AF5 neuronal cells protected the cells from N-methyl-D-aspartate (NMDA)-induced excitotoxic cell death (Chen et al. 2007).

Of relevance to this dissertation, 14-3-3η has also been implicated in neurodegeneration and PD. Most 14-3-3 proteins are abundantly found in LB's of PD brains (Kawamoto et al. 2002), while the 14-3-3γ, -ε and η isoforms in particular are enriched at the synaptic junction and the synaptic membrane, similarly to α-synuclein (Berg et al. 2003). Interestingly, 14-3-3 proteins share amino acid sequence homology with α-synuclein (Ostrerova et al. 1999). Soluble α-synuclein and 14-3-3 protein complexes were observed in neurons of *SNCA* transgenic mice (Shirakashi et al. 2006), and a direct interaction of 14-3-3η with α-synuclein was confirmed by immunoprecipitating this complex from the SNpc of PD patients (Sato et al 2006). A recent and insightful study examined the relationship between 14-3-3η and α-synuclein, which found that the fibrillization and aggregation process of α-synuclein is heavily influenced by the presence of 14-3-3η (Plotegher et al. 2014). Their study showed that, while 14-3-3η was unable to bind monomeric α-synuclein, it strongly interacted with oligomeric α-synuclein aggregation intermediates and diverted the aggregation process. However, when the level of α-synuclein was overwhelmingly higher than 14-3-3η, the fibrillization process in effect sequestered 14-3-3η. This sequestration of 14-3-3η by excessive α-synuclein may contribute to PD pathogenesis via the loss of appropriate 14-3-3η function. Indeed, 14-3-3η overexpression rescued the toxic effects of early-stage α-synuclein aggregation in cell models (Plotegher et al. 2014).

LRRK2 has been shown to bind several 14-3-3 isoforms, especially 14-3-3η, where PD-causing mutations in *LRRK2* abolished the interaction with 14-3-3η (Nichols et al. 2010; Li et al. 2011b). Moreover, disruption of the interaction between 14-3-3η and LRRK2 altered the cytoplasmic

localization of LRRK2, resulting in the accumulation of this normally diffusely-spread protein (Dzamko et al. 2010). Further evidence suggests that 14-3-3η mediates the extracellular release of LRRK2 in exosomes (Fraser et al. 2013). Hence, 14-3-3η regulates LRRK2 localization and sorting, while PD-linked mutations impair this regulatory action. This may be of considerable relevance as aberrant LRRK2 sorting has been implicated in PD pathogenesis (MacLeod et al. 2013).

Of note, 14-3-3η has been previously shown to interact with parkin (Sato et al 2006). Sato et al. co-immunoprecipitated parkin and 14-3-3η from mouse brain homogenates, and found that the association with parkin was specific to this isoform. Furthermore, they used parkin deletion constructs to demonstrate that the region containing parkin's RING0 domain was critical for 14-3-3η binding. Upon investigation of the effect of 14-3-3η binding on parkin's activity, it was discovered that 14-3-3η suppressed parkin's intrinsic auto-ubiquitination ability; 14-3-3η furthermore inhibited the interaction of parkin with its substrate synphilin-1. Surprisingly, Sato et al. found that wild-type α-synuclein relieved this negative regulation of parkin activity via its interaction with 14-3-3η, while PD-causing A30P and A53T SNCA mutants could not rescue parkin activity.

These insightful findings suggest that 14-3-3η-bound parkin is present in a latent state in the cells, where 14-3-3η functionally links parkin and α-synuclein. It could be that an imbalance of the three-way interactions between parkin, 14-3-3η and α-synuclein may contribute to the neurodegenerative process. While this has not been properly explored, the interaction of 14-3-3η with parkin might protect parkin from cellular stresses, such as its previously-reported sensitivity to nitrosative stress (Yao et al. 2004). Furthermore, while 14-3-3η may negatively regulate parkin activity, it may paradoxically play a positive role in maintaining a large pool of parkin in the cell by inhibiting its auto-ubiquitination and subsequent degradation. Physiological α-synuclein might fine-tune this regulation by binding to 14-3-3η and activating the latent parkin-14-3-3η complex in an appropriate manner. In fact, immunoprecipitation of 14-3-3η from midbrain lysates showed that 14-3-3η-bound parkin is significantly decreased in PD patients compared to controls, whereas levels of 14-3-3η-bound α-synuclein is clearly elevated in PD patients (Sato et al 2006). This supports the hypothesis that a disruption of the careful balance between the positive and negative regulation of parkin contributes to PD. Moreover, the demonstration that 14-3-3η interacts with numerous PD-associated proteins, including α-synuclein, LRRK2 and parkin, might suggest that 14-3-3η is involved in the regulation of multiple pathogenic processes in PD.

The present study independently verified the previously-described interaction of parkin with 14-3-3η (Sato et al 2006). Furthermore, the protein expression levels of 14-3-3η was found to not differ significantly between parkin-null and wild-type parkin fibroblasts, which is consistent with the regulation of parkin by 14-3-3η, instead of *vice versa*. While the curious negative regulation of parkin by 14-3-3η was not investigated further, as this was beyond the scope of this study, future

investigation of the precise molecular mechanisms and consequences of this regulatory effect may be of interest to PD research. Also, modulating the regulation of parkin by 14-3-3η may be a novel target for the prevention and therapy of PD, as may be the interactions by 14-3-3η with α-synuclein or LRRK2. Recent efforts have discovered many natural and synthetic compounds that modulate the binding of 14-3-3 proteins with their targets (Zhao et al. 2011a; Milroy et al. 2013; Ottmann 2013); however, such compounds would need to selectively target specific 14-3-3 isoforms and isoform interactions before they can be used *in vivo*.

4.2.2.4 *Cytoskeletal actin*

β-Actin and γ-actin are two ubiquitously-expressed cytoplasmic members of the actin protein family; this family includes four other actin paralogs that are predominantly expressed in muscle (Rubenstein 1990). These two non-muscle cytoskeletal actins share an exceptionally high amino acid sequence similarity, differing by only four amino acids clustered at their respective N-terminals (Vandekerckhove and Weber 1978). In the present study, a Y2H screen identified an interaction between parkin and a cDNA clone encoding a large fragment of γ-actin. However, as the peptide sequence encoded by this clone is also found in β-actin, it can be assumed that parkin interacts with both actin paralogs. Hence, the relevance of the interaction between parkin and cytoskeletal actin will be discussed here.

The cytoskeleton consists of the three essential components: actin filaments, tubulin-containing microtubules and intermediate filaments. Actin participates in many important cellular functions as part of the cytoskeleton, including cell signaling, vesicle trafficking, organelle movement, and structural organization (Pollard and Cooper 2009). Crucial to these roles is the ability of actins to self-assemble into filaments (F-actin). The assembly of F-actin is a highly dynamic process which can be modulated by numerous actin-associated proteins in the cell, and perturbation of F-actin dynamics can impair proper cellular functioning.

Numerous studies have highlighted a link between actin, vesicle trafficking and PD. For example, α-synuclein is known to alter actin cytoskeletal structure and dynamics. Wild-type α-synuclein was found to interact with actin, slowing its polymerization and promoting its depolymeration (Sousa et al. 2009). A30P mutant α-synuclein, on the other hand accelerated polymerization (Sousa et al. 2009). This interaction of α-synuclein and F-actin is thought to underlie α-synuclein's role in synaptic vesicle trafficking and synaptic function (Bellani et al. 2010). Similarly, accumulating evidence also implicate LRRK2 in actin dynamics. It was shown that LRRK2 depolymerized F-actin *in vitro*, and that PD-causing *LRRK2* mutations accelerated actin disassembly in SH-SY5Y cells (Chan et al. 2011a; Meixner et al. 2011) Fibroblasts from PD patients with *LRRK2* mutations had decreased F-

actin stability which were more susceptible to the F-actin depolymerizing agent Latrunculin A (Caesar et al. 2014). Moreover, such fibroblasts had a significant increase in F-actin bundles, possibly a compensatory mechanism to protect F-actin from the depolymerizing effect of mutant LRRK2 (Caesar 2014.) LRRK2 also phosphorylates moesin, a protein that anchors F-actin to the plasma membrane (Jaleel et al. 2007); phosphorylation of moesin alters the arrangement of the actin cytoskeleton and modifies synaptic vesicular function (Parisiadou et al. 2009). This important role of LRRK2 in modulating synaptic transmission is increasingly being recognized as a key feature of PD (Belluzzi et al. 2012; Lee et al. 2012a).

Parkin has been previously associated with the cytoskeleton in the literature. Huynh et al. (2000) used confocal microscopy to demonstrate that parkin co-localized with actin fibers in COS1 cells. To further differentiate whether parkin associated with actin filaments or microtubules, cells were treated with cytochalastin D, an actin depolymerizing agent, or nocodazole, which selectively destabilizes microtubules. Cytochalastin D treatment disrupted both actin and parkin staining behavior, further supporting parkin-actin co-localization. Nocodazole, however, had no effect on parkin staining, suggesting that parkin did not co-localize with microtubules. In contrast to this, Ren et al. (2003) found that parkin is a microtubule-binding protein. This study demonstrated that parkin co-immunoprecipitated with both α- and β-tubulin and co-localized to α/β tubulin heterodimers in SH-SY5Y cells. These contradictory findings by Huynh at al. and Ren et al. may be explained by differences in experimental conditions. Ubiquitination assays demonstrated that wild-type parkin ubiquitinated both monomeric α- and β-tubulin, and targeted these proteins for proteasomal degradation (Ren et al. 2003). The authors speculated that parkin may selectively ubiquitinate misfolded monomeric tubulins, which are cytotoxic upon accumulation in the cell. However, parkin also interacts with assembled tubulins, albeit in a non-enzymatic manner. It was demonstrated that parkin interacted with and stabilized microtubules independently of its E3 ligase activity, supporting the association of parkin and the microtubule cytoskeleton (Yang et al. 2005).

There are other studies which support the functional association of parkin and actin. Parkin interacts with and ubiquitinates LIM kinase 1 (LIMK1), which then attenuates LIMK1-dependendent phosphorylation and inactivation of cofilin (Lim et al. 2007). Cofilin is known to bind to F-actin and promotes actin turnover (Lappalainen and Drubin 1997). Hence, parkin modulates the actin cytoskeleton indirectly via its interaction with LIMK1. A further study investigated the functional link between PINK1 and parkin, and found that RNAi-mediated *PINK1* knockdown dramatically increased parkin's interaction with F-actin (Kim and Son 2010). Further investigation demonstrated that loss of PINK1 induced F-actin bundling in neuronal cells via the increased inactivation of cofilin, which then promoted the recruitment of parkin to F-actin. Interestingly, induction of oxidative stress and treatment with rotenone similarly increased the association of parkin with F-actin (Kim and Son

2010). Collectively, these results support a model whereby parkin binds and stabilizes F-actin, and this stabilization is increased as a neuroprotective response to cellular stress. This is similar to the stabilizing binding of parkin to microtubules (Yang et al. 2005).

Of note, this study by Kim and Son is the only report of the successful co-IP of parkin and actin prior to the present study. However, Kim and Son used overexpressed and FLAG-tagged parkin to perform the co-IP assay, whereas the present study demonstrates this interaction with endogenous parkin. Hence, the present study confirmed the interaction between parkin and actin in a more biologically relevant experimental setting. This is of importance as the presence of N-terminal epitope tags are known to alter the biochemical function of parkin by artificially inducing an auto-activated state (Burchell et al. 2012). It is strongly suggested that any results obtained using tagged parkin should be confirmed with endogenously-expressed parkin, as has been done for the parkin-actin interaction in the present study.

The absence of parkin was found to have no effect on the steady-state level of total γ-actin (and β-actin) protein. This suggests that the interaction of parkin with actin does not promote the turnover of actin, which is consistent with reports that the degradation of actin is instead mediated by the E3 ligase TRIM23 (Kudryashova et al. 2005). However, it is conceivable that the absence of parkin may have an effect on the assembly state of F-actin, which would not have been reflected in denaturing western blot analyses as performed in the present study. While the functional relevance of this interaction is currently unclear, parkin's association with actin may promote proper actin dynamics, which is supported by studies that suggest a stabilizing role of parkin at F-actin, similar to parkin's role at microtubules. Alternatively, parkin may associate with actin as a general means of "anchoring" itself in various subcellular localizations. This would allow for the efficient ubiquitination of parkin substrates that are being transported along actin filaments. Further investigation of the interaction of parkin with actin may be fruitful, as the relevance of actin dynamics to PD has been highlighted by the numerous studies showing that α-synuclein and LRRK2 also interact with actin. The actin cytoskeleton may therefore represent a functional link between several PD-causing genes.

4.3 FUNCTIONAL STUDIES IN A PARKIN-DEFICIENT CELLULAR MODEL

Patient-derived fibroblasts with *parkin* mutations are valuable models for investigating the functions of parkin in an *in vivo* setting. However, published results of such investigations of parkin-mutant fibroblasts have not been wholly consistent (Mortiboys et al. 2008; Grunewald et al. 2010; Pacelli et al. 2011). Therefore, the present study aimed to functionally compare *parkin*-mutant fibroblasts from South African PD patients with wild-type control fibroblasts using a variety of assays of cellular health and function (Section 3.3).

It was shown that patient-derived fibroblasts have comparable cell viabilities (as detected by a MTT assay) to wild-type control fibroblasts under basal conditions. Surprisingly, it was also found that the cell growth (as measured by a CyQUANT® assay) is significantly higher in the *parkin*-mutant fibroblasts under basal conditions (p=0.0001). This is in contrast to the established literature. For example, Mortiboys et al. (2008) reported that both cell viability and growth rates were similar in fibroblasts from controls and patients with *parkin* mutations, whereas Pacelli et al. (2011) reported that *parkin* mutant fibroblasts displayed a significantly lower growth rate than control fibroblasts. Both of these studies reported cell viability and growth under basal, unstressed conditions. The increased cell growth detected in the present study may reflect methodological differences, as neither the study by Mortiboys et al. or Pacelli et al. used a CyQUANT® assay to determine cell growth. It is also conceivable that the increased cell proliferation in the absence of parkin is a result of a metabolic shift in response to parkin deficiency, which is known to promote cell proliferation in various cancers (Xu et al. 2014).

In contrast to these observations, the cell growth of *parkin*-mutant fibroblasts is significantly inhibited after treatment with CCCP (p=0.0013), while wild-type fibroblasts demonstrate a much smaller response. This is indicative of an increased susceptibility to CCCP in the absence of parkin. Treatment with CCCP reduces the $\Delta\psi_m$ and promotes the recruitment of parkin from the cytoplasm to depolarized mitochondria (Narendra et al. 2008). Parkin is subsequently involved in the isolation and mitophagic clearance of CCCP-damaged mitochondria (Narendra et al. 2008). Hence, parkin deficiency in patient-derived fibroblasts may reduce cell growth after CCCP treatment via the failure to properly clear damaged mitochondria. The resulting accumulation of depolarized mitochondria in the absence of parkin may impair cell growth by being a significant source of oxidative stress (Henchcliffe and Beal 2008).

The present study found interesting differences in the mitochondrial network morphologies of patient and wild-type fibroblasts (Section 3.3.4). Whereas the degree of mitochondrial elongation (aspect ratio) was comparable between patient-derived and wild-type fibroblasts, the amount of mitochondrial branching (form factor) was significantly decreased in patients (p=0.0306). This decrease in form factor is consistent with increased fragmentation of the mitochondrial network (Burbulla et al. 2010).

Other studies which investigated mitochondrial network morphology in fibroblasts from patients with *parkin* mutations found conflicting results. In contrast to the results obtained here, Mortiboys et al. (2008) found that fibroblasts with *parkin* mutations had a marked increase in mitochondrial branching, as quantified by the form factor. This was suggestive of an increased mitochondrial fusion in the absence of parkin. Two other studies found that *parkin* mutant and wild-type fibroblasts demonstrated comparable form factors under basal conditions (Grunewald et al. 2010; Rakovic et al. 2011). However, both studies found that treatment with mitochondrial stressors (paraquat and

valinomycin, respectively) decreased the form factor and induced mitochondrial network fragmentation in *parkin* mutant and wild-type fibroblasts; these decreases was only statistically significant in the fibroblasts with *parkin* mutations. These findings are supported by the results of Pacelli et al. (2011), who observed a noticeably more fragmented mitochondrial network in *parkin*-mutant fibroblasts even under basal conditions; however, this difference was not quantified in terms of form factor. Hence, the majority of studies reported a decreased mitochondrial form factor, indicating increased fragmentation, in the absence of parkin. The results obtained here support these established findings, but not the contrasting findings of Mortiboys et al. (2008).

Of note, all of the above-mentioned studies which quantified the mitochondrial network morphology reported that the degree of mitochondrial elongation (as expressed by the aspect ratio) was comparable in *parkin*-mutant and wild-type fibroblasts (Mortiboys et al. 2008; Grunewald et al. 2010; Rakovic et al. 2011). Hence, the similar mitochondrial aspect ratios observed in the present study is in concordance with the established literature.

Several other studies have implicated increased mitochondrial fission in the pathogenesis of PD. For example, mutations in *PINK1* and *DJ-1* induce mitochondrial fragmentation in cultured neurons (Exner et al. 2007; Krebiehl et al. 2010). Similarly, overexpression of α-synuclein and LRRK2 were found to promote mitochondrial fragmentation (Wang et al. 2012b; Xie and Chung 2012). In addition to the above-described reports of fragmented mitochondrial networks in *parkin* mutant fibroblasts, RNAi-mediated knockdown of parkin in neuronal cells had a similar pro-fragmentation effect (Lutz et al. 2009). This enhanced mitochondrial fragmentation in the absence of parkin can be explained by an abrogation of parkin's interaction with the mitochondrial fission factor Drp1. Parkin ubiquitinates and promotes the proteasomal degradation of Drp1 (Wang et al. 2011a); therefore, loss of parkin would reduce the level of Drp1 ubiquitination, resulting excessive mitochondrial fission and fragmentation of the mitochondrial network. In fact, the fragmented phenotype of parkin mutant cells was found to be dependent of Drp1, and Drp1 knockdown could rescue these morphological abnormalities (Lutz et al. 2009).

However, this is contradicted by other studies demonstrating that, in *Drosophila*, wild-type parkin promotes fission, and loss of parkin resulted in increased mitochondrial fusion and branching, which can be rescued by Drp1 overexpression (Poole et al. 2008; Ziviani et al. 2010). In support of the relevance of these observations is the finding that parkin ubiquitinates Mfn1 and Mfn2 even in mammalian cells, promoting the degradation of these pro-fusion factors (Glauser et al. 2011; Sun et al. 2012). According to this model, wild-type parkin ubiquitinates Mfn1/2 in response to mitochondrial damage in order to inhibit fusion of damaged mitochondria with healthy mitochondria. This fission promotes the selective isolation and mitophagy of dysfunctional mitochondria (Rakovic

et al. 2011). In the absence of parkin, dysregulation of Mfn1/2 may contribute to increased mitochondrial fusion, as seen in some *parkin*-mutant fibroblasts (Mortiboys et al. 2008).

It is difficult to reconcile the described pro-fusion (via Drp1 ubiquitination) and pro-fission (via Mfn1/2 ubiquitination) functions of parkin. It is likely that these contradictory roles of parkin reflect the complex nature of the regulation of mitochondrial dynamics, where a delicate balance between fusion and fission promotes optimal mitochondrial functioning. Hence, the enhanced fission and fragmentation in the absence of parkin, as seen in the present study, may indicate a disruption of mitochondrial dynamics that cannot be easily reduced to one-way interactions between parkin and fission/fusion proteins.

Mitochondrial morphology is thought to be intimately connected to various parameters of mitochondrial health, including $\Delta\psi_m$. However, the current study found that $\Delta\psi_m$ is similar in *parkin*-mutant and wild-type fibroblasts, irrespective of the degree of mitochondrial branching (Section 3.3.3). This lack of $\Delta\psi_m$ impairment is in contrast to the findings by Mortiboys et al. (2008), who reported a 30% decrease in $\Delta\psi_m$ in *parkin*-mutant fibroblasts relative to wild-type controls. The reported decrease in $\Delta\psi_m$ was even more pronounced when the fibroblast culture media was switched to include galactose as an energy source rather than glucose, which saw a 70% decrease in $\Delta\psi_m$ in fibroblasts with *parkin* mutations under these oxidative conditions (Mortiboys et al. 2008). Cultured fibroblasts predominantly use glycolysis to generate ATP, rather than oxidative phosphorylation (Benard et al. 2007). Culturing fibroblasts in glucose-deficient media obligates their use of oxidative phosphorylation for ATP production, which explains why possible mitochondrial impairments are enhanced under these conditions (Rossignol et al. 2004).

Grunewald et al. (2010) found that $\Delta\psi_m$ was similar in *parkin*-mutant and wild-type fibroblasts under basal conditions, in concordance to the results of the present study. However, a decrease in $\Delta\psi_m$ was observed in the patient fibroblasts after the induction of oxidative stress by treatment with paraquat. While the present study only investigated $\Delta\psi_m$ under basal conditions, it is conceivable that possible impairments in $\Delta\psi_m$ in *parkin*-mutant fibroblasts may only be readily observable under highly oxidative conditions, where the cells are more reliant on mitochondria for ATP production. Hence, culturing the fibroblasts in glucose-free media may have unmasked impairments in $\Delta\psi_m$ which are not apparent under the experimental conditions used in the present study.

Surprisingly, the present study found that the rate of mitochondrial respiration is increased in *parkin*-mutant fibroblasts in comparison to wild-type fibroblasts (Section 3.3.2). Further investigation of respiratory activity after the addition of various inhibitory compounds demonstrated that, in addition to an increased mitochondrial respiratory rate under basal conditions (p=0.0355), patient fibroblasts have an elevated ATP-coupled respiration (p=0.0481), increased respiration due to passive proton

leak across the inner mitochondrial membrane (p=0.0273) and an increased maximal respiratory rate (p=0.0081).

The unanticipated overall increase in mitochondrial respiration is in contrast to numerous studies which have reported decreased respiratory activity in fibroblasts from PD patients with *parkin* mutations. For example, Mortiboys et al. (2008) described significant impairment of mitochondrial complex I activity in *parkin*-mutant fibroblasts, which was linked to a loss of $\Delta\psi_m$ and decreased cellular ATP content. Similarly, Pacelli et al. (2011) reported that both the basal and maximal respiratory rate was significantly decreased in patient fibroblasts with *parkin* mutations. Further investigation of the specific respiratory complexes contributing to the decline in respiratory flux demonstrated that complex I, III and IV (but not complex II) activity was significantly reduced in patient fibroblasts (Pacelli et al. 2011).

The paradoxically improved mitochondrial respiration in the absence of parkin seen in the present study is difficult to explain, but it likely reflects a compensatory response in these *parkin*-mutant fibroblasts. Indeed, the increase in respiration that is coupled to ATP strongly suggests an upregulation of mitochondrial function, which will be discussed in more detail below. However, it is telling that the patient fibroblasts also had an increased passive proton leakage, and the resulting oxygen consumption from this leakage (which does not contribute to ATP production) is elevated to a higher extent than the ATP-linked oxygen consumption. This is reflected by the trend towards lower ATP coupling efficiency of the *parkin*-mutant fibroblasts, although this difference did not reach statistical significance (p=0.0983). It is possible that the increased proton leakage and lower ATP coupling efficiency points towards an underlying mitochondrial defect caused by parkin deficiency, which is then overcome and masked by a compensatory response.

Conversely, it is also possible that the higher proton leakage is in itself a compensatory response aimed at lowering ETC-linked ROS production. Studies have demonstrated that the elevation of proton leakage can be induced by uncoupling proteins (UCPs) in response to oxidative stress (Brand 2000; Porter 2001). Here, UCPs promote the passive movement of protons across the inner mitochondrial membrane which lowers $\Delta\psi_m$ in a controlled fashion; UCPs therefore decrease further ROS production at the expense of decreased ATP production (Toime and Brand 2010).

As stated, it is speculated that the significant increase in basal and ATP-linked respiration in *parkin*-mutant fibroblasts is due to a compensatory effect. In fact, several compensatory responses to parkin deficiency have been described in the literature. Pacelli et al. (2011) found that the defective ATP production by oxidative phosphorylation in *parkin*-mutant fibroblasts was compensated by an upregulation of the glycolytic pathway. They furthermore reported that the protein expression of PGC1-α was significantly higher in *parkin*-mutant fibroblasts; PGC1-α is a key promoter of the

compensatory increase in mitochondrial biogenesis (Kelly and Scarpulla 2004). However, the expression of several PGC1-α target genes directly involved in mitochondrial biogenesis (including *NRF1*, *TFAM* and *COX II*) were unchanged or even decreased in patient-derived fibroblasts. Pacelli et al. postulated that an unknown post-translational modification of PGC1-α modulated its function in *parkin*-mutant fibroblasts, preventing a compensatory increase in mitochondrial biogenesis. It is interesting to speculate that the genetic backgrounds of the patient-derived fibroblasts in the current study may allow for the PGC1-α-mediated increase in mitochondrial biogenesis, in contrast to fibroblasts used by Pacelli et al. This may, in part, explain the conflicting results obtained here and by Pacelli et al. Clearly, additional studies will be necessary to support such a mechanism.

Other studies have also hinted at a compensatory increase in mitochondrial biogenesis in parkin deficient fibroblasts. Grunewald et al. (2010) investigated the citrate synthase activity of *parkin*-mutant fibroblasts as an index of total mitochondrial mass, and found that such activity was significantly higher in *parkin*-mutant fibroblasts than wild-type controls. Indeed, Grunewald et al. did not observe any impairments of mitochondrial complexes I-IV under basal conditions. This in in contrast to Pacelli et al. (2011) who reported that citrate synthase activity was significantly decreased in *parkin*-mutant fibroblasts, suggesting a decrease in total mitochondrial content, which was associated with marked defects in complexes I, III and IV. Hence, increased citrate synthase activity, and elevated mitochondrial biogenesis in general, may explain the milder phenotype of parkin mutant fibroblasts observed by Grunewald et al. While markers of mitochondrial biogenesis were not specifically assayed in the present study, increased biogenesis may underlie the compensatory increase in mitochondrial respiration seen here.

It is noted that a possible compensatory elevation of mitochondrial biogenesis in the parkin-deficient fibroblasts would be paradoxical: parkin is involved in the promotion of mitochondrial biogenesis; hence, these processes are expected to be decreased in the absence of parkin (Kuroda et al. 2006a). However, future investigation of the exact nature and mechanism of the respiratory compensation seen here in parkin-mutant fibroblasts may reveal a more complex and nuanced view of parkin and its interaction with mitochondria.

It is furthermore found that patient fibroblasts have a higher maximal respiration, with this effect being particularly pronounced in the fibroblasts of patient P2 (Section 3.3.2). This is reflected in the significantly higher spare respiratory capacity of the P2 fibroblasts over the wild-type control fibroblasts, whereas the fibroblasts of patient P3 have a spare capacity comparable to the controls. These differences between the two patients' fibroblasts may be explained by genetic differences, which results in additional compensatory mechanisms specific to the P2 fibroblasts. It is interesting to compare this to the results of the parkin interactor accumulation experiments (Section 3.2.4.2), which also suggested a compensatory response in the P2 fibroblasts. While the nature of this patient-specific

compensation is unclear, previous studies have found compensatory mitochondrial biogenesis and upregulation of lysosomal degradation pathways *PINK1* knockout mice (Wood-Kaczmar et al. 2008), as well as upregulation of various RING and RBR E3 ubiquitin ligases in *parkin* knockout mice (Bhandari et al. 2014). It is interesting to speculate that P2 fibroblasts may be compensating for the loss of parkin by upregulating alternative mitochondrial and/or protein degradation pathways, which is not occurring in P3 cells to the same extent. Indeed, a clinical comparison of the PD phenotypes of patients P2 and P3 is suggestive of such a possible compensatory effect. P2 and P3 harbor identical *parkin* mutations and, as siblings, share approximately 50% of their genetic makeup; however, P2 has a markedly less severe PD phenotype and slower disease progression than her sibling (personal communication with research nurse, Sr. Debbie Joubert). The possible compensatory mechanism which attenuates PD severity and cellular impairments in P2 should be investigated in future studies.

Spare respiratory capacity is the extent to which cells can increase oxidative phosphorylation in the case of a sudden increase in energy demand, and reflects the cells' abilities to respond to stressful conditions (Nicholls 2009). The marked increase in maximal respiration and spare respiratory capacity of the P2 fibroblasts specifically is therefore unexpected, and may represent an "overshoot" of the compensatory response to the absence of parkin. However, is should be noted that compensatory adaptions due to the upregulation of parallel or alternative pathways are almost certainly less efficient, and may only result in a seemingly "improved" phenotype when the cells are not exposed to any additional sources of stress. Indeed, the fibroblasts in the present study were cultured under optimal growth conditions prior to respiratory rate analysis, and the perturbations with pharmacological stressors during analysis were performed in short time spans of minutes – hardly enough time for the ablation of compensatory responses under prolonged stress. It would be interesting to investigate whether similar respiratory compensation is in effect for cells cultured in glucose-free galactose media.

These compensatory responses are likely dependent on cell- and tissue-specific metabolic capacity and adaptations (Akundi et al. 2013). Hence, the observations made here on patient-derived fibroblasts should not be extrapolated to possible effects in a neuronal environment, as neurons may be more restricted in their compensatory repertoire than dermal fibroblasts. In particular, the inability of neurons to upregulate glycolysis may increase their vulnerability to mitochondrial dysfunction (Bolaños et al. 2010). Furthermore, many of the described functional roles of parkin are cell-type specific which will result in different functional effects of parkin deficiency in fibroblasts and neurons. For example, it was found that parkin has anti-apoptotic and anti-oxidative properties in neuronal and myogenic cells, but not in COS-1 kidney cells (Kuroda et al. 2006b). Ideally, the observations made in this study should be verified in a neuronal model, such as iPSC-derived neurons with *parkin* mutations.

4.4 VITAMIN K_2 AS A POTENTIAL THERAPEUTIC MODALITY

Patient-derived fibroblasts, with pre-defined genotypes, are particularly useful in the evaluation of the effects of various compounds on underlying disease mechanisms in human cells (Auburger et al. 2012). In fact, fibroblasts from PD patients with *parkin* mutations have been successfully used to investigate the rescue effect of glutathione precursor compounds on mitochondrial impairment (Mortiboys et al. 2008). Similarly, it has been demonstrated that rapamycin partially rescued mitochondrial defects in parkin-mutant fibroblasts (Tain et al. 2009). Here, the effects of treatment with the potential therapeutic agent vitamin K_2 on mitochondrial function were assessed in a cellular model of parkin deficiency.

It was shown that vitamin K_2 (in the form of MK-4) had no overall effect on cell growth when comparing vitamin K_2-treated fibroblasts with untreated cells, either for patient-derived or wild-type control fibroblasts. Similarly, vitamin K_2 co-treatment did not significantly alter overall cell growth of CCCP-stressed fibroblasts. Furthermore, vitamin K_2 did not rescue the increased susceptibility to CCCP in *parkin*-mutant fibroblast discussed in Section 4.3. When considering assays of cell viability, it was found that vitamin K_2 slightly decreased cell viability in comparison to untreated cells, but this effect was not significantly different between patient-derived and wild-type fibroblasts. In other words, the observed decrease in cell viability is a global effect not related to *parkin* mutation status. This decline in cell viability after vitamin K_2 treatment may be explained by the previously-described pro-apoptotic effect of vitamin K_2 (Yokoyama et al. 2008). It is unclear why similar effects on cell viability were not seen during the initial optimization of vitamin K_2 treatment conditions (Section 3.4.1).

The effect of vitamin K_2 on the morphology of the mitochondrial network had a similarly global, parkin-independent effect. Vitamin K_2 increased both the mitochondrial length (aspect ratio; $p<0.0001$) and degree of branching (form factor; $p<0.0001$) of all investigated fibroblast cell lines. The observed increases in aspect ratio and form factor following vitamin K_2 treatment are indicative of an increase in mitochondrial fusion and decrease in fission, respectively; hence, vitamin K_2 is thought to promote a more interconnected mitochondrial network. Previous studies have shown that increased mitochondrial fusion has protective effects. It was reported that enhanced fusion enabled equal distribution of mitochondrial proteins and metabolites, and reduced the accumulation of mtDNA mutations, thereby protecting against mitochondrial damage (Nakada et al. 2001; Ono et al. 2001). Thus, the elevation of mitochondrial fusion may serve to maintain bioenergetic function by acting as a "rescue" pathway (Twig and Shirihai 2011). Increased mitochondrial fusion was also found to be protective against ischemia in heart tissue (Ong et al. 2010). Interestingly, Rambold et al (2011) found that the fusion-driven elongation of mitochondria increased ATP production; this was ascribed to the enhanced cristae density and ATP synthase dimerization of elongated mitochondria.

Given these functional links between mitochondrial dynamics and bioenergetics, it can be speculated that the higher interconnectedness of mitochondria of vitamin K_2-treated fibroblasts seen in the present study is associated with altered mitochondrial respiration. In fact, mitochondrial respiration analysis revealed that vitamin K_2 increased the rates of basal respiration (p=0.0459), ATP-linked respiration (p=0.0465), the oxygen consumption due to proton leakage (p=0.025) and the maximum respiration (p=0.0331) of all fibroblasts cell lines. While treatment with vitamin K_2 increased these measures of absolute respiration, it did not significantly affect ATP coupling efficiency or spare respiratory capacity. Importantly, the observed increases in basal and ATP-linked respiration were global effects of vitamin K_2 treatment, irrespective of the *parkin* mutation status of the fibroblasts. It was speculated that the enhanced respiratory rates may be due to increased polarization of $\Delta\psi_m$ following treatment; however, further experiments found that vitamin K_2 had no observable effect on $\Delta\psi_m$ .This suggests that vitamin K_2 may act as a general promoter of mitochondrial respiration, which is in accordance to its previously-described role as a mitochondrial electron carrier in the ETC of *Drosophila* (Vos et al. 2012).

It is interesting to contrast the results obtained here to those reported by Vos et al: while they found that vitamin K_2 supplementation rescued mitochondrial dysfunction in *PINK1*-mutant flies, wild-type control flies did not experience any enhancement of mitochondrial function. For example, measurements of OCR and ATP synthesis were comparable between wild-type flies fed on vitamin K_2 and control media. Similarly, whereas vitamin K_2 rescued the swollen, clumped mitochondrial phenotype of *PINK1*- and *parkin*-mutant flies, treatment had no effect on the mitochondrial morphology of wild-type *Drosophila*. This is in contrast to the increased interconnectedness of mitochondrial networks and elevated respiratory rates seen in even wild-type fibroblasts following vitamin K_2 treatment. This discrepancy may point toward significant differences in the molecular action of vitamin K_2 in *Drosophila* and human cells, which should be followed up in future studies.

Some interesting disparities between patient and wild-type fibroblasts in their respective vitamin K_2 treatment responses were observed. For instance, the increase in proton leakage following treatment was significantly more pronounced in patients than the increase in wild-types (p=0.0082). Also, vitamin K_2 increased the maximum respiratory rates of *parkin*-mutant fibroblasts to a greater extent than control fibroblasts (p=0.0105). Whereas it was originally anticipated that vitamin K_2 may rescue defects in mitochondrial respiration in *parkin*-mutant fibroblasts, this study found a compensatory increase of respiratory rates in response to parkin deficiency (Section 4.3), which is enhanced by vitamin K_2 treatment. The enhancement of this compensatory effect in *parkin*-mutant fibroblasts by vitamin K_2 may point towards an interaction of vitamin K_2 with the patient-specific compensatory response.

It is noted that the global effects of vitamin K_2 seen in patient and unaffected control fibroblasts, such as elevated mitochondrial respiration and enhanced interconnectivity of mitochondrial network, may itself be indirect cellular responses to vitamin K_2 treatment. This may repudiate the specific action of vitamin K_2 as an ETC molecule in human fibroblasts, as seen in *Drosophila* (Vos et al. 2012). However, potentially promising therapeutic compounds do not necessarily have to target specific cellular pathways to prove beneficial: compounds which induce compensatory mechanisms may sufficiently overcome underlying cellular defects to provide a protective effect.

While this study of parkin-deficient fibroblasts does not support a role for vitamin K_2 to treat PD pathology specifically, vitamin K_2 may have appeal as a general promoter of mitochondrial respiratory function. As such, vitamin K_2 supplementation could potentially support the function of cells and tissues that are particularly reliant on proper mitochondrial function, including neurons. Hence, this compound may prove beneficial as a general neuroprotective agent. Other studies have described various neuroprotective effects of vitamin K_2; for example, vitamin K_2 was found to protect against oxidative stress-induced cell death in cultured neurons and oligodendrocytes (Li et al. 2003; Sakaue et al. 2011). Vitamin K_2 is also known to promote neuroprotection via its activation of the anti-apoptotic protein Gas6 (Shankar et al. 2003). Moreover, the vitamin K analog β-lapachone has been shown to enhance mitochondrial function in the brain and prevent motor function decline in aged mice (Lee et al. 2012b). In fact, low levels of vitamin K_2 in the brain, as well as low dietary intake of vitamin K_2, have been associated with an increased susceptibility to Alzheimer's disease (Allison 2001; Presse et al. 2008).

Vitamin K_2 may also be of benefit in PD therapy by targeting other neurodegenerative pathways. A recent study demonstrated that vitamin K_2 can directly interact with α-synuclein and inhibit its fibrillization *in vitro* (da Silva et al. 2013). In contrast to the non-specific hydrophobic interactions exhibited by most other anti-fibrillogenic compounds, vitamin K_2 delayed fibrillization via a specific interaction with α-synuclein residues, which promoted the formation of short fibrils rather than cytotoxic oligomers. These anti-fibrillogenic properties of vitamin K_2, in combination with its enhancement of mitochondrial function seen in the present study, suggest that vitamin K_2 has potential as a multi-target PD therapeutic agent.

However, it should be emphasized that the interesting effects described in this pilot study were observed in cultured fibroblasts, and that these results cannot necessarily be extrapolated to neurons. Fibroblasts are markedly different from neurons in their bioenergetic requirements (Connolly 1998), and the increased mitochondrial respiration of fibroblasts in the presence of vitamin K_2 may reflect cell-type specific responses. Therefore, the promising mitochondrial effects seen here should be verified in an appropriate neuronal environment to support the potential of vitamin K_2 as a neuroprotective compound.

4.5 LIMITATIONS OF THE STUDY

4.5.1 Limitations of the PD study group

The major drawback of the study group used for *parkin* mutation screening is the limited number of South African PD patients available for inclusion. Furthermore, out of the 229 recruited PD patients, only seventeen were of Black African ancestry. This under-studied population group is therefore not adequately represented in the present study, which prohibits informed conclusions being made regarding the frequency of *parkin* mutations in the Black South African population. The limited number of Black PD patients may reflect a recruitment bias, as the majority of the study participants were recruited at the Movement Disorders clinic at Tygerberg Hospital (Cape Town, South Africa). This hospital mainly serves the predominantly Caucasian and mixed ancestry communities of the surrounding area, due to the complex socio-economic legacies of the apartheid regime. Black PD patients in rural areas may be under-diagnosed, as there are currently very few trained neurologists available to such rural communities. It is possible that this bias of ascertainment contributed to the low recruitment of Black PD patients in the present study. Despite intensive efforts, no additional Black patients could be recruited: this was due to a lack of contact details, loss of patients to follow-up and a lack of willingness of family members to participate in the research.

The South African Indian population is also under-represented amongst the study participants, with only four PD patients of Indian descent; however, this limitation is of less concern as the contribution of *parkin* mutations to PD in this population group has been well studied on the Indian subcontinent (Biswas et al. 2006; Vinish et al. 2010; Padmaja et al. 2012). While separate genetic screening for PD genes in the South African Indian population would be of benefit, this is perhaps not as urgent as investigations of the population groups that are predominantly found in South Africa.

4.5.2 Limitations of mutation detection techniques

HRM analysis is a fast, simple and cost-effective method to screen for genetic variants; however, HRM is susceptible to both false positive and false negative results. Several studies have established the sensitivity and specificity of this technique to be in the range of 90-100% (Dobrowolski et al. 2007; Montgomery et al. 2007; Taylor 2009). Small insertions and deletions may be more difficult to detect than nucleotide substitutions, and homozygous substitutions or A>T substitutions may not significantly alter the melting profile (van der Stoep et al. 2009). Hence, all samples demonstrating altered melting behavior need to be verified, and their variants identified, by direct sequencing. This need for subsequent verification incurs additional costs on the HRM screening method.

The MLPA technique allows for the targeted, simultaneous analysis of many genomic regions for exonic rearrangements, using standard PCR and capillary electrophoresis equipment (Hömig-Hölzel and Savola 2012). However, MLPA is susceptible to false positive results, specifically false exonic deletions. Such false positives may arise from DNA sequence polymorphisms in the target sequence that are located close to the probe ligation site, which may interfere with proper probe annealing. This particular limitation is evident in the present study, as the presence of the M192L *parkin* polymorphism was shown to produce a false positive result (Section 3.1.2). Hence, it is advisable that all exonic rearrangements detected via MLPA analysis be verified using a second, independent experimental approach. This alternative exonic rearrangement detection method may introduce additional reagent and labor costs. Furthermore, probe signal analysis requires the proper binding of reference probes to their target sequences. While these reference probes are designed to target chromosomal regions that are not expected to harbor structural variants, probe design is mostly based on genomic data from Caucasian individuals. It is possible that the great genetic diversity observed in African populations may influence the binding of reference probes to target regions, which may yield false results. It is therefore important to independently verify MLPA results obtained for samples from non-Caucasian origin.

4.5.3 Limitations of Y2H

The Y2H method is a simple, inexpensive and powerful high-throughput genetic technique to detect interactions between bait and prey proteins in an *in vivo* environment (Fields and Song 1989). This makes Y2H a widely-used screening method with broad applications in the study of interactomics. However, this approach presents several limitations, particularly in regards to false positive and false negative results.

False positive bait-prey interactions, i.e. detection of spurious interactions in the Y2H setting which are biologically meaningless, may arise for a number of reasons. Firstly, proteins observed to interact in yeast do so in a very artificial setting: they are directed to the nucleus (forced co-localization), are overexpressed in the same cell (forced co-expression), are expressed as fusion proteins, and they interact in a non-native yeast environment, all of which may facilitate their interaction (Gietz 2006; Brückner et al. 2009). Hence, protein interactions observed in a Y2H setting need to be independently verified in more biologically appropriate environment. Secondly, bait or prey proteins may activate a reporter gene independently of an interacting partner: this limitation was mitigated in this study by testing for auto-activation of the parkin bait prior to Y2H analysis, the use of multiple reporter genes, and by performing rigorous interaction specificity testing of prey proteins after Y2H analysis. Nonetheless, false positives remain a serious drawback, with an estimated 25-45% false positive rate for the Y2H system (Deane et al. 2002; Huang et al. 2007).

While steps can be taken to mitigate the detection of false positive interactions, it is more difficult to address the high false negative rate, estimated at 45-96% (Edwards et al. 2004). A major source of false negatives, i.e. authentic protein interactions which were not detected in the Y2H setting, is the necessity of bait and prey proteins to enter the yeast nucleus. Membrane proteins, mitochondrial proteins and other proteins with strong localization signals may not appropriately translocate to the yeast nucleus, despite their fusion to a nuclear localization signal (Koegl and Uetz 2007). Moreover, bait and preys are expressed as fusion proteins, where the presence of fused domains may interfere with proper folding of the proteins or sterically obstruct protein interactions. Furthermore, relevant cofactors required for protein interaction, such as post-translation protein modifications or adaptor proteins, may not be present in the yeast host organism, leading to a false negative result (Sprinzak et al. 2003). Importantly, parkin requires PINK1-mediated phosphorylation to activate the mitophagy cascade (Shiba-Fukushima et al. 2012); important mitophagic targets of parkin may therefore have been overlooked due to the absence of the proper phosphorylation signal in the Y2H setting.

False negatives may also arise from proteins that are toxic to the host cell when overexpressed (Suter et al. 2008). Although initial testing of the parkin bait showed no toxic effect on the host strain, one cannot rule out such an effect for certain prey proteins. Furthermore, the high stringency of the interaction specificity tests used to reduce false positives may have excluded authentic protein interactions. One of the heterologous bait controls used in the present study encodes murine p53; parkin is a known target of p53 (Zhang et al. 2011) Hence, parkin interactors which are likewise targets of p53 would have been spuriously excluded as false positives, including the often-reported interaction of parkin with itself (Zhang et al. 2000; Imai et al. 2001).

These false negatives drastically affect the reproducibility of Y2H screens. Per illustration, two independent Y2H screens using identical methods showed less than 30% overlap and only 12% of known interactions were detected in each screen (Ito et al. 2001). This considerable limitation is the likely explanation for why most of the previously-described parkin interactors were not detected here.

4.5.4 Limitations of verification techniques

The current study used a combination of immunofluorescent and biochemical approaches to verify selected protein interactions. Independent verification of such interactions greatly supported their authenticity and biological relevance, as the interacting proteins were expressed under the influence of their native promoters (endogenous expression), in mammalian cells in their natural cellular compartments, and without the presence of artificial fusion domains. However, verification techniques are labor-intensive and can only be applied to a small number of interactions detected via Y2H. Hence, most of the interactions found in the Y2H screen remain to be verified in a future study.

In vivo co-localization was used to demonstrate that parkin and each of its interactors share subcellular environments, thereby supporting the biological relevance of these interactions. However, as fluorescence microscopy is limited by the optical resolution of the microscope (typically 200nm for confocal microscopy), apparent co-localization of proteins cannot be taken as evidence of physical interaction *per se* (Lalonde et al. 2008). The present study used vertical Z-stacking to acquire fluorescent signal in all three dimensions, which allowed for the resolution of signals that might have deceptively appeared to co-localize in two-dimensional analyses. Common problems when performing immunofluorescence experiments include cellular autofluorescence and spectral bleed-through between different fluorescent signals (Zinchuk et al. 2007; Dunn et al. 2011). However, the present study used careful selection of appropriate fluorophores, suitable negative controls, and assessment of primary and secondary antibodies for cross-reactivity and specificity of fluorescent signals, to minimize such effects.

Co-IP of endogenous proteins is generally considered to be the "gold standard" technique for the demonstration of protein interactions (Berggård et al. 2007). However, co-IP requires careful consideration and optimization in order to overcome the limitations of this approach. A commonly experienced problem is high background signals resulting from antibody cross-reactivity; here, antibodies were selected in such a way as to avoid cross-reactivity. Furthermore, co-immunoprecipitation is less adept at detecting transient interactions, and detected interactions may represent the association of proteins in a common complex, rather than direct interactions. An additional consideration when using homogenized cell lysates is that proteins from different cellular compartments are likely to come into contact with each other; however, in this study, co-localization analyses did illustrate that parkin and each of its interactors share subcellular environments *in vivo*.

Co-IP relies on proper antibody binding to isolate protein complexes. Hence, the 3D structure of an interacting pair may obstruct an antibody epitope, and prevent immunoprecipitation of that protein complex (Zhou and Veenstra 2007). This limitation was encountered in the co-IP of parkin and SEPT9 (Section 3.2.3.2), where the use of a different anti-parkin antibody (recognizing a different parkin epitope) circumvented this obstacle.

4.5.5 Limitations of parkin-deficient cell models

Originally, it was attempted to use siRNA-mediated gene knockdown in SH-SY5Y cells to create a parkin-deficient neuronal cell model. However, this approach was reconsidered after several technical issues were encountered. Firstly, of the four unvalidated *parkin*-targeted siRNA molecules tested, only two had any demonstrable effect on parkin mRNA expression. When considering the two siRNA molecules that did suppress *parkin* mRNA expression, this knockdown was limited to only 50% of *parkin* expression observed in non-silenced control cells. This partial knockdown effect would have

been problematic in subsequent experiments, as cells from heterozygous parkin mutation carriers (with presumably 50% functional parkin) typically do not demonstrate significant functional impairments (Mortiboys et al. 2008; Pacelli et al. 2011). This is in accordance with the recessive inheritance pattern of *parkin* mutations, suggesting that a 50% loss of parkin is mostly insufficient to result in PD. Secondly, the two tested siRNA molecules had greatly inconsistent effects on the parkin protein expression, despite the fact that similar transfection conditions were used in all replicate experiments. Ultimately, the inconsistent knockdown efficiency at the protein level precluded downstream siRNA experiments, in which implicitly reliable parkin knockdown would be critical.

Furthermore, the necessity for recurring transfections in all downstream applications made the transient siRNA-mediated gene knockdown approach impractical in the present study, which employed a large range of repeated functional assays. It is suggested that alternative approaches to transient siRNA-mediated gene knockdown, such as stable knockdown with small hairpin RNA (shRNA) or genomic editing with CRISPR (clustered regularly interspaced short palindromic repeats)/Cas9, may be more appropriate for future use (Lambeth and Smith 2013; Liu and Fan 2014).

The current study used PD patient-derived parkin-null fibroblasts as a model of parkin deficiency. These patient-derived cell lines have the advantage of harboring predefined *parkin* mutations, without the need for genetic manipulation. Furthermore, such cell models reflect the cumulative cell damage at the age of the patients. However, the use of patient-derived fibroblasts has several limitations which need to be considered (Auburger et al. 2012). Firstly, the gene expression profile of dermal fibroblasts differs significantly from neurons, which limit their use as models of PD. *SNCA* in particular is expressed at a relatively low level in fibroblasts, and in addition fibroblasts are resistant to the mitochondrial toxin rotenone (Harper et al. 2007). Fibroblast models therefore do not recapitulate the neuronal environment, particularly not the susceptible dopaminergic neuronal environment. This limitation may be overcome by reprogramming patient-derived fibroblasts into induced pluripotent stem cells (iPSCs), after which they may be differentiated into an appropriate dopaminergic neuronal PD model (Beevers et al. 2013).

Secondly, the use of derived cell models is significantly limited by the inherent genomic variability between cell lines from different individuals. It is therefore recommended that several biological replicate and control cell lines be investigated in any given study, which may improve the signal-to-noise ratio caused by this variability. In the current study, fibroblasts could only be obtained from three patients with *parkin*-null mutations, of which one fibroblast culture was lost to microbial contamination. The results obtained here are therefore limited by the low number of biological replicates (two). Furthermore, the two patients recruited for this study were siblings. The limited sample size is a major drawback of the study, and verification of the findings reporter here in a larger group of patients and controls would be necessary.

4.5.6 Limitations of functional assays

MTT assays are widely used to assess cell viability (Berridge et al. 2005). These assessments are based on the capacity of cellular dehydrogenases to reduce MTT to insoluble formazan, which is limited to viable cells. However, MTT measurements are particularly susceptible to biochemical influences of added compounds, which may artificially inflate viability measurements (Ulukaya et al. 2004; Ahmad et al. 2006; Ganapathy-Kanniappan et al. 2010). In fact, several studies have reported conflicting results from MTT-based cell viability assays and cell growth assays due to such MTT artefacts (Jabbar et al. 1989; Pagliacci et al. 1993; Belyanskaya et al. 2007). This limitation was also seen in the present study, as treatment of fibroblasts with CCCP greatly enhanced the ostensible viability measurements (Section 3.3.1). It has been suggested that MTT assays should be supplemented with additional assays of cellular health in order to detect such MTT-induced artefacts. This was done here, as CyQUANT® assays were performed in parallel with MTT assays. While CyQUANT® assays are based on measurements of total DNA content and are therefore not susceptible to the same artefacts as MTT assays, CyQUANT® assays are less adept at discriminating between viable and apoptotic cells. Hence, the simultaneous use of these two complementary assays provides a more reliable estimate of cellular health than either assay by itself.

Mitochondrial respiration analysis using a Seahorse Extracellular Flux Analyzer provides a simple, accurate and high-throughput method to investigate respiratory flux in in intact cells (Ferrick et al. 2008). However, it should be noted that the respiratory state of isolated dermal fibroblasts are not representative of cell respiration in more energetically-demanding cells such as neurons, as fibroblasts are known to have a lower metabolic rate than most cells (Connolly 1998). Furthermore, OCR measurements are very sensitive to inhibitor compound concentrations; therefore, these parameters were extensively optimized for the fibroblast cell lines prior to the experiment. It is particularly important that all OCR measurements should be normalized to account for quantitative differences between cell samples; in the present study, OCR measurements were normalized to cell number. While measurements of cell number or total protein content is generally regarded as a sufficient means of normalization (Perron et al. 2013; Wills et al. 2013), it should be noted that this does not correct for possible differences in mitochondrial densities between cells. Hence, cells may increase mitochondrial biogenesis as a compensatory response to mitochondrial impairment, which would greatly affect cellular respiration. This compensation would not be accounted for when only considering cell number or total protein concentration. Analyzing isolated mitochondria would allow for a respiratory analysis of comparable mitochondrial numbers; however, this approach is susceptible to several other limitations and artefacts (Brand and Nicholls 2011).

Functional assays that employ fluorescent dyes, such as the JC-1 dye in $\Delta\psi_m$ analysis and the Mitotracker Red dye used for mitochondrial network analysis, should be carefully optimized in order

to minimize dye-induced cytotoxicity. Such dye-induced cytotoxicity may increase cellular stress and apoptosis, which may result in artefacts. In the present study, the JC-1 and Mitotracker Red live-cell staining conditions were first optimized in order to minimize dye-induced cytotoxicity in the fibroblast cell cultures. Additionally, care was taken to keep all dye incubation periods and fluorescence imaging procedures consistent between experimental runs.

4.6 OVERVIEW AND FUTURE DIRECTIONS OF THE STUDY

It was concluded from the present study that *parkin* mutations do not significantly contribute to the genetic etiology of PD in South African patients. This finding is consistent with parallel studies from our research group which found that mutations in the known PD genes are rare in the South African PD population. The large percentage of South African PD patients without any detected mutations in known PD genes raises the interesting possibility of the South African population harboring novel mutations or novel PD-causing genes. Hence, our research group is currently employing various approaches to identify new PD candidate genes for screening in the South African population. For example, a NGS-based exome sequencing approach is currently underway to identify candidate PD genes in an extended Afrikaner family. Alternatively, genes and proteins that contribute to PD may be identified by a hypothesis-driven approach, whereby proteins acting in common pathways with known PD genes are prioritized for investigation and genetic screening. This approach may identify new genetic risk factors of PD. The present study identified and verified four parkin-interacting proteins; future studies should be aimed at screening the genes encoding 14-3-3η, ATPAF1, β- and γ-actin and SEPT9 for variants in a group of South African PD patients. Ultimately, the identification of the genes and mutations underlying PD in the unique Black, Afrikaner and Mixed ancestry sub-populations of South Africa may reveal novel disease mechanisms underlying the etiology of PD in South Africa.

Of the four parkin interactors, two are wholly novel and should be prioritized for future research. It was found that ATPAF1 and SEPT9 both accumulate in the absence of parkin, which strongly suggests that these proteins are substrates of parkin-mediated ubiquitination. The obvious next step would be to confirm that this is indeed the case, using either *in vitro* or *in vivo* ubiquitination assays. Furthermore, the ubiquitination signals should be analyzed with chain-specific anti-ubiquitin antibodies, which would establish the mode of ubiquitination (whether mono-, poly-, K48- or K63-ubiquitination). This approach would provide further insight into the nature and consequences of these protein interactions.

It is recommended that the functional consequences of parkin's interaction with both ATPAF1 and SEPT9 should be investigated further, as these two proteins are novel and exciting members of the parkin interactome. For example, it should be determined whether the accumulation of ATPAF1 alters

the assembly of the F_1-ATP synthase, as this has not been investigated to date. This may be performed by overexpressing ATPAF1 in an appropriate cell line and using non-denaturing PAGE and immunoblotting with an antibody directed against the β-subunit of F_1-ATP synthase, which would indicate the incorporation of the β-subunit into various stages of ATP synthase assembly. This investigation should also be performed in parkin-deficient cell models, which accumulate ATPAF1 without the need for transgenic overexpression. In terms of SEPT9, future studies should investigate how accumulating SEPT9, either as a result of overexpression or due to parkin deficiency, impacts on the assembly of septin filaments. Cell imaging approaches would be appropriate towards this end. The particular role of SEPT9 in neurons should also be investigated, as this is currently unknown. A previous study has suggested that SEPT9 accumulation in neurons may have a pro-apoptotic effect (Mao et al. 2013); this should be investigated further in the context of its interaction with parkin.

This study also identified 25 other putative parkin-interacting proteins in a Y2H screen which were not prioritized for verification. However, these proteins may be authentic parkin interactors of significant relevance to PD, and should be verified in the future. Based on recent findings, three of the putative interactors could be prioritized for further verification and study: EXOC4, CCDC56 and HGS. EXOC4, also known as Sec8, is a component of the exocyst complex with important roles in vesicular trafficking (Heider and Munson 2012). Interestingly, it was recently reported that accumulation of EXOC4 activated the JNK pro-apoptosis signaling cascade (Tanaka et al. 2014). CCDC56 has only very recently been characterized as a mitochondrial transmembrane protein and essential factor in mitochondrial complex IV biogenesis (Clemente et al. 2013). This may be of significant relevance to neurodegeneration, and future studies should aim to verify this protein interaction. Lastly, the putative parkin interactor HGS is a component of the endosomal sorting complex required for transport (ESCRT), and has recently been implicated in xenophagy directed against mycobacterial pathogens (Mehra et al. 2013). Hence, parkin and HGS may interact in the mediation of xenophagy. While this is perhaps not related to PD, this interesting finding may have significant implications for research into cellular defense responses.

The investigation of the functional effects of parkin deficiency in fibroblasts obtained from South African PD patients has delivered some surprising results. Whereas these *parkin*-mutant fibroblasts are more susceptible to CCCP-induced cytotoxicity and have more fragmented mitochondrial networks than wild-type control fibroblasts; the respiratory capacity of these fibroblasts are not impaired in the absence of parkin. In fact, measurements of respiratory rates were markedly enhanced in patient-derived fibroblasts, strongly suggesting a compensatory response in these cells. Future studies should aim at investigating the molecular mechanism of such mitochondrial compensation in the absence of parkin. In particular, it should be determined whether mitochondrial biogenesis is in fact increased in the patient-derived fibroblasts. This may be done by performing q-PCR to quantify mtDNA content, or by using western blotting to evaluate the protein expression of key mitochondrial

proteins. Alternatively, indirect measures of mitochondrial content (such as citrate synthase activity) may be performed, as has been done in previous studies (Grunewald et al. 2010; Pacelli et al. 2011).

It is also suggested that future studies should confirm that the interesting impairments and compensatory effects observed in the patient-derived fibroblasts are due to parkin deficiency itself, rather than an unknown secondary mechanisms. For example, Mortiboys et al. (2008) used an RNAi approach to demonstrate the parkin-dependent nature of the mitochondrial impairments they initially observed in *parkin*-mutant fibroblasts, and which were recapitulated following parkin knockdown in wild-type fibroblasts. Similar RNAi approaches or genomic editing with CRISPR/Cas9 may be suitable to this end. Moreover, this study could be expanded to include fibroblasts from patients with sporadic PD, which may be more appropriate controls for the *parkin*-mutant fibroblasts than cells obtained from unaffected individuals.

Importantly, all of the functional effects of parkin deficiency observed in this pilot study were performed on fibroblasts cultured under basal, unstressed conditions. Given parkin's important role in the cellular stress response, future studies should aim to compare the results obtained here to fibroblasts cultured under more stressed or oxidative conditions. This may be achieved by exposing the cells to low concentrations of cytotoxic agents, or by culturing the fibroblasts in glucose-free galactose media.

This study also evaluated the effects of vitamin K_2 treatment on mitochondrial health in a parkin-deficient cell model. It was found that vitamin K_2 increased the interconnectedness of the mitochondrial network and enhanced respiratory rates of all the fibroblasts investigated, irrespective of parkin mutation status. This suggests that vitamin K_2 may be a promising pro-mitochondrial compound, and its specific molecular action at the mitochondria should be investigated further. Particularly, it is still unclear whether vitamin K_2 increases mitochondrial function by acting as an electron carrier in the fibroblasts (as it does in *Drosophila*) or whether respiratory rates are increased as a secondary cellular response to vitamin K_2 treatment. It is therefore suggested that the action of vitamin K_2 at the ETC should be determined in human cells. This may be done by isolating mitochondria and determining the effect of direct application of vitamin K_2 on the rate of oxygen consumption or ATP production, as was done by Vos et al. (2012).

Finally, the results obtained here from both the functional investigations of parkin deficiency and the evaluation of the effects of vitamin K_2 treatment would benefit significantly from a more comprehensive analysis of cellular and mitochondrial function, and from using a larger sample size. Our results may be substantiated and informed by measurements of total ATP levels, ATP synthesis rates, activities of the individual ETC complexes, NADH/NADPH levels, glycolysis, and/or ROS generation. Furthermore, whole proteome or transcriptome analyses would provide valuable and

unbiased insights into cellular differences between parkin-deficient and wild-type cells, as well as between vitamin K_2-treated and untreated cells.

4.7 CONCLUSION

This study has described several interesting findings on the *parkin* gene, its protein product and parkin deficiency, which provided valuable insight into how parkin dysfunction contributes to neurodegeneration. However, the reported findings, plausible explanations and proposed mechanisms may only be scratching the surface of the biological processes involved. It is almost inevitable that the exploratory approaches used in the current study raise more questions than provide answers; however, such questions are fertile ground for future research. Ultimately, it is hoped that a more comprehensive understanding of parkin and its role in PD would be translated into novel and more effective PD therapeutic approaches, in order to better treat patients suffering from this debilitating disorder.

REFERENCES

Aarsland, D., Larsen, J.P., Tandberg, E., et al. (2000). Predictors of nursing home placement in Parkinson's disease: a population-based, prospective study. *Journal of the American Geriatrics Society*. *48*, 938–942.

Aarsland, D., Andersen, K., Larsen, J.P., et al. (2001). Risk of dementia in Parkinson's disease: a community-based, prospective study. *Neurology*. *56*, 730–736.

Aarsland, D., Zaccai, J., and Brayne, C. (2005). A systematic review of prevalence studies of dementia in Parkinson's disease. *Movement disorders: official journal of the Movement Disorder Society*. *20*, 1255–1263.

Aasly, J.O., Toft, M., Fernandez-Mata, I., et al. (2005). Clinical features of LRRK2-associated Parkinson's disease in central Norway. *Annals of neurology*. *57*, 762–765.

Abraham, V.C., Towne, D.L., Waring, J.F., et al. (2008). Application of a high-content multiparameter cytotoxicity assay to prioritize compounds based on toxicity potential in humans. *Journal of Biomolecular Screening*. *13*, 527–537.

Ackerman, S.H. (2002). Atp11p and Atp12p are chaperones for F1-ATPase biogenesis in mitochondria. *Biochimica et Biophysica Acta (BBA) - Bioenergetics*. *1555*, 101–105.

Ackerman, S.H., and Tzagoloff, A. (2005). Function, structure, and biogenesis of mitochondrial ATP synthase. *Progress in Nucleic Acid Research and Molecular Biology*. *80*, 95–133.

Adzhubei, I.A., Schmidt, S., Peshkin, L., et al. (2010). A method and server for predicting damaging missense mutations. *Nature methods*. *7*, 248–249.

Aharon-Peretz, J., Rosenbaum, H., and Gershoni-Baruch, R. (2004). Mutations in the glucocerebrosidase gene and Parkinson's disease in Ashkenazi Jews. *The New England journal of medicine*. *351*, 1972–1977.

Ahlskog, J.E. (2009). Parkin and PINK1 parkinsonism may represent nigral mitochondrial cytopathies distinct from Lewy body Parkinson's disease. *Parkinsonism & Related Disorders*. *15*, 721–727.

Ahmad, S., Ahmad, A., Schneider, K.B., et al. (2006). Cholesterol interferes with the MTT assay in human epithelial-like (A549) and endothelial (HLMVE and HCAE) cells. *International Journal of Toxicology*. *25*, 17–23.

Ahmed, M.R., Zhan, X., Song, X., et al. (2011). Ubiquitin ligase parkin promotes Mdm2-arrestin interaction but inhibits arrestin ubiquitination. *Biochemistry*. *50*, 3749–3763.

Ahn, T.-B., Kim, S.Y., Kim, J.Y., et al. (2008). alpha-Synuclein gene duplication is present in sporadic Parkinson disease. *Neurology*. *70*, 43–49.

Akundi, R.S., Zhi, L., Sullivan, P.G., et al. (2013). Shared and cell type-specific mitochondrial defects and metabolic adaptations in primary cells from PINK1-deficient mice. *Neuro-Degenerative Diseases*. *12*, 136–149.

Ali, S., Vollaard, A.M., Widjaja, S., et al. (2006). PARK2/PACRG polymorphisms and susceptibility to typhoid and paratyphoid fever. *Clinical and Experimental Immunology*. *144*, 425–431.

Allen, M.T., and Levy, L.S. (2013). Parkinson's disease and pesticide exposure--a new assessment. *Critical reviews in toxicology*. *43*, 515–534.

Allison, A.C. (2001). The possible role of vitamin K deficiency in the pathogenesis of Alzheimer's disease and in augmenting brain damage associated with cardiovascular disease. *Medical Hypotheses*. *57*, 151–155.

Alvarez-Erviti, L., Rodriguez-Oroz, M.C., Cooper, J.M., et al. (2010). Chaperone-mediated autophagy markers in Parkinson disease brains. *Archives of neurology*. *67*, 1464–1472.

Alvarez-Erviti, L., Seow, Y., Schapira, A.H., et al. (2011). Lysosomal dysfunction increases exosome-mediated alpha-synuclein release and transmission. *Neurobiology of disease*. *42*, 360–367.

Alves, G., Forsaa, E.B., Pedersen, K.F., et al. (2008). Epidemiology of Parkinson's disease. *Journal of neurology*. *255 Suppl 5*, 18–32.

Amir, S., Wang, R., Matzkin, H., et al. (2006). MSF-A interacts with hypoxia-inducible factor-1alpha and augments hypoxia-inducible factor transcriptional activation to affect tumorigenicity and angiogenesis. *Cancer Research*. *66*, 856–866.

Amir, S., Wang, R., Simons, J.W., et al. (2009). SEPT9_v1 up-regulates hypoxia-inducible factor 1 by preventing its RACK1-mediated degradation. *Journal of Biological Chemistry*. *284*, 11142–11151.

Amir, S., Golan, M., and Mabjeesh, N.J. (2010). Targeted knockdown of SEPT9_v1 inhibits tumor growth and angiogenesis of human prostate cancer cells concomitant with disruption of hypoxia-inducible factor-1 pathway. *Molecular Cancer Research*. *8*, 643–652.

Anantharam, V., Lehrmann, E., Kanthasamy, A., et al. (2007). Microarray analysis of oxidative stress regulated genes in mesencephalic dopaminergic neuronal cells: relevance to oxidative damage in Parkinson's disease. *Neurochemistry international*. *50*, 834–847.

Ando, M., Funayama, M., Li, Y., et al. (2012). VPS35 mutation in Japanese patients with typical Parkinson's disease. *Movement disorders: official journal of the Movement Disorder Society*. *27*, 1413–1417.

Anglade, P., Vyas, S., Javoy-Agid, F., et al. (1997). Apoptosis and autophagy in nigral neurons of patients with Parkinson's disease. *Histology and Histopathology*. *12*, 25–31.

Antonini, A., Tolosa, E., Mizuno, Y., et al. (2009). A reassessment of risks and benefits of dopamine agonists in Parkinson's disease. *Lancet neurology*. *8*, 929–937.

Appel-Cresswell, S., Vilarino-Guell, C., Encarnacion, M., et al. (2013). Alpha-synuclein p.H50Q, a novel pathogenic mutation for Parkinson's disease. *Movement disorders: official journal of the Movement Disorder Society*. *28*, 811–813.

Asakawa, S., Tsunematsu Ki, Takayanagi, A., et al. (2001). The genomic structure and promoter region of the human parkin gene. *Biochemical and biophysical research communications*. *286*, 863–868.

Ascherio, A., Chen, H., Schwarzschild, M.A., et al. (2003). Caffeine, postmenopausal estrogen, and risk of Parkinson's disease. *Neurology*. *60*, 790–795.

Ashok, P.P., Radhakrishnan, K., Sridharan, R., et al. (1986). Epidemiology of Parkinson's disease in Benghazi, North-East Libya. *Clinical neurology and neurosurgery*. *88*, 109–113.

Auburger, G., Klinkenberg, M., Drost, J., et al. (2012). Primary skin fibroblasts as a model of Parkinson's disease. *Molecular Neurobiology*. *46*, 20–27.

Avraham, E., Rott, R., Liani, E., et al. (2007). Phosphorylation of parkin by the cyclin-dependent kinase 5 at the linker region modulates its ubiquitin-ligase activity and aggregation. *Journal of Biological Chemistry*. *282*, 12842–12850.

Azuma, K., Urano, T., Ouchi, Y., et al. (2009). Vitamin K2 suppresses proliferation and motility of hepatocellular carcinoma cells by activating steroid and xenobiotic receptor. *Endocrine Journal*. *56*, 843–849.

Bagheri, H., Damase-Michel, C., Lapeyre-Mestre, M., et al. (1999). A study of salivary secretion in Parkinson's disease. *Clinical neuropharmacology*. *22*, 213–215.

Bai, J.J., Safadi, S.S., Mercier, P., et al. (2013). Ataxin-3 is a multivalent ligand for the Parkin Ubl domain. *Biochemistry*. *52*, 7369–7376.

Bandopadhyay, R., Kingsbury, A.E., Muqit, M.M., et al. (2005). Synphilin-1 and parkin show overlapping expression patterns in human brain and form aggresomes in response to proteasomal inhibition. *Neurobiology of Disease*. *20*, 401–411.

Barbosa, M.T., Caramelli, P., Maia, D.P., et al. (2006). Parkinsonism and Parkinson's disease in the elderly: a community-based survey in Brazil (the Bambuí study). *Movement disorders: official journal of the Movement Disorder Society*. *21*, 800–808.

Bardien, S., Keyser, R., Yako, Y., et al. (2009). Molecular analysis of the parkin gene in South African patients diagnosed with Parkinson's disease. *Parkinsonism & Related Disorders*. *15*, 116–121.

Barone, P., Aarsland, D., Burn, D., et al. (2011). Cognitive impairment in nondemented Parkinson's disease. *Movement disorders: official journal of the Movement Disorder Society*. *26*, 2483–2495.

Bedford, L., Hay, D., Devoy, A., et al. (2008). Depletion of 26S proteasomes in mouse brain neurons causes neurodegeneration and Lewy-like inclusions resembling human pale bodies. *The Journal of Neuroscience*. *28*, 8189–8198.

Bedford, L., Paine, S., Sheppard, P.W., et al. (2010). Assembly, structure, and function of the 26S proteasome. *Trends in cell biology*. *20*, 391–401.

Beevers, J.E., Caffrey, T.M., and Wade-Martins, R. (2013). Induced pluripotent stem cell (iPSC)-derived dopaminergic models of Parkinson's disease. *Biochemical Society transactions*. *41*, 1503–1508.

Beites, C.L., Xie, H., Bowser, R., et al. (1999). The septin CDCrel-1 binds syntaxin and inhibits exocytosis. *Nature Neuroscience*. *2*, 434–439.

Bellani, S., Sousa, V.L., Ronzitti, G., et al. (2010). The regulation of synaptic function by alpha-synuclein. *Communicative & Integrative Biology*. *3*, 106–109.

Belluzzi, E., Greggio, E., and Piccoli, G. (2012). Presynaptic dysfunction in Parkinson's disease: a focus on LRRK2. *Biochemical Society Transactions*. *40*, 1111–1116.

Belyanskaya, L., Manser, P., Spohn, P., et al. (2007). The reliability and limits of the MTT reduction assay for carbon nanotubes–cell interaction. *Carbon*. *45*, 2643–2648.

Benard, G., Bellance, N., James, D., et al. (2007). Mitochondrial bioenergetics and structural network organization. *Journal of Cell Science*. *120*, 838–848.

Bender, A., Krishnan, K.J., Morris, C.M., et al. (2006a). High levels of mitochondrial DNA deletions in substantia nigra neurons in aging and Parkinson disease. *Nature Genetics*. *38*, 515–517.

Bender, A., Koch, W., Elstner, M., et al. (2006b). Creatine supplementation in Parkinson disease: a placebo-controlled randomized pilot trial. *Neurology*. *67*, 1262–1264.

Benito-León, J., Bermejo-Pareja, F., Rodríguez, J., et al. (2003). Prevalence of PD and other types of parkinsonism in three elderly populations of central Spain. *Movement disorders: official journal of the Movement Disorder Society*. *18*, 267–274.

Benito-León, J., Bermejo-Pareja, F., Morales-González, J.M., et al. (2004). Incidence of Parkinson disease and parkinsonism in three elderly populations of central Spain. *Neurology*. *62*, 734–741.

Berardelli, A., Rothwell, J.C., Thompson, P.D., et al. (2001). Pathophysiology of bradykinesia in Parkinson's disease. *Brain: a journal of neurology*. *124*, 2131–2146.

Berg, D., Holzmann, C., and Riess, O. (2003). 14-3-3 proteins in the nervous system. *Nature Reviews. Neuroscience*. *4*, 752–762.

Berger, A.K., Cortese, G.P., Amodeo, K.D., et al. (2009). Parkin selectively alters the intrinsic threshold for mitochondrial cytochrome c release. *Human molecular genetics*. *18*, 4317–4328.

Berggård, T., Linse, S., and James, P. (2007). Methods for the detection and analysis of protein–protein interactions. *Proteomics*. *7*, 2833–2842.

Bernal-Pacheco, O., Limotai, N., Go, C.L., et al. (2012). Nonmotor manifestations in Parkinson disease. *The neurologist*. *18*, 1–16.

Berridge, M.V., Herst, P.M., and Tan, A.S. (2005). Tetrazolium dyes as tools in cell biology: new insights into their cellular reduction. *Biotechnology Annual Review*. *11*, 127–152.

Bertolin, G., Ferrando-Miguel, R., Jacoupy, M., et al. (2013). The TOMM machinery is a molecular switch in PINK1 and PARK2/PARKIN-dependent mitochondrial clearance. *Autophagy*. *9*, 1801–1817.

Bertoncini, C.W., Fernandez, C.O., Griesinger, C., et al. (2005). Familial mutants of alpha-synuclein with increased neurotoxicity have a destabilized conformation. *The Journal of biological chemistry*. *280*, 30649–30652.

Betarbet, R., Sherer, T.B., MacKenzie, G., et al. (2000). Chronic systemic pesticide exposure reproduces features of Parkinson's disease. *Nature neuroscience*. *3*, 1301–1306.

Beulens, J.W.J., Bots, M.L., Atsma, F., et al. (2009). High dietary menaquinone intake is associated with reduced coronary calcification. *Atherosclerosis*. *203*, 489–493.

Beulens, J.W.J., Booth, S.L., van den Heuvel, E.G.H.M., et al. (2013). The role of menaquinones (vitamin K2) in human health. *British Journal of Nutrition*. *110*, 1357–1368.

Beyer, M.K., Herlofson, K., Arsland, D., et al. (2001). Causes of death in a community-based study of Parkinson's disease. *Acta neurologica Scandinavica*. *103*, 7–11.

Bhandari, P., Song, M., Chen, Y., et al. (2014). Mitochondrial contagion induced by parkin deficiency in Drosophila hearts and its containment by suppressing mitofusin. *Circulation Research*. *114*, 257–265.

Biedler, J.L., Roffler-Tarlov, S., Schachner, M., et al. (1978). Multiple neurotransmitter synthesis by human neuroblastoma cell lines and clones. *Cancer research*. *38*, 3751–3757.

Biswas, A., Gupta, A., Naiya, T., et al. (2006). Molecular pathogenesis of Parkinson's disease: identification of mutations in the Parkin gene in Indian patients. *Parkinsonism & related disorders*. *12*, 420–426.

Blanckenberg, J., Bardien, S., Glanzmann, B., et al. (2013). The prevalence and genetics of Parkinson's disease in sub-Saharan Africans. *Journal of the Neurological Sciences*. *335*, 22–25.

Blanckenberg, J., Ntsapi, C., Carr, J.A., et al. (2014). EIF4G1 R1205H and VPS35 D620N mutations are rare in Parkinson's disease from South Africa. *Neurobiology of Aging*. *35*, 445.e1–e3.

Blocq, P., and Marinesco, G. (1894). Sur un cas de tremblement parkinsonien hemiplegique symptomatique d'une tumeur du peduncule cerebrale. *Revue neurologique*. 2.

Bolam, J.P., and Pissadaki, E.K. (2012). Living on the edge with too many mouths to feed: why dopamine neurons die. *Movement Disorders: Official Journal of the Movement Disorder Society*. *27*, 1478–1483.

Bolaños, J.P., Almeida, A., and Moncada, S. (2010). Glycolysis: a bioenergetic or a survival pathway? *Trends in Biochemical Sciences*. *35*, 145–149.

Bonifati, V. (2014). Genetics of Parkinson's disease--state of the art, 2013. *Parkinsonism & related disorders*. *20 Suppl 1*, S23–S28.

Bonifati, V., Rizzu, P., van Baren, M.J., et al. (2003). Mutations in the DJ-1 gene associated with autosomal recessive early-onset parkinsonism. *Science*. *299*, 256–259.

Bonifati, V., Rohé, C.F., Breedveld, G.J., et al. (2005). Early-onset parkinsonism associated with PINK1 mutations: frequency, genotypes, and phenotypes. *Neurology*. *65*, 87–95.

Bower, J.H., Maraganore, D.M., McDonnell, S.K., et al. (1999). Incidence and distribution of parkinsonism in Olmsted County, Minnesota, 1976-1990. *Neurology*. *52*, 1214–1220.

Boyer, P.D. (1997). The ATP synthase - a splendid molecular machine. *Annual Review of Biochemistry*. *66*, 717–749.

Braak, H., and Braak, E. (2000). Pathoanatomy of Parkinson's disease. *Journal of neurology*. *247 Suppl 2*, II3–II10.

Braak, H., Tredici, K.D., Rüb, U., et al. (2003). Staging of brain pathology related to sporadic Parkinson's disease. *Neurobiology of Aging*. *24*, 197–211.

Brand, M.D. (2000). Uncoupling to survive? The role of mitochondrial inefficiency in ageing. *Experimental Gerontology*. *35*, 811–820.

Brand, M.D., and Nicholls, D.G. (2011). Assessing mitochondrial dysfunction in cells. *The Biochemical Journal*. *435*, 297–312.

Bras, J., Verloes, A., Schneider, S.A., et al. (2012). Mutation of the parkinsonism gene ATP13A2 causes neuronal ceroid-lipofuscinosis. *Human molecular genetics*. *21*, 2646–2650.

Brissaud, E. (1895). Nature et pathogenie de la maladie de Parkinson (leçon 23). In *Leçons Sur Les Maladies Du Systeme Nerveux*, pp. 488–501.

Brückner, A., Polge, C., Lentze, N., et al. (2009). Yeast two-hybrid, a powerful tool for systems biology. *International Journal of Molecular Sciences*. *10*, 2763–2788.

Bukhatwa, S., Zeng, B.-Y., Rose, S., et al. (2010). A comparison of changes in proteasomal subunit expression in the substantia nigra in Parkinson's disease, multiple system atrophy and progressive supranuclear palsy. *Brain Research*. *1326*, 174–183.

Burbulla, L.F., Krebiehl, G., and Krüger, R. (2010). Balance is the challenge--the impact of mitochondrial dynamics in Parkinson's disease. *European Journal of Clinical Investigation*. *40*, 1048–1060.

Burchell, L., Chaugule, V.K., and Walden, H. (2012). Small, N-terminal tags activate Parkin E3 ubiquitin ligase activity by disrupting its autoinhibited conformation. *PloS One*. *7*, e34748.

Burnett, B., Li, F., and Pittman, R.N. (2003). The polyglutamine neurodegenerative protein ataxin-3 binds polyubiquitylated proteins and has ubiquitin protease activity. *Human Molecular Genetics*. *12*, 3195–3205.

Caesar, M., Felk, S., Aasly, J.O., et al. (2014). Changes in actin dynamics and F-actin structure both in synaptoneurosomes of LRRK2(R1441G) mutant mice and in primary human fibroblasts of LRRK2(G2019S) mutation carriers. *Neuroscience*. *284*, 311–324.

Camacho, J.L.G., Jaramillo, N.M., Gómez, P.Y., et al. (2012). High frequency of Parkin exon rearrangements in Mexican-mestizo patients with early-onset Parkinson's disease. *Movement Disorders*. *27*, 1047–1051.

Caneda-Ferrón, B., De Girolamo, L.A., Costa, T., et al. (2008). Assessment of the direct and indirect effects of MPP+ and dopamine on the human proteasome: implications for Parkinson's disease aetiology. *Journal of Neurochemistry*. *105*, 225–238.

Canet-Avilés, R.M., Wilson, M.A., Miller, D.W., et al. (2004). The Parkinson's disease protein DJ-1 is neuroprotective due to cysteine-sulfinic acid-driven mitochondrial localization. *Proceedings of the National Academy of Sciences of the United States of America*. *101*, 9103–9108.

Cao, K., Liu, W., Nakamura, H., et al. (2009). Vitamin K2 downregulates the expression of fibroblast growth factor receptor 3 in human hepatocellular carcinoma cells. *Hepatology Research*. *39*, 1108–1117.

Carlsson, A., Lindqvist, M., Magnusson, T., et al. (1958). On the presence of 3-hydroxytyramine in brain. *Science*. *127*, 471.

Castrioto, A., Lozano, A.M., Poon, Y.-Y., et al. (2011). Ten-year outcome of subthalamic stimulation in Parkinson disease: a blinded evaluation. *Archives of neurology*. *68*, 1550–1556.

Cazeneuve, C., Sân, C., Ibrahim, S.A., et al. (2009). A new complex homozygous large rearrangement of the PINK1 gene in a Sudanese family with early onset Parkinson's disease. *Neurogenetics*. *10*, 265–270.

Cerveira, N., Bizarro, S., and Teixeira, M.R. (2011). MLL-SEPTIN gene fusions in hematological malignancies. *Biological Chemistry*. *392*, 713–724.

Cesari, R., Martin, E.S., Calin, G.A., et al. (2003). Parkin, a gene implicated in autosomal recessive juvenile parkinsonism, is a candidate tumor suppressor gene on chromosome 6q25-q27. *Proceedings of the National Academy of Sciences of the United States of America*. *100*, 5956–5961.

Cha, G.-H., Kim, S., Park, J., et al. (2005). Parkin negatively regulates JNK pathway in the dopaminergic neurons of Drosophila. *Proceedings of the National Academy of Sciences of the United States of America*. *102*, 10345–10350.

Chan, N.L., and Hill, C.P. (2001). Defining polyubiquitin chain topology. *Nature structural biology*. *8*, 650–652.

Chan, D., Citro, A., Cordy, J.M., et al. (2011a). Rac1 protein rescues neurite retraction caused by G2019S leucine-rich repeat kinase 2 (LRRK2). *The Journal of Biological Chemistry*. *286*, 16140–16149.

Chan, N.C., Salazar, A.M., Pham, A.H., et al. (2011b). Broad activation of the ubiquitin-proteasome system by Parkin is critical for mitophagy. *Human Molecular Genetics*. *20*, 1726–1737.

Charcot, J.-M. (1880). Leçons sur les Maladies du Système Nerveux Faites a la Salpêtrière (Paris: Masson).

Chartier-Harlin, M.-C., Dachsel, J.C., Vilariño-Güell, C., et al. (2011). Translation initiator EIF4G1 mutations in familial Parkinson disease. *American Journal of Human Genetics*. *89*, 398–406.

Chau, V., Tobias, J.W., Bachmair, A., et al. (1989). A multiubiquitin chain is confined to specific lysine in a targeted short-lived protein. *Science*. *243*, 1576–1583.

Chaudhuri, K.R., and Odin, P. (2010). The challenge of non-motor symptoms in Parkinson's disease. *Progress in brain research*. *184*, 325–341.

Chaugule, V.K., Burchell, L., Barber, K.R., et al. (2011). Autoregulation of Parkin activity through its ubiquitin-like domain. *EMBO J*. *30*, 2853–2867.

Chen, Z.J., and Sun, L.J. (2009). Nonproteolytic functions of ubiquitin in cell signaling. *Molecular cell*. *33*, 275–286.

Chen, D., Xiao, H., Zhang, K., et al. (2010a). Retromer is required for apoptotic cell clearance by phagocytic receptor recycling. *Science*. *327*, 1261–1264.

Chen, D., Gao, F., Li, B., et al. (2010b). Parkin mono-ubiquitinates Bcl-2 and regulates autophagy. *Journal of Biological Chemistry*. *285*, 38214–38223.

Chen, J., Lee, C.-T., Errico, S.L., et al. (2007). Increases in expression of 14-3-3 eta and 14-3-3 zeta transcripts during neuroprotection induced by Δ9-tetrahydrocannabinol in AF5 cells. *Journal of neuroscience research*. *85*, 1724–1733.

Chen, X.Q., Liu, S., Qin, L.Y., et al. (2005). Selective regulation of 14-3-3η in primary culture of cerebral cortical neurons and astrocytes during development. *Journal of Neuroscience Research*. *79*, 114–118.

Chew, K.C.M., Matsuda, N., Saisho, K., et al. (2011). Parkin mediates apparent E2-independent monoubiquitination in vitro and contains an intrinsic activity that catalyzes polyubiquitination. *PloS one*. *6*, e19720.

Choi, P. (2003). SEPT5_v2 is a parkin-binding protein. *Molecular Brain Research*. *117*, 179–189.

Choi, J.M., Woo, M.S., Ma, H.-I., et al. (2008). Analysis of PARK genes in a Korean cohort of early-onset Parkinson disease. *Neurogenetics*. *9*, 263–269.

Choi, P., Golts, N., Snyder, H., et al. (2001). Co-association of parkin and alpha-synuclein. *Neuroreport*. *12*, 2839–2843.

Choo, Y.S., Vogler, G., Wang, D., et al. (2012). Regulation of parkin and PINK1 by neddylation. *Human Molecular Genetics*. *21*, 2514–2523.

Choubey, V., Cagalinec, M., Liiv, J., et al. (2014). BECN1 is involved in the initiation of mitophagy: It facilitates PARK2 translocation to mitochondria. *Autophagy*. *10*, 1105–1119.

Chung, J.-Y., Park, H.R., Lee, S.-J., et al. (2013). Elevated TRAF2/6 expression in Parkinson's disease is caused by the loss of Parkin E3 ligase activity. *Laboratory Investigation; a Journal of Technical Methods and Pathology*. *93*, 663–676.

Chung, K.K., Zhang, Y., Lim, K.L., et al. (2001). Parkin ubiquitinates the alpha-synuclein-interacting protein, synphilin-1: implications for Lewy-body formation in Parkinson disease. *Nature Medicine*. *7*, 1144–1150.

Ciccarone, V., Spengler, B.A., Meyers, M.B., et al. (1989). Phenotypic diversification in human neuroblastoma cells: expression of distinct neural crest lineages. *Cancer research*. *49*, 219–225.

Clague, M.J., Liu, H., and Urbé, S. (2012). Governance of endocytic trafficking and signaling by reversible ubiquitylation. *Developmental cell*. *23*, 457–467.

Clark, I.E., Dodson, M.W., Jiang, C., et al. (2006). Drosophila pink1 is required for mitochondrial function and interacts genetically with parkin. *Nature*. *441*, 1162–1166.

Clavería, L.E., Duarte, J., Sevillano, M.D., et al. (2002). Prevalence of Parkinson's disease in Cantalejo, Spain: a door-to-door survey. *Movement disorders: official journal of the Movement Disorder Society*. *17*, 242–249.

Clemente, P., Peralta, S., Cruz-Bermudez, A., et al. (2013). hCOA3 stabilizes cytochrome c oxidase 1 (COX1) and promotes cytochrome c oxidase assembly in human mitochondria. *The Journal of biological chemistry*. *288*, 8321–8331.

Connolly, G.P. (1998). Fibroblast models of neurological disorders: fluorescence measurement studies. *Trends in Pharmacological Sciences*. *19*, 171–177.

Connolly, D., Hoang, H.G., Adler, E., et al. (2014). Septin 9 amplification and isoform-specific expression in peritumoral and tumor breast tissue. *Biological Chemistry*. *395*, 157–167.

Conway, K.A., Lee, S.J., Rochet, J.C., et al. (2000). Acceleration of oligomerization, not fibrillization, is a shared property of both alpha-synuclein mutations linked to early-onset Parkinson's disease: implications for pathogenesis and therapy. *Proceedings of the National Academy of Sciences of the United States of America*. *97*, 571–576.

Corfield, V.A., Moolman, J.C., Martell, R., et al. (1993). Polymerase chain reaction-based detection of MN blood group-specific sequences in the human genome. *Transfusion*. *33*, 119–124.

Corti, O., and Brice, A. (2013). Mitochondrial quality control turns out to be the principal suspect in parkin and PINK1-related autosomal recessive Parkinson's disease. *Current Opinion in Neurobiology*. *23*, 100–108.

Corti, O., Hampe, C., Koutnikova, H., et al. (2003). The p38 subunit of the aminoacyl-tRNA synthetase complex is a Parkin substrate: linking protein biosynthesis and neurodegeneration. *Human Molecular Genetics*. *12*, 1427–1437.

Corti, O., Lesage, S., and Brice, A. (2011). What genetics tells us about the causes and mechanisms of Parkinson's disease. *Physiological Reviews*. *91*, 1161–1218.

Da Costa, C.A., Sunyach, C., Giaime, E., et al. (2009). Transcriptional repression of p53 by parkin and impairment by mutations associated with autosomal recessive juvenile Parkinson's disease. *Nature cell biology*. *11*, 1370–1375.

Van Criekinge, W., and Beyaert, R. (1999). Yeast two-hybrid: state of the art. *Biological Procedures Online*. *2*, 1–38.

Cronin, K.D., Ge, D., Manninger, P., et al. (2009). Expansion of the Parkinson disease-associated SNCA-Rep1 allele upregulates human alpha-synuclein in transgenic mouse brain. *Human molecular genetics*. *18*, 3274–3285.

Crosiers, D., Ceulemans, B., Meeus, B., et al. (2011). Juvenile dystonia-parkinsonism and dementia caused by a novel ATP13A2 frameshift mutation. *Parkinsonism & related disorders*. *17*, 135–138.

Cuervo, A.M., Stefanis, L., Fredenburg, R., et al. (2004). Impaired degradation of mutant alpha-synuclein by chaperone-mediated autophagy. *Science*. *305*, 1292–1295.

Dächsel, J.C., Lücking, C.B., Deeg, S., et al. (2005). Parkin interacts with the proteasome subunit alpha4. *FEBS letters*. *579*, 3913–3919.

Dächsel, J.C., Behrouz, B., Yue, M., et al. (2010). A comparative study of Lrrk2 function in primary neuronal cultures. *Parkinsonism & related disorders*. *16*, 650–655.

Danzer, K.M., Krebs, S.K., Wolff, M., et al. (2009). Seeding induced by alpha-synuclein oligomers provides evidence for spreading of alpha-synuclein pathology. *Journal of neurochemistry*. *111*, 192–203.

Darios, F., Corti, O., Lücking, C.B., et al. (2003). Parkin prevents mitochondrial swelling and cytochrome c release in mitochondria-dependent cell death. *Human Molecular Genetics*. *12*, 517–526.

Dauer, W., and Przedborski, S. (2003). Parkinson's disease: mechanisms and models. *Neuron*. *39*, 889–909.

Davison, E.J., Pennington, K., Hung, C.-C., et al. (2009). Proteomic analysis of increased Parkin expression and its interactants provides evidence for a role in modulation of mitochondrial function. *PROTEOMICS*. *9*, 4284–4297.

Dawson, T.M., and Dawson, V.L. (2010). The role of parkin in familial and sporadic Parkinson's disease. *Movement Disorders: Official Journal of the Movement Disorder Society*. *25 Suppl 1*, S32–S39.

Deane, C.M., Salwiński, Ł., Xenarios, I., et al. (2002). Protein interactions: two methods for assessment of the reliability of high throughput observations. *Molecular & cellular proteomics: MCP*. *1*, 349–356.

Dehvari, N., Sandebring, A., Flores-Morales, A., et al. (2009). Parkin-mediated ubiquitination regulates phospholipase C-γ1. *Journal of Cellular and Molecular Medicine*. *13*, 3061–3068.

Van Den Eeden, S.K., Tanner, C.M., Bernstein, A.L., et al. (2003). Incidence of Parkinson's disease: variation by age, gender, and race/ethnicity. *American Journal of Epidemiology*. *157*, 1015–1022.

Deng, H., Dodson, M.W., Huang, H., et al. (2008). The Parkinson's disease genes pink1 and parkin promote mitochondrial fission and/or inhibit fusion in Drosophila. *Proceedings of the National Academy of Sciences of the United States of America*. *105*, 14503–14508.

Deng, N., Goh, L.K., Wang, H., et al. (2012). A comprehensive survey of genomic alterations in gastric cancer reveals systematic patterns of molecular exclusivity and co-occurrence among distinct therapeutic targets. *Gut*. *61*, 673–684.

Denison, S.R., Wang, F., Becker, N.A., et al. (2003). Alterations in the common fragile site gene Parkin in ovarian and other cancers. *Oncogene*. *22*, 8370–8378.

Desplats, P., Lee, H.-J., Bae, E.-J., et al. (2009). Inclusion formation and neuronal cell death through neuron-to-neuron transmission of alpha-synuclein. *Proceedings of the National Academy of Sciences of the United States of America*. *106*, 13010–13015.

Detmer, S.A., and Chan, D.C. (2007). Functions and dysfunctions of mitochondrial dynamics. *Nature Reviews. Molecular Cell Biology*. *8*, 870–879.

Deuschl, G., Raethjen, J., Baron, R., et al. (2000). The pathophysiology of parkinsonian tremor: a review. *Journal of neurology*. *247 Suppl 5*, V33–V48.

Djarmati, A., Hedrich, K., Svetel, M., et al. (2004). Detection of Parkin (PARK2) and DJ1 (PARK7) mutations in early-onset Parkinson disease: Parkin mutation frequency depends on ethnic origin of patients. *Human Mutation*. *23*, 525–525.

Dobrowolski, S.F., Ellingson, C.E., Caldovic, L., et al. (2007). Streamlined assessment of gene variants by high resolution melt profiling utilizing the ornithine transcarbamylase gene as a model system. *Human Mutation*. *28*, 1133–1140.

Doherty, K.M., Silveira-Moriyama, L., Parkkinen, L., et al. (2013). Parkin disease: a clinicopathologic entity? *JAMA neurology*. *70*, 571–579.

Dolat, L., Hu, Q., and Spiliotis, E.T. (2014). Septin functions in organ system physiology and pathology. *Biological Chemistry*. *395*, 123–141.

Dong, Z., Ferger, B., Paterna, J.-C., et al. (2003). Dopamine-dependent neurodegeneration in rats induced by viral vector-mediated overexpression of the parkin target protein, CDCrel-1. *Proceedings of the National Academy of Sciences of the United States of America*. *100*, 12438–12443.

Dorsey, E.R., Constantinescu, R., Thompson, J.P., et al. (2007). Projected number of people with Parkinson disease in the most populous nations, 2005 through 2030. *Neurology*. *68*, 384–386.

Doss-Pepe, E.W., Chen, L., and Madura, K. (2005). Alpha-synuclein and parkin contribute to the assembly of ubiquitin lysine 63-linked multiubiquitin chains. *The Journal of Biological Chemistry*. *280*, 16619–16624.

Dove, K.K., and Klevit, R.E. (2013). Structural Biology: Parkin's Serpentine Shape Revealed in the Year of the Snake. *Current biology: CB*. *23*, R691–R693.

Driver, J.A., Kurth, T., Buring, J.E., et al. (2008). Parkinson disease and risk of mortality: a prospective comorbidity-matched cohort study. *Neurology*. *70*, 1423–1430.

Driver, J.A., Logroscino, G., Gaziano, J.M., et al. (2009). Incidence and remaining lifetime risk of Parkinson disease in advanced age. *Neurology*. *72*, 432–438.

Dunn, K.W., Kamocka, M.M., and McDonald, J.H. (2011). A practical guide to evaluating colocalization in biological microscopy. *American Journal of Physiology. Cell Physiology*. *300*, C723–C742.

Den Dunnen, J.T., and Antonarakis, S.E. (2000). Mutation nomenclature extensions and suggestions to describe complex mutations: a discussion. *Human mutation*. *15*, 7–12.

Duplan, E., Sevalle, J., Viotti, J., et al. (2013). Parkin differently regulates presenilin-1 and presenilin-2 functions by direct control of their promoter transcription. *Journal of Molecular Cell Biology*. *5*, 132–142.

Durcan, T.M., and Fon, E.A. (2011). Mutant ataxin-3 promotes the autophagic degradation of parkin. *Autophagy*. *7*, 233–234.

Durcan, T.M., Kontogiannea, M., Thorarinsdottir, T., et al. (2011). The Machado-Joseph disease-associated mutant form of ataxin-3 regulates parkin ubiquitination and stability. *Human Molecular Genetics*. *20*, 141–154.

Dzamko, N., Deak, M., Hentati, F., et al. (2010). Inhibition of LRRK2 kinase activity leads to dephosphorylation of Ser(910)/Ser(935), disruption of 14-3-3 binding and altered cytoplasmic localization. *The Biochemical Journal*. *430*, 405–413.

Edvardson, S., Cinnamon, Y., Ta-Shma, A., et al. (2012). A deleterious mutation in DNAJC6 encoding the neuronal-specific clathrin-uncoating co-chaperone auxilin, is associated with juvenile parkinsonism. *PloS one*. *7*, e36458.

Edwards, A.M., Kus, B., Jansen, R., et al. (2004). Bridging structural biology and genomics: assessing protein interaction data with known complexes. *Drug Discovery Today*. *9*, S32–S40.

Edwards, T.L., Scott, W.K., Almonte, C., et al. (2010). Genome-wide association study confirms SNPs in SNCA and the MAPT region as common risk factors for Parkinson disease. *Annals of human genetics*. *74*, 97–109.

Eisenhaber, B., Chumak, N., Eisenhaber, F., et al. (2007). The ring between ring fingers (RBR) protein family. *Genome biology*. *8*, 209.

Ekholm-Reed, S., Goldberg, M.S., Schlossmacher, M.G., et al. (2013). Parkin-dependent degradation of the F-box protein Fbw7β promotes neuronal survival in response to oxidative stress by stabilizing Mcl-1. *Molecular and cellular biology*. *33*, 3627–3643.

Eslamboli, A., Romero-Ramos, M., Burger, C., et al. (2007). Long-term consequences of human alpha-synuclein overexpression in the primate ventral midbrain. *Brain: a journal of neurology*. *130*, 799–815.

Exner, N., Treske, B., Paquet, D., et al. (2007). Loss-of-function of human PINK1 results in mitochondrial pathology and can be rescued by parkin. *The Journal of Neuroscience: The Official Journal of the Society for Neuroscience*. *27*, 12413–12418.

Exner, N., Lutz, A.K., Haass, C., et al. (2012). Mitochondrial dysfunction in Parkinson's disease: molecular mechanisms and pathophysiological consequences. *The EMBO journal*. *31*, 3038–3062.

Fallon, L., Moreau, F., Croft, B.G., et al. (2002). Parkin and CASK/LIN-2 associate via a PDZ-mediated interaction and are co-localized in lipid rafts and postsynaptic densities in brain. *The Journal of biological chemistry*. *277*, 486–491.

Fallon, L., Bélanger, C.M.L., Corera, A.T., et al. (2006). A regulated interaction with the UIM protein Eps15 implicates parkin in EGF receptor trafficking and PI(3)K-Akt signalling. *Nature cell biology*. *8*, 834–842.

Farias, F.H.G., Zeng, R., Johnson, G.S., et al. (2011). A truncating mutation in ATP13A2 is responsible for adult-onset neuronal ceroid lipofuscinosis in Tibetan terriers. *Neurobiology of disease*. *42*, 468–474.

Farrer, M., Chan, P., Chen, R., et al. (2001). Lewy bodies and parkinsonism in families with parkin mutations. *Annals of neurology*. *50*, 293–300.

Fearnley, J.M., and Lees, A.J. (1991). Ageing and Parkinson's disease: substantia nigra regional selectivity. *Brain: a journal of neurology*. *114 (Pt 5)*, 2283–2301.

Fénelon, G. (2008). Psychosis in Parkinson's disease: phenomenology, frequency, risk factors, and current understanding of pathophysiologic mechanisms. *CNS spectrums*. *13*, 18–25.

Ferrick, D.A., Neilson, A., and Beeson, C. (2008). Advances in measuring cellular bioenergetics using extracellular flux. *Drug Discovery Today*. *13*, 268–274.

Field, C.M., and Kellogg, D. (1999). Septins: cytoskeletal polymers or signalling GTPases? *Trends in cell biology*. *9*, 387–394.

Fields, S., and Song, O. (1989). A novel genetic system to detect protein-protein interactions. *Nature*. *340*, 245–246.

Di Fonzo, A., Wu-Chou, Y.-H., Lu, C.-S., et al. (2006). A common missense variant in the LRRK2 gene, Gly2385Arg, associated with Parkinson's disease risk in Taiwan. *Neurogenetics*. *7*, 133–138.

Di Fonzo, A., Dekker, M.C.J., Montagna, P., et al. (2009). FBXO7 mutations cause autosomal recessive, early-onset parkinsonian-pyramidal syndrome. *Neurology*. *72*, 240–245.

Fornai, F., Schlüter, O.M., Lenzi, P., et al. (2005). Parkinson-like syndrome induced by continuous MPTP infusion: convergent roles of the ubiquitin-proteasome system and alpha-synuclein. *Proceedings of the National Academy of Sciences of the United States of America*. *102*, 3413–3418.

Foroud, T., Uniacke, S.K., Liu, L., et al. (2003). Heterozygosity for a mutation in the parkin gene leads to later onset Parkinson disease. *Neurology*. *60*, 796–801.

Fox, J. (2003). Effect displays in R for generalised linear models. *Journal of Statistical Software*. *8*, 1–27.

Fraser, K.B., Moehle, M.S., Daher, J.P.L., et al. (2013). LRRK2 secretion in exosomes is regulated by 14-3-3. *Human Molecular Genetics*. *22*, 4988–5000.

Fuchs, J., Nilsson, C., Kachergus, J., et al. (2007). Phenotypic variation in a large Swedish pedigree due to SNCA duplication and triplication. *Neurology*. *68*, 916–922.

Fujiwara, M., Marusawa, H., Wang, H.-Q., et al. (2008). Parkin as a tumor suppressor gene for hepatocellular carcinoma. *Oncogene*. *27*, 6002–6011.

Fukae, J., Sato, S., Shiba, K., et al. (2009). Programmed cell death-2 isoform1 is ubiquitinated by parkin and increased in the substantia nigra of patients with autosomal recessive Parkinson's disease. *FEBS Letters*. *583*, 521–525.

Fulga, T.A., Elson-Schwab, I., Khurana, V., et al. (2007). Abnormal bundling and accumulation of F-actin mediates tau-induced neuronal degeneration in vivo. *Nature Cell Biology*. *9*, 139–148.

Fung, H.C., Xiromerisiou, G., Gibbs, J.R., et al. (2006). Association of tau haplotype-tagging polymorphisms with Parkinson's disease in diverse ethnic Parkinson's disease cohorts. *Neuro-degenerative diseases*. *3*, 327–333.

Gallagher, D.A., Lees, A.J., and Schrag, A. (2010). What are the most important nonmotor symptoms in patients with Parkinson's disease and are we missing them? *Movement disorders: official journal of the Movement Disorder Society*. *25*, 2493–2500.

Ganapathy-Kanniappan, S., Geschwind, J.-F.H., Kunjithapatham, R., et al. (2010). The pyruvic acid analog 3-bromopyruvate interferes with the tetrazolium reagent MTS in the evaluation of cytotoxicity. *Assay and Drug Development Technologies*. *8*, 258–262.

Gegg, M.E., Cooper, J.M., Chau, K.-Y., et al. (2010). Mitofusin 1 and mitofusin 2 are ubiquitinated in a PINK1/parkin-dependent manner upon induction of mitophagy. *Human Molecular Genetics*. *19*, 4861–4870.

Geisler, S., Holmström, K.M., Skujat, D., et al. (2010). PINK1/Parkin-mediated mitophagy is dependent on VDAC1 and p62/SQSTM1. *Nature Cell Biology*. *12*, 119–131.

Geleijnse, J.M., Vermeer, C., Grobbee, D.E., et al. (2004). Dietary intake of menaquinone is associated with a reduced risk of coronary heart disease: the Rotterdam Study. *The Journal of Nutrition*. *134*, 3100–3105.

Giasson, B.I., Uryu, K., Trojanowski, J.Q., et al. (1999). Mutant and wild type human alpha-synucleins assemble into elongated filaments with distinct morphologies in vitro. *The Journal of Biological Chemistry*. *274*, 7619–7622.

Gibb, W.R., and Lees, A.J. (1988a). The relevance of the Lewy body to the pathogenesis of idiopathic Parkinson's disease. *Journal of neurology, neurosurgery, and psychiatry*. *51*, 745–752.

Gibb, W.R., and Lees, A.J. (1988b). A comparison of clinical and pathological features of young- and old-onset Parkinson's disease. *Neurology*. *38*, 1402–1406.

Gietz, R.D. (2006). Yeast two-hybrid system screening. *Methods in Molecular Biology*. *313*, 345–371.

Giladi, N., Kao, R., and Fahn, S. (1997). Freezing phenomenon in patients with parkinsonian syndromes. *Movement disorders: official journal of the Movement Disorder Society*. *12*, 302–305.

Glauser, L., Sonnay, S., Stafa, K., et al. (2011). Parkin promotes the ubiquitination and degradation of the mitochondrial fusion factor mitofusin 1. *Journal of Neurochemistry*. *118*, 636–645.

Golan, M., and Mabjeesh, N.J. (2013). SEPT9_i1 is required for the association between HIF-1α and importin-α to promote efficient nuclear translocation. *Cell Cycle*. *12*, 2297–2308.

Gourlay, C.W., and Ayscough, K.R. (2005). The actin cytoskeleton: a key regulator of apoptosis and ageing? *Nature Reviews. Molecular Cell Biology*. *6*, 583–589.

Greene, J.C., Whitworth, A.J., Kuo, I., et al. (2003). Mitochondrial pathology and apoptotic muscle degeneration in Drosophila parkin mutants. *Proceedings of the National Academy of Sciences of the United States of America*. *100*, 4078.

Greenfield, J., and Bosanquet, F. (1953). The brain-stem lesions in Parkinsonism. *Journal of neurology, neurosurgery, and psychiatry*. *16*, 213–226.

Greffard, S., Verny, M., Bonnet, A.-M., et al. (2006). Motor score of the Unified Parkinson Disease Rating Scale as a good predictor of Lewy body-associated neuronal loss in the substantia nigra. *Archives of neurology*. *63*, 584–588.

Gregory, A., Westaway, S.K., Holm, I.E., et al. (2008). Neurodegeneration associated with genetic defects in phospholipase A(2). *Neurology*. *71*, 1402–1409.

Grover, D., Verma, R., Goes, F.S., et al. (2009). Family-based association of YWHAH in psychotic bipolar disorder. *American journal of medical genetics. Part B, Neuropsychiatric genetics : the official publication of the International Society of Psychiatric Genetics*. *150B*, 977–983.

Grünblatt, E., Mandel, S., Jacob-Hirsch, J., et al. (2004). Gene expression profiling of parkinsonian substantia nigra pars compacta; alterations in ubiquitin-proteasome, heat shock protein, iron and oxidative stress regulated proteins, cell adhesion/cellular matrix and vesicle trafficking genes. *Journal of Neural Transmission. 111*, 1543–1573.

Grunewald, A., Voges, L., Rakovic, A., et al. (2010). Mutant parkin impairs mitochondrial function and morphology in human fibroblasts. *PLoS ONE*. *5*, e12962.

Grützmann, R., Molnar, B., Pilarsky, C., et al. (2008). Sensitive detection of colorectal cancer in peripheral blood by septin 9 DNA methylation assay. *PloS One*. *3*, e3759.

Gu, J., Ajani, J.A., Hawk, E.T., et al. (2010). Genome-wide catalogue of chromosomal aberrations in barrett's esophagus and esophageal adenocarcinoma: a high-density single nucleotide polymorphism array analysis. *Cancer Prevention Research*. *3*, 1176–1186.

Guo, D., Rajamäki, M.-L., and Valkonen, J. (2008). Protein-protein interactions: the yeast two-hybrid system. *Methods in Molecular Biology*. *451*, 421–439.

Guo, J., Wang, L., He, D., et al. (2011). Clinical features and [11C]-CFT PET analysis of PARK2, PARK6, PARK7-linked autosomal recessive early onset Parkinsonism. *Neurological Sciences: Official Journal of the Italian Neurological Society and of the Italian Society of Clinical Neurophysiology*. *32*, 35–40.

Gwinn-Hardy, K., Mehta, N.D., Farrer, M., et al. (2000). Distinctive neuropathology revealed by alpha-synuclein antibodies in hereditary parkinsonism and dementia linked to chromosome 4p. *Acta neuropathologica*. *99*, 663–672.

Gwinn-Hardy, K., Singleton, A., O'Suilleabhain, P., et al. (2001). Spinocerebellar ataxia type 3 phenotypically resembling parkinson disease in a black family. *Archives of Neurology*. *58*, 296–299.

Habu, D., Shiomi, S., Tamori, A., et al. (2004). Role of vitamin K2 in the development of hepatocellular carcinoma in women with viral cirrhosis of the liver. *JAMA*. *292*, 358–361.

Haddock, B.A., and Jones, C.W. (1977). Bacterial respiration. *Bacteriological Reviews*. *41*, 47–99.

Hall, T. (1999). BioEdit: a user-friendly biological sequence alignment editor and analysis program for Windows 95/98/NT. *Nucleic acids symposium series*. *41*, 95–98.

Hall, P.A., Jung, K., Hillan, K.J., et al. (2005). Expression profiling the human septin gene family. *The Journal of Pathology*. *206*, 269–278.

Halliday, G.M., McRitchie, D.A., Cartwright, H., et al. (1996). Midbrain neuropathology in idiopathic Parkinson's disease and diffuse Lewy body disease. *Journal of Clinical Neuroscience: Official Journal of the Neurosurgical Society of Australasia*. *3*, 52–60.

Hampe, C., Ardila-Osorio, H., Fournier, M., et al. (2006). Biochemical analysis of Parkinson's disease-causing variants of Parkin, an E3 ubiquitin–protein ligase with monoubiquitylation capacity. *Human molecular genetics*. *15*, 2059.

Hansen, C., Angot, E., Bergström, A.-L., et al. (2011). α-Synuclein propagates from mouse brain to grafted dopaminergic neurons and seeds aggregation in cultured human cells. *The Journal of clinical investigation*. *121*, 715–725.

Harper, J.M., Salmon, A.B., Leiser, S.F., et al. (2007). Skin-derived fibroblasts from long-lived species are resistant to some, but not all, lethal stresses and to the mitochondrial inhibitor rotenone. *Aging Cell*. *6*, 1–13.

Harper, J.W., Adami, G.R., Wei, N., et al. (1993). The p21 Cdk-interacting protein Cip1 is a potent inhibitor of G1 cyclin-dependent kinases. *Cell*. *75*, 805–816.

Harterink, M., Port, F., Lorenowicz, M.J., et al. (2011). A SNX3-dependent retromer pathway mediates retrograde transport of the Wnt sorting receptor Wntless and is required for Wnt secretion. *Nature cell biology*. *13*, 914–923.

Hasegawa, T., Treis, A., Patenge, N., et al. (2008). Parkin protects against tyrosinase-mediated dopamine neurotoxicity by suppressing stress-activated protein kinase pathways. *Journal of neurochemistry*. *105*, 1700–1715.

Haskin, J., Szargel, R., Shani, V., et al. (2013). AF-6 is a positive modulator of the PINK1/parkin pathway and is deficient in Parkinson's disease. *Human Molecular Genetics*. *22*, 2083–2096.

Hassler, R. (1938). Zur Pathologie der Paralysis agitans und des postenzephalitischen Parkinsonismus. *Journal für Psychologie und Neurologie*. *48*, 387–476.

Hasson, S.A., Kane, L.A., Yamano, K., et al. (2013). High-content genome-wide RNAi screens identify regulators of parkin upstream of mitophagy. *Nature*. *504*, 291–295.

Haylett, W.L., Keyser, R.J., du Plessis, M.C., et al. (2012). Mutations in the parkin gene are a minor cause of Parkinson's disease in the South African population. *Parkinsonism & Related Disorders*. *18*, 89–92.

Healy, D.G., Falchi, M., O'Sullivan, S.S., et al. (2008). Phenotype, genotype, and worldwide genetic penetrance of LRRK2-associated Parkinson's disease: a case-control study. *Lancet Neurology*. *7*, 583–590.

Hebron, M.L., Lonskaya, I., Sharpe, K., et al. (2013). Parkin ubiquitinates Tar-DNA binding protein-43 (TDP-43) and promotes its cytosolic accumulation via interaction with histone deacetylase 6 (HDAC6). *The Journal of Biological Chemistry*. *288*, 4103–4115.

Hedrich, K., Kann, M., Lanthaler, A.J., et al. (2001). The importance of gene dosage studies: mutational analysis of the parkin gene in early-onset parkinsonism. *Human Molecular Genetics*. *10*, 1649–1656.

Hedrich, K., Marder, K., Harris, J., et al. (2002). Evaluation of 50 probands with early-onset Parkinson's disease for Parkin mutations. *Neurology*. *58*, 1239–1246.

Hedrich, K., Eskelson, C., Wilmot, B., et al. (2004). Distribution, type, and origin of Parkin mutations: review and case studies. *Movement disorders: official journal of the Movement Disorder Society*. *19*, 1146–1157.

Van der Heiden, M.G., Cantley, L.C., and Thompson, C.B. (2009). Understanding the Warburg effect: the metabolic requirements of cell proliferation. *Science*. *324*, 1029–1033.

Heider, M.R., and Munson, M. (2012). Exorcising the exocyst complex. *Traffic*. *13*, 898–907.

Henchcliffe, C., and Beal, M.F. (2008). Mitochondrial biology and oxidative stress in Parkinson disease pathogenesis. *Nature Clinical Practice. Neurology*. *4*, 600–609.

Henn, I.H., Bouman, L., Schlehe, J.S., et al. (2007). Parkin mediates neuroprotection through activation of IkappaB kinase/nuclear factor-kappaB signaling. *The Journal of neuroscience: the official journal of the Society for Neuroscience*. *27*, 1868–1878.

Herlofson, K., Lie, S.A., Arsland, D., et al. (2004). Mortality and Parkinson disease: A community based study. *Neurology*. *62*, 937–942.

Hernán, M.A., Takkouche, B., Caamaño-Isorna, F., et al. (2002). A meta-analysis of coffee drinking, cigarette smoking, and the risk of Parkinson's disease. *Annals of Neurology*. *52*, 276–284.

Hershko, A., and Ciechanover, A. (1998). The ubiquitin system. *Annual Review of Biochemistry*. *67*, 425–479.

Hirtz, D., Thurman, D.J., Gwinn-Hardy, K., et al. (2007). How common are the "common" neurologic disorders? *Neurology*. *68*, 326–337.

Hömig-Hölzel, C., and Savola, S. (2012). Multiplex ligation-dependent probe amplification (MLPA) in tumor diagnostics and prognostics. *Diagnostic Molecular Pathology: The American Journal of Surgical Pathology, Part B. 21*, 189–206.

Hornykiewicz, O. (2008). Basic research on dopamine in Parkinson's disease and the discovery of the nigrostriatal dopamine pathway: the view of an eyewitness. *Neuro-degenerative diseases*. *5*, 114–117.

Hristova, V.A., Beasley, S.A., Rylett, R.J., et al. (2009). Identification of a Novel Zn2+-binding Domain in the Autosomal Recessive Juvenile Parkinson-related E3 Ligase Parkin. *Journal of Biological Chemistry*. *284*, 14978–14986.

Hsu, S.C., Hazuka, C.D., Roth, R., et al. (1998). Subunit composition, protein interactions, and structures of the mammalian brain sec6/8 complex and septin filaments. *Neuron*. *20*, 1111–1122.

Huang, H., Jedynak, B.M., and Bader, J.S. (2007). Where have all the interactions gone? Estimating the coverage of two-hybrid protein interaction maps. *PLoS computational biology*. *3*, e214.

Hughes, A.J., Daniel, S.E., Blankson, S., et al. (1993). A clinicopathologic study of 100 cases of Parkinson's disease. *Archives of neurology*. *50*, 140–148.

Hughes, A.J., Daniel, S.E., and Lees, A.J. (2001). Improved accuracy of clinical diagnosis of Lewy body Parkinson's disease. *Neurology*. *57*, 1497–1499.

Humbeeck, C.V., Cornelissen, T., Hofkens, H., et al. (2011). Parkin interacts with Ambra1 to induce mitophagy. *The Journal of Neuroscience*. *31*, 10249–10261.

Hunot, S., Vila, M., Teismann, P., et al. (2004). JNK-mediated induction of cyclooxygenase 2 is required for neurodegeneration in a mouse model of Parkinson's disease. *Proceedings of the National Academy of Sciences of the United States of America*. *101*, 665–670.

Huynh, D.P., Scoles, D.R., Ho, T.H., et al. (2000). Parkin is associated with actin filaments in neuronal and nonneural cells. *Annals of Neurology*. *48*, 737–744.

Huynh, D.P., Scoles, D.R., Nguyen, D., et al. (2003). The autosomal recessive juvenile Parkinson disease gene product, parkin, interacts with and ubiquitinates synaptotagmin XI. *Human Molecular Genetics*. *12*, 2587–2597.

Huynh, D.P., Nguyen, D.T., Pulst-Korenberg, J.B., et al. (2007). Parkin is an E3 ubiquitin-ligase for normal and mutant ataxin-2 and prevents ataxin-2-induced cell death. *Experimental neurology*. *203*, 531–541.

Ibáñez, P., Lesage, S., Janin, S., et al. (2009). Alpha-synuclein gene rearrangements in dominantly inherited parkinsonism: frequency, phenotype, and mechanisms. *Archives of neurology*. *66*, 102–108.

Ichikawa, T., Horie-Inoue, K., Ikeda, K., et al. (2007). Vitamin K2 induces phosphorylation of protein kinase A and expression of novel target genes in osteoblastic cells. *Journal of Molecular Endocrinology*. *39*, 239–247.

Ihara, M., Tomimoto, H., Kitayama, H., et al. (2003). Association of the cytoskeletal GTP-binding protein Sept4/H5 with cytoplasmic inclusions found in Parkinson's disease and other synucleinopathies. *Journal of Biological Chemistry*. *278*, 24095–24102.

Ihara, M., Yamasaki, N., Hagiwara, A., et al. (2007). Sept4, a component of presynaptic scaffold and Lewy bodies, is required for the suppression of alpha-synuclein neurotoxicity. *Neuron*. *53*, 519–533.

Ii, K., Ito, H., Tanaka, K., et al. (1997). Immunocytochemical co-localization of the proteasome in ubiquitinated structures in neurodegenerative diseases and the elderly. *Journal of Neuropathology and Experimental Neurology*. *56*, 125–131.

Ikeuchi, K., Marusawa, H., Fujiwara, M., et al. (2009). Attenuation of proteolysis-mediated cyclin E regulation by alternatively spliced Parkin in human colorectal cancers. *International Journal of Cancer*. *125*, 2029–2035.

Imai, Y., Soda, M., and Takahashi, R. (2000). Parkin suppresses unfolded protein stress-induced cell death through its E3 ubiquitin-protein ligase activity. *The Journal of biological chemistry*. *275*, 35661–35664.

Imai, Y., Soda, M., Inoue, H., et al. (2001). An unfolded putative transmembrane polypeptide, which can lead to endoplasmic reticulum stress, is a substrate of Parkin. *Cell*. *105*, 891–902.

Imai, Y., Soda, M., Hatakeyama, S., et al. (2002). CHIP is associated with Parkin, a gene responsible for familial Parkinson's disease, and enhances its ubiquitin ligase activity. *Molecular Cell*. *10*, 55–67.

Imai, Y., Soda, M., Murakami, T., et al. (2003). A product of the human gene adjacent to parkin is a component of Lewy bodies and suppresses Pael receptor-induced cell death. *The Journal of Biological Chemistry*. *278*, 51901–51910.

Imam, S.Z., Zhou, Q., Yamamoto, A., et al. (2011). Novel regulation of parkin function through c-Abl-mediated tyrosine phosphorylation: implications for Parkinson's disease. *The Journal of Neuroscience: The Official Journal of the Society for Neuroscience*. *31*, 157–163.

Inestrosa, N.C., Marzolo, M.P., and Bonnefont, A.B. (1998). Cellular and molecular basis of estrogen's neuroprotection. Potential relevance for Alzheimer's disease. *Molecular neurobiology*. *17*, 73–86.

International Parkinson's Disease Genomics Consortium (IPDGC), and Wellcome Trust Case Control Consortium 2 (WTCCC2) (2011). A two-stage meta-analysis identifies several new loci for Parkinson's disease. *PLoS genetics*. *7*, e1002142.

Iranzo, A., Molinuevo, J.L., Santamaría, J., et al. (2006). Rapid-eye-movement sleep behaviour disorder as an early marker for a neurodegenerative disorder: a descriptive study. *Lancet neurology*. *5*, 572–577.

Ito, A., Shirakawa, H., Takumi, N., et al. (2011). Menaquinone-4 enhances testosterone production in rats and testis-derived tumor cells. *Lipids in Health and Disease*. *10*, 158–177.

Ito, T., Chiba, T., Ozawa, R., et al. (2001). A comprehensive two-hybrid analysis to explore the yeast protein interactome. *Proceedings of the National Academy of Sciences of the United States of America*. *98*, 4569–4574.

Iwakawa, R., Okayama, H., Kohno, T., et al. (2012). Contribution of germline mutations to PARK2 gene inactivation in lung adenocarcinoma. *Genes, Chromosomes & Cancer*. *51*, 462–472.

Jabbar, S.A., Twentyman, P.R., and Watson, J.V. (1989). The MTT assay underestimates the growth inhibitory effects of interferons. *British Journal of Cancer*. *60*, 523–528.

Jaleel, M., Nichols, R.J., Deak, M., et al. (2007). LRRK2 phosphorylates moesin at threonine-558: characterization of how Parkinson's disease mutants affect kinase activity. *The Biochemical Journal*. *405*, 307–317.

James, P., Halladay, J., and Craig, E.A. (1996). Genomic libraries and a host strain designed for highly efficient two-hybrid selection in yeast. *Genetics*. *144*, 1425–1436.

Janetzky, B., Hauck, S., Youdim, M.B., et al. (1994). Unaltered aconitase activity, but decreased complex I activity in substantia nigra pars compacta of patients with Parkinson's disease. *Neuroscience Letters*. *169*, 126–128.

Jankovic, J. (2008). Parkinson's disease: clinical features and diagnosis. *Journal of Neurology, Neurosurgery & Psychiatry*. *79*, 368–376.

Jiang, H., Jiang, Q., and Feng, J. (2004). Parkin increases dopamine uptake by enhancing the cell surface expression of dopamine transporter. *The Journal of Biological Chemistry*. *279*, 54380–54386.

Jiang, H., Jiang, Q., Liu, W., et al. (2006). Parkin suppresses the expression of monoamine oxidases. *The Journal of biological chemistry*. *281*, 8591–8599.

Jiang, Q., Ren, Y., and Feng, J. (2008). Direct binding with histone deacetylase 6 mediates the reversible recruitment of parkin to the centrosome. *The Journal of Neuroscience: The Official Journal of the Society for Neuroscience*. *28*, 12993–13002.

Joch, M., Ase, A.R., Chen, C.X.-Q., et al. (2007). Parkin-mediated monoubiquitination of the PDZ protein PICK1 regulates the activity of acid-sensing ion channels. *Molecular biology of the cell*. *18*, 3105–3118.

Johnson, B.N., Berger, A.K., Cortese, G.P., et al. (2012). The ubiquitin E3 ligase parkin regulates the proapoptotic function of Bax. *Proceedings of the National Academy of Sciences of the United States of America*. *109*, 6283–6288.

Jonckheere, A.I., Smeitink, J.A.M., and Rodenburg, R.J.T. (2012). Mitochondrial ATP synthase: architecture, function and pathology. *Journal of Inherited Metabolic Disease*. *35*, 211–225.

Jones, L.J., Gray, M., Yue, S.T., et al. (2001). Sensitive determination of cell number using the CyQUANT cell proliferation assay. *Journal of Immunological Methods*. *254*, 85–98.

Jost, W.H. (1997). Gastrointestinal motility problems in patients with Parkinson's disease. Effects of antiparkinsonian treatment and guidelines for management. *Drugs & aging*. *10*, 249–258.

Jucker, M., and Walker, L.C. (2013). Self-propagation of pathogenic protein aggregates in neurodegenerative diseases. *Nature*. *501*, 45–51.

Kahle, P.J., and Haass, C. (2004). How does parkin ligate ubiquitin to Parkinson's disease? *EMBO reports*. *5*, 681–685.

Kalaitzakis, M.E., Graeber, M.B., Gentleman, S.M., et al. (2008). Controversies over the staging of alpha-synuclein pathology in Parkinson's disease. *Acta neuropathologica*. *116*, 125–128.

Kalia, S.K., Lee, S., Smith, P.D., et al. (2004). BAG5 inhibits parkin and enhances dopaminergic neuron degeneration. *Neuron*. *44*, 931–945.

Kalikin, L.M., Sims, H.L., and Petty, E.M. (2000). Genomic and expression analyses of alternatively spliced transcripts of the MLL septin-like fusion gene (MSF) that map to a 17q25 region of loss in breast and ovarian tumors. *Genomics*. *63*, 165–172.

Kamel, F., Tanner, C., Umbach, D., et al. (2007). Pesticide exposure and self-reported Parkinson's disease in the agricultural health study. *American journal of epidemiology*. *165*, 364–374.

Kann, M., Jacobs, H., Mohrmann, K., et al. (2002). Role of parkin mutations in 111 community-based patients with early-onset parkinsonism. *Annals of neurology*. *51*, 621–625.

Kao, S.-Y. (2009). Regulation of DNA repair by parkin. *Biochemical and Biophysical Research Communications*. *382*, 321–325.

Kawajiri, S., Saiki, S., Sato, S., et al. (2011). Genetic mutations and functions of PINK1. *Trends in pharmacological sciences*. *32*, 573–580.

Kawamoto, Y., Akiguchi, I., Nakamura, S., et al. (2002). 14-3-3 proteins in Lewy bodies in Parkinson disease and diffuse Lewy body disease brains. *Journal of Neuropathology and Experimental Neurology*. *61*, 245–253.

Kay, D.M., Moran, D., Moses, L., et al. (2007). Heterozygous parkin point mutations are as common in control subjects as in Parkinson's patients. *Annals of Neurology*. *61*, 47–54.

Kay, D.M., Stevens, C.F., Hamza, T.H., et al. (2010). A comprehensive analysis of deletions, multiplications, and copy number variations in PARK2. *Neurology*. *75*, 1189–1194.

Keegan, L., Gill, G., and Ptashne, M. (1986). Separation of DNA binding from the transcription-activating function of a eukaryotic regulatory protein. *Science*. *231*, 699–704.

Kelly, D.P., and Scarpulla, R.C. (2004). Transcriptional regulatory circuits controlling mitochondrial biogenesis and function. *Genes & Development*. *18*, 357–368.

Kemeny, S., Dery, D., Loboda, Y., et al. (2012). Parkin promotes degradation of the mitochondrial pro-apoptotic ARTS protein. *PloS one*. *7*, e38837.

Keyser, R.J. (2011). Investigation of the genetic aetiology of Parkinson's disease in South Africa. Stellenbosch: University of Stellenbosch.

Keyser, R.J., Lombard, D., Veikondis, R., et al. (2009). Analysis of exon dosage using MLPA in South African Parkinson's disease patients. *Neurogenetics*. *11*, 305–312.

Khoo, T.K., Yarnall, A.J., Duncan, G.W., et al. (2013). The spectrum of nonmotor symptoms in early Parkinson disease. *Neurology*. *80*, 276–281.

Kieburtz, K., and Wunderle, K.B. (2013). Parkinson's disease: evidence for environmental risk factors. *Movement disorders: official journal of the Movement Disorder Society*. *28*, 8–13.

Kilarski, L.L., Pearson, J.P., Newsway, V., et al. (2012). Systematic review and UK-based study of PARK2 (parkin), PINK1, PARK7 (DJ-1) and LRRK2 in early-onset Parkinson's disease. *Movement disorders: official journal of the Movement Disorder Society*. *27*, 1522–1529.

Kim, K.-H., and Son, J.H. (2010). PINK1 gene knockdown leads to increased binding of parkin with actin filament. *Neuroscience Letters*. *468*, 272–276.

Kim, K., Kim, S.-H., Kim, J., et al. (2012). Glutathione s-transferase omega 1 activity is sufficient to suppress neurodegeneration in a Drosophila model of Parkinson disease. *The Journal of Biological Chemistry*. *287*, 6628–6641.

Kim, M.S., Froese, C.D., Estey, M.P., et al. (2011). SEPT9 occupies the terminal positions in septin octamers and mediates polymerization-dependent functions in abscission. *The Journal of Cell Biology*. *195*, 815–826.

Kinoshita, A., Kinoshita, M., Akiyama, H., et al. (1998). Identification of septins in neurofibrillary tangles in Alzheimer's disease. *The American journal of pathology*. *153*, 1551–1560.

Kitada, T., Asakawa, S., Hattori, N., et al. (1998). Mutations in the parkin gene cause autosomal recessive juvenile parkinsonism. *Nature*. *392*, 605–608.

Klein, C., Hedrich, K., Wellenbrock, C., et al. (2003). Frequency of parkin mutations in late-onset Parkinson's disease. *Annals of neurology*. *54*, 415–416.

Klein, C., Djarmati, A., Hedrich, K., et al. (2005). PINK1, Parkin, and DJ-1 mutations in Italian patients with early-onset parkinsonism. *European journal of human genetics: EJHG*. *13*, 1086–1093.

Klucken, J., Poehler, A.-M., Ebrahimi-Fakhari, D., et al. (2012). Alpha-synuclein aggregation involves a bafilomycin A 1-sensitive autophagy pathway. *Autophagy*. *8*, 754–766.

Ko, H.S. (2005). Accumulation of the authentic parkin substrate aminoacyl-tRNA synthetase cofactor, p38/JTV-1, leads to catecholaminergic cell death. *Journal of Neuroscience*. *25*, 7968–7978.

Ko, H.S. (2006). Identification of far upstream element-binding protein-1 as an authentic parkin substrate. *Journal of Biological Chemistry*. *281*, 16193–16196.

Ko, H.S., Lee, Y., Shin, J.-H., et al. (2010). Phosphorylation by the c-Abl protein tyrosine kinase inhibits parkin's ubiquitination and protective function. *Proceedings of the National Academy of Sciences of the United States of America*. *107*, 16691–16696.

Koegl, M., and Uetz, P. (2007). Improving yeast two-hybrid screening systems. *Briefings in Functional Genomics & Proteomics*. *6*, 302–312.

Koh, H., and Chung, J. (2012). PINK1 as a molecular checkpoint in the maintenance of mitochondrial function and integrity. *Molecules and cells*. *34*, 7–13.

Komander, D., and Rape, M. (2012). The ubiquitin code. *Annual review of biochemistry*. *81*, 203–229.

Kondapalli, C., Kazlauskaite, A., Zhang, N., et al. (2012). PINK1 is activated by mitochondrial membrane potential depolarization and stimulates Parkin E3 ligase activity by phosphorylating Serine 65. *Open Biology*. *2*, 120080.

Kordower, J.H., Chu, Y., Hauser, R.A., et al. (2008). Lewy body-like pathology in long-term embryonic nigral transplants in Parkinson's disease. *Nature medicine*. *14*, 504–506.

Koressaar, T., and Remm, M. (2007). Enhancements and modifications of primer design program Primer3. *Bioinformatics (Oxford, England)*. *23*, 1289–1291.

Köroğlu, Ç., Baysal, L., Cetinkaya, M., et al. (2013). DNAJC6 is responsible for juvenile parkinsonism with phenotypic variability. *Parkinsonism & related disorders*. *19*, 320–324.

Korutla, L., Furlong IV, H.A., and Mackler, S.A. (2014). NAC1, A POZ/BTB protein interacts with Parkin and may contribute to Parkinson's disease. *Neuroscience*. *257*, 86–95.

Koyano, F., Okatsu, K., Ishigaki, S., et al. (2013). The principal PINK1 and Parkin cellular events triggered in response to dissipation of mitochondrial membrane potential occur in primary neurons. *Genes to Cells: Devoted to Molecular & Cellular Mechanisms*. *18*, 672–681.

Koziorowski, D., Hoffman-Zacharska, D., Sławek, J., et al. (2010). Low frequency of the PARK2 gene mutations in Polish patients with the early-onset form of Parkinson disease. *Parkinsonism & related disorders*. *16*, 136–138.

Kravtsova-Ivantsiv, Y., and Ciechanover, A. (2012). Non-canonical ubiquitin-based signals for proteasomal degradation. *Journal of cell science*. *125*, 539–548.

Krebiehl, G., Ruckerbauer, S., Burbulla, L.F., et al. (2010). Reduced basal autophagy and impaired mitochondrial dynamics due to loss of Parkinson's disease-associated protein DJ-1. *PLoS ONE*. *5*, e9367.

Krebs, C.E., Karkheiran, S., Powell, J.C., et al. (2013). The Sac1 domain of SYNJ1 identified mutated in a family with early-onset progressive Parkinsonism with generalized seizures. *Human mutation*. *34*, 1200–1207.

Krüger, R., Vieira-Saecker, A.M., Kuhn, W., et al. (1999). Increased susceptibility to sporadic Parkinson's disease by a certain combined alpha-synuclein/apolipoprotein E genotype. *Annals of neurology*. *45*, 611–617.

Ku, S., and Glass, G.A. (2010). Age of Parkinson's disease onset as a predictor for the development of dyskinesia. *Movement disorders: official journal of the Movement Disorder Society*. *25*, 1177–1182.

Kubo, S.I., Kitami, T., Noda, S., et al. (2001). Parkin is associated with cellular vesicles. *Journal of neurochemistry*. *78*, 42–54.

Kudryashova, E., Kudryashov, D., Kramerova, I., et al. (2005). Trim32 is a ubiquitin ligase mutated in limb girdle muscular dystrophy type 2H that binds to skeletal muscle myosin and ubiquitinates actin. *Journal of Molecular Biology*. *354*, 413–424.

Kuhlenbäumer, G., Hannibal, M.C., Nelis, E., et al. (2005). Mutations in SEPT9 cause hereditary neuralgic amyotrophy. *Nature Genetics*. *37*, 1044–1046.

Kuopio, A.M., Marttila, R.J., Helenius, H., et al. (1999). Changing epidemiology of Parkinson's disease in southwestern Finland. *Neurology*. *52*, 302–308.

Kuroda, Y., Mitsui, T., Kunishige, M., et al. (2006a). Parkin enhances mitochondrial biogenesis in proliferating cells. *Human molecular genetics*. *15*, 883–895.

Kuroda, Y., Mitsui, T., Kunishige, M., et al. (2006b). Parkin affects mitochondrial function and apoptosis in neuronal and myogenic cells. *Biochemical and Biophysical Research Communications*. *348*, 787–793.

Kuroda, Y., Sako, W., Goto, S., et al. (2012). Parkin interacts with Klokin1 for mitochondrial import and maintenance of membrane potential. *Human Molecular Genetics*. *21*, 991–1003.

Kuzuhara, S., Mori, H., Izumiyama, N., et al. (1988). Lewy bodies are ubiquitinated. A light and electron microscopic immunocytochemical study. *Acta Neuropathologica*. *75*, 345–353.

Kwak, S., Masaki, T., Ishiura, S., et al. (1991). Multicatalytic proteinase is present in Lewy bodies and neurofibrillary tangles in diffuse Lewy body disease brains. *Neuroscience Letters*. *128*, 21–24.

Lai, B.C.L., Marion, S.A., Teschke, K., et al. (2002). Occupational and environmental risk factors for Parkinson's disease. *Parkinsonism & related disorders*. *8*, 297–309.

Lalonde, S., Ehrhardt, D.W., Loqué, D., et al. (2008). Molecular and cellular approaches for the detection of protein–protein interactions: latest techniques and current limitations. *The Plant Journal*. *53*, 610–635.

Lambeth, L.S., and Smith, C.A. (2013). Short hairpin RNA-mediated gene silencing. *Methods in Molecular Biology (Clifton, N.J.)*. *942*, 205–232.

Langston, J.W. (2006). The Parkinson's complex: parkinsonism is just the tip of the iceberg. *Annals of neurology*. *59*, 591–596.

Langston, J.W., Ballard, P., Tetrud, J.W., et al. (1983). Chronic Parkinsonism in humans due to a product of meperidine-analog synthesis. *Science*. *219*, 979–980.

Lappalainen, P., and Drubin, D.G. (1997). Cofilin promotes rapid actin filament turnover in vivo. *Nature*. *388*, 78–82.

Larisch, S., Yi, Y., Lotan, R., et al. (2000). A novel mitochondrial septin-like protein, ARTS, mediates apoptosis dependent on its P-loop motif. *Nature Cell Biology*. *2*, 915–921.

De Lau, L.M.L., and Breteler, M.M.B. (2006). Epidemiology of Parkinson's disease. *Lancet Neurology*. *5*, 525–535.

De Lau, L.M.L., Giesbergen, P.C.L.M., de Rijk, M.C., et al. (2004). Incidence of parkinsonism and Parkinson disease in a general population: the Rotterdam Study. *Neurology*. *63*, 1240–1244.

De Lau, L.M.L., Verbaan, D., Marinus, J., et al. (2014). Survival in Parkinson's disease. Relation with motor and non-motor features. *Parkinsonism & related disorders*. *20*, 613–616.

Lee, D.W., Rajagopalan, S., Siddiq, A., et al. (2009). Inhibition of prolyl hydroxylase protects against 1-methyl-4-phenyl-1,2,3,6-tetrahydropyridine-induced neurotoxicity: model for the potential involvement of the hypoxia-inducible factor pathway in Parkinson disease. *The Journal of Biological Chemistry*. *284*, 29065–29076.

Lee, J., Park, A.H., Lee, S.-H., et al. (2012a). Beta-lapachone, a modulator of NAD metabolism, prevents health declines in aged mice. *PloS One*. *7*, e47122.

Lee, S., Imai, Y., Gehrke, S., et al. (2012b). The synaptic function of LRRK2. *Biochemical Society Transactions*. *40*, 1047–1051.

Lee, Y., Karuppagounder, S.S., Shin, J.-H., et al. (2013). Parthanatos mediates AIMP2-activated age-dependent dopaminergic neuronal loss. *Nature neuroscience*. *16*, 1392–1400.

Lefebvre-Legendre, L., Salin, B., Schaëffer, J., et al. (2005). Failure to assemble the alpha 3 beta 3 subcomplex of the ATP synthase leads to accumulation of the alpha and beta subunits within inclusion bodies and the loss of mitochondrial cristae in Saccharomyces cerevisiae. *The Journal of Biological Chemistry*. *280*, 18386–18392.

Lennox, G., Lowe, J., Morrell, K., et al. (1989). Anti-ubiquitin immunocytochemistry is more sensitive than conventional techniques in the detection of diffuse Lewy body disease. *Journal of Neurology, Neurosurgery, and Psychiatry*. *52*, 67–71.

Lesage, S., Ibanez, P., Lohmann, E., et al. (2005). G2019S LRRK2 mutation in French and North African families with Parkinson's disease. *Annals of neurology*. *58*, 784–787.

Lesage, S., Dürr, A., Tazir, M., et al. (2006). LRRK2 G2019S as a cause of Parkinson's disease in North African Arabs. *The New England Journal of Medicine*. *354*, 422–423.

Lesage, S., Magali, P., Lohmann, E., et al. (2007). Deletion of the parkin and PACRG gene promoter in early-onset parkinsonism. *Human mutation*. *28*, 27–32.

Lesage, S., Condroyer, C., Klebe, S., et al. (2012a). Identification of VPS35 mutations replicated in French families with Parkinson disease. *Neurology*. *78*, 1449–1450.

Lesage, S., Condroyer, C., Klebe, S., et al. (2012b). EIF4G1 in familial Parkinson's disease: pathogenic mutations or rare benign variants? *Neurobiology of aging*. *33*, 2233.e1–e2233.e5.

Lesage, S., Anheim, M., Letournel, F., et al. (2013). G51D α-synuclein mutation causes a novel parkinsonian-pyramidal syndrome. *Annals of neurology*. *73*, 459–471.

Lev, N., Barhum, Y., Pilosof, N.S., et al. (2013). DJ-1 protects against dopamine toxicity: implications for Parkinson's disease and aging. *The journals of gerontology. Series A, Biological sciences and medical sciences*. *68*, 215–225.

Lewis, P.A., and Alessi, D.R. (2012). Deciphering the function of leucine-rich repeat kinase 2 and targeting its dysfunction in disease. *Biochemical Society transactions*. *40*, 1039–1041.

Lewis, P.A., Greggio, E., Beilina, A., et al. (2007). The R1441C mutation of LRRK2 disrupts GTP hydrolysis. *Biochemical and biophysical research communications*. *357*, 668–671.

Lewy, F. (1912). Paralysis agitans. I. Pathologische anatomie. In *Handbuch Der Neurologie*, pp. 920–933.

Li, J., Lin, J.C., Wang, H., et al. (2003). Novel role of vitamin k in preventing oxidative injury to developing oligodendrocytes and neurons. *The Journal of Neuroscience: The Official Journal of the Society for Neuroscience*. *23*, 5816–5826.

Li, J.-Y., Englund, E., Holton, J.L., et al. (2008). Lewy bodies in grafted neurons in subjects with Parkinson's disease suggest host-to-graft disease propagation. *Nature medicine*. *14*, 501–503.

Li, J.-Y., Englund, E., Widner, H., et al. (2010). Characterization of Lewy body pathology in 12- and 16-year-old intrastriatal mesencephalic grafts surviving in a patient with Parkinson's disease. *Movement disorders: official journal of the Movement Disorder Society*. *25*, 1091–1096.

Li, L., Wang, X., Fei, X., et al. (2011a). Parkinson's disease involves autophagy and abnormal distribution of cathepsin L. *Neuroscience Letters*. *489*, 62–67.

Li, X., Wang, Q.J., Pan, N., et al. (2011b). Phosphorylation-dependent 14-3-3 binding to LRRK2 is impaired by common mutations of familial Parkinson's disease. *PLoS ONE*. *6*, e17153.

Li, Y., Tomiyama, H., Sato, K., et al. (2005). Clinicogenetic study of PINK1 mutations in autosomal recessive early-onset parkinsonism. *Neurology*. *64*, 1955–1957.

Li, Y., Wan, O.W., Xie, W., et al. (2011c). p32 regulates mitochondrial morphology and dynamics through parkin. *Neuroscience*. *199*, 346–358.

Liang, C.-L., Wang, T.T., Luby-Phelps, K., et al. (2007). Mitochondria mass is low in mouse substantia nigra dopamine neurons: implications for Parkinson's disease. *Experimental Neurology*. *203*, 370–380.

Lieberman, A. (2006). Depression in Parkinson's disease -- a review. *Acta neurologica Scandinavica*. *113*, 1–8.

Lim, K.L. (2005). Parkin mediates nonclassical, proteasomal-independent ubiquitination of synphilin-1: implications for Lewy body formation. *Journal of Neuroscience*. *25*, 2002–2009.

Lim, K.L., Dawson, V.L., and Dawson, T.M. (2006). Parkin-mediated lysine 63-linked polyubiquitination: a link to protein inclusions formation in Parkinson's and other conformational diseases? *Neurobiology of aging*. *27*, 524–529.

Lim, M.K., Kawamura, T., Ohsawa, Y., et al. (2007). Parkin interacts with LIM Kinase 1 and reduces its cofilin-phosphorylation activity via ubiquitination. *Experimental Cell Research*. *313*, 2858–2874.

Lim, S.-Y., Fox, S.H., and Lang, A.E. (2009). Overview of the extranigral aspects of Parkinson disease. *Archives of neurology*. *66*, 167–172.

Lincoln, S., Wiley, J., Lynch, T., et al. (2003). Parkin-proven disease: common founders but divergent phenotypes. *Neurology*. *60*, 1605–1610.

Linder, J., Stenlund, H., and Forsgren, L. (2010). Incidence of Parkinson's disease and parkinsonism in northern Sweden: a population-based study. *Movement disorders: official journal of the Movement Disorder Society*. *25*, 341–348.

Lindersson, E., Beedholm, R., Højrup, P., et al. (2004). Proteasomal inhibition by alpha-synuclein filaments and oligomers. *The Journal of biological chemistry*. *279*, 12924–12934.

Litvan, I., Bhatia, K.P., Burn, D.J., et al. (2003). Movement Disorders Society Scientific Issues Committee report: SIC Task Force appraisal of clinical diagnostic criteria for Parkinsonian disorders. *Movement disorders: official journal of the Movement Disorder Society*. *18*, 467–486.

Liu, L., and Fan, X.-D. (2014). CRISPR-Cas system: a powerful tool for genome engineering. *Plant Molecular Biology*. *85*, 209–218.

Lonskaya, I., Shekoyan, A.R., Hebron, M.L., et al. (2013). Diminished parkin solubility and co-localization with intraneuronal amyloid-β are associated with autophagic defects in Alzheimer's disease. *Journal of Alzheimer's Disease*. *33*, 231–247.

Low, P.A. (2008). Prevalence of orthostatic hypotension. *Clinical autonomic research: official journal of the Clinical Autonomic Research Society*. *18 Suppl 1*, 8–13.

Lowe, J., McDermott, H., Landon, M., et al. (1990). Ubiquitin carboxyl-terminal hydrolase (PGP 9.5) is selectively present in ubiquitinated inclusion bodies characteristic of human neurodegenerative diseases. *The Journal of Pathology*. *161*, 153–160.

Lu, C.-S., Chang, H.-C., Kuo, P.-C., et al. (2004). The parkinsonian phenotype of spinocerebellar ataxia type 3 in a Taiwanese family. *Parkinsonism & Related Disorders*. *10*, 369–373.

Lücking, C.B., D\ürr, A., Bonifati, V., et al. (2000). Association between early-onset Parkinson's disease and mutations in the parkin gene. *New England Journal of Medicine*. *342*, 1560–1567.

Ludlam, A., Brunzelle, J., Pribyl, T., et al. (2009). Chaperones of F1-ATPase. *Journal of Biological Chemistry*. *284*, 17138–17146.

Luk, K.C., Song, C., O'Brien, P., et al. (2009). Exogenous alpha-synuclein fibrils seed the formation of Lewy body-like intracellular inclusions in cultured cells. *Proceedings of the National Academy of Sciences of the United States of America*. *106*, 20051–20056.

Luk, K.C., Kehm, V.M., Zhang, B., et al. (2012). Intracerebral inoculation of pathological α-synuclein initiates a rapidly progressive neurodegenerative α-synucleinopathy in mice. *The Journal of experimental medicine*. *209*, 975–986.

Lundblad, M., Decressac, M., Mattsson, B., et al. (2012). Impaired neurotransmission caused by overexpression of α-synuclein in nigral dopamine neurons. *Proceedings of the National Academy of Sciences of the United States of America*. *109*, 3213–3219.

Lutz, A.K., Exner, N., Fett, M.E., et al. (2009). Loss of parkin or PINK1 function increases Drp1-dependent mitochondrial fragmentation. *The Journal of Biological Chemistry*. *284*, 22938–22951.

Maass, A., and Reichmann, H. (2013). Sleep and non-motor symptoms in Parkinson's disease. *Journal of neural transmission (Vienna, Austria: 1996)*. *120*, 565–569.

Macedo, M.G., Anar, B., Bronner, I.F., et al. (2003). The DJ-1L166P mutant protein associated with early onset Parkinson's disease is unstable and forms higher-order protein complexes. *Human molecular genetics*. *12*, 2807–2816.

Mackintosh, C. (2004). Dynamic interactions between 14-3-3 proteins and phosphoproteins regulate diverse cellular processes. *The Biochemical Journal*. *381*, 329–342.

Macleod, A.D., Taylor, K.S.M., and Counsell, C.E. (2014). Mortality in Parkinson's disease: A systematic review and meta-analysis. *Movement Disorders*. n/a – n/a.

MacLeod, D.A., Rhinn, H., Kuwahara, T., et al. (2013). RAB7L1 interacts with LRRK2 to modify intraneuronal protein sorting and Parkinson's disease risk. *Neuron*. *77*, 425–439.

Mahdavi, M.A., and Lin, Y.-H. (2007). False positive reduction in protein-protein interaction predictions using gene ontology annotations. *BMC bioinformatics*. *8*, 262–272.

Malgieri, G., and Eliezer, D. (2008). Structural effects of Parkinson's disease linked DJ-1 mutations. *Protein science: a publication of the Protein Society*. *17*, 855–868.

Manyam, B.V. (1990). Paralysis agitans and levodopa in "Ayurveda": ancient Indian medical treatise. *Movement disorders*. *5*, 47–48.

Manzanillo, P.S., Ayres, J.S., Watson, R.O., et al. (2013). PARKIN ubiquitin ligase mediates resistance to intracellular pathogens. *Nature*. *501*, 512–516.

Mao, H., Liu, J., Shi, W., et al. (2013). The expression patterns of Septin-9 after traumatic brain injury in rat brain. *Journal of Molecular Neuroscience*. *51*, 558–566.

Maraganore, D.M., de Andrade, M., Elbaz, A., et al. (2006). Collaborative analysis of alpha-synuclein gene promoter variability and Parkinson disease. *JAMA: the journal of the American Medical Association*. *296*, 661–670.

Martin, L.J., Pan, Y., Price, A.C., et al. (2006). Parkinson's disease alpha-synuclein transgenic mice develop neuronal mitochondrial degeneration and cell death. *The Journal of neuroscience: the official journal of the Society for Neuroscience*. *26*, 41–50.

Martinez-Martin, P., Schapira, A.H.V., Stocchi, F., et al. (2007). Prevalence of nonmotor symptoms in Parkinson's disease in an international setting; study using nonmotor symptoms questionnaire in 545 patients. *Movement disorders: official journal of the Movement Disorder Society*. *22*, 1623–1629.

Masliah, E., Rockenstein, E., Veinbergs, I., et al. (2000). Dopaminergic loss and inclusion body formation in alpha-synuclein mice: implications for neurodegenerative disorders. *Science*. *287*, 1265–1269.

Mata, I.F., Kachergus, J.M., Taylor, J.P., et al. (2005). Lrrk2 pathogenic substitutions in Parkinson's disease. *Neurogenetics*. *6*, 171–177.

Matinolli, M., Korpelainen, J.T., Korpelainen, R., et al. (2009). Orthostatic hypotension, balance and falls in Parkinson's disease. *Movement disorders: official journal of the Movement Disorder Society*. *24*, 745–751.

Matsuda, N., Sato, S., Shiba, K., et al. (2010). PINK1 stabilized by mitochondrial depolarization recruits Parkin to damaged mitochondria and activates latent Parkin for mitophagy. *The Journal of cell biology*. *189*, 211–221.

Matsuda, W., Furuta, T., Nakamura, K.C., et al. (2009). Single nigrostriatal dopaminergic neurons form widely spread and highly dense axonal arborizations in the neostriatum. *The Journal of Neuroscience: The Official Journal of the Society for Neuroscience*. *29*, 444–453.

Mayeux, R., Marder, K., Cote, L.J., et al. (1995). The frequency of idiopathic Parkinson's disease by age, ethnic group, and sex in northern Manhattan, 1988-1993. *American journal of epidemiology*. *142*, 820–827.

Mazzulli, J.R., Xu, Y.-H., Sun, Y., et al. (2011). Gaucher disease glucocerebrosidase and α-synuclein form a bidirectional pathogenic loop in synucleinopathies. *Cell*. *146*, 37–52.

McCoy, M.K., Kaganovich, A., Rudenko, I.N., et al. (2014). Hexokinase activity is required for recruitment of parkin to depolarized mitochondria. *Human Molecular Genetics*. *23*, 145–156.

McGough, I.J., and Cullen, P.J. (2011). Recent advances in retromer biology. *Traffic (Copenhagen, Denmark)*. *12*, 963–971.

McIlhatton, M.A., Burrows, J.F., Donaghy, P.G., et al. (2001). Genomic organization, complex splicing pattern and expression of a human septin gene on chromosome 17q25.3. *Oncogene*. *20*, 5930–5939.

McInerney-Leo, A., Gwinn-Hardy, K., and Nussbaum, R.L. (2004). Prevalence of Parkinson's disease in populations of African ancestry: a review. *Journal of the National Medical Association*. *96*, 974–979.

McLelland, G.-L., Soubannier, V., Chen, C.X., et al. (2014). Parkin and PINK1 function in a vesicular trafficking pathway regulating mitochondrial quality control. *The EMBO Journal*. *33*, 282–295.

McNaught, K.S., and Jenner, P. (2001). Proteasomal function is impaired in substantia nigra in Parkinson's disease. *Neuroscience Letters*. *297*, 191–194.

McNaught, K.S.P., and Olanow, C.W. (2003). Proteolytic stress: a unifying concept for the etiopathogenesis of Parkinson's disease. *Annals of neurology*. *53 Suppl 3*, S73–S84; discussion S84–S86.

McNaught, K.S.P., Belizaire, R., Isacson, O., et al. (2003). Altered proteasomal function in sporadic Parkinson's disease. *Experimental Neurology*. *179*, 38–46.

Meerloo, J. van, Kaspers, G.J.L., and Cloos, J. (2011). Cell Sensitivity Assays: The MTT Assay. In *Cancer Cell Culture*, I.A. Cree, ed. (Humana Press), pp. 237–245.

Mehdi, S.J., Alam, M.S., Batra, S., et al. (2011). Allelic loss of 6q25-27, the PARKIN tumor suppressor gene locus, in cervical carcinoma. *Medical Oncology*. *28*, 1520–1526.

Mehra, A., Zahra, A., Thompson, V., et al. (2013). Mycobacterium tuberculosis type VII secreted effector EsxH targets host ESCRT to impair trafficking. *PLoS pathogens*. *9*, e1003734.

Meixner, A., Boldt, K., Van Troys, M., et al. (2011). A QUICK screen for Lrrk2 interaction partners--leucine-rich repeat kinase 2 is involved in actin cytoskeleton dynamics. *Molecular & cellular proteomics: MCP*. *10*, M110.001172.

Melcon, M.O., Anderson, D.W., Vergara, R.H., et al. (1997). Prevalence of Parkinson's disease in Junín, Buenos Aires Province, Argentina. *Movement disorders: official journal of the Movement Disorder Society*. *12*, 197–205.

Mellick, G., Siebert, G., Funayama, M., et al. (2009). Screening PARK genes for mutations in early-onset Parkinson's disease patients from Queensland, Australia. *Parkinsonism & Related Disorders*. *15*, 105–109.

Mhawech, P. (2005). 14-3-3 proteins--an update. *Cell Research*. *15*, 228–236.

Miller, D.W., Ahmad, R., Hague, S., et al. (2003). L166P mutant DJ-1, causative for recessive Parkinson's disease, is degraded through the ubiquitin-proteasome system. *The Journal of Biological Chemistry*. *278*, 36588–36595.

Milroy, L.-G., Brunsveld, L., and Ottmann, C. (2013). Stabilization and inhibition of protein-protein interactions: the 14-3-3 case study. *ACS chemical biology*. *8*, 27–35.

Mira, M.T., Alcaïs, A., Nguyen, V.T., et al. (2004). Susceptibility to leprosy is associated with PARK2 and PACRG. *Nature*. *427*, 636–640.

Miyakawa, S., Ogino, M., Funabe, S., et al. (2013). Lewy body pathology in a patient with a homozygous parkin deletion. *Movement disorders: official journal of the Movement Disorder Society*. *28*, 388–391.

Mizuta, I., Satake, W., Nakabayashi, Y., et al. (2006a). Multiple candidate gene analysis identifies alpha-synuclein as a susceptibility gene for sporadic Parkinson's disease. *Human molecular genetics*. *15*, 1151–1158.

Mizuta, T., Ozaki, I., Eguchi, Y., et al. (2006b). The effect of menatetrenone, a vitamin K2 analog, on disease recurrence and survival in patients with hepatocellular carcinoma after curative treatment: a pilot study. *Cancer*. *106*, 867–872.

Montesinos, M.L., Castellano-Muñoz, M., García-Junco-Clemente, P., et al. (2005). Recycling and EH domain proteins at the synapse. *Brain research. Brain research reviews*. *49*, 416–428.

Montgomery, J., Wittwer, C.T., Palais, R., et al. (2007). Simultaneous mutation scanning and genotyping by high-resolution DNA melting analysis. *Nature Protocols*. *2*, 59–66.

Moore, D.J., Zhang, L., Troncoso, J., et al. (2005). Association of DJ-1 and parkin mediated by pathogenic DJ-1 mutations and oxidative stress. *Human Molecular Genetics*. *14*, 71–84.

Morens, D.M., Davis, J.W., Grandinetti, A., et al. (1996). Epidemiologic observations on Parkinson's disease: incidence and mortality in a prospective study of middle-aged men. *Neurology*. *46*, 1044–1050.

Morgan, N.V., Westaway, S.K., Morton, J.E.V., et al. (2006). PLA2G6, encoding a phospholipase A2, is mutated in neurodegenerative disorders with high brain iron. *Nature genetics*. *38*, 752–754.

Morioka, S., Sakata, K., Yoshida, S., et al. (2002). Incidence of Parkinson disease in Wakayama, Japan. *Journal of epidemiology / Japan Epidemiological Association*. *12*, 403–407.

Mortiboys, H., Thomas, K.J., Koopman, W.J.., et al. (2008). Mitochondrial function and morphology are impaired in parkin-mutant fibroblasts. *Annals of neurology*. *64*, 555–565.

Mostowy, S., and Cossart, P. (2012). Septins: the fourth component of the cytoskeleton. *Nature Reviews. Molecular Cell Biology*. *13*, 183–194.

Mougenot, A.-L., Nicot, S., Bencsik, A., et al. (2012). Prion-like acceleration of a synucleinopathy in a transgenic mouse model. *Neurobiology of aging*. *33*, 2225–2228.

Mueller, J.C., Fuchs, J., Hofer, A., et al. (2005). Multiple regions of alpha-synuclein are associated with Parkinson's disease. *Annals of neurology*. *57*, 535–541.

Muñoz-Soriano, V., Nieto-Arellano, R., and Paricio, N. (2012). Septin 4, the drosophila ortholog of human CDCrel-1, accumulates in parkin mutant brains and is functionally related to the Nedd4 E3 ubiquitin ligase. *Journal of molecular neuroscience: MN*. *48*, 136–143.

Myers, A.J., Pittman, A.M., Zhao, A.S., et al. (2007). The MAPT H1c risk haplotype is associated with increased expression of tau and especially of 4 repeat containing transcripts. *Neurobiology of disease*. *25*, 561–570.

Myhre, R., Toft, M., Kachergus, J., et al. (2008). Multiple alpha-synuclein gene polymorphisms are associated with Parkinson's disease in a Norwegian population. *Acta neurologica Scandinavica*. *118*, 320–327.

Nakada, K., Inoue, K., Ono, T., et al. (2001). Inter-mitochondrial complementation: Mitochondria-specific system preventing mice from expression of disease phenotypes by mutant mtDNA. *Nature Medicine*. *7*, 934–940.

Nakagawa, K., Hirota, Y., Sawada, N., et al. (2010). Identification of UBIAD1 as a novel human menaquinone-4 biosynthetic enzyme. *Nature*. *468*, 117–121.

Narendra, D., Tanaka, A., Suen, D.-F., et al. (2008). Parkin is recruited selectively to impaired mitochondria and promotes their autophagy. *The Journal of Cell Biology*. *183*, 795–803.

Narendra, D., Jin, S.M., Tanaka, A., et al. (2010a). PINK1 Is selectively stabilized on impaired mitochondria to activate parkin. *PLoS Biol*. *8*, e1000298.

Narendra, D., Kane, L.A., Hauser, D.N., et al. (2010b). p62/SQSTM1 is required for Parkin-induced mitochondrial clustering but not mitophagy; VDAC1 is dispensable for both. *Autophagy*. *6*, 1090–1106.

Neudorfer, O., Giladi, N., Elstein, D., et al. (1996). Occurrence of Parkinson's syndrome in type I Gaucher disease. *QJM: monthly journal of the Association of Physicians*. *89*, 691–694.

Newmeyer, D.D., and Ferguson-Miller, S. (2003). Mitochondria: releasing power for life and unleashing the machineries of death. *Cell*. *112*, 481–490.

Nicholls, D.G. (2009). Spare respiratory capacity, oxidative stress and excitotoxicity. *Biochemical Society Transactions*. *37*, 1385–1388.

Nichols, R.J., Dzamko, N., Morrice, N.A., et al. (2010). 14-3-3 binding to LRRK2 is disrupted by multiple Parkinson's disease-associated mutations and regulates cytoplasmic localization. *The Biochemical Journal*. *430*, 393–404.

Nishioka, K., Hayashi, S., Farrer, M.J., et al. (2006). Clinical heterogeneity of alpha-synuclein gene duplication in Parkinson's disease. *Annals of neurology*. *59*, 298–309.

Nishioka, K., Funayama, M., Vilariño-Güell, C., et al. (2014). EIF4G1 gene mutations are not a common cause of Parkinson's disease in the Japanese population. *Parkinsonism & related disorders*. *20*, 659–661.

Nuytemans, K., Theuns, J., Cruts, M., et al. (2010). Genetic etiology of Parkinson disease associated with mutations in the SNCA, PARK2, PINK1, PARK7, and LRRK2 genes: a mutation update. *Human Mutation*. *31*, 763–780.

Ogawa, M., Nakai, S., Deguchi, A., et al. (2007). Vitamins K2, K3 and K5 exert antitumor effects on established colorectal cancer in mice by inducing apoptotic death of tumor cells. *International Journal of Oncology*. *31*, 323–331.

Okano, T., Shimomura, Y., Yamane, M., et al. (2008). Conversion of phylloquinone (Vitamin K1) into menaquinone-4 (Vitamin K2) in mice: two possible routes for menaquinone-4 accumulation in cerebra of mice. *The Journal of Biological Chemistry*. *283*, 11270–11279.

Okatsu, K., Iemura, S., Koyano, F., et al. (2012). Mitochondrial hexokinase HKI is a novel substrate of the Parkin ubiquitin ligase. *Biochemical and Biophysical Research Communications*. *428*, 197–202.

Okubadejo, N.U., Bower, J.H., Rocca, W.A., et al. (2006). Parkinson's disease in Africa: A systematic review of epidemiologic and genetic studies. *Movement disorders: official journal of the Movement Disorder Society*. *21*, 2150–2156.

Okui, M., Yamaki, A., Takayanagi, A., et al. (2005). Transcription factor single-minded 2 (SIM2) is ubiquitinated by the RING-IBR-RING-type E3 ubiquitin ligases. *Experimental Cell Research*. *309*, 220–228.

Okun, M.S. (2012). Deep-brain stimulation for Parkinson's disease. *The New England journal of medicine*. *367*, 1529–1538.

Olanow, C.W., Perl, D.P., DeMartino, G.N., et al. (2004). Lewy-body formation is an aggresome-related process: a hypothesis. *Lancet neurology*. *3*, 496–503.

Olanow, C.W., Rascol, O., Hauser, R., et al. (2009). A double-blind, delayed-start trial of rasagiline in Parkinson's disease. *The New England journal of medicine*. *361*, 1268–1278.

Olzmann, J.A., Li, L., Chudaev, M.V., et al. (2007). Parkin-mediated K63-linked polyubiquitination targets misfolded DJ-1 to aggresomes via binding to HDAC6. *The Journal of Cell Biology*. *178*, 1025–1038.

Ondo, W.G., Dat Vuong, K., Khan, H., et al. (2001). Daytime sleepiness and other sleep disorders in Parkinson's disease. *Neurology*. *57*, 1392–1396.

Ong, S.-B., Subrayan, S., Lim, S.Y., et al. (2010). Inhibiting mitochondrial fission protects the heart against ischemia/reperfusion injury. *Circulation*. *121*, 2012–2022.

Ono, T., Isobe, K., Nakada, K., et al. (2001). Human cells are protected from mitochondrial dysfunction by complementation of DNA products in fused mitochondria. *Nature Genetics*. *28*, 272–275.

Osley, M.A., Fleming, A.B., and Kao, C.-F. (2006). Histone ubiquitylation and the regulation of transcription. *Results and problems in cell differentiation*. *41*, 47–75.

Ostrerova, N., Petrucelli, L., Farrer, M., et al. (1999). alpha-Synuclein shares physical and functional homology with 14-3-3 proteins. *The Journal of Neuroscience: The Official Journal of the Society for Neuroscience*. *19*, 5782–5791.

Otsuka, M., Kato, N., Shao, R.-X., et al. (2004). Vitamin K2 inhibits the growth and invasiveness of hepatocellular carcinoma cells via protein kinase A activation. *Hepatology*. *40*, 243–251.

Ottmann, C. (2013). Small-molecule modulators of 14-3-3 protein–protein interactions. *Bioorganic & Medicinal Chemistry*. *21*, 4058–4062.

Ozaki, I., Zhang, H., Mizuta, T., et al. (2007). Menatetrenone, a vitamin K2 analogue, inhibits hepatocellular carcinoma cell growth by suppressing cyclin D1 expression through inhibition of nuclear factor kappaB activation. *Clinical Cancer Research: An Official Journal of the American Association for Cancer Research*. *13*, 2236–2245.

Pacelli, C., De Rasmo, D., Signorile, A., et al. (2011). Mitochondrial defect and PGC-1α dysfunction in parkin-associated familial Parkinson's disease. *Biochimica et Biophysica Acta (BBA) - Molecular Basis of Disease*. *1812*, 1041–1053.

Padmaja, M.V., Jayaraman, M., Srinivasan, A.V., et al. (2012). PARK2 gene mutations in early onset Parkinson's disease patients of South India. *Neuroscience Letters*. *523*, 145–147.

Pagliacci, M.C., Spinozzi, F., Migliorati, G., et al. (1993). Genistein inhibits tumour cell growth in vitro but enhances mitochondrial reduction of tetrazolium salts: a further pitfall in the use of the MTT assay for evaluating cell growth and survival. *European Journal of Cancer*. *29A*, 1573–1577.

Paisán-Ruiz, C., Jain, S., Evans, E.W., et al. (2004). Cloning of the gene containing mutations that cause PARK8-linked Parkinson's disease. *Neuron*. *44*, 595–600.

Paisán-Ruiz, C., Bhatia, K.P., Li, A., et al. (2009). Characterization of PLA2G6 as a locus for dystonia-parkinsonism. *Annals of neurology*. *65*, 19–23.

Paisán-Ruiz, C., Guevara, R., Federoff, M., et al. (2010). Early-onset L-dopa-responsive parkinsonism with pyramidal signs due to ATP13A2, PLA2G6, FBXO7 and spatacsin mutations. *Movement disorders: official journal of the Movement Disorder Society*. *25*, 1791–1800.

Palacios, N., Gao, X., McCullough, M.L., et al. (2012). Caffeine and risk of Parkinson's disease in a large cohort of men and women. *Movement disorders: official journal of the Movement Disorder Society*. *27*, 1276–1282.

Pankratz, N., Pauciulo, M.W., Elsaesser, V.E., et al. (2006). Mutations in DJ-1 are rare in familial Parkinson disease. *Neuroscience letters*. *408*, 209–213.

Pankratz, N., Wilk, J.B., Latourelle, J.C., et al. (2009a). Genomewide association study for susceptibility genes contributing to familial Parkinson disease. *Human genetics*. *124*, 593–605.

Pankratz, N., Kissell, D.K., Pauciulo, M.W., et al. (2009b). Parkin dosage mutations have greater pathogenicity in familial PD than simple sequence mutations. *Neurology*. *73*, 279–286.

Parelkar, S.S., Cadena, J.G., Kim, C., et al. (2012). The parkin-like human homolog of Drosophila Ariadne-1 (HHARI) can induce aggresome formation in mammalian cells and is immunologically detectable in Lewy bodies. *Journal of Molecular Neuroscience*. *46*, 109–121.

Parisiadou, L., Xie, C., Cho, H.J., et al. (2009). Phosphorylation of ezrin/radixin/moesin proteins by LRRK2 promotes the rearrangement of actin cytoskeleton in neuronal morphogenesis. *The Journal of Neuroscience: The Official Journal of the Society for Neuroscience*. *29*, 13971–13980.

Park, H.-M., Kim, G.-Y., Nam, M.-K., et al. (2009). The serine protease HtrA2/Omi cleaves Parkin and irreversibly inactivates its E3 ubiquitin ligase activity. *Biochemical and Biophysical Research Communications*. *387*, 537–542.

Park, J., Lee, S.B., Lee, S., et al. (2006). Mitochondrial dysfunction in Drosophila PINK1 mutants is complemented by parkin. *Nature*. *441*, 1157–1161.

Parkinson, J. (1817). An Essay on the Shaking Palsy (London: Sherwood, Needly and Jones).

Parkkinen, L., Pirttilä, T., and Alafuzoff, I. (2008). Applicability of current staging/categorization of alpha-synuclein pathology and their clinical relevance. *Acta neuropathologica*. *115*, 399–407.

Parrish, J.R., Gulyas, K.D., and Finley, R.L. (2006). Yeast two-hybrid contributions to interactome mapping. *Current Opinion in Biotechnology*. *17*, 387–393.

Parsons, T.D., Rogers, S.A., Braaten, A.J., et al. (2006). Cognitive sequelae of subthalamic nucleus deep brain stimulation in Parkinson's disease: a meta-analysis. *Lancet neurology*. *5*, 578–588.

Patil, A., and Nakamura, H. (2005). Filtering high-throughput protein-protein interaction data using a combination of genomic features. *BMC bioinformatics*. *6*, 100–117.

Patterson, N., Petersen, D.C., van der Ross, R.E., et al. (2009). Genetic structure of a unique admixed population: implications for medical research. *Human Molecular Genetics*. *19*, 411–419.

Pavese, N., and Brooks, D.J. (2009). Imaging neurodegeneration in Parkinson's disease. *Biochimica et Biophysica Acta (BBA)-Molecular Basis of Disease*. *1792*, 722–729.

Pearce, R.K., Hawkes, C.H., and Daniel, S.E. (1995). The anterior olfactory nucleus in Parkinson's disease. *Movement disorders: official journal of the Movement Disorder Society*. *10*, 283–287.

Pellicano, C., Benincasa, D., Pisani, V., et al. (2007). Prodromal non-motor symptoms of Parkinson's disease. *Neuropsychiatric disease and treatment*. *3*, 145–152.

Periquet, M. (2003). Parkin mutations are frequent in patients with isolated early-onset parkinsonism. *Brain*. *126*, 1271–1278.

Periquet, M., Lücking, C., Vaughan, J., et al. (2001). Origin of the mutations in the parkin gene in Europe: exon rearrangements are independent recurrent events, whereas point mutations may result from Founder effects. *American journal of human genetics*. *68*, 617–626.

Periquet, M., Corti, O., Jacquier, S., et al. (2005). Proteomic analysis of parkin knockout mice: alterations in energy metabolism, protein handling and synaptic function. *Journal of Neurochemistry*. *95*, 1259–1276.

Perneger, T.V. (1998). What's wrong with Bonferroni adjustments. *BMJ (Clinical research ed.)*. *316*, 1236–1238.

Perron, N.R., Beeson, C., and Rohrer, B. (2013). Early alterations in mitochondrial reserve capacity; a means to predict subsequent photoreceptor cell death. *Journal of Bioenergetics and Biomembranes*. *45*, 101–109.

Peters, C.M., Gartner, C.E., Silburn, P.A., et al. (2006). Prevalence of Parkinson's disease in metropolitan and rural Queensland: a general practice survey. *Journal of clinical neuroscience: official journal of the Neurosurgical Society of Australasia*. *13*, 343–348.

Peterson, E., and Petty, E. (2010). Conquering the complex world of human septins: implications for health and disease. *Clinical Genetics*. *77*, 511–524.

Petrozzi, L., Ricci, G., Giglioli, N.J., et al. (2007). Mitochondria and neurodegeneration. *Bioscience Reports*. *27*, 87–104.

Petrucelli, L., O'Farrell, C., Lockhart, P.J., et al. (2002). Parkin protects against the toxicity associated with mutant alpha-synuclein: proteasome dysfunction selectively affects catecholaminergic neurons. *Neuron*. *36*, 1007–1019.

Petrucelli, L., Dickson, D., Kehoe, K., et al. (2004). CHIP and Hsp70 regulate tau ubiquitination, degradation and aggregation. *Human Molecular Genetics*. *13*, 703–714.

Piccini, P., Burn, D.J., Ceravolo, R., et al. (1999). The role of inheritance in sporadic Parkinson's disease: evidence from a longitudinal study of dopaminergic function in twins. *Annals of neurology*. *45*, 577–582.

Pícková, A., Potocký, M., and Houštěk, J. (2005). Assembly factors of F1Fo-ATP synthase across genomes. *Proteins: Structure, Function, and Bioinformatics*. *59*, 393–402.

Pinheiro, J., Bates, D., DebRoy, S., et al. (2014). R Core Team (2013) nlme: Linear and nonlinear mixed effects models R package version 3.1-117. Available at: http://CRAN.R-project.org/package=nlme

Pícková, A., Paul, J., Petruzzella, V., et al. (2003). Differential expression of ATPAF1 and ATPAF2 genes encoding F1-ATPase assembly proteins in mouse tissues. *FEBS Letters*. *551*, 42–46.

Plotegher, N., Kumar, D., Tessari, I., et al. (2014). The chaperone-like protein 14-3-3η interacts with human α-synuclein aggregation intermediates rerouting the amyloidogenic pathway and reducing α-synuclein cellular toxicity. *Human Molecular Genetics*. *23*, 5615–5629.

Pollard, T.D., and Cooper, J.A. (2009). Actin, a central player in cell shape and movement. *Science*. *326*, 1208–1212.

Polymeropoulos, M.H., Lavedan, C., Leroy, E., et al. (1997). Mutation in the α-synuclein gene identified in families with Parkinson's disease. *Science*. *276*, 2045–2047.

Ponsen, M.M., Stoffers, D., Booij, J., et al. (2004). Idiopathic hyposmia as a preclinical sign of Parkinson's disease. *Annals of neurology*. *56*, 173–181.

Poole, A.C., Thomas, R.E., Andrews, L.A., et al. (2008). The PINK1/Parkin pathway regulates mitochondrial morphology. *Proceedings of the National Academy of Sciences of the United States of America*. *105*, 1638–1643.

Poole, A.C., Thomas, R.E., Yu, S., et al. (2010). The mitochondrial fusion-promoting factor mitofusin is a substrate of the PINK1/parkin pathway. *PLoS ONE*. *5*, e10054.

Porter, R.K. (2001). Mitochondrial proton leak: a role for uncoupling proteins 2 and 3? *Biochimica et Biophysica Acta (BBA) - Bioenergetics*. *1504*, 120–127.

Poulogiannis, G., McIntyre, R.E., Dimitriadi, M., et al. (2010). PARK2 deletions occur frequently in sporadic colorectal cancer and accelerate adenoma development in Apc mutant mice. *Proceedings of the National Academy of Sciences of the United States of America*. *107*, 15145–15150.

Pramstaller, P.P., Schlossmacher, M.G., Jacques, T.S., et al. (2005). Lewy body Parkinson's disease in a large pedigree with 77 Parkin mutation carriers. *Annals of neurology*. *58*, 411–422.

Presse, N., Shatenstein, B., Kergoat, M.-J., et al. (2008). Low vitamin K intakes in community-dwelling elders at an early stage of Alzheimer's disease. *Journal of the American Dietetic Association*. *108*, 2095–2099.

Quadri, M., Fang, M., Picillo, M., et al. (2013). Mutation in the SYNJ1 gene associated with autosomal recessive, early-onset Parkinsonism. *Human mutation*. *34*, 1208–1215.

Quadri, M., Yang, X., Cossu, G., et al. (2014). An exome study of Parkinson's disease in Sardinia, a Mediterranean genetic isolate. *Neurogenetics*. [Epub ahead of print].

Quik, M., Perez, X.A., and Bordia, T. (2012). Nicotine as a potential neuroprotective agent for Parkinson's disease. *Movement disorders: official journal of the Movement Disorder Society*. *27*, 947–957.

Racette, B.A., Good, L.M., Kissel, A.M., et al. (2009). A population-based study of parkinsonism in an Amish community. *Neuroepidemiology*. *33*, 225–230.

Rakovic, A., Gr\ünewald, A., Seibler, P., et al. (2010). Effect of endogenous mutant and wild-type PINK1 on Parkin in fibroblasts from Parkinson disease patients. *Human molecular genetics*. *19*, 3124–3137.

Rakovic, A., Grunewald, A., Kottwitz, J., et al. (2011). Mutations in PINK1 and parkin impair ubiquitination of mitofusins in human fibroblasts. *PLoS ONE*. *6*, e16746.

Rambold, A.S., Kostelecky, B., Elia, N., et al. (2011). Tubular network formation protects mitochondria from autophagosomal degradation during nutrient starvation. *Proceedings of the National Academy of Sciences of the United States of America*. *108*, 10190–10195.

Ramirez, A., Heimbach, A., Gründemann, J., et al. (2006). Hereditary parkinsonism with dementia is caused by mutations in ATP13A2, encoding a lysosomal type 5 P-type ATPase. *Nature Genetics*. *38*, 1184–1191.

Rankin, C.A., Roy, A., Zhang, Y., et al. (2011). Parkin, a top level manager in the cell's sanitation department. *The open biochemistry journal*. *5*, 9–26.

Rascol, O., Brooks, D.J., Melamed, E., et al. (2005). Rasagiline as an adjunct to levodopa in patients with Parkinson's disease and motor fluctuations (LARGO, Lasting effect in Adjunct therapy with Rasagiline Given Once daily, study): a randomised, double-blind, parallel-group trial. *Lancet*. *365*, 947–954.

Raudino, F. (2012). The Parkinson disease before James Parkinson. *Neurological sciences*. *33*, 945–948.

Rawal, N., Corti, O., Sacchetti, P., et al. (2009). Parkin protects dopaminergic neurons from excessive Wnt/beta-catenin signaling. *Biochemical and Biophysical Research Communications*. *388*, 473–478.

R Core Team (2012). R: A language and environment for statistical computing. R Foundation for Statistical Computing, Vienna, Austria. Available at: http://www.R-project.org/

Reed, G.H., Kent, J.O., and Wittwer, C.T. (2007). High-resolution DNA melting analysis for simple and efficient molecular diagnostics. *Pharmacogenomics*. *8*, 597–608.

Reers, M., Smiley, S.T., Mottola-Hartshorn, C., et al. (1995). Mitochondrial membrane potential monitored by JC-1 dye. *Methods in Enzymology*. *260*, 406–417.

Reeve, A., Simcox, E., and Turnbull, D. (2014). Ageing and Parkinson's disease: Why is advancing age the biggest risk factor? *Ageing research reviews*. *14C*, 19–30.

Ren, Y., Zhao, J., and Feng, J. (2003). Parkin binds to alpha/beta tubulin and increases their ubiquitination and degradation. *The Journal of Neuroscience: The Official Journal of the Society for Neuroscience*. *23*, 3316–3324.

Ren, Y., Jiang, H., Yang, F., et al. (2009). Parkin protects dopaminergic neurons against microtubule-depolymerizing toxins by attenuating microtubule-associated protein kinase activation. *The Journal of biological chemistry*. *284*, 4009–4017.

Ren, Y., Jiang, H., Ma, D., et al. (2011). Parkin degrades estrogen-related receptors to limit the expression of monoamine oxidases. *Human Molecular Genetics*. *20*, 1074–1083.

Rideout, H.J., and Stefanis, L. (2002). Proteasomal inhibition-induced inclusion formation and death in cortical neurons require transcription and ubiquitination. *Molecular and Cellular Neurosciences*. *21*, 223–238.

Rideout, H.J., Larsen, K.E., Sulzer, D., et al. (2001). Proteasomal inhibition leads to formation of ubiquitin/alpha-synuclein-immunoreactive inclusions in PC12 cells. *Journal of Neurochemistry*. *78*, 899–908.

Riederer, P., and Laux, G. (2011). MAO-inhibitors in Parkinson's Disease. *Experimental neurobiology*. *20*, 1–17.

Ries, V., Henchcliffe, C., Kareva, T., et al. (2006). Oncoprotein Akt/PKB induces trophic effects in murine models of Parkinson's disease. *Proceedings of the National Academy of Sciences of the United States of America*. *103*, 18757–18762.

De Rijk, M.C., Breteler, M.M., Graveland, G.A., et al. (1995). Prevalence of Parkinson's disease in the elderly: the Rotterdam Study. *Neurology*. *45*, 2143–2146.

De Rijk, M.C., Launer, L.J., Berger, K., et al. (2000). Prevalence of Parkinson's disease in Europe: A collaborative study of population-based cohorts. Neurologic Diseases in the Elderly Research Group. *Neurology*. *54*, S21–S23.

Riley, B.E., Lougheed, J.C., Callaway, K., et al. (2013). Structure and function of Parkin E3 ubiquitin ligase reveals aspects of RING and HECT ligases. *Nature Communications*. *4*, 1982.

Rocca, W.A., McDonnell, S.K., Strain, K.J., et al. (2004). Familial aggregation of Parkinson's disease: The Mayo Clinic family study. *Annals of neurology*. *56*, 495–502.

Rodriguez-Oroz, M.C., Jahanshahi, M., Krack, P., et al. (2009). Initial clinical manifestations of Parkinson's disease: features and pathophysiological mechanisms. *Lancet neurology*. *8*, 1128–1139.

Ron, I., Rapaport, D., and Horowitz, M. (2010). Interaction between parkin and mutant glucocerebrosidase variants: a possible link between Parkinson disease and Gaucher disease. *Human Molecular Genetics*. *19*, 3771–3781.

Rosen, K.M., Moussa, C.E.-H., Lee, H.-K., et al. (2010). Parkin reverses intracellular β-amyloid accumulation and its negative effects on proteasome function. *Journal of neuroscience research*. *88*, 167–178.

Ross, G.W., Abbott, R.D., Petrovitch, H., et al. (2000). Association of coffee and caffeine intake with the risk of Parkinson disease. *JAMA: the journal of the American Medical Association*. *283*, 2674–2679.

Ross, G.W., Petrovitch, H., Abbott, R.D., et al. (2008a). Association of olfactory dysfunction with risk for future Parkinson's disease. *Annals of neurology*. *63*, 167–173.

Ross, O.A., Braithwaite, A.T., Skipper, L.M., et al. (2008b). Genomic investigation of alpha-synuclein multiplication and parkinsonism. *Annals of neurology*. *63*, 743–750.

Ross, O.A., Wu, Y.-R., Lee, M.-C., et al. (2008c). Analysis of Lrrk2 R1628P as a risk factor for Parkinson's disease. *Annals of neurology*. *64*, 88–92.

Ross, O.A., Soto-Ortolaza, A.I., Heckman, M.G., et al. (2011). Association of LRRK2 exonic variants with susceptibility to Parkinson's disease: a case-control study. *Lancet neurology*. *10*, 898–908.

Rossignol, R., Gilkerson, R., Aggeler, R., et al. (2004). Energy substrate modulates mitochondrial structure and oxidative capacity in cancer cells. *Cancer Research*. *64*, 985–993.

Roth, J.A., Singleton, S., Feng, J., et al. (2010). Parkin regulates metal transport via proteasomal degradation of the 1B isoforms of divalent metal transporter 1. *Journal of Neurochemistry*. *113*, 454–464.

Rothfuss, O., Fischer, H., Hasegawa, T., et al. (2009). Parkin protects mitochondrial genome integrity and supports mitochondrial DNA repair. *Human Molecular Genetics*. *18*, 3832–3850.

Rubenstein, P.A. (1990). The functional importance of multiple actin isoforms. *BioEssays: News and Reviews in Molecular, Cellular and Developmental Biology*. *12*, 309–315.

Saito, E., Wachi, H., Sato, F., et al. (2007). Treatment with vitamin k(2) combined with bisphosphonates synergistically inhibits calcification in cultured smooth muscle cells. *Journal of Atherosclerosis and Thrombosis. 14*, 317–324.

Saito, K., Adachi, N., Koyama, H., et al. (2010). OGFOD1, a member of the 2-oxoglutarate and iron dependent dioxygenase family, functions in ischemic signaling. *FEBS Letters*. *584*, 3340–3347.

Sakata, E., Yamaguchi, Y., Kurimoto, E., et al. (2003). Parkin binds the Rpn10 subunit of 26S proteasomes through its ubiquitin-like domain. *EMBO reports*. *4*, 301–306.

Sakaue, M., Mori, N., Okazaki, M., et al. (2011). Vitamin K has the potential to protect neurons from methylmercury-induced cell death in vitro. *Journal of Neuroscience Research*. *89*, 1052–1058.

Salama, M., Yuan, T.-F., Machado, S., et al. (2013). Co-enzyme Q10 to treat neurological disorders: basic mechanisms, clinical outcomes, and future research direction. *CNS & neurological disorders drug targets*. *12*, 641–664.

Samaranch, L., Lorenzo-Betancor, O., Arbelo, J.M., et al. (2010). PINK1-linked parkinsonism is associated with Lewy body pathology. *Brain: a journal of neurology*. *133*, 1128–1142.

Santoro, L., Breedveld, G.J., Manganelli, F., et al. (2011). Novel ATP13A2 (PARK9) homozygous mutation in a family with marked phenotype variability. *Neurogenetics*. *12*, 33–39.

Sarraf, S.A., Raman, M., Guarani-Pereira, V., et al. (2013). Landscape of the PARKIN-dependent ubiquitylome in response to mitochondrial depolarization. *Nature*. *496*, 372–376.

Satake, W., Nakabayashi, Y., Mizuta, I., et al. (2009). Genome-wide association study identifies common variants at four loci as genetic risk factors for Parkinson's disease. *Nature Genetics*. *41*, 1303–1307.

Sato, S., Chiba, T., Sakata, E., et al. (2006). 14-3-3eta is a novel regulator of parkin ubiquitin ligase. *The EMBO Journal*. *25*, 211–221.

Satoh, J., and Kuroda, Y. (1999). Association of codon 167 Ser/Asn heterozygosity in the parkin gene with sporadic Parkinson's disease. *Neuroreport*. *10*, 2735–2739.

Le Saux, O., Beck, K., Sachsinger, C., et al. (2002). Evidence for a founder effect for pseudoxanthoma elasticum in the Afrikaner population of South Africa. *Human genetics*. *111*, 331–338.

Schapira, A.H., Cooper, J.M., Dexter, D., et al. (1989). Mitochondrial complex I deficiency in Parkinson's disease. *Lancet*. *1*, 1269.

Schapira, A.H.V., Emre, M., Jenner, P., et al. (2009). Levodopa in the treatment of Parkinson's disease. *European journal of neurology: the official journal of the European Federation of Neurological Societies*. *16*, 982–989.

Schauberger, E.M., Ewart, S.L., Arshad, S.H., et al. (2011). Identification of ATPAF1 as a novel candidate gene for asthma in children. *The Journal of allergy and clinical immunology*. *128*, 753–760.

Schenck, C.H., and Mahowald, M.W. (2002). REM sleep behavior disorder: clinical, developmental, and neuroscience perspectives 16 years after its formal identification in SLEEP. *Sleep*. *25*, 120–138.

Scherfler, C., Khan, N.L., Pavese, N., et al. (2004). Striatal and cortical pre- and postsynaptic dopaminergic dysfunction in sporadic parkin-linked parkinsonism. *Brain: A Journal of Neurology*. *127*, 1332–1342.

Schinke, E.N., Bii, V., Nalla, A., et al. (2014). A novel approach to identify driver genes involved in androgen-independent prostate cancer. *Molecular Cancer*. *13*, 120.

Schlitter, A.M., Kurz, M., Larsen, J.P., et al. (2006). Parkin gene variations in late-onset Parkinson's disease: comparison between Norwegian and German cohorts. *Acta neurologica Scandinavica*. *113*, 9–13.

Schneider, C.A., Rasband, W.S., and Eliceiri, K.W. (2012). NIH Image to ImageJ: 25 years of image analysis. *Nature Methods*. *9*, 671–675.

Schoenberg, B.S., Osuntokun, B.O., Adeuja, A.O., et al. (1988). Comparison of the prevalence of Parkinson's disease in black populations in the rural United States and in rural Nigeria: door-to-door community studies. *Neurology*. *38*, 645–646.

Schrag, A., and Schott, J.M. (2006). Epidemiological, clinical, and genetic characteristics of early-onset parkinsonism. *Lancet Neurology*. *5*, 355–363.

Schulte, E.C., Mollenhauer, B., Zimprich, A., et al. (2012). Variants in eukaryotic translation initiation factor 4G1 in sporadic Parkinson's disease. *Neurogenetics*. *13*, 281–285.

Schwarz, J.M., Rödelsperger, C., Schuelke, M., et al. (2010). MutationTaster evaluates disease-causing potential of sequence alterations. *Nature Methods*. *7*, 575–576.

Scott, D., and Roy, S. (2012). α-Synuclein inhibits intersynaptic vesicle mobility and maintains recycling-pool homeostasis. *The Journal of neuroscience: the official journal of the Society for Neuroscience*. *32*, 10129–10135.

Scott, M., Hyland, P.L., McGregor, G., et al. (2005). Multimodality expression profiling shows SEPT9 to be overexpressed in a wide range of human tumours. *Oncogene*. *24*, 4688–4700.

Sellin, M.E., Sandblad, L., Stenmark, S., et al. (2011). Deciphering the rules governing assembly order of mammalian septin complexes. *Molecular Biology of the Cell*. *22*, 3152–3164.

Sellin, M.E., Stenmark, S., and Gullberg, M. (2012). Mammalian SEPT9 isoforms direct microtubule-dependent arrangements of septin core heteromers. *Molecular biology of the cell*. *23*, 4242–4255.

Semenza, G.L. (2010). Defining the role of hypoxia-inducible factor 1 in cancer biology and therapeutics. *Oncogene*. *29*, 625–634.

Senior, A.E., Nadanaciva, S., and Weber, J. (2002). The molecular mechanism of ATP synthesis by F1F0-ATP synthase. *Biochimica Et Biophysica Acta*. *1553*, 188–211.

Serebriiskii, I., Estojak, J., Berman, M., et al. (2000). Approaches to detecting false positives in yeast two-hybrid systems. *BioTechniques*. *28*, 328–330, 332–336.

Sha, D., Chin, L.-S., and Li, L. (2009). Phosphorylation of parkin by Parkinson disease-linked kinase PINK1 activates parkin E3 ligase function and NF- B signaling. *Human Molecular Genetics*. *19*, 352–363.

Shah, S.P., Roth, A., Goya, R., et al. (2012). The clonal and mutational evolution spectrum of primary triple-negative breast cancers. *Nature*. *486*, 395–399.

Shan, G. (2010). RNA interference as a gene knockdown technique. *The International Journal of Biochemistry & Cell Biology*. *42*, 1243–1251.

Shankar, S.L., O'Guin, K., Cammer, M., et al. (2003). The growth arrest-specific gene product Gas6 promotes the survival of human oligodendrocytes via a phosphatidylinositol 3-kinase-dependent pathway. *The Journal of Neuroscience: The Official Journal of the Society for Neuroscience*. *23*, 4208–4218.

Sharma, M., Ioannidis, J.P.A., Aasly, J.O., et al. (2012). A multi-centre clinico-genetic analysis of the VPS35 gene in Parkinson disease indicates reduced penetrance for disease-associated variants. *Journal of medical genetics*. *49*, 721–726.

Shearer, M.J., and Newman, P. (2008). Metabolism and cell biology of vitamin K. *Thrombosis and Haemostasis*. *100*, 530–547.

Shehadeh, L., Mitsi, G., Adi, N., et al. (2009). Expression of Lewy body protein septin 4 in postmortem brain of Parkinson's disease and control subjects. *Movement Disorders*. *24*, 204–210.

Sheluho, D., and Ackerman, S.H. (2001). An accessible hydrophobic surface is a key element of the molecular chaperone action of Atp11p. *The Journal of Biological Chemistry*. *276*, 39945–39949.

Sheng, Z.-H., and Cai, Q. (2012). Mitochondrial transport in neurons: impact on synaptic homeostasis and neurodegeneration. *Nature Reviews. Neuroscience*. *13*, 77–93.

Shiba, K., Arai, T., Sato, S., et al. (2009). Parkin stabilizes PINK1 through direct interaction. *Biochemical and Biophysical Research Communications*. *383*, 331–335.

Shiba-Fukushima, K., Imai, Y., Yoshida, S., et al. (2012). PINK1-mediated phosphorylation of the Parkin ubiquitin-like domain primes mitochondrial translocation of Parkin and regulates mitophagy. *Scientific Reports*. *2*, 1002.

Shimura, H., Hattori, N., Kubo, S., et al. (1999). Immunohistochemical and subcellular localization of Parkin protein: absence of protein in autosomal recessive juvenile parkinsonism patients. *Annals of neurology*. *45*, 668–672.

Shimura, H., Hattori, N., Kubo, S. i, et al. (2000). Familial Parkinson disease gene product, parkin, is a ubiquitin-protein ligase. *Nature Genetics*. *25*, 302–305.

Shimura, H., Schlossmacher, M.G., Hattori, N., et al. (2001). Ubiquitination of a new form of alpha-synuclein by parkin from human brain: implications for Parkinson's disease. *Science*. *293*, 263–269.

Shin, J.-H., Ko, H.S., Kang, H., et al. (2011). PARIS (ZNF746) repression of PGC-1α contributes to neurodegeneration in Parkinson's disease. *Cell*. *144*, 689–702.

Shirakashi, Y., Kawamoto, Y., Tomimoto, H., et al. (2006). alpha-Synuclein is colocalized with 14-3-3 and synphilin-1 in A53T transgenic mice. *Acta Neuropathologica*. *112*, 681–689.

Shojaee, S., Sina, F., Banihosseini, S.S., et al. (2008). Genome-wide linkage analysis of a Parkinsonian-pyramidal syndrome pedigree by 500 K SNP arrays. *American journal of human genetics*. *82*, 1375–1384.

Sidransky, E., Nalls, M.A., Aasly, J.O., et al. (2009). Multicenter analysis of glucocerebrosidase mutations in Parkinson's disease. *The New England journal of medicine*. *361*, 1651–1661.

Da Silva, F.L., Coelho Cerqueira, E., de Freitas, M.S., et al. (2013). Vitamins K interact with N-terminus α-synuclein and modulate the protein fibrillization in vitro. Exploring the interaction between quinones and α-synuclein. *Neurochemistry International*. *62*, 103–112.

Simón-Sánchez, J., Schulte, C., Bras, J.M., et al. (2009). Genome-wide association study reveals genetic risk underlying Parkinson's disease. *Nature genetics*. *41*, 1308–1312.

Sina, F., Shojaee, S., Elahi, E., et al. (2009). R632W mutation in PLA2G6 segregates with dystonia-parkinsonism in a consanguineous Iranian family. *European journal of neurology: the official journal of the European Federation of Neurological Societies*. *16*, 101–104.

Sironi, F., Primignani, P., Zini, M., et al. (2008). Parkin analysis in early onset Parkinson's disease. *Parkinsonism & related disorders*. *14*, 326–333.

Skipper, L., Wilkes, K., Toft, M., et al. (2004). Linkage disequilibrium and association of MAPT H1 in Parkinson disease. *American journal of human genetics*. *75*, 669–677.

Smith, W.W., Pei, Z., Jiang, H., et al. (2005). Leucine-rich repeat kinase 2 (LRRK2) interacts with parkin, and mutant LRRK2 induces neuronal degeneration. *Proceedings of the National Academy of Sciences of the United States of America*. *102*, 18676–18681.

Snyder, H., Mensah, K., Theisler, C., et al. (2003). Aggregated and monomeric alpha-synuclein bind to the S6' proteasomal protein and inhibit proteasomal function. *The Journal of biological chemistry*. *278*, 11753–11759.

Song, D.D., Shults, C.W., Sisk, A., et al. (2004). Enhanced substantia nigra mitochondrial pathology in human alpha-synuclein transgenic mice after treatment with MPTP. *Experimental neurology*. *186*, 158–172.

Sousa, V.L., Bellani, S., Giannandrea, M., et al. (2009). {alpha}-synuclein and its A30P mutant affect actin cytoskeletal structure and dynamics. *Molecular Biology of the Cell*. *20*, 3725–3739.

Spillantini, M.G., and Goedert, M. (2013). Tau pathology and neurodegeneration. *The Lancet Neurology*. *12*, 609–622.

Spillantini, M.G., Schmidt, M.L., Lee, V.M., et al. (1997). Alpha-synuclein in Lewy bodies. *Nature*. *388*, 839–840.

Spratt, D.E., Julio Martinez-Torres, R., Noh, Y.J., et al. (2013). A molecular explanation for the recessive nature of parkin-linked Parkinson's disease. *Nature Communications*. *4*, 1983.

Sprinzak, E., Sattath, S., and Margalit, H. (2003). How reliable are experimental protein-protein interaction data? *Journal of Molecular Biology*. *327*, 919–923.

Sriram, S.R., Li, X., Ko, H.S., et al. (2005). Familial-associated mutations differentially disrupt the solubility, localization, binding and ubiquitination properties of parkin. *Human Molecular Genetics*. *14*, 2571–2586.

Stamey, W., Davidson, A., and Jankovic, J. (2008). Shoulder pain: a presenting symptom of Parkinson disease. *Journal of clinical rheumatology: practical reports on rheumatic & musculoskeletal diseases*. *14*, 253–254.

Staropoli, J.F., McDermott, C., Martinat, C., et al. (2003). Parkin is a component of an SCF-like ubiquitin ligase complex and protects postmitotic neurons from kainate excitotoxicity. *Neuron*. *37*, 735–749.

Stichel, C.C., Augustin, M., Kühn, K., et al. (2000). Parkin expression in the adult mouse brain. *The European journal of neuroscience*. *12*, 4181–4194.

Van der Stoep, N., van Paridon, C.D.M., Janssens, T., et al. (2009). Diagnostic guidelines for high-resolution melting curve (HRM) analysis: an interlaboratory validation of BRCA1 mutation scanning using the 96-well LightScanner. *Human Mutation*. *30*, 899–909.

Storch, A., Jost, W.H., Vieregge, P., et al. (2007). Randomized, double-blind, placebo-controlled trial on symptomatic effects of coenzyme Q(10) in Parkinson disease. *Archives of Neurology*. *64*, 938–944.

St-Pierre, J., Drori, S., Uldry, M., et al. (2006). Suppression of reactive oxygen species and neurodegeneration by the PGC-1 transcriptional coactivators. *Cell*. *127*, 397–408.

Sul, J.-W., Park, M.-Y., Shin, J., et al. (2013). Accumulation of the parkin substrate, FAF1, plays a key role in the dopaminergic neurodegeneration. *Human Molecular Genetics*. *22*, 1558–1573.

Sulzer, D. (2007). Multiple hit hypotheses for dopamine neuron loss in Parkinson's disease. *Trends in Neurosciences*. *30*, 244–250.

Sulzer, D., and Surmeier, D.J. (2013). Neuronal vulnerability, pathogenesis, and Parkinson's disease. *Movement Disorders: Official Journal of the Movement Disorder Society*. *28*, 41–50.

Sun, M., Latourelle, J.C., Wooten, G.F., et al. (2006a). Influence of heterozygosity for parkin mutation on onset age in familial Parkinson disease: the GenePD study. *Archives of neurology*. *63*, 826–832.

Sun, M., Latourelle, J.C., Wooten, G.F., et al. (2006b). Influence of heterozygosity for parkin mutation on onset age in familial Parkinson disease: the GenePD study. *Archives of neurology*. *63*, 826–832.

Sun, Y., Vashisht, A.A., Tchieu, J., et al. (2012). Voltage-dependent anion channels (VDACs) recruit Parkin to defective mitochondria to promote mitochondrial autophagy. *The Journal of Biological Chemistry*. *287*, 40652–40660.

Sunada, Y., Saito, F., Matsumura, K., et al. (1998). Differential expression of the parkin gene in the human brain and peripheral leukocytes. *Neuroscience letters*. *254*, 180–182.

Surka, M.C., Tsang, C.W., and Trimble, W.S. (2002). The mammalian septin MSF localizes with microtubules and is required for completion of cytokinesis. *Molecular Biology of the Cell*. *13*, 3532–3545.

Suter, B., Kittanakom, S., and Stagljar, I. (2008). Two-hybrid technologies in proteomics research. *Current Opinion in Biotechnology*. *19*, 316–323.

Sveinbjörnsdottir, S., Hicks, A.A., Jonsson, T., et al. (2000). Familial aggregation of Parkinson's disease in Iceland. *The New England journal of medicine*. *343*, 1765–1770.

Swan, M., and Saunders-Pullman, R. (2013). The association between ß-glucocerebrosidase mutations and parkinsonism. *Current neurology and neuroscience reports*. *13*, 368.

Taba, P., and Asser, T. (2003). Incidence of Parkinson's disease in Estonia. *Neuroepidemiology*. *22*, 41–45.

Tain, L.S., Mortiboys, H., Tao, R.N., et al. (2009). Rapamycin activation of 4E-BP prevents parkinsonian dopaminergic neuron loss. *Nature Neuroscience*. *12*, 1129–1135.

Takahashi, Y. (2003). The 14-3-3 proteins: gene, gene expression, and function. *Neurochemical Research*. *28*, 1265–1273.

Tan, E.-K. (2007). The role of common genetic risk variants in Parkinson disease. *Clinical genetics*. *72*, 387–393.

Tan, E.-K., and Skipper, L.M. (2007). Pathogenic mutations in Parkinson disease. *Human mutation*. *28*, 641–653.

Tan, E.K., Shen, H., Tan, J.M.M., et al. (2005). Differential expression of splice variant and wild-type parkin in sporadic Parkinson's disease. *Neurogenetics*. *6*, 179–184.

Tan, E.-K., Yew, K., Chua, E., et al. (2006). PINK1 mutations in sporadic early-onset Parkinson's disease. *Movement disorders: official journal of the Movement Disorder Society*. *21*, 789–793.

Tan, E.-K., Zhao, Y., Skipper, L., et al. (2007). The LRRK2 Gly2385Arg variant is associated with Parkinson's disease: genetic and functional evidence. *Human genetics*. *120*, 857–863.

Tanaka, T., Iino, M., and Goto, K. (2014). Knockdown of Sec8 enhances the binding affinity of c-Jun N-terminal kinase (JNK)-interacting protein 4 for mitogen-activated protein kinase kinase 4 (MKK4) and suppresses the phosphorylation of MKK4, p38, and JNK, thereby inhibiting apoptosis. *The FEBS journal*. *281*, 5237–5250.

Tanji, K., Mori, F., Kakita, A., et al. (2011). Alteration of autophagosomal proteins (LC3, GABARAP and GATE-16) in Lewy body disease. *Neurobiology of Disease*. *43*, 690–697.

Tanner, C.M., Ottman, R., Goldman, S.M., et al. (1999). Parkinson disease in twins: an etiologic study. *JAMA: the journal of the American Medical Association*. *281*, 341–346.

Tanner, C.M., Kamel, F., Ross, G.W., et al. (2011). Rotenone, paraquat, and Parkinson's disease. *Environmental health perspectives*. *119*, 866–872.

Tay, S.-P., Yeo, C.W.S., Chai, C., et al. (2010). Parkin enhances the expression of cyclin-dependent kinase 6 and negatively regulates the proliferation of breast cancer cells. *The Journal of Biological Chemistry*. *285*, 29231–29238.

Tayebi, N., Walker, J., Stubblefield, B., et al. (2003). Gaucher disease with parkinsonian manifestations: does glucocerebrosidase deficiency contribute to a vulnerability to parkinsonism? *Molecular genetics and metabolism*. *79*, 104–109.

Taylor, C.F. (2009). Mutation scanning using high-resolution melting. *Biochemical Society Transactions*. *37*, 433–437.

Taylor, K.S.M., Cook, J.A., and Counsell, C.E. (2007). Heterogeneity in male to female risk for Parkinson's disease. *Journal of neurology, neurosurgery, and psychiatry*. *78*, 905–906.

Teismann, P., and Schulz, J.B. (2004). Cellular pathology of Parkinson's disease: astrocytes, microglia and inflammation. *Cell and Tissue Research*. *318*, 149–161.

Thaler, A., Ash, E., Gan-Or, Z., et al. (2009). The LRRK2 G2019S mutation as the cause of Parkinson's disease in Ashkenazi Jews. *Journal of neural transmission*. *116*, 1473–1482.

Thrower, J.S., Hoffman, L., Rechsteiner, M., et al. (2000). Recognition of the polyubiquitin proteolytic signal. *The EMBO journal*. *19*, 94–102.

Tinazzi, M., Del Vesco, C., Fincati, E., et al. (2006). Pain and motor complications in Parkinson's disease. *Journal of neurology, neurosurgery, and psychiatry*. *77*, 822–825.

Tobin, J.E., Latourelle, J.C., Lew, M.F., et al. (2008). Haplotypes and gene expression implicate the MAPT region for Parkinson disease: the GenePD Study. *Neurology*. *71*, 28–34.

Toime, L.J., and Brand, M.D. (2010). Uncoupling protein-3 lowers reactive oxygen species production in isolated mitochondria. *Free Radical Biology & Medicine*. *49*, 606–611.

Tokita, H., Tsuchida, A., Miyazawa, K., et al. (2006). Vitamin K2-induced antitumor effects via cell-cycle arrest and apoptosis in gastric cancer cell lines. *International Journal of Molecular Medicine*. *17*, 235–243.

Toma, M.I., Grosser, M., Herr, A., et al. (2008). Loss of heterozygosity and copy number abnormality in clear cell renal cell carcinoma discovered by high-density affymetrix 10K single nucleotide polymorphism mapping array. *Neoplasia*. *10*, 634–642.

Toyooka, K., Muratake, T., Tanaka, T., et al. (1999). 14-3-3 protein eta chain gene (YWHAH) polymorphism and its genetic association with schizophrenia. *American Journal of Medical Genetics*. *88*, 164–167.

Trempe, J.-F., Sauvé, V., Grenier, K., et al. (2013). Structure of parkin reveals mechanisms for ubiquitin ligase activation. *Science*. *340*, 1451–1455.

Tretiakoff, C. (1919). Contribution a l'etude de l'anatomie pathologique du locus niger de Soemmering avec quelques deductions relatives a la pathogenie des troubles du tonus musculaire et de la maladie de Parkinson (Paris: Jouve and Co).

Trinh, J., and Farrer, M. (2013). Advances in the genetics of Parkinson disease. *Nature reviews. Neurology*. *9*, 445–454.

Tsai, Y.C., Fishman, P.S., Thakor, N.V., et al. (2003). Parkin facilitates the elimination of expanded polyglutamine proteins and leads to preservation of proteasome function. *The Journal of Biological Chemistry*. *278*, 22044–22055.

Tsang, C.W., Estey, M.P., DiCiccio, J.E., et al. (2011). Characterization of presynaptic septin complexes in mammalian hippocampal neurons. *Biological Chemistry*. *392*, 739–749.

Turrens, J.F. (2003). Mitochondrial formation of reactive oxygen species. *The Journal of Physiology*. *552*, 335–344.

Twig, G., and Shirihai, O.S. (2011). The interplay between mitochondrial dynamics and mitophagy. *Antioxidants & Redox Signaling*. *14*, 1939–1951.

Uchiki, T., Kim, H.T., Zhai, B., et al. (2009). The ubiquitin-interacting motif protein, S5a, is ubiquitinated by all types of ubiquitin ligases by a mechanism different from typical substrate recognition. *The Journal of Biological Chemistry*. *284*, 12622–12632.

Ulmer, T.S., Bax, A., Cole, N.B., et al. (2005). Structure and dynamics of micelle-bound human alpha-synuclein. *The Journal of biological chemistry*. *280*, 9595–9603.

Ulukaya, E., Colakogullari, M., and Wood, E.J. (2004). Interference by anti-cancer chemotherapeutic agents in the MTT-tumor chemosensitivity assay. *Chemotherapy*. *50*, 43–50.

Um, J.W., and Chung, K.C. (2006). Functional modulation of parkin through physical interaction with SUMO-1. *Journal of Neuroscience Research*. *84*, 1543–1554.

Um, J.W., Min, D.S., Rhim, H., et al. (2006). Parkin ubiquitinates and promotes the degradation of RanBP2. *Journal of Biological Chemistry*. *281*, 3595–3603.

Um, J.W., Im, E., Lee, H.J., et al. (2010). Parkin directly modulates 26S proteasome activity. *The Journal of Neuroscience: The Official Journal of the Society for Neuroscience*. *30*, 11805–11814.

Um, J.W., Han, K.A., Im, E., et al. (2012). Neddylation positively regulates the ubiquitin E3 ligase activity of parkin. *Journal of Neuroscience Research*. *90*, 1030–1042.

Valente, E.M. (2004). Hereditary early-onset Parkinson's disease caused by mutations in PINK1. *Science*. *304*, 1158–1160.

Valente, E.M., Arena, G., Torosantucci, L., et al. (2012). Molecular pathways in sporadic PD. *Parkinsonism & Related Disorders*. *18 Suppl 1*, S71–S73.

Vandekerckhove, J., and Weber, K. (1978). At least six different actins are expressed in a higher mammal: an analysis based on the amino acid sequence of the amino-terminal tryptic peptide. *Journal of Molecular Biology*. *126*, 783–802.

Vandesompele, J., De Preter, K., Pattyn, F., et al. (2002). Accurate normalization of real-time quantitative RT-PCR data by geometric averaging of multiple internal control genes. *Genome biology*. *3*, 1–11.

Venda, L.L., Cragg, S.J., Buchman, V.L., et al. (2010). α-Synuclein and dopamine at the crossroads of Parkinson's disease. *Trends in Neurosciences*. *33*, 559–568.

Ventura-Clapier, R., Garnier, A., and Veksler, V. (2008). Transcriptional control of mitochondrial biogenesis: the central role of PGC-1alpha. *Cardiovascular Research*. *79*, 208–217.

Vermeer, C. (1990). Gamma-carboxyglutamate-containing proteins and the vitamin K-dependent carboxylase. *The Biochemical Journal*. *266*, 625–636.

Vernon, A.C., Johansson, S.M., and Modo, M.M. (2010). Non-invasive evaluation of nigrostriatal neuropathology in a proteasome inhibitor rodent model of Parkinson's disease. *BMC neuroscience*. *11*, 1.

Vilariño-Güell, C., Wider, C., Ross, O.A., et al. (2011). VPS35 mutations in Parkinson disease. *American Journal of Human Genetics*. *89*, 162–167.

Vincow, E.S., Merrihew, G., Thomas, R.E., et al. (2013). The PINK1-Parkin pathway promotes both mitophagy and selective respiratory chain turnover in vivo. *Proceedings of the National Academy of Sciences of the United States of America*. *110*, 6400–6405.

Vingerhoets, F.J., Schulzer, M., Calne, D.B., et al. (1997). Which clinical sign of Parkinson's disease best reflects the nigrostriatal lesion? *Annals of neurology*. *41*, 58–64.

Vinish, M., Prabhakar, S., Khullar, M., et al. (2010). Genetic screening reveals high frequency of PARK2 mutations and reduced Parkin expression conferring risk for Parkinsonism in North West India. *Journal of Neurology, Neurosurgery, and Psychiatry*. *81*, 166–170.

Vives-Bauza, C., de Vries, R.L.., Tocilescu, M.A., et al. (2009). Is there a pathogenic role for mitochondria in Parkinson's disease? *Parkinsonism & Related Disorders*. *15*, S241–S244.

Volpicelli-Daley, L.A., Luk, K.C., Patel, T.P., et al. (2011). Exogenous α-synuclein fibrils induce Lewy body pathology leading to synaptic dysfunction and neuron death. *Neuron*. *72*, 57–71.

Vos, M., Esposito, G., Edirisinghe, J.N., et al. (2012). Vitamin K2 is a mitochondrial electron carrier that rescues pink1 deficiency. *Science*. *336*, 1306–1310.

Wakabayashi, K., Tanji, K., Odagiri, S., et al. (2013). The Lewy body in Parkinson's disease and related neurodegenerative disorders. *Molecular neurobiology*. *47*, 495–508.

Wang, Z.G., and Ackerman, S.H. (2000). The assembly factor Atp11p binds to the beta-subunit of the mitochondrial F(1)-ATPase. *The Journal of Biological Chemistry*. *275*, 5767–5772.

Wang, C., Lu, R., Ouyang, X., et al. (2007). Drosophila overexpressing parkin R275W mutant exhibits dopaminergic neuron degeneration and mitochondrial abnormalities. *The Journal of neuroscience: the official journal of the Society for Neuroscience*. *27*, 8563–8570.

Wang, H., Song, P., Du, L., et al. (2011a). Parkin ubiquitinates Drp1 for proteasome-dependent degradation: implication of dysregulated mitochondrial dynamics in Parkinson's disease. *Journal of Biological Chemistry*. *286*, 11649–11658.

Wang, X., Winter, D., Ashrafi, G., et al. (2011b). PINK1 and Parkin target Miro for phosphorylation and degradation to arrest mitochondrial motility. *Cell*. *147*, 893–906.

Wang, X., Petrie, T.G., Liu, Y., et al. (2012a). Parkinson's disease-associated DJ-1 mutations impair mitochondrial dynamics and cause mitochondrial dysfunction. *Journal of neurochemistry*. *121*, 830–839.

Wang, X., Yan, M.H., Fujioka, H., et al. (2012b). LRRK2 regulates mitochondrial dynamics and function through direct interaction with DLP1. *Human Molecular Genetics*. *21*, 1931–1944.

Wang, Y.S., Shi, Y.M., Wu, Z.Y., et al. (1991). Parkinson's disease in China. Coordinational Group of Neuroepidemiology, PLA. *Chinese medical journal*. *104*, 960–964.

Wang, Z.G., White, P.S., and Ackerman, S.H. (2001). Atp11p and Atp12p are assembly factors for the F(1)-ATPase in human mitochondria. *The Journal of Biological Chemistry*. *276*, 30773–30778.

Wauer, T., and Komander, D. (2013). Structure of the human Parkin ligase domain in an autoinhibited state. *The EMBO journal*. *32*, 2099–2112.

Wenzel, D.M., Lissounov, A., Brzovic, P.S., et al. (2011). UBCH7 reactivity profile reveals parkin and HHARI to be RING/HECT hybrids. *Nature*. *474*, 105–108.

West, A.B., Lockhart, P.J., O'Farell, C., et al. (2003). Identification of a novel gene linked to parkin via a bi-directional promoter. *Journal of molecular biology*. *326*, 11–19.

West, A.B., Moore, D.J., Biskup, S., et al. (2005). Parkinson's disease-associated mutations in leucine-rich repeat kinase 2 augment kinase activity. *Proceedings of the National Academy of Sciences of the United States of America*. *102*, 16842–16847.

Westermann, B. (2010). Mitochondrial fusion and fission in cell life and death. *Nature Reviews. Molecular Cell Biology*. *11*, 872–884.

Whitworth, A.J., Theodore, D.A., Greene, J.C., et al. (2005). Increased glutathione S-transferase activity rescues dopaminergic neuron loss in a Drosophila model of Parkinson's disease. *Proceedings of the National Academy of Sciences of the United States of America*. *102*, 8024–8029.

Wider, C., Dickson, D.W., and Wszolek, Z.K. (2010). Leucine-rich repeat kinase 2 gene-associated disease: redefining genotype-phenotype correlation. *Neuro-degenerative diseases*. *7*, 175–179.

Williams, D.R., Watt, H.C., and Lees, A.J. (2006). Predictors of falls and fractures in bradykinetic rigid syndromes: a retrospective study. *Journal of neurology, neurosurgery, and psychiatry*. *77*, 468–473.

Wills, L.P., Beeson, G.C., Trager, R.E., et al. (2013). High-throughput respirometric assay identifies predictive toxicophore of mitochondrial injury. *Toxicology and Applied Pharmacology*. *272*, 490–502.

Winklhofer, K.F. (2014). Parkin and mitochondrial quality control: toward assembling the puzzle. *Trends in cell biology*.

Wirdefeldt, K., Gatz, M., Schalling, M., et al. (2004). No evidence for heritability of Parkinson disease in Swedish twins. *Neurology*. *63*, 305–311.

Wirdefeldt, K., Adami, H.-O., Cole, P., et al. (2011). Epidemiology and etiology of Parkinson's disease: a review of the evidence. *European journal of epidemiology*. *26 Suppl 1*, S1–S58.

Witten, L., Sager, T., Thirstrup, K., et al. (2009). HIF prolyl hydroxylase inhibition augments dopamine release in the rat brain in vivo. *Journal of Neuroscience Research*. *87*, 1686–1694.

Wong, A.H.C., Macciardi, F., Klempan, T., et al. (2003). Identification of candidate genes for psychosis in rat models, and possible association between schizophrenia and the 14-3-3eta gene. *Molecular Psychiatry*. *8*, 156–166.

Wood, S.J., Wypych, J., Steavenson, S., et al. (1999). Alpha-synuclein fibrillogenesis is nucleation-dependent. Implications for the pathogenesis of Parkinson's disease. *The Journal of Biological Chemistry*. *274*, 19509–19512.

Wood-Kaczmar, A., Gandhi, S., Yao, Z., et al. (2008). PINK1 is necessary for long term survival and mitochondrial function in human dopaminergic neurons. *PloS One*. *3*, e2455.

Wooten, G.F., Currie, L.J., Bovbjerg, V.E., et al. (2004). Are men at greater risk for Parkinson's disease than women? *Journal of neurology, neurosurgery, and psychiatry*. *75*, 637–639.

Xie, W., and Chung, K.K.K. (2012). Alpha-synuclein impairs normal dynamics of mitochondria in cell and animal models of Parkinson's disease. *Journal of Neurochemistry*. *122*, 404–414.

Xie, W., Li, X., Li, C., et al. (2010). Proteasome inhibition modeling nigral neuron degeneration in Parkinson's disease. *Journal of Neurochemistry*. *115*, 188–199.

Xiong, H., Wang, D., Chen, L., et al. (2009). Parkin, PINK1, and DJ-1 form a ubiquitin E3 ligase complex promoting unfolded protein degradation. *The Journal of Clinical Investigation*. *119*, 650–660.

Xu, K., Xu, Y.-H., Chen, J.-F., et al. (2010). Neuroprotection by caffeine: time course and role of its metabolites in the MPTP model of Parkinson's disease. *Neuroscience*. *167*, 475–481.

Xu, L., Lin, D., Yin, D., et al. (2014). An emerging role of PARK2 in cancer. *Journal of Molecular Medicine*. *92*, 31–42.

Yaguchi, M., Miyazawa, K., Katagiri, T., et al. (1997). Vitamin K2 and its derivatives induce apoptosis in leukemia cells and enhance the effect of all-trans retinoic acid. *Leukemia*. *11*, 779–787.

Yamamoto, A., Friedlein, A., Imai, Y., et al. (2005). Parkin phosphorylation and modulation of its E3 ubiquitin ligase activity. *The Journal of Biological Chemistry*. *280*, 3390–3399.

Yang, F., Jiang, Q., Zhao, J., et al. (2005). Parkin stabilizes microtubules through strong binding mediated by three independent domains. *Journal of Biological Chemistry*. *280*, 17154–17162.

Yang, H., Zhou, X., Liu, X., et al. (2011). Mitochondrial dysfunction induced by knockdown of mortalin is rescued by Parkin. *Biochemical and Biophysical Research Communications*. *410*, 114–120.

Yang, Y., Gehrke, S., Imai, Y., et al. (2006). Mitochondrial pathology and muscle and dopaminergic neuron degeneration caused by inactivation of Drosophila Pink1 is rescued by Parkin. *Proceedings of the National Academy of Sciences of the United States of America*. *103*, 10793–10798.

Yao, D., Gu, Z., Nakamura, T., et al. (2004). Nitrosative stress linked to sporadic Parkinson's disease: S-nitrosylation of parkin regulates its E3 ubiquitin ligase activity. *Proceedings of the National Academy of Sciences of the United States of America*. *101*, 10810–10814.

Yao, Y., Li, L., Zhang, H., et al. (2012). Enhanced therapeutic efficacy of vitamin K2 by silencing BCL-2 expression in SMMC-7721 hepatocellular carcinoma cells. *Oncology Letters*. *4*, 163–167.

Yeo, C.W.S., Ng, F.S.L., Chai, C., et al. (2012). Parkin pathway activation mitigates glioma cell proliferation and predicts patient survival. *Cancer Research*. *72*, 2543–2553.

Yin, D., Ogawa, S., Kawamata, N., et al. (2009). High-resolution genomic copy number profiling of glioblastoma multiforme by single nucleotide polymorphism DNA microarray. *Molecular cancer research: MCR*. *7*, 665–677.

Yokoyama, T., Miyazawa, K., Naito, M., et al. (2008). Vitamin K2 induces autophagy and apoptosis simultaneously in leukemia cells. *Autophagy*. *4*, 629–640.

Yonova-Doing, E., Atadzhanov, M., Quadri, M., et al. (2012). Analysis of LRRK2, SNCA, Parkin, PINK1, and DJ-1 in Zambian patients with Parkinson's disease. *Parkinsonism & Related Disorders*. *18*, 567–571.

Yoshii, S.R., Kishi, C., Ishihara, N., et al. (2011). Parkin mediates proteasome-dependent protein degradation and rupture of the outer mitochondrial membrane. *The Journal of Biological Chemistry*. *286*, 19630–19640.

Yu, W., Sun, Y., Guo, S., et al. (2011). The PINK1/Parkin pathway regulates mitochondrial dynamics and function in mammalian hippocampal and dopaminergic neurons. *Human Molecular Genetics*. *20*, 3227–3240.

Zabetian, C.P., Hutter, C.M., Factor, S.A., et al. (2007). Association analysis of MAPT H1 haplotype and subhaplotypes in Parkinson's disease. *Annals of neurology*. *62*, 137–144.

Zarate-Lagunes, M., Gu, W.J., Blanchard, V., et al. (2001). Parkin immunoreactivity in the brain of human and non-human primates: an immunohistochemical analysis in normal conditions and in Parkinsonian syndromes. *The Journal of comparative neurology*. *432*, 184–196.

Zeng, B.-Y., Iravani, M.M., Lin, S.-T., et al. (2006). MPTP treatment of common marmosets impairs proteasomal enzyme activity and decreases expression of structural and regulatory elements of the 26S proteasome. *The European Journal of Neuroscience*. *23*, 1766–1774.

Zhang, Z.X., and Román, G.C. (1993). Worldwide occurrence of Parkinson's disease: an updated review. *Neuroepidemiology*. *12*, 195–208.

Zhang, C., Lin, M., Wu, R., et al. (2011). Parkin, a p53 target gene, mediates the role of p53 in glucose metabolism and the Warburg effect. *Proceedings of the National Academy of Sciences of the United States of America*. *108*, 16259–16264.

Zhang, L., Shimoji, M., Thomas, B., et al. (2005). Mitochondrial localization of the Parkinson's disease related protein DJ-1: implications for pathogenesis. *Human molecular genetics*. *14*, 2063–2073.

Zhang, Y., Gao, J., Chung, K.K., et al. (2000). Parkin functions as an E2-dependent ubiquitin- protein ligase and promotes the degradation of the synaptic vesicle-associated protein, CDCrel-1. *Proceedings of the National Academy of Sciences of the United States of America*. *97*, 13354–13359.

Zhang, Z.-X., Roman, G.C., Hong, Z., et al. (2004). Parkinson's disease in China: prevalence in Beijing, Xian, and Shanghai. *Lancet*. *365*, 595–597.

Zhang, Z.-X., Dong, Z.-H., and Román, G.C. (2006). Early descriptions of Parkinson disease in ancient China. *Archives of neurology*. *63*, 782–784.

Zhao, J., Meyerkord, C.L., Du, Y., et al. (2011a). 14-3-3 proteins as potential therapeutic targets. *Seminars in Cell & Developmental Biology*. *22*, 705–712.

Zhao, T., De Graaff, E., Breedveld, G.J., et al. (2011b). Loss of nuclear activity of the FBXO7 protein in patients with parkinsonian-pyramidal syndrome (PARK15). *PloS one*. *6*, e16983.

Zhao, T., Severijnen, L.-A., van der Weiden, M., et al. (2013). FBXO7 immunoreactivity in α-synuclein-containing inclusions in Parkinson disease and multiple system atrophy. *Journal of neuropathology and experimental neurology*. *72*, 482–488.

Zhong, L. (2004). RING finger ubiquitin-protein isopeptide ligase Nrdp1/FLRF regulates parkin stability and activity. *Journal of Biological Chemistry*. *280*, 9425–9430.

Zhou, M., and Veenstra, T.D. (2007). Proteomic analysis of protein complexes. *Proteomics*. *7*, 2688–2697.

Zimprich, A., Biskup, S., Leitner, P., et al. (2004). Mutations in LRRK2 cause autosomal-dominant parkinsonism with pleomorphic pathology. *Neuron*. *44*, 601–607.

Zimprich, A., Benet-Pagès, A., Struhal, W., et al. (2011). A mutation in VPS35, encoding a subunit of the retromer complex, causes late-onset Parkinson disease. *American Journal of Human Genetics*. *89*, 168–175.

Zinchuk, V., Zinchuk, O., and Okada, T. (2007). Quantitative colocalization analysis of multicolor confocal immunofluorescence microscopy images: pushing pixels to explore biological phenomena. *Acta Histochemica Et Cytochemica*. *40*, 101–111.

Ziviani, E., Tao, R.N., and Whitworth, A.J. (2010). Drosophila parkin requires PINK1 for mitochondrial translocation and ubiquitinates mitofusin. *Proceedings of the National Academy of Sciences of the United States of America*. *107*, 5018–5023.

APPENDIX I

UK Parkinson's Disease Society Brain Bank criteria for the diagnosis of PD

Step 1: Diagnosis of parkinsonian syndrome
Bradykinesia (slowness of initiation of voluntary movement with progressive reduction in speed and amplitude or repetitive actions)
And at least one of the following:
Muscular rigidity
4–6 Hz rest tremor
Postural instability not caused by primary visual, vestibular, cerebellar, or proprioceptive dysfunction

Step 2: Exclusion criteria for PD
History of repeated strokes with stepwise progression of parkinsonian features
History of repeated head injury
History of definite encephalitis
Oculogyric crises
Neuroleptic treatment at onset of symptoms
More than one affected relative*
Sustained remission
Strictly unilateral features after three years
Supranuclear gaze palsy
Cerebellar signs
Early severe autonomic involvement
Early severe dementia with disturbances of memory, language, and praxis
Babinski sign
Presence of a cerebral tumor or communicating hydrocephalus on CT scan
Negative response to large doses of levodopa (if malabsorption excluded)
MPTP exposure

Step 3: Supportive positive criteria of PD
Three or more required for diagnosis of definite PD:
Unilateral onset
Rest tremor present
Progressive disorder
Persistent asymmetry affecting the side of onset most
Excellent response (70%–100%) to levodopa
Severe levodopa-induced chorea
Levodopa response for five years or more
Clinical course of ten years or more

*This criteria is no longer used (Hughes et al. 2001). Adapted from Gibbs & Lees (1988b).

APPENDIX II

1. DNA EXTRACTION SOLUTIONS

Cell lysis buffer

Sucrose	109.54g
Triton X-100	10ml
$MgCl_2$	476mg
1M Tris-HCl stock solution, pH 8	10ml

Add ddH_2O to a final volume of 1 liter.

3M Na-Ac solution

Sodium acetate	40.81g
ddH_2O	50ml

Adjust pH to 5.2 with glacial acetic acid. Add ddH_2O to a final volume of 100ml.

Na-EDTA solution

4mM NaCl stock solution	18.75ml
100mM EDTA stock solution	250ml

Phenol-chloroform

Phenol	50ml
Chloroform	48ml
8-hydroxyquinone	2ml

Store at 4˚C.

Chloroform-octanol (24:1)

Chloroform	96ml
Octanol	4ml

Store at 4˚C.

10X TE stock solution

1M Tris-HCl stock, pH 8	10ml
500mM EDTA stock solution, pH 8	20ml

Add ddH_2O to a final volume of 100ml.

1X TE buffer

10X TE stock solution	10ml

Add ddH_2O to a final volume of 100ml.

2. ELECTROPHORESIS SOLUTIONS

20X SB stock solution

Sodium tetraborate decahydrate	38.14g

Add ddH_2O to a final volume of 1 liter.

1X SB buffer

20X SB stock solution	50ml

Add ddH_2O to a final volume of 1 liter.

4X SDS-PAGE resolving gel buffer

Tris base	109.2g
ddH_2O	330ml
10% SDS	24ml

Adjust pH to 8.8 using 1M HCl. Add ddH_2O to a final volume of 600ml.

4X SDS-PAGE stacking gel buffer

Tris base	36.3g
ddH_2O	330ml
10% SDS	24ml

Adjust pH to 6.8 using 1M HCl. Add ddH_2O to a final volume of 600ml.

10% Sodium dodecyl sulfate (SDS)

SDS	50g

Add ddH_2O to a final volume of 500ml.

10X SDS-PAGE running buffer

Tris base	30g
Glycine	144g
10% SDS	100ml

Add ddH_2O to a final volume of 1 liter.

1X SDS-PAGE running buffer

10X SDS-PAGE running buffer	100ml

Add ddH_2O to a final volume of 1 liter.

10% Ammonium persulfate (APS)

Ammonium persulfate	10g

Add ddH_2O to a final volume of 100ml. Mix well and store at 4^oC.

Transfer buffer

Tris base	3.03g
Glycine	14.4g
Methanol	200ml

Add ddH_2O to a final volume of 1 liter.

3. GELS

1% Agarose gel

Agarose	1g
1X SB buffer	100ml

Dissolve the mixture by microwaving for 1-2min on maximum power. Allow to cool to approximately 55^oC. Add 5µl ethidium bromide (10mg/ml).

2% Agarose gel

Agarose	2g
1X SB buffer	100ml

Dissolve the mixture by microwaving for 1-2min on maximum power. Allow to cool to approximately 55^oC. Add 5µl ethidium bromide (10mg/ml).

3.75% SDS-PAGE stacking gel

ddH_2O	2.53ml
10% SDS	40µl
4X SDS-PAGE stacking buffer	1ml
40% Acrylamide	390µl
TEMED	6µl
10% APS	30µl

Makes two gels for the Bio-Rad Mini gel apparatus system (Bio-Rad Laboratories, Hercules, California, USA)

12% SDS-PAGE resolving gel

ddH_2O	5.57ml
10% SDS	100µl
4X SDS-PAGE resolving buffer	1.25ml
40% Acrylamide	3ml
TEMED	5µl
10% APS	75µl

Makes two gels for the Bio-Rad Mini gel apparatus system (Bio-Rad Laboratories, Hercules, California, USA)

15% SDS-PAGE resolving gel

ddH_2O	4.82ml
10% SDS	100µl
4X SDS-PAGE resolving buffer	1.25ml
40% Acrylamide	3.75ml
TEMED	5µl
10% APS	75µl

Makes two gels for the Bio-Rad Mini gel apparatus system (Bio-Rad Laboratories, Hercules, California, USA)

4. LOADING DYES

Ethidium bromide stock (10mg/ml)

Ethidium bromide	500mg
ddH_2O	50ml

Stir well on a magnetic stirrer for 4h and store aliquots in a dark container at 4˚C.

Bromophenol blue loading dye

1% Bromophenol blue	10ml
Glycerol	50ml

Add ddH_2O to a final volume of 100ml. Mix well and store aliquots at 4˚C.

2X SDS loading buffer

10% SDS	600µl
1M Tris-HCl (pH 6.8)	1.5ml
1% Bromophenol blue	600µl
DTT	464mg
Glycerol	3ml

Add ddH_2O to a final volume of 15ml. Mix well and store aliquots at -20˚C.

5X SDS loading buffer

10% SDS	1.5ml
1M Tris-HCl (pH 6.8)	3.75ml
1% Bromophenol blue	1.5ml
DTT	1.16g
Glycerol	7.5ml

Add ddH_2O to a final volume of 15ml. Mix well and store aliquots at -20˚C.

5. BACTERIAL MEDIA

Luria-Bertani (LB) media

Bacto tryptone	5g
Yeast extract	2.5g
NaCl	5g

Add ddH_2O to a final volume of 500ml. Autoclave at 121˚C for 20min and allow cooling to approximately 55˚C. Add appropriate antibiotic (Ampicillin 25mg/liter; Kanamycin 5mg/liter).

LB agar plates

Bacto tryptone	5g
Yeast extract	2.5g
NaCl	5g
Bacto agar	8g

Add ddH_2O to a final volume of 500ml. Autoclave at 121˚C for 20min and allow cooling to approximately 55˚C. Add appropriate antibiotic (Ampicillin 25µg/ml; Kanamycin 5µg/ml). Pour into plates and allow 2-3h to set. Store at room temperature for up to three weeks.

6. YEAST MEDIA

YPDA media

Difco peptone	10g
Yeast extract	10g
Glucose	10g
0.2% L-adenine hemisulfate	7.5ml

Add ddH_2O to a final volume of 500ml. Autoclave at 121˚C for 20min.

2X YPDA media

Difco peptone	20g
Yeast extract	10g
Glucose	20
0.2% L-adenine hemisulfate	1.5ml

Add ddH_2O to a final volume of 500ml. Autoclave at 121˚C for 20min.

0.5X YPDA media

Difco peptone	2g
Yeast extract	1g
Glucose	2g
0.2% L-adenine hemisulfate	1.5ml

Add ddH_2O to a final volume of 200ml. Autoclave at 121˚C for 20min.

YPDA agar plates

Difco peptone	10g
Yeast extract	10g
Glucose	10g
0.2% L-adenine hemisulfate	7.5ml
Bacto agar	10g

Add ddH_2O to a final volume of 500ml. Autoclave at 121˚C for 20min and allow cooling to approximately 55˚C. Pour into plates and allow 2-3h to set. Store at room temperature for up to three weeks.

SD^{-Ade} agar plates

Glucose	12g
Yeast nitrogen base without amino acids	4g
SD^{-Ade} amino acid supplement	0.4g
Bacto agar	12g

Add ddH_2O to a final volume of 600ml. Autoclave at 121˚C for 20min and allow cooling to approximately 55˚C. Pour into plates and allow 2-3h to set. Store at room temperature for up to three weeks.

SD^{-His} agar plates

Glucose	12g
Yeast nitrogen base without amino acids	4g
SD^{-His} amino acid supplement	0.4g
Bacto agar	12g

Add ddH_2O to a final volume of 600ml. Autoclave at 121˚C for 20min and allow cooling to approximately 55˚C. Pour into plates and allow 2-3h to set. Store at room temperature for up to three weeks.

SD^{-Ura} agar plates

Glucose	12g
Yeast nitrogen base without amino acids	4g
SD^{-Ura} amino acid supplement	0.4g
Bacto agar	12g

Add ddH_2O to a final volume of 600ml. Autoclave at 121˚C for 20min and allow cooling to approximately 55˚C. Pour into plates and allow 2-3h to set. Store at room temperature for up to three weeks.

SD^{-Leu} media

Glucose	12g
Yeast nitrogen base without amino acids	4g
SD^{-His} amino acid supplement	0.4g

Add ddH_2O to a final volume of 600ml. Autoclave at 121˚C for 20min.

SD^{-Leu} agar plates

Glucose	12g
Yeast nitrogen base without amino acids	4g
SD^{-Leu} amino acid supplement	0.4g
Bacto agar	12g

Add ddH_2O to a final volume of 600ml. Autoclave at 121˚C for 20min and allow cooling to approximately 55˚C. Pour into plates and allow 2-3h to set. Store at room temperature for up to three weeks.

SD^{-Trp} media

Glucose	12g
Yeast nitrogen base without amino acids	4g
SD^{-Trp} amino acid supplement	0.4g

Add ddH_2O to a final volume of 600ml. Autoclave at 121˚C for 20min.

SD^{-Trp} agar plates

Glucose	12g
Yeast nitrogen base without amino acids	4g
SD^{-Trp} amino acid supplement	0.4g
Bacto agar	12g

Add ddH_2O to a final volume of 600ml. Autoclave at 121˚C for 20min and allow cooling to approximately 55˚C. Pour into plates and allow 2-3h to set. Store at room temperature for up to three weeks.

SD$^{-Leu-Trp}$ media

Glucose	12g
Yeast nitrogen base without amino acids	4g
SD$^{-Leu-Trp}$ amino acid supplement	0.4g

Add ddH_2O to a final volume of 600ml. Autoclave at 121˚C for 20min.

SD$^{-Leu-Trp}$ agar plates

Glucose	12g
Yeast nitrogen base without amino acids	4g
SD$^{-Leu-Trp}$ amino acid supplement	0.4g
Bacto agar	12g

Add ddH_2O to a final volume of 600ml. Autoclave at 121˚C for 20min and allow cooling to approximately 55˚C. Pour into plates and allow 2-3h to set. Store at room temperature for up to three weeks.

TDO media

Glucose	12g
Yeast nitrogen base without amino acids	4g
SD$^{-Leu-Trp-His}$ amino acid supplement	0.4g

Add ddH_2O to a final volume of 600ml. Autoclave at 121˚C for 20min.

TDO agar plates

Glucose	12g
Yeast nitrogen base without amino acids	4g
SD$^{-Leu-Trp-His}$ amino acid supplement	0.4g
Bacto agar	12g

Add ddH_2O to a final volume of 600ml. Autoclave at 121˚C for 20min and allow cooling to approximately 55˚C. Pour into plates and allow 2-3h to set. Store at room temperature for up to three weeks.

QDO media

Glucose	12g
Yeast nitrogen base without amino acids	4g
SD$^{-Leu-Trp-His-Ade}$ amino acid supplement	0.4g

Add ddH_2O to a final volume of 600ml. Autoclave at 121˚C for 20min.

QDO agar plates

Glucose	12g
Yeast nitrogen base without amino acids	4g
$SD^{-Leu-Trp-His-Ade}$ amino acid supplement	0.4g
Bacto agar	12g

Add ddH_2O to a final volume of 600ml. Autoclave at 121˚C for 20min and allow cooling to approximately 55˚C. Pour into plates and allow 2-3h to set. Store at room temperature for up to three weeks.

X-α-galactosidase (X-α-gal) solution (5mg/ml)

X-α-gal	25mg
Dimethylformamide	1ml

Makes a 25mg/ml stock solution. Dilute with dimethylformamide to a 5mg/ml working solution. Store in a dark container at -20˚C.

7. MAMMALIAN CELL CULTURE MEDIA

Fibroblast isolation media

Amniochrome II complete media	95ml
Chang Medium® D	95ml
Non-essential amino acids (NEAA)	5ml
Penicillin-streptomycin	5ml

Pre-warm to 37˚C before use. Store at 4˚C.

Fibroblast culture media

DMEM (4.5g/liter glucose, with L-glutamine)	450ml
Fetal bovine serum	50ml
Penicillin-streptomycin	5ml

Pre-warm to 37˚C before use. Store at 4˚C.

SH-SY5Y culture media

DMEM (4.5g/liter glucose, with L-glutamine)	222.5ml
Ham's F12 (with L-glutamine)	222.5ml
Fetal bovine serum	50ml
Penicillin-streptomycin	5ml

Pre-warm to 37˚C before use. Store at 4˚C.

SH-SY5Y serum-free media

DMEM (4.5g/liter glucose, with L-glutamine)	50ml
Ham's F12 (with L-glutamine)	50ml

Pre-warm to 37˚C before use. Store at 4˚C.

8. SOLUTIONS FOR THE GENERATION OF BACTERIAL COMPETENT CELLS

CAP buffer

$CaCl_2$	2.21g
Glycerol	37.5ml
PIPES	0.76g

Add ddH_2O to a final volume of 250ml. Adjust pH to 7.0 and store at 4˚C.

9. YEAST TRANSFORMATION SOLUTIONS

1M Lithium acetate (LiAc)

LiAc	5.1g

Add ddH_2O to a final volume of 50ml.

100mM LiAc

1M LiAc	5ml

Add ddH_2O to a final volume of 50ml.

50% Polyethylene glycol (PEG)

PEG 4000	25g

Add ddH_2O to a final volume of 50ml.

10. YEAST PLASMID PURIFICATION SOLUTIONS

Yeast lysis buffer

10% SDS	10ml
Triton X-100	2ml
5M NaCl stock solution	2ml
1M Tris-HCl stock solution, pH 8	1ml
500mM EDTA stock solution, pH 8	200µl

Add ddH_2O to a final volume of 100ml.

12. WESTERN BLOT SOLUTIONS

Passive lysis buffer

1M HEPES stock solution	10ml
5M NaCl stock solution	4ml
500mM EDTA stock solution, pH 8	4ml
Triton X-100	2ml
10mM Sodium pyrophosphate (NaPPi)	8ml
1M Na_3VO_4	400µl

Add ddH_2O to a final volume of 200ml. Aliquot and store at 4˚C. Prior to use, add 100µl of 50mM PMSF and one quarter protease inhibitor tablet (Roche) to 5ml passive lysis buffer.

Bradford protein reagent

Coomassie Brilliant Blue	100mg
Phosphoric acid	100ml
96% Ethanol	50ml

Add ddH_2O to a final volume of 1 liter. Filter 2-5 times until solution is light brown in color. Store in lightproof container at room temperature.

TBST

5M NaCl stock solution	30ml
1M Tris-HCl stock solution (pH 7.6)	20ml
Tween-20	1ml

Add ddH_2O to a final volume of 1 liter.

Membrane stripping buffer

Glycine	15g
10% SDS	10ml
Tween-20	10ml

Adjust pH to 2.2. Add ddH_2O to a final volume of 1 liter.

13. CO-LOCALIZATION SOLUTIONS

Phosphate buffered saline (PBS)

NaCl	8g
KCl	200mg
$Na_2HPO_4 \cdot 2H_2O$	1.42g
KH_2PO_4	200mg

Add ddH_2O to a final volume of 1 liter.

4% Paraformaldehyde

Paraformaldehyde	8g
PBS	200ml

Dissolve by adding 1ml of 1M NaOH and heating at 50˚C for 30min with constant stirring. Once dissolved, adjust final pH to 7.4-7.6.

Mounting media

Mowiol 4-88	12g
Glycerol	30g
ddH_2O	30ml

Add 60ml of a 0.2M Tris stock solution (pH 8.5) and stir overnight at room temperature. Dissolve remaining Mowiol by heating to 50˚C with constant stirring. Centrifuge at 5000g for 15 min. Aliquot and store supernatant at -20˚C. Prior to use, add a small quantity (<10mg) anti-fading agent (n-propylgallate) to 1ml mounting media and dissolve by heating to 50˚C for 1h. Centrifuge at 5000g for 2 min to remove residual sediment. Store in the dark at 4˚C for up to three weeks.

14. SOLUTIONS FOR CELL FUNCTION ASSAYS

5mg/ml MTT stock solution

Thiazolyl blue tetrazolium bromide	10mg
PBS	2ml

Filter through a 0.2µm filter before use. Store in the dark at 4˚C for up to two weeks.

0.1N Acidified isopropanol

38% HCl	990µl
Isopropanol	99.1ml

Store at room temperature.

40mM MK-4 (Vitamin K_2) stock solution

MK-4	35.6mg
Ethanol	2ml

Vortex well. Aliquot and store in the dark at -20˚C. Stable at 4˚C for up to two weeks.

40µM MK-4 (Vitamin K_2) working solution

MK-4 stock solution	20µl
Fibroblast culture media	20ml

Make up fresh before each use.

40mM CCCP stock solution

Carbonyl cyanide m-chlorophenyl hydrazone	16.2mg
DMSO	2ml

Aliquot and store in the dark at -20˚C. Stable at 4˚C for up to two weeks.

10µM CCCP working solution

40mM CCCP stock solution	5µl
Fibroblast culture media	20ml

Make up fresh before each use.

5mg/ml JC-1 stock solution

Tetraethyl benzimidazolyl carbocyanine iodide	5mg
DMSO	1ml

Aliquot in 40µl volumes and store in lightproof container at -20˚C.

0.5µg/ml JC-1 working solution

5mg/ml JC-1 stock solution	2µl
Fibroblast culture media	20ml

Make up fresh before each use. Keep in a lightproof tube.

APPENDIX III

1. YEAST CALCULATIONS (obtained from Clontech Manual)

Library titer

Count number of colonies on all plates with 30-300 colonies after four days

$$\text{\#colony forming units (cfu)/ml} = \frac{\text{\#cfu x 1000µl/1ml}}{\text{volume plated (µl) x dilution factor}}$$

Yeast mating efficiency

Number of cfu/ml on SD^{-Leu} plates indicates viability of prey partner

Number of cfu/ml on SD^{-Trp} plates indicates viability of bait partner

Number of cfu/ml on $SD^{-Leu-Trp}$ plates indicates viability of diploids

The lowest number of cfu/ml on SD^{-Leu} or SD^{-Trp} plates indicates which of the bait or prey partners is the limiting partner

$$\text{Mating efficiency} = \frac{\text{\#cfu/ml of diploids x 100}}{\text{\#cfu/ml of limiting partner}}$$

Number of clones screened

#clones screened = #cfu/ml of diploids x resuspension volume (ml)

2. HEMOCYTOMETRIC CELL COUNT

A hemocytometric yeast cell count was performed in order to obtain a bait culture titer prior to the use of the culture in Y2H library mating. Hemocytometric cell counting was also used to obtain the correct mammalian cell count for the accurate seeding of SH-SY5Y cells. A glass coverslip was placed on the counting surface of a Neubauer hemocytometer (Superior, Berlin, Germany) after both the coverslip and the hemocytometer were cleaned with ethanol. Approximately 50µl of a 1 in 10 dilution of cell suspension was loaded onto the counting surface, which filled the area underneath the coverslip through capillary action. The counting chamber was viewed under a microscope (Nikon TMS, Nikon Instruments, New York, USA) and the number of cells in the large central quadrant was counted. The number of cells per milliliter was calculated as follows:

#cells/ml = #cells in central quadrant x dilution factor x 10^4 (a constant used as the volume of the central quadrant is 10^{-4}ml)

APPENDIX IV

BACTERIAL STRAIN PHENOTYPES

E. coli strain DH5α

Φ 80d *lacZ*Δ*M15* recA1, *end*A1, *Gry* A96 *thi*-1, *hsd*R17 *sup*E44, *rel*A1, *deoR* Δ(*lac*ZYA *argF*)u169

YEAST STRAIN PHENOTYPES

S. cerevisiae strain AH109

*MAT*a, *trp1-901, leu2-3, ura3-5, his3-200, gal4*Δ, *gal80*Δ, *LYS::GAL1*$_{UAS}$*-GAL*$_{TATA}$*-HIS3, GAL2*$_{UAS}$*-GA2*$_{TATA}$*-ADE2, URA3:: MEL1*$_{UAS}$*-MEL1*$_{TATA}$*-lacZ* (James et al. 1996)

S. cerevisiae strain Y187

*MATα, ura3-52, his3-200, ade2-101, trp1-901, leu2-3, 112, gal4*Δ, *met-, gal80*Δ, *URA3:: GAL1*$_{UAS}$*-GAL1*$_{TATA}$*-lacZ* (Harper et al. 1993)

APPENDIX V

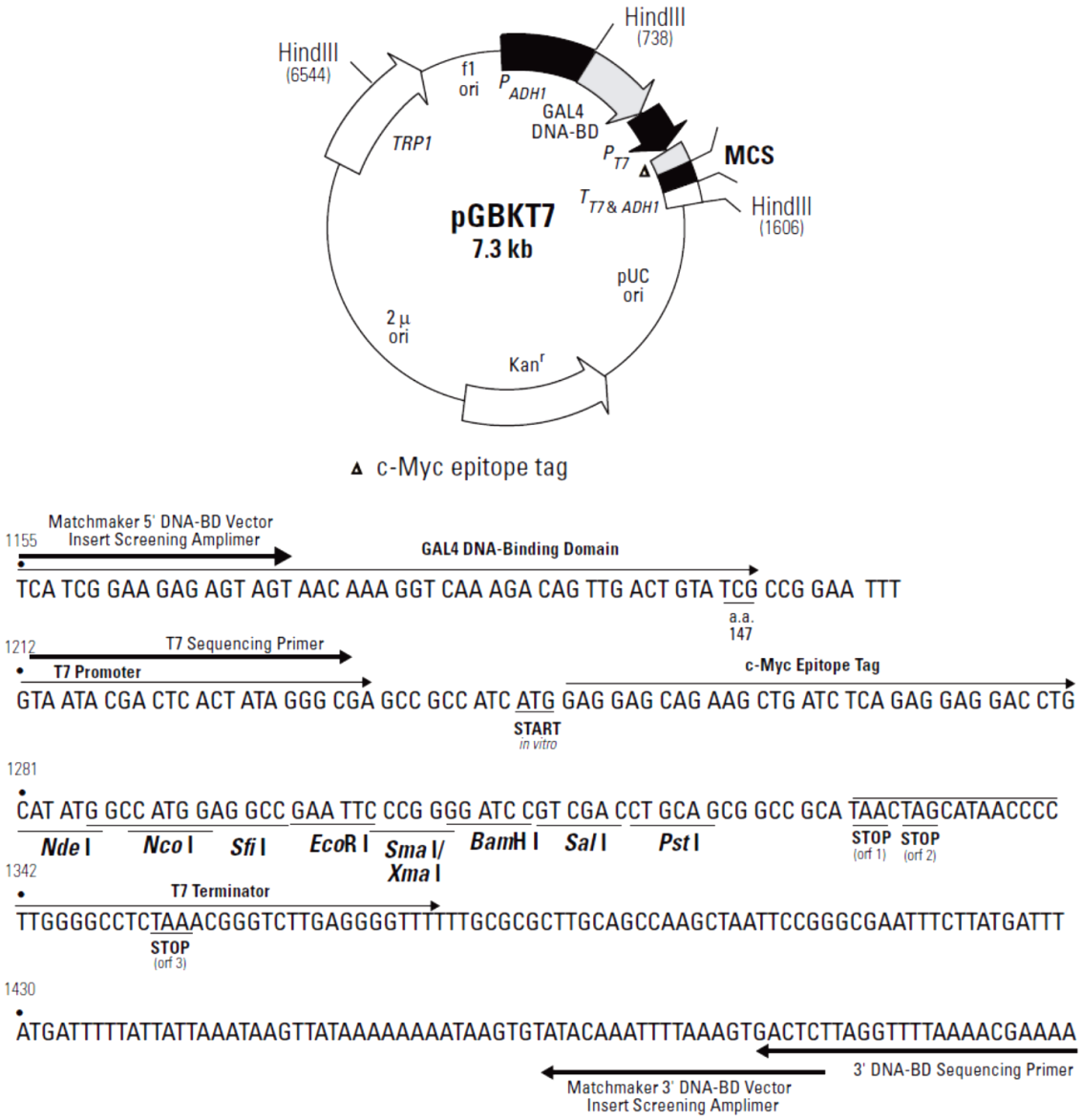

pGBKT7 restriction map and multiple cloning site (MCS). This vector expresses proteins fused to amino acids 1-47 of the GAL4 DNA binding domain (DNA-BD) as well as a c-Myc epitope tag. Expression in yeast is driven by the constitutive *ADH1* promoter (P_{ADH1}) whereas transcription is terminated by the *T7* and *ADH1* transcription termination sequence ($T_{T7\&ADH1}$). The vector also contains a *T7* RNA polymerase promoter. Unique restriction sites in the MCS are indicated in bold. The vector replicates from pUC ori and 2µ ori in *E. coli* and *S. cerevisiae*, respectively. The kanamycin resistance gene (Kan^r) and the *TRP1* nutritional marker respectively facilitate selection in *E. coli* and *S. cerevisiae*. (Taken from Clontech MATCHMAKER™ vector handbook)

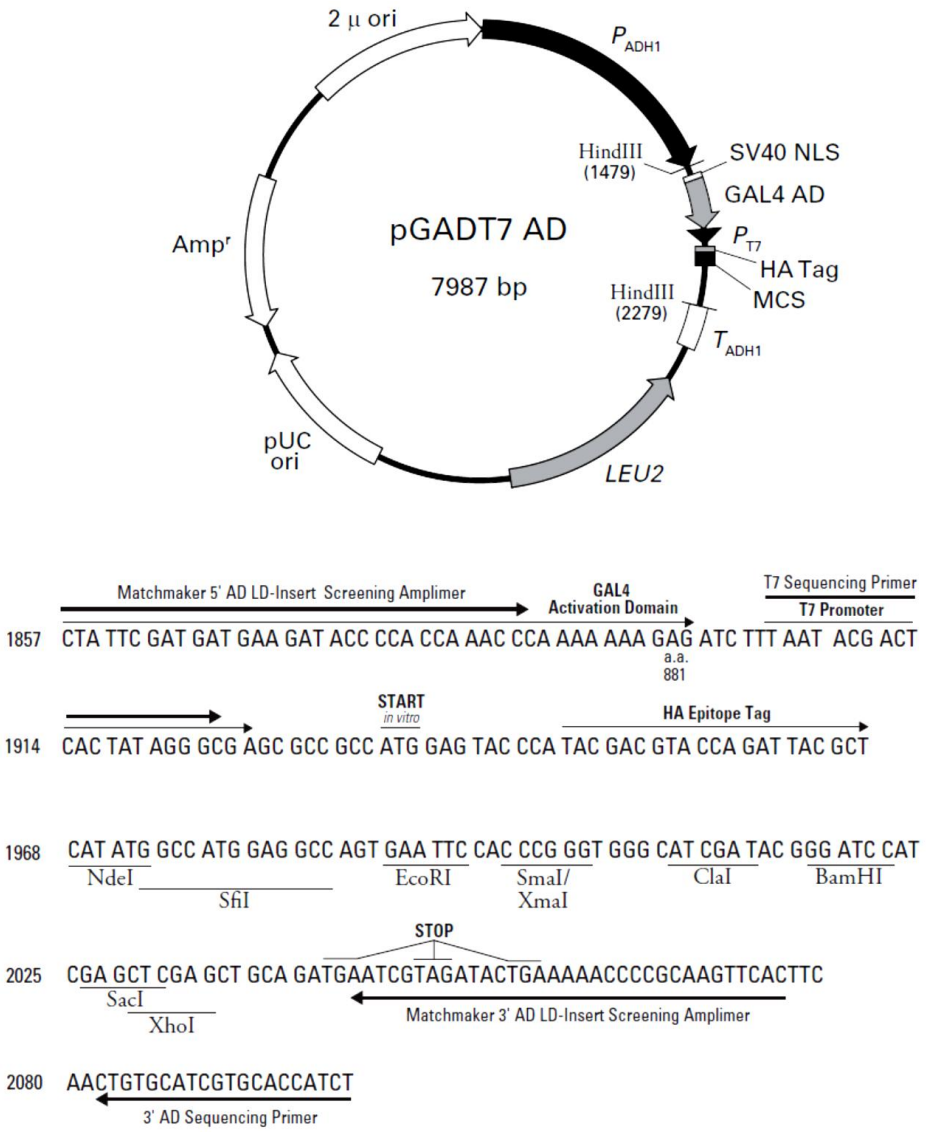

pGADT7 AD restriction map and multiple cloning site (MCS). This vector expresses proteins fused to amino acids 768-881 of the GAL4 DNA activation domain (DNA-AD), a SV40 nuclear localization signal (SV40 NLS) and a haemagglutinin (HA) epitope tag. Expression in yeast is driven by the constitutive *ADH1* promoter (P_{ADH1}) whereas transcription is terminated by the *ADH1* transcription termination sequence (T_{ADH1}). The vector also contains a *T7* RNA polymerase promoter. Unique restriction sites in the MCS are indicated. The vector replicates from pUC ori and 2μ ori in *E. coli* and *S. cerevisiae*, respectively. The ampicillin resistance gene (Amp^r) and the *LEU2* nutritional marker respectively facilitate selection in *E. coli* and *S. cerevisiae*. (Taken from Clontech MATCHMAKER™ vector handbook)

APPENDIX VI

Complete list of clones illustrating scoring of *HIS3*, *ADE2* and *MEL1* reporter genes activation during Y2H analysis

Clone ID	Growth on TDO (*HIS3* activation)	Growth on QDO (*ADE2* activation)	X-α-galactosidase assay (*MEL1* activation)
1	++++	+++	Pale blue
2	+++	+	No blue
3	+++	-	-
4	++++	++++	Pale blue
5	**++++**	**++++**	**Dark blue**
6	++++	+++	Pale blue
7	+++	-	-
8	**++++**	**++++**	**Medium blue**
9	++	++	Medium blue
10	++++	-	-
11	+++	++	Pale blue
12	+++	-	-
13	+	-	-
14	**++++**	**+++**	**Dark blue**
15	++	-	-
16	+	-	-
17	++	+	Dark blue
18	+	-	-
19	++++	++	Pale blue
20	**++++**	**+++**	**Dark blue**
21	**++++**	**++++**	**Dark blue**
22	**++++**	**++++**	**Dark blue**
23	**++++**	**+++**	**Dark blue**
24	**++++**	**+++**	**Dark blue**
25	++	-	-
26	+++	+	Pale blue
27	+++	+++	Pale blue
28	++++	+++	No blue
29	+++	++	Medium blue
30	+++	+	Medium blue
31	+	-	-
32	++++	++++	Pale blue
33	+++	+	Pale blue
34	+	-	-
35	+++	++	No blue
36	++++	+++	Pale blue
37	++++	++++	Pale blue
38	++++	++++	Pale blue
39	++	-	-
40	++	++	Pale blue
41	++	-	-
42	+	-	-
43	**++++**	**++++**	**Dark blue**
44	+	-	-
45	++++	++++	Pale blue

Clone ID	Growth on TDO (*HIS3* activation)	Growth on QDO (*ADE2* activation)	X-α-galactosidase assay (*MEL1* activation)
46	++++	++++	Pale blue
47	++++	++++	Pale blue
48	**++++**	**++++**	**Dark blue**
49	+++	-	-
50	+++	++	Pale blue
51	+	-	-
52	++	-	-
53	+	-	-
54	+++	+++	Pale blue
55	++	-	-
56	++	++	Medium blue
57	+	+	Pale blue
58	+	-	-
59	++++	++	Medium blue
60	++	-	-
61	++	+	Pale blue
62	**++++**	**++++**	**Dark blue**
63	+++	++	Medium blue
64	**++++**	**+++**	**Dark blue**
65	**++++**	**+++**	**Dark blue**
66	**+++**	**+++**	**Dark blue**
67	**++++**	**+++**	**Dark blue**
68	++	++	Pale blue
69	**++++**	**++**	**Dark blue**
70	++	+	Dark blue
71	**++++**	**+++**	**Dark blue**
72	++++	+	Medium blue
73	++++	+	Dark blue
74	+++	+	Dark blue
75	**++++**	**+++**	**Dark blue**
76	++	+	Medium blue
77	++	+	Medium blue
78	+++	+	Dark blue
79	++	+	Dark blue
80	++	++	Medium blue
81	++++	+	Dark blue
82	++	-	-
83	+	-	-
84	+++	-	-
85	++	-	-
86	+++	++	Medium blue
87	+++	+	Medium blue
88	+	-	-
89	+	-	-
90	**++++**	**++++**	**Dark blue**
91	+++	+	Pale blue
92	+++	+	Medium blue
93	++	-	-
94	+	-	-
95	++	-	-
96	++	-	-
97	+	-	-

Clone ID	Growth on TDO (*HIS3* activation)	Growth on QDO (*ADE2* activation)	X-α-galactosidase assay (*MEL1* activation)
98	+++	-	-
99	+++	+++	Pale blue
100	**++++**	**++++**	**Dark blue**
101	**++++**	**++++**	**Dark blue**
102	**++++**	**++++**	**Dark blue**
103	++++	++	Medium blue
104	**++++**	**++++**	**Dark blue**
105	++++	+++	No blue
106	**++++**	**++++**	**Dark blue**
107	+	-	-
108	+++	++	Medium blue
109	+++	+	Medium blue
110	++	+	Pale blue
111	++	+	Pale blue
112	+	-	-
113	**++++**	**++++**	**Dark blue**
114	++	-	-
115	+	-	-
116	**++++**	**+++**	**Dark blue**
117	+	-	-
118	++	-	-
119	++	-	-
120	+	-	-
121	+++	+++	Pale blue
122	+++	++	Pale blue
123	**++++**	**+++**	**Dark blue**
124	+++	+	Medium blue
125	+++	+++	Pale blue
126	+++	+++	No blue
127	+++	+++	Pale blue
128	++++	+++	No blue
129	++	+	Medium blue
130	+++	+++	Pale blue
131	++	++	Pale blue
132	++	++	No blue
133	++	+	Medium blue
134	+++	++	Pale blue
135	++	+	Pale blue
136	+++	+++	Pale blue
137	+	-	-
138	++++	++++	Pale blue
139	++++	++	Medium blue
140	**++++**	**+++**	**Dark blue**
141	**++++**	**++**	**Dark blue**
142	**++++**	**++++**	**Medium blue**
143	++	++	Medium blue
144	++	+	Pale blue
145	+	-	-
146	++	++	Medium blue
147	**+++**	**+++**	**Dark blue**
148	++	-	-
149	**++++**	**+++**	**Dark blue**

Clone ID	Growth on TDO (*HIS3* activation)	Growth on QDO (*ADE2* activation)	X-α-galactosidase assay (*MEL1* activation)
150	**+++**	**+++**	**Dark blue**
151	++++	++++	No blue
152	++	-	-
153	++	++	No blue
154	++++	++++	No blue
155	+	-	-
156	+++	+	Medium blue
157	++	-	-
158	++	+	Dark blue
159	++++	+	Dark blue
160	++	++	Medium blue
161	**++++**	**++++**	**Dark blue**
162	**++++**	**+++**	**Dark blue**
163	++	-	-
164	**++++**	**++++**	**Dark blue**
165	**++++**	**++++**	**Dark blue**
166	+++	++	Dark blue
167	++++	-	-
168	++++	++++	No blue
169	++	-	-
170	+	-	-
171	**++++**	**+++**	**Dark blue**
172	++++	++	Pale blue
173	++++	+	Medium blue
174	**++++**	**+++**	**Dark blue**
175	+++	+	Medium blue
176	+++	+	Pale blue
177	++	+	Pale blue
178	++	+	Pale blue
179	++++	+	Pale blue
180	++++	+	Medium blue
181	++	+	Pale blue
182	++	+	Pale blue
183	+++	+++	Pale blue
184	+++	+++	Pale blue
185	+++	+	Medium blue
186	++++	+++	Pale blue
187	+++	+++	Pale blue
188	**++++**	**+++**	**Dark blue**
189	+++	+	Medium blue
190	+++	+++	No blue
191	++	-	-
192	+	-	-
193	+	-	-
194	++	++	Medium blue
195	++++	+	Dark blue
196	+++	-	-
197	+++	++	Medium blue
198	**++++**	**+++**	**Dark blue**
199	**++++**	**+++**	**Dark blue**
200	++	-	-
201	++	-	-

Clone ID	Growth on TDO (*HIS3* activation)	Growth on QDO (*ADE2* activation)	X-α-galactosidase assay (*MEL1* activation)
202	**++++**	**+++**	**Dark blue**
203	++++	++	Medium blue
204	**++++**	**+++**	**Dark blue**
205	++++	++	Medium blue
206	+	-	-
207	**++++**	**++++**	**Dark blue**
208	**++++**	**+++**	**Dark blue**
209	++	-	-
210	+	-	-
211	+	-	-
212	++	-	-
213	++	-	-
214	+++	+++	Pale blue
215	+++	++	Medium blue
216	+	-	-
217	++++	+	Dark blue
218	**++++**	**+++**	**Dark blue**
219	+++	++	Medium blue
220	++++	++	Medium blue
221	**++++**	**++++**	**Dark blue**
222	**++++**	**++++**	**Dark blue**
223	**++++**	**++++**	**Dark blue**
224	**++++**	**+++**	**Dark blue**
225	**++++**	**+++**	**Dark blue**
226	++	-	-
227	+	-	-
228	+	-	-
229	+	-	-
230	++++	++++	Pale blue
231	+++	-	-
232	**++++**	**++++**	**Dark blue**
233	++	+	Medium blue
234	++	-	-
235	++	++	Dark blue
236	+++	+++	Pale blue
237	++	-	-
238	+	-	-
239	+++	+++	Pale blue
240	++	-	-
241	++	-	-
242	**++++**	**++++**	**Medium blue**
243	++	-	-
244	+++	+	Pale blue
245	+	-	-
246	+++	+++	Pale blue
247	++	+	Pale blue
248	++	+	Pale blue
249	+++	+	Pale blue
250	+	-	-
251	++++	+++	Pale blue
252	**++++**	**++++**	**Medium blue**
253	++	++	Pale blue

Clone ID	Growth on TDO (*HIS3* activation)	Growth on QDO (*ADE2* activation)	X-α-galactosidase assay (*MEL1* activation)
254	+++	++	Pale blue
255	++++	++	Pale blue
256	**++++**	**++++**	**Dark blue**
257	**++++**	**++++**	**Dark blue**
258	**++++**	**++++**	**Dark blue**
259	**++++**	**++++**	**Medium blue**
260	++++	++++	Pale blue
261	+++	+++	Pale blue
262	+	-	-
263	++	++	Pale blue
264	++	-	-
265	+	-	-
266	+	-	-
267	+	-	-
268	++	-	-
269	+++	+++	Pale blue
270	+	-	-
271	**++++**	**+++**	**Dark blue**
272	+	-	-
273	++	-	-
274	**+++**	**+++**	**Dark blue**
275	**++++**	**++++**	**Dark blue**
276	**++++**	**++++**	**Dark blue**
277	**++++**	**++++**	**Dark blue**
278	**++++**	**++++**	**Medium blue**
279	++++	++	Medium Blue
280	++	++	Medium blue
281	++	-	-
282	++	++	Medium blue
283	++	-	-
284	+++	++	Pale blue
285	++++	++	Pale blue
286	++	++	Pale blue
287	+++	+++	Pale blue
288	++	+	Medium blue
289	++	++	Pale blue
290	+++	++	Pale blue
291	++++	++++	No blue
292	+	-	-
293	+++	+++	Pale blue
294	+++	+++	Pale blue
295	+++	+++	Pale blue
296	++++	+++	No blue
297	++++	++++	No blue
298	++++	+++	No blue
299	+	-	-
300	+	+	No blue
301	+++	+++	Pale blue
302	+++	+++	Pale blue
303	+++	++	Pale blue
304	+	-	-
305	++	++	Pale blue

Clone ID	Growth on TDO (*HIS3* activation)	Growth on QDO (*ADE2* activation)	X-α-galactosidase assay (*MEL1* activation)
306	+++	+	Medium blue
307	++	+	Pale blue
308	++++	++++	No blue
309	+++	+++	Pale blue
310	++++	++++	Pale blue
311	+++	++	Medium blue
312	+++	++	Medium blue
313	+++	++	Pale blue
314	+++	++	Pale blue
315	++++	++	Pale blue
316	++++	++++	Pale blue
317	**++++**	**++++**	**Dark blue**
318	**+++**	**+++**	**Dark blue**
319	**+++**	**+++**	**Dark blue**
320	**+++**	**+++**	**Dark blue**
321	**++++**	**+++**	**Dark blue**
322	+	-	-
323	++	-	-
324	++++	+++	Pale blue
325	++	-	-
326	++	-	-
327	++	-	-
328	+	-	-
329	**++++**	**++++**	**Dark blue**
330	**++++**	**++++**	**Dark blue**
331	++++	++	Pale blue
332	**++++**	**+++**	**Dark blue**
333	**++++**	**+++**	**Dark blue**
334	**++++**	**++++**	**Dark blue**
335	++	-	-
336	++	-	-
337	**++++**	**+++**	**Dark blue**
338	+	-	-
339	+	-	-
340	**++++**	**+++**	**Dark blue**
341	++	-	-
342	+++	++	Pale blue
343	++	+	Medium blue
344	++++	++	Medium blue
345	**++++**	**+++**	**Dark blue**
346	+	-	-
347	**++++**	**++++**	**Dark blue**
348	**++++**	**++++**	**Dark blue**
349	++	-	-
350	+	-	-
351	+	-	-
352	++	+	Pale blue
353	+	-	-
354	+	-	-
355	+	-	-
356	++	-	-
357	++	++	Pale blue

Clone ID	Growth on TDO (*HIS3* activation)	Growth on QDO (*ADE2* activation)	X-α-galactosidase assay (*MEL1* activation)
358	+++	++	Pale blue
359	+	-	-
360	++++	++++	No blue
361	**++++**	**++++**	**Dark blue**
362	++	+	Pale blue
363	++++	++++	Pale blue
364	++	-	-
365	++	-	-
366	+	-	-
367	+	-	-
368	+	-	-
369	+	-	-
370	+++	+++	Pale blue
371	++++	+++	Pale blue
372	+	-	-
373	+	-	-
374	++	++	No blue
375	+	-	-
376	+	-	-
377	**++++**	**++++**	**Dark blue**
378	**++++**	**+++**	**Dark blue**
379	**++++**	**++++**	**Dark blue**
380	++	-	-
381	**++++**	**++++**	**Dark blue**
382	**++++**	**++++**	**Dark blue**
383	++	-	-
384	++	-	-
385	+	-	-
386	**+++**	**++++**	**Dark blue**
387	**++++**	**++++**	**Dark blue**
388	++	-	-
389	+++	-	-
390	**++++**	**++++**	**Dark blue**
391	++	-	-
392	+	-	-
393	++++	+	Dark blue
394	++	-	-
395	**++**	**++++**	**Dark blue**
396	++	-	-
397	+++	-	-
398	++++	++++	No blue
399	++	-	-
400	+	-	-
401	+++	+++	No blue
402	**++++**	**++++**	**Dark blue**
403	++	-	-
404	++	-	-
405	+++	-	-
406	+	-	-
407	++	-	-
408	++	-	-
409	++	-	-

Clone ID	Growth on TDO (*HIS3* activation)	Growth on QDO (*ADE2* activation)	X-α-galactosidase assay (*MEL1* activation)
410	+	-	-
411	+	-	-
412	+	-	-
413	++++	+	Pale blue
414	++	-	-
415	+	-	-
416	++++	++++	Pale blue
417	++	-	-
418	+++	-	-
419	+	-	-
420	++	-	-
421	++	-	-
422	+	-	-
423	**++++**	**++++**	**Dark blue**
424	++	-	-
425	++	-	-
426	+	-	-
427	+	-	-
428	+++	+++	Pale blue
429	+++	-	-
430	+	-	-
431	+	-	-
432	**++++**	**++++**	**Dark blue**
433	**++++**	**+++**	**Dark blue**
434	++++	+++	Pale blue
435	**++++**	**+++**	**Dark blue**
436	**++++**	**+++**	**Dark blue**
437	**++++**	**++++**	**Dark blue**
438	+++	-	-
439	**++++**	**++++**	**Dark blue**
440	++	+	Pale blue
441	**++++**	**+++**	**Dark blue**
442	**++++**	**+++**	**Dark blue**
443	**++++**	**+++**	**Dark blue**
444	++++	+	Medium blue
445	++	-	-
446	+	-	-
447	++++	++	Pale blue
448	++	-	-
449	++	-	-
450	+	-	-
451	+	-	-
452	**++++**	**+++**	**Dark blue**
453	+	-	-
454	+	-	-
455	+	-	-
456	+	-	-
457	++	-	-
458	++	-	-
459	+	-	-
460	++	-	-
461	+++	-	-

Clone ID	Growth on TDO (*HIS3* activation)	Growth on QDO (*ADE2* activation)	X-α-galactosidase assay (*MEL1* activation)
462	++++	++++	**Dark blue**
463	+++	-	-
464	+	-	-
465	++++	++++	**Dark blue**
466	++	-	-
467	++	-	-
468	++	-	-
469	++	-	-
470	+	-	-
471	+	-	-
472	++++	++++	**Dark blue**
473	+	-	-
474	++	-	-
475	+	-	-
476	+++	+++	**Dark blue**
477	++	-	-
478	++++	++++	No blue
479	+	+	No blue
480	+	+	No blue
481	++	+	Pale blue
482	+	-	-
483	++++	+++	**Dark blue**
484	+	-	-
485	+	-	-
486	++	-	-
487	++	++	Medium blue
488	+++	++	Pale blue
489	++++	+++	**Dark blue**
490	+++	+++	**Dark blue**
491	+++	++	Medium blue
492	+	-	-
493	++	-	-
494	++++	++++	**Dark blue**
495	+++	+++	**Dark blue**
496	++++	++++	**Dark blue**
497	++++	++	Pale blue
498	++	-	-
499	+	-	-
500	+	-	-
501	+	-	-
502	++	-	-
503	+++	-	-
504	++	++	Medium blue
505	++	-	-

Clones in **blue** font were designated as primary clones. Abbreviations: ++++, excellent growth; +++ fair growth; ++ weak growth; +, very weak growth; -, no growth; QDO, quadruple dropout (SD media lacking tryptophan, leucine, histidine and adenine); TDO, triple dropout (SD media lacking tryptophan, leucine and histidine); Y2H, yeast two-hybrid

APPENDIX VII

Complete list of clones scored for bait-prey interaction specificity

Clone ID	pGBKT7-*parkin*	pGBKT7	pGBKT7-*53*	pGBKT7-*TTN*
5	++++	+++	+	+
8	++++	+	-	+
14	++++	-	+	-
20	++++	++	-	+
21	++++	-	+++	-
22	++++	++	-	++
23	++++	+	-	-
24	++++	+	-	+
43	+++++	+	-	+
48	++++	+	+	+
62	++++	+	+	-
64	++++	+	-	+
65	++++	++++	+	+++
66	++++	+	+	+
69	++++	+	+	+
71	+++++	++++	+++	++
75	+++++	++++	+	+
90	++++	+++	+	+
100	++++	+	+	+
101	++++	-	-	+
102	++++	+	-	+
104	++++	+	++++	-
113	+++++	+	+++	+
116	++++	+	++++	-
123	++++	++	+++	+++
140	++++	+	++++	+
141	++++	+	+	-
142	++++	+	+	+
147	+++++	+	-	-
149	++++	+++	-	-
150	+++++	-	+++	+
161	++++	+	+	+
162	+++++	+	+++	+
164	++++	+	+	+
165	++++	+	+	+
166	++++	+	-	+
171	++++	-	++++	++++
174	+++++	-	+	+
188	++++	+	+	+
198	++++	+	+	+
199	++++	+	-	+++

Clone ID	pGBKT7-*parkin*	pGBKT7	pGBKT7-*53*	pGBKT7-*TTN*
202	++++	+++	-	-
204	++++	+	+	+
207	++++	+++	-	+
208	++++	+	-	+
218	++++	+	-	+
221	+++++	+	+	-
222	++++	-	-	-
223	++++	++	+	+
224	++++	+	-	+
225	++++	+	+	+
232	++++	+	++++	+
242	++++	+	-	-
252	++++	-	+	+
256	++++	+	+++	++
257	++++	+	+	+
258	+++++	+	-	-
259	++++	+	+	+
271	+++++	+	+	++++
274	++++	+	+	+
275	++++	+	++++	+
276	++++	+	+	+
277	++++	+	+	+
278	++++	+	+	+
317	++++	+	-	+
318	++++	+	+	+
319	+++++	+	+	+
320	++++	+++	+++	+
321	++++	+	-	+
329	++++	+	+	+
330	++++	+	+	+
332	++++	+++	+	+
333	++++	+	+++	++++
334	++++	++++	+	+
337	++++	+	+	+
340	++++	++	+	+
345	++++	+	+++	+
361	++++	++	++	++
372	++++	-	+	+
377	++++	+	+	+
378	++++	++	+++	-
379	++++	+	-	+
386	++++	++	+++	++
387	++++	++	++	++
390	++++	++	++	++
395	++++	+	+	+

Clone ID	pGBKT7-*parkin*	pGBKT7	pGBKT7-*53*	pGBKT7-*TTN*
423	++++	-	+	-
432	++++	+	+	+
433	+++++	++++	++++	++++
435	++++	-	+	+
436	++++	+	-	+
437	+++++	+	+	+
439	++++	+	+	+
441	++++	+++	+	++++
442	++++	++	++++	-
443	++++	+	+	+
452	++++	+	+	+
462	++++	-	++++	+
465	++++	++	-	++
472	++++	+++	-	+
476	+++++	+	+	+
483	++++	+	-	+
489	++++	-	+	+
490	++++	++++	++++	-
494	++++	+	+	+
495	++++	-	-	-
496	++++	+	+	+

Clones in **blue** font were considered to demonstrate specific parkin-bait interactions. All colonies were scored after 7 days on QDO plates. Abbreviations: ++++, excellent growth; +++ fair growth; ++ weak growth; +, very weak growth; -, no growth; QDO, quadruple dropout (SD media lacking tryptophan, leucine, histidine and adenine

APPENDIX VIII

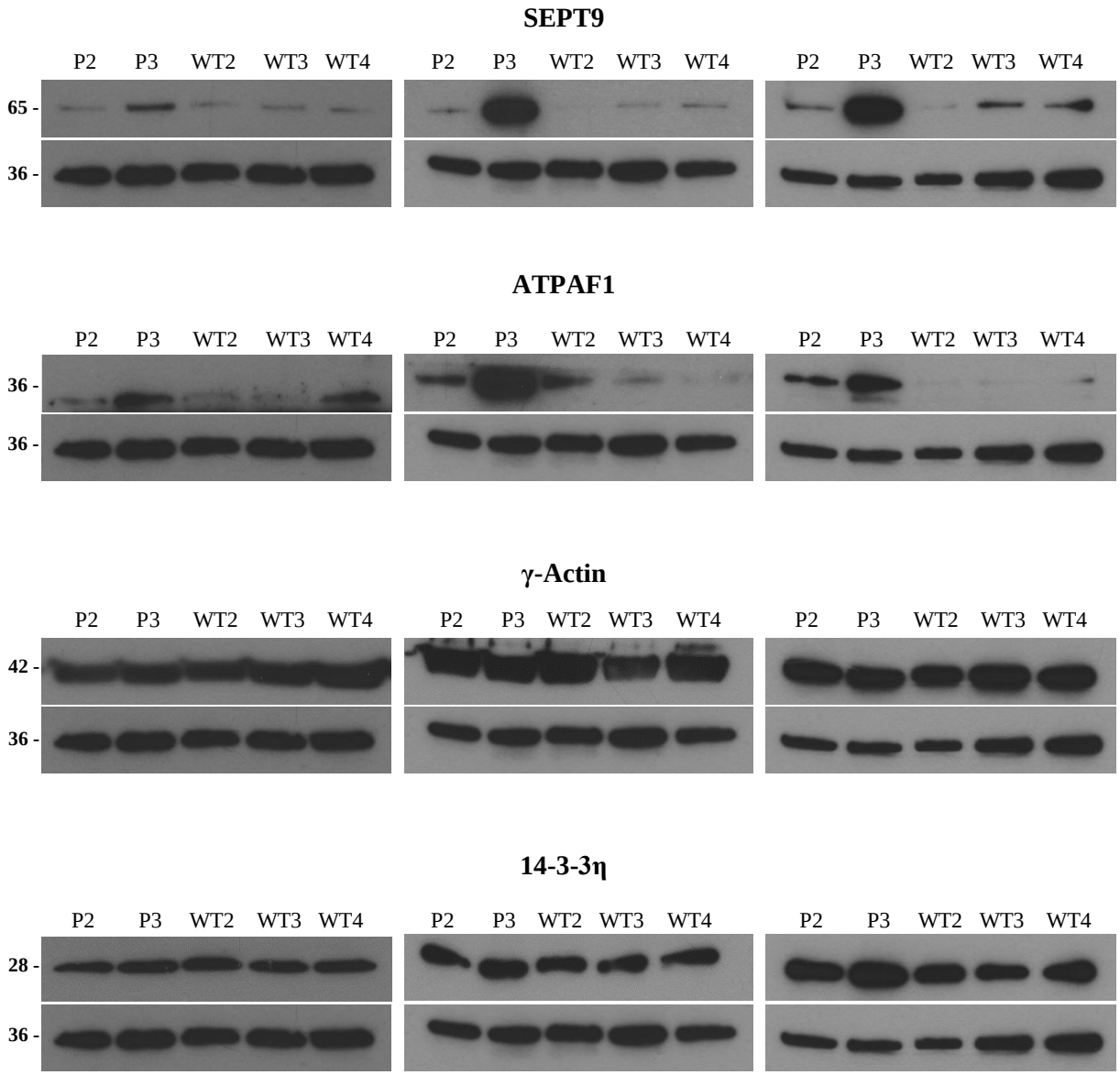

Protein expression of parkin interactors in parkin-null and wild-type fibroblasts over three experimental runs. Relative protein expression of SEPT9, ATPAF1, γ-actin and 14-3-3η were assayed with western blots in fibroblasts from parkin-null patients (P2 and P3) and wild-type controls (WT2, WT3, WT4). Expression of interactors (top lanes) was normalized to GAPDH expression (bottom lanes). Experiments were performed in triplicate (N=3) and western blots of all three replicate runs are shown. Numbers on the side of western blots denote protein sizes (in kiloDalton).

APPENDIX IX

GRAPHICAL OUTPUTS OF FUNCTIONAL ASSAYS

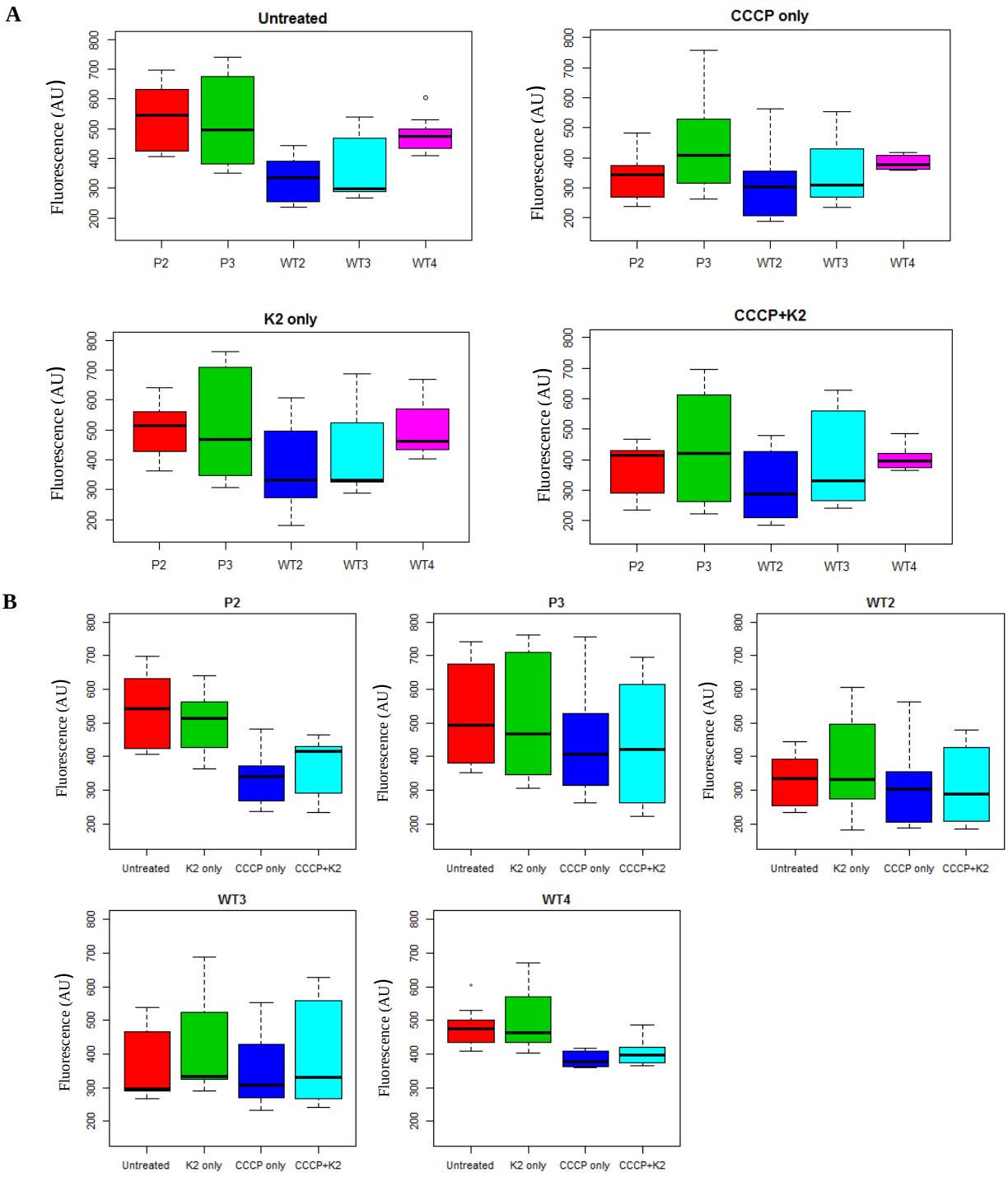

Cell growth in patient-derived and wild-type fibroblasts under basal and CCCP-stressed conditions, with and with Vitamin K_2 treatment. Cell growth was assessed by a CyQUANT® assay. Box-and-whisker plots depict measurements for each fibroblast cell line for three experimental runs. **A**, cell growth in different cell lines under each treatment category. **B**, comparison of cell growth under different treatments within a given cell line.

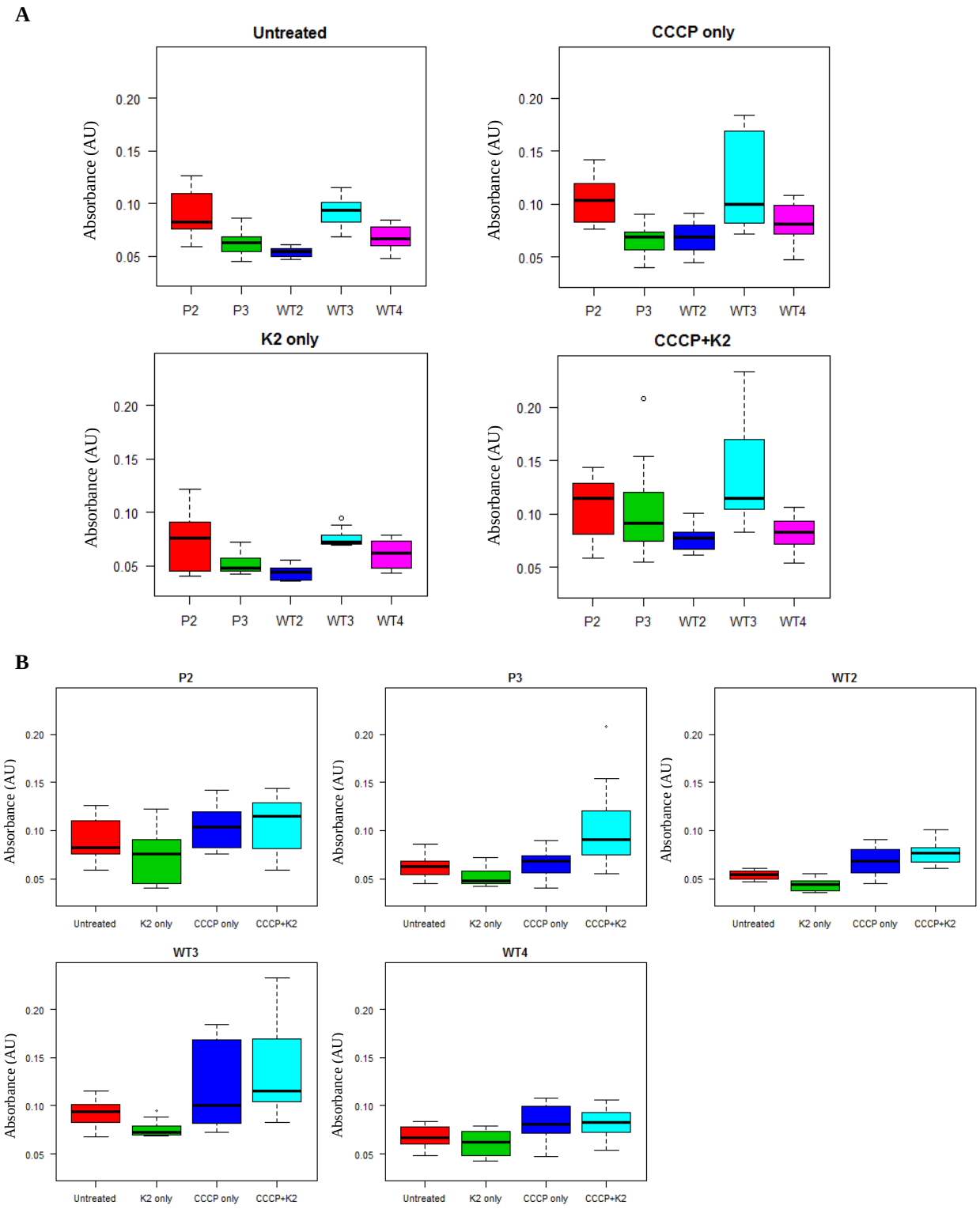

Cell viability in patient-derived and wild-type fibroblasts under basal and CCCP-stressed conditions, with and with Vitamin K_2 treatment. Cell viability was assessed by a MTT assay. Box-and-whisker plots depict measurements for each fibroblast cell line for three experimental runs. **A**, cell viability in different cell lines under each treatment category. **B**, comparison of cell viability under different treatments within a given cell line.

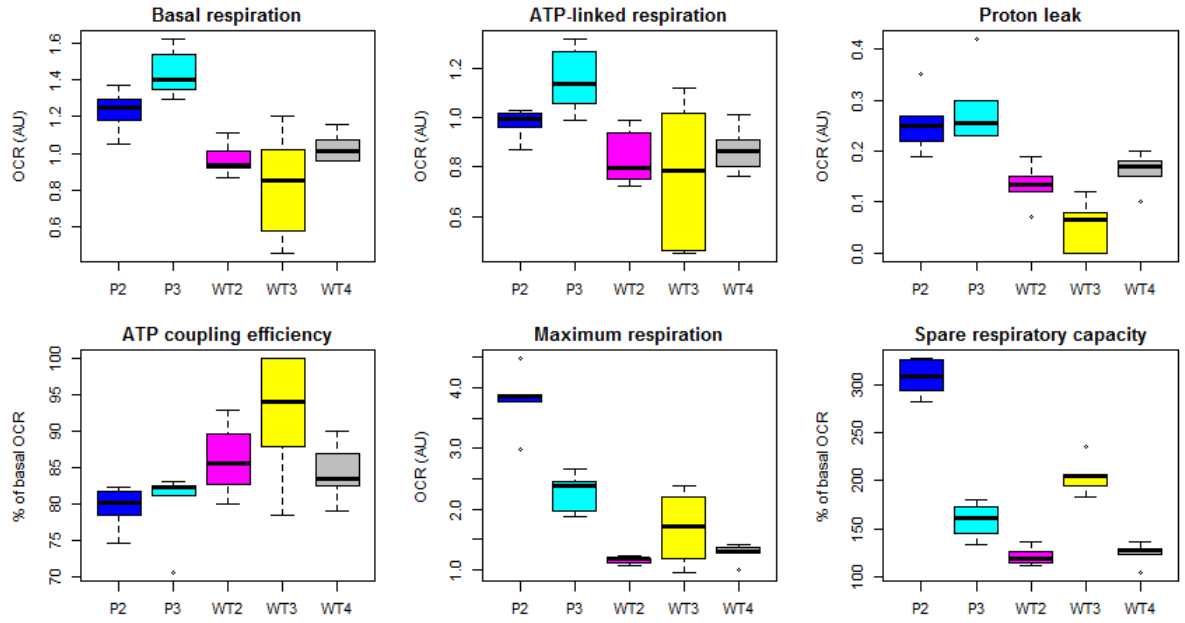

Parameters of respiratory control in patient-derived and wild-type fibroblasts. Box-and-whisker plots depict values for each fibroblast cell line, with 6 replicate measurements.

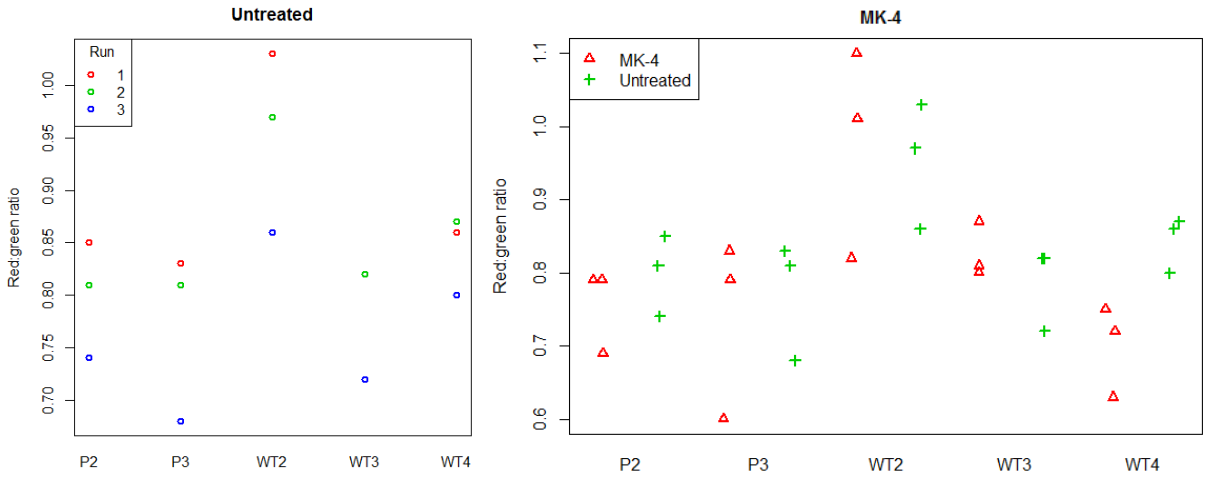

Relative $\Delta\psi_m$ of untreated patient-derived and wild-type fibroblasts, with and with Vitamin K_2 treatment. Relative $\Delta\psi_m$ was determined by JC-1 red:green fluorescent emission ratios, across 3 experimental runs. Red:green ratios for each fibroblast cell line is shown in the left panel, whereas the effect of treatment with vitamin K_2 (MK-4) on the red:green ratio of each cell line is shown in the right panel.

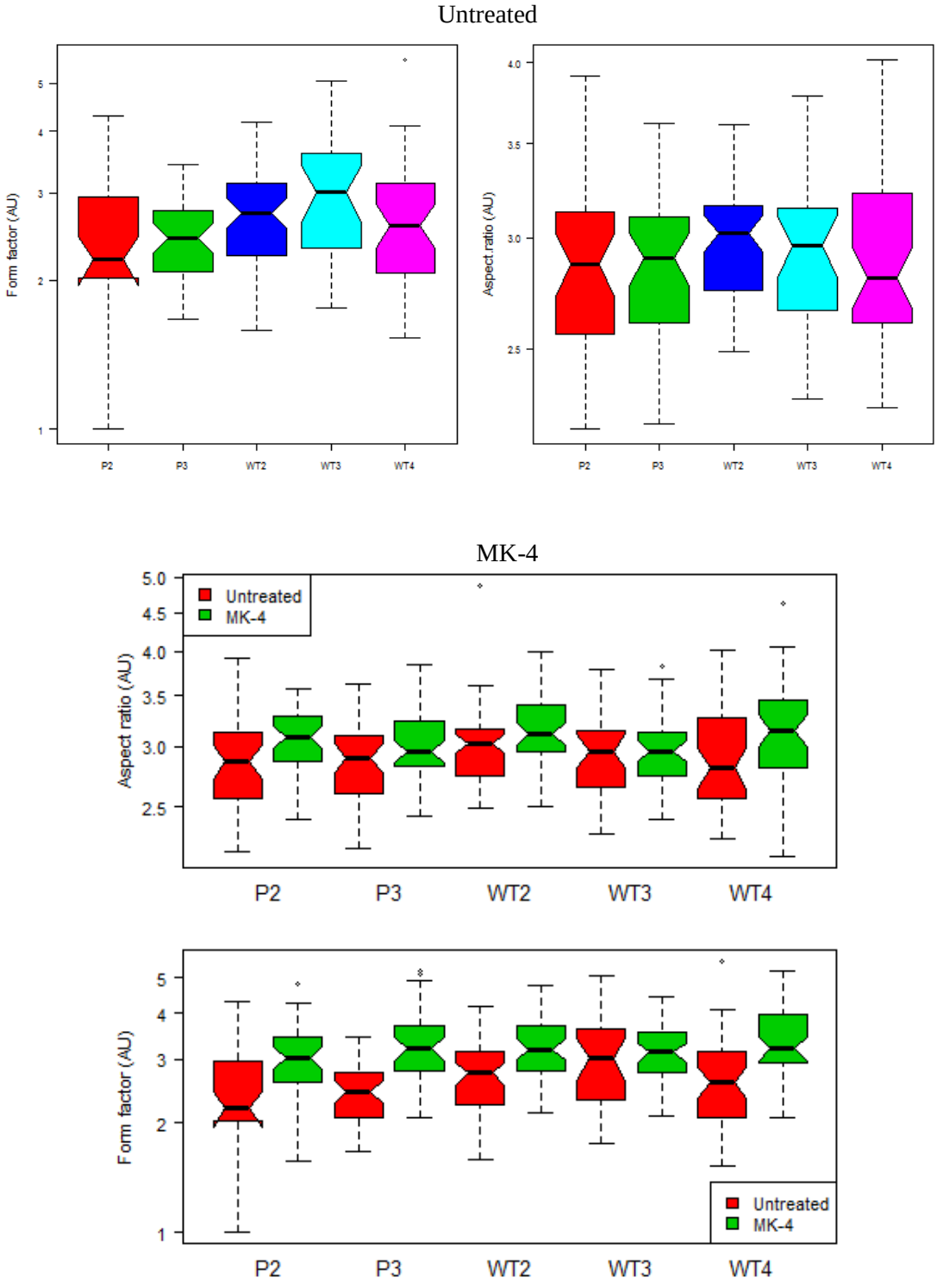

Mitochondrial network analysis of patient-derived and wild-type fibroblasts, with and with Vitamin K_2 treatment. Mitotracker Red and live-cell microscopy was used to visualize the mitochondrial network. All images were assessed in regards to the degree of mitochondrial branching (form factor) and degree of mitochondrial elongation (aspect ratio), with approximately 40 cell analyzed per fibroblast cell line. The distribution of these parameters in each fibroblast cell line are represented on logarithmic scale in box-and-whisker-plots.

APPENDIX X

```
SEPT9_v1      MKKSYSGGTRTSSGRLRRLGDSSGPALKRSFEVEEVETPNSTPPRRVQTPLLRATVASST   60
SEPT9_v2      MSDP------AVNAQLDG-IISDFEALKRSFEVEEVETPNSTPPRRVQTPLLRATVASST   53
SEPT9_v3      ------------------MERDRISALKRSFEVEEVETPNSTPPRRVQTPLLRATVASST   42
ORF           ------------------------------------------------------------   0

SEPT9_v1      QKFQDLGVKNSEPSARHVDSLSQRSPKASLRRVELSGPKAAEPVSRRTELSIDISSKQVE   120
SEPT9_v2      QKFQDLGVKNSEPSARHVDSLSQRSPKASLRRVELSGPKAAEPVSRRTELSIDISSKQVE   113
SEPT9_v3      QKFQDLGVKNSEPSARHVDSLSQRSPKASLRRVELSGPKAAEPVSRRTELSIDISSKQVE   102
ORF           ----------------------------------------------LSIDISSKQVE   11
                                                             ***********

SEPT9_v1      NAGAIGPSRFGLKRAEVLGHKTPEPAPRRTEITIVKPQESAHRRMEPPASKVPEVPTAPA   180
SEPT9_v2      NAGAIGPSRFGLKRAEVLGHKTPEPAPRRTEITIVKPQESAHRRMEPPASKVPEVPTAPA   173
SEPT9_v3      NAGAIGPSRFGLKRAEVLGHKTPEPAPRRTEITIVKPQESAHRRMEPPASKVPEVPTAPA   162
ORF           NAGAIGPSRFGLKRAEVLGHKTPEPAPRRTEITIVKPQESAHRRMEPPASKVPEVPTAPA   71
              ************************************************************

SEPT9_v1      TDAAPKRVEIQMPKPAEAPTAPSPAQTLENSEPAPVSQLQSRLEPKPQPPVAEATPRSQE   240
SEPT9_v2      TDAAPKRVEIQMPKPAEAPTAPSPAQTLENSEPAPVSQLQSRLEPKPQPPVAEATPRSQE   233
SEPT9_v3      TDAAPKRVEIQMPKPAEAPTAPSPAQTLENSEPAPVSQLQSRLEPKPQPPVAEATPRSQE   222
ORF           TDAAPKRVEIQMPKPAEAPTAPSPAQTLENSEPAPVSQLQSRLEPKPQPPVAEATPRSQE   131
              ************************************************************

SEPT9_v1      ATEAAPSCVGDMADTPRDAGLKQAPASRNEKAPVDFGYVGIDSILEQMRRKAMKQGFEFN   300
SEPT9_v2      ATEAAPSCVGDMADTPRDAGLKQAPASRNEKAPVDFGYVGIDSILEQMRRKAMKQGFEFN   293
SEPT9_v3      ATEAAPSCVGDMADTPRDAGLKQAPASRNEKAPVDFGYVGIDSILEQMRRKAMKQGFEFN   282
ORF           ATEAAPSCVGDMADTPRDAGLKQAPASRNEKAPVDFGYVGIDSILEQMRRKAMKQGFEFN   191
              ************************************************************

SEPT9_v1      IMVVGQSGLGKSTLINTLFKSKISRKSVQPTSEERIPKTIEIKSITHDIEEKGVRMKLTV   360
SEPT9_v2      IMVVGQSGLGKSTLINTLFKSKISRKSVQPTSEERIPKTIEIKSITHDIEEKGVRMKLTV   353
SEPT9_v3      IMVVGQSGLGKSTLINTLFKSKISRKSVQPTSEERIPKTIEIKSITHDIEEKGVRMKLTV   342
ORF           IMVVGQSGLGKSTLINTLFKSKISRKSVQPTSEERIPKTIEIKSITHDIEEKGVRMKLTV   251
              ************************************************************

SEPT9_v1      IDTPGFGDHINNENCWQPIMKFINDQYEKYLQEEVNINRKKRIPDTRVHCCLYFIPATGH   420
SEPT9_v2      IDTPGFGDHINNENCWQPIMKFINDQYEKYLQEEVNINRKKRIPDTRVHCCLYFIPATGH   413
SEPT9_v3      IDTPGFGDHINNENCWQPIMKFINDQYEKYLQEEVNINRKKRIPDTRVHCCLYFIPATGH   402
ORF           IDTPGFGDHINNENCWQPIMKFINDQYEKYLQEEVNINRKKRIPDTRVHCCLYFIPATGH   311
              ************************************************************

SEPT9_v1      SLRPLDIEFMKRLSKVVNIVPVIAKADTLTLEERVHFKQRITADLLSNGIDVYPQKEFDE   480
SEPT9_v2      SLRPLDIEFMKRLSKVVNIVPVIAKADTLTLEERVHFKQRITADLLSNGIDVYPQKEFDE   473
SEPT9_v3      SLRPLDIEFMKRLSKVVNIVPVIAKADTLTLEERVHFKQRITADLLSNGIDVYPQKEFDE   462
ORF           SLRPLDIEFMKRLSKVVNIVPVIAKADTLTLEERVHFKQRITADLLSNGIDVYPQKEFDE   371
              ************************************************************

SEPT9_v1      DSEDRLVNEKFREMIPFAVVGSDHEYQVNGKRILGRKTKWGTIEVENTTHCEFAYLRDLL   540
SEPT9_v2      DSEDRLVNEKFREMIPFAVVGSDHEYQVNGKRILGRKTKWGTIEVENTTHCEFAYLRDLL   533
SEPT9_v3      DSEDRLVNEKFREMIPFAVVGSDHEYQVNGKRILGRKTKWGTIEVENTTHCEFAYLRDLL   522
ORF           DSEDRLVNEKFREMIPFAVVGSDHEYQVNGKRILGRKTKWGTIEVENTTHCEFAYLRDLL   431
              ************************************************************

SEPT9_v1      IRTHMQNIKDITSSIHFEAYRVKRLNEGSSAMANGMEEKEPEAPEM                 586
SEPT9_v2      IRTHMQNIKDITSSIHFEAYRVKRLNEGSSAMANGMEEKEPEAPEM                 579
SEPT9_v3      IRTHMQNIKDITSSIHFEAYRVKRLNEGSSAMANGMEEKEPEAPEM                 568
ORF           IRTHMQNIKDITSSIHFEAYRVKRLNEGSSAMANGMEEKEPEAPEM                 477
              *********************************************
```

Protein alignment of translated ORF sequence of Y2H clone 318 with SEPT9 isoforms. Three representative SEPT9 isoforms (SEPT9_v1, SEPT9_v2 and SEPT9_v3) were selected; clone 318 had a 100% identity to all isoforms. Hence, clone 318 encodes a peptide common to all SEPT9 isoforms. The isoform-variable region of SEPT9 is shown in red font, whereas the GTPase domain-containing region is shown in blue font. *In silico* alignment was performed with CLUSTAL O 1.2.1 (http://www.ebi.ac.uk/Tools/msa/clustalo).